

**A Comparative Study of the Complex Formation of
Molybdenum(VI) and Tungsten(VI) with Ligands
Derived from Carboxylic Acids**



**Dissertation Presented for the Degree of
Doctor of Philosophy (Chemistry)
at the
University of Stellenbosch**

**Promoter
Prof. J.J. Cruywagen**

**Stellenbosch
February 2000**

Declaration

I, the undersigned, hereby declare that the work contained in this dissertation is my own original work and that I have not previously in its entirety or in part submitted it at any university for a degree.

SUMMARY

A comparative study of the complex formation of Molybdenum(VI) and Tungsten(VI) with ligands derived from carboxylic acids

Complexation of molybdenum(VI) and tungsten(VI) with eight common organic ligands, namely oxalic, lactic, mandelic, malic, citric, tartaric, aspartic and nitrilotriacetic acids, were investigated by potentiometry, spectrophotometry and calorimetry in a 1 M (Na)Cl aqueous medium at 25°C over a wide pH range. The aim was to identify the likely complex species in terms of their stoichiometric coefficients of reagents (MoO_4^{2-} or WO_4^{2-} , Ligand^{n-} , H^+) and to calculate the formation constants and the values for the change in free energy, enthalpy and entropy associated with their formation.

A comprehensive potentiometric study led to the identification of many molybdate complexes, typically with the metal-to-ligand ratio of 1:1, 1:2, 2:2, 2:1, 4:2, 4:4. Most of the tungstate complexes identified had analogues in the related molybdate-ligand systems. The complexes for which the ratio metal:ligand > 1 and with a relatively high degree of condensation were better represented in the molybdate systems than in the tungstate systems. All the complexes which have previously been determined by X-ray crystallographic analysis were identified and characterized by potentiometry. The formation constants of the complexes were determined. By analysis of spectrophotometric data the spectra of some molybdate complexes were calculated and their formation constants verified.

Calorimetric data were collected for all the complex systems and used to calculate the ΔH° values (and indirectly the $T\Delta S^\circ$ values) for the formation of some of the complexes identified by potentiometry. With due consideration of the thermodynamic quantities, structures for all the identified complexes were proposed with expected features like MO_2 , MO_3 or dimeric metalate cores and didentate or tridentate chelation by the ligands. Some unique tartrate complexes were proposed to have chain structures, which are believed to be the result of the two chemically identical vicinal α -hydroxycarboxylate groups of tartrate.

The change in free energy for the formation of tungstate complexes of the α -hydroxycarboxylic acids is generally $\sim 9 \text{ kJ mol}^{-1}$ per metal greater than that of the related molybdate complexes with the same proposed structure. The difference in stability of most oxalate and nta-complexes of molybdate and tungstate is not so marked. The particularly weak aspartate complexation is the result of a weaker metal-nitrogen bond compared to the metal-oxygen bond. Tridentate and didentate chelation seems to be indicated by a significant difference in the change of enthalpy and entropy (more bonds at the cost of entropy). Tungstate has a greater tendency to increase its coordination number from four to six than molybdate. This is reflected by the greater ΔH° value for the formation of almost all the tungstate complexes compared to molybdate complexes with the same stoichiometry and structure.

The models and the thermodynamic values obtained show consistent and plausible trends, which, in turn give more credence to the individual models. The models are also consistent with structures of complexes isolated in the solid state as well as with results from previous NMR, polarimetric and other investigations.

OPSOMMING

'n Vergelykende studie van die kompleksvorming van Molibdeen(VI) en Wolfram(VI) met ligande wat afgelei is van karboksielsure

Kompleksvorming van molibdeen(VI) en wolfram(VI) met agt eenvoudige organiese ligande, naamlik oksaal-, melk-, amandel-, appel-, sitroen-, wynsteen-, aspartien- en nitrilo-triasynsuur, is potensiomeries, spektrofotometries en kalorimetries ondersoek in 1 M (Na)Cl watermedium by 25°C oor 'n wye pH-gebied. Die doel was om die waarskynlike kompleksspesies te identifiseer in terme van die stoïgiometriese koëffisiënte van die samestellende reaktante (MoO_4^{2-} of WO_4^{2-} , Ligand^n , H^+) en om die vormingskonstantes en die waardes vir die verandering in vrye energie, entalpie en entropie wat met hul vorming geassosieer is, te bereken.

'n Deeglike potensiometriese ondersoek het gelei tot die identifikasie van 'n groot aantal tipiese molibdaatkomplekse met metaal-ligand verhouding 1:1, 1:2, 2:2, 2:1, 4:2, 4:4, en die vormingskonstantes van die komplekse is bereken. Die meeste wolframaatkomplekse het analoë in die verwante molibdaat-ligand sisteme. Komplekse met metaal-ligand verhouding > 1 en van 'n relatief hoë kondensasiegraad kom meer algemeen voor in die molibdaat-sisteme as in die wolframaat-sisteme. Die spektra van sekere molibdaatkomplekse is bereken uit spektrofotometriese data, en hul vormingskonstantes is ook uit dié data geverifieer.

Kalorimetriese data is vir al die kompleks-sisteme verkry. Hiermee is die ΔH° -waardes (asook, op indirekte wyse, die $T\Delta S^\circ$ -waardes) vir die vorming van die potensiomeries geïdentifiseerde komplekse bereken. Strukture is vir al die komplekse voorgestel met inagneming van hierdie termodinamiese waardes. Die strukture het verwagte kenmerke soos MO_2 , MO_3 of dimeriese metalaat-keme met die ligand didentaat of tridentaat gebind. Sommige unieke tartraatkomplekse is as kettingstrukture voorgestel; die gevolg van twee chemies ekwivalente, naasliggende α -hidroksikarboksilaat groepe van tartraat.

Die verandering in vrye energie vir die vorming van wolframaatkomplekse van die α -hidroksikarboksielsure is oor die algemeen $\sim 9 \text{ kJ mol}^{-1}$ per metaal groter as dié van die verwante molibdaatkompleks met dieselfde voorgestelde struktuur. Die verskil in die stabiliteit van die meeste oksalaat- en nta-komplekse van molybdaat en wolframaat is kleiner. Die besonder swak kompleksvorming met aspartaat is die gevolg van 'n swakker metaal-stikstof binding, vergeleke met 'n metaal-suurstof binding. Dit blyk dat tridentate en didentate chelaatvorming aangedui word deur 'n beduidende verskil in entalpie en entropie (meer bindings ten koste van entropie). Wolframaat is meer geneig om koördinasie-uitbreiding (van vier na ses) te ondergaan as molibdaat. Dit word weerspieël deur die groter ΔH° -waarde vir die vorming van die meeste wolframaatkomplekse, vergeleke met molibdaatkomplekse met dieselfde stoïgiometrie en struktuur.

Die verkreeë modelle en termodinamiese waardes toon konsekwente tendense. Dit verleen meer geloofwaardigheid aan die individuele modelle. Die modelle is ook versoenbaar met die strukture van die komplekse wat in vaste toestand geïsoleer en gekarakteriseer is, asook met resultate van vorige KMR-, polarimetriese- en ander ondersoeke.

Acknowledgements

I thank

Prof. J.J. Cruywagen for his guidance and support, and for collecting
most of the calorimetric data,

Prof. J.B.B. Heyns for his advice and for proof-reading the thesis,

Dr. G.F.C. Wessels for the polarographic measurements,

Prof. H. Stafast for his interest and constructive criticism.

Index

	page
1. Introduction	1
2. Experimental and methods of analysis	5
2.1 Reagents, Solutions, Standardizations	5
2.2 Potentiometry	6
2.3 Spectrophotometry	8
2.4 Calorimetry	9
2.5 Differential pulse polarography	10
2.6 Methods of data analysis	11
2.6.1 Potentiometric analysis	11
2.6.1.1 Molybdenum(VI) and Tungsten(VI)-proton model	12
2.6.1.2 Ligand-proton model	14
2.6.1.3 Model search strategy with SUPERQUAD	15
2.6.2 Spectrophotometric analysis	16
2.6.3 Calorimetric analysis	17
3. Experimental results and data analysis	20
3.1 Complexation with oxalate	21
3.1.1 Molybdenum(VI)-oxalate system	21
3.1.1.1 Potentiometric data and analysis	21
3.1.1.2 Enthalpimetric data and analysis	25
3.1.2 Tungsten(VI)-oxalate system	27
3.1.2.1 Potentiometric data and analysis	27
3.1.2.2 Enthalpimetric data and analysis	30
3.2 Complexation with lactate	33
3.2.1 Molybdenum(VI)-lactate system	33
3.2.1.1 Potentiometric data and analysis	33
3.2.1.2 Enthalpimetric data and analysis	35
3.2.2 Tungsten(VI)-lactate system	37
3.2.2.1 Potentiometric data and analysis	37
3.2.2.2 Enthalpimetric data and analysis	39
3.3 Complexation with mandelate	40
3.3.1 Molybdenum(VI)-mandelate system	40
3.3.1.1 Potentiometric data and analysis	40
3.3.1.2 Spectrophotometric data and analysis	42
3.3.1.3 Enthalpimetric data and analysis	45
3.3.2 Tungsten-mandelate system	46
3.3.2.1 Potentiometric data and analysis	46

3.3.2.2	Enthalpimetric data and analysis	48
3.4	Complexation with malate	49
3.4.1	Molybdenum(VI)-malate system	49
3.4.1.1	Potentiometric data and analysis	49
3.4.1.2	Spectrophotometric data and analysis	52
3.4.1.3	Enthalpimetric data and analysis	54
3.4.2	Tungstate(VI)-malate system	57
3.4.2.1	Potentiometric data and analysis	57
3.4.2.2	Enthalpimetric data and analysis	60
3.5	Complexation with citrate	62
3.5.1	Molybdenum(VI)-citrate system	62
3.5.1.1	Potentiometric data and analysis	62
3.5.1.2	Spectrophotometric data and analysis	64
3.5.1.3	Analysis of Differential Pulse Polarograms	68
3.5.1.4	Enthalpimetric data and analysis	75
3.5.2	Tungsten(VI)-citrate system	77
3.5.2.1	Potentiometric data and analysis	77
3.5.2.2	Enthalpimetric data and analysis	79
3.6	Complexation with tartrate	80
3.6.1	Molybdenum(VI)-tartrate system	80
3.6.1.1	Potentiometric data and analysis	80
3.6.1.2	Enthalpimetric data and analysis	83
3.6.2	Tungsten(VI)-tartrate system	85
3.6.2.1	Potentiometric data and analysis	85
3.6.2.2	Enthalpimetric data and analysis	88
3.7	Complexation with aspartate	90
3.7.1	Molybdenum(VI)-aspartate system	90
3.7.1.1	Potentiometric data and analysis	90
3.7.1.2	Spectrophotometric data and analysis	93
3.7.1.3	Enthalpimetric data and analysis	95
3.7.2	Tungsten(VI)-aspartate system	97
3.7.2.1	Potentiometric data and analysis	97
3.7.2.2	Enthalpimetric data and analysis	100
3.8	Complexation with nitrilotriacetate (nta)	104
3.8.1	Molybdenum(VI)-nta system	104
3.8.1.1	Potentiometric data and analysis	104
3.8.1.2	Spectrophotometric data and analysis	106
3.8.1.3	Enthalpimetric data and analysis	109
3.8.2	Tungsten(VI)-nta system	111
3.8.2.1	Potentiometric data and analysis	111
3.8.2.2	Enthalpimetric data and analysis	116

4. Discussion	120
4.1 Comparison of Mo(VI) and W(VI) complexation	120
4.2 Proposed structures for the complexes	134
4.3 Structure and Thermodynamic values	150
4.3.1 [1,2, <i>r</i>] complexes	150
4.3.2 [1,1, <i>r</i>] and [2,2, <i>r</i>] complexes	152
4.3.2.1 didentate chelation to one metal alone	152
4.3.2.2 tridentate chelation to one metal alone	155
4.3.2.3 monodentate chelation to two different metal centres	157
4.3.2.4 dimerization of monomeric octahedral Mo	159
4.3.3 [2,1, <i>r</i>] complexes	159
4.3.4 [4,2, <i>r</i>] complexes	162
4.3.5 [3,4, <i>r</i>] , [4,3, <i>r</i>], [4,4, <i>r</i>], [4,5, <i>r</i>] and [2,4,8] complexes	163
4.3.6 Protonations	165
4.3.7 Comparison of [1,2,2] and [1,1,2] complexes	166
4.3.8 Comparison of [2,1, <i>r</i>] and [2,2, <i>r</i>] complexes	170
4.4 Comparison with literature	172
4.4.1 Oxalate complexes	172
4.4.2 Lactate and mandelate complexes	172
4.4.3 Malate complexes	173
4.4.3.1 Previous NMR investigation (Mo-malate)	173
4.4.3.2 Previous polarimetric study (Mo-malate)	174
4.4.3.3 Previous NMR investigation(W-malate)	174
4.4.3.4 Previous polarimetric study (W-malate)	174
4.4.4 Citrate complexes	178
4.4.5 Tartrate complexes	179
4.4.6 Aspartate complexes	180
4.4.7 Nta complexes	181
5. Concluding remarks	182
Appendix 1 Summary of titrations (potentiometric, spectrophotometric and calorimetric)	187
Appendix 2 Distribution of the ligand species	195
Appendix 3 Structures previously determined	197
Appendix 4 Summary of thermodynamic values (calculated and proposed)	200
Appendix 5 Explanatory notes on <i>F</i> curves	206
References	208
Publications based on this work	212

List of tables

Table 2.1	Reagents used in the investigation	5
Table 2.2	Molybdenum(VI)-proton model for 25°C and 2°C used in calculations	13
Table 2.3	Tungsten(VI)-proton model used in calculations (25°C)	14
Table 2.4	General ligand-proton model	14
Table 2.5	Ligand-species used as "reactants" in this investigation	15
Table 2.6	Values for the ΔH° for the formation of molybdenum(VI) species	18
Table 2.7	Values for the ΔH° for the formation of tungsten(VI) species	18
Table 3.1.1	Molybdate(VI)-oxalate complexes identified and calculated $\log\beta$ and ΔG° values	22
Table 3.1.2	Calculated ΔH° and $T\Delta S^\circ$ values for the formation of some Mo(VI)-oxalate complexes	26
Table 3.1.3	Tungstate(VI)-oxalate complexes identified and calculated $\log\beta$ and ΔG° values	28
Table 3.1.4	Calculated ΔH° and $T\Delta S^\circ$ values for the formation of some W(VI)-oxalate complexes	32
Table 3.2.1	Molybdate(VI)-lactate complexes identified and calculated $\log\beta$ and ΔG° values	34
Table 3.2.2	Calculated ΔH° and $T\Delta S^\circ$ values for the formation of some Mo(VI)-lactate complexes	36
Table 3.2.3	Tungstate(VI)-lactate complexes identified and calculated $\log\beta$ and ΔG° values	38
Table 3.2.4	Calculated ΔH° and $T\Delta S^\circ$ values for the formation of some W(VI)-lactate complexes	39
Table 3.3.1	Molybdate(VI)-mandelate complexes identified and calculated $\log\beta$ and ΔG° values	41
Table 3.3.2	Calculated ΔH° and $T\Delta S^\circ$ values for the formation of some Mo(VI)-mandelate complexes	45
Table 3.3.3	Tungstate(VI)-mandelate complexes identified and calculated $\log\beta$ and ΔG° values	47
Table 3.3.4	Calculated ΔH° and $T\Delta S^\circ$ values for the formation of some W(VI)-mandelate complexes	48
Table 3.4.1	Molybdate(VI)-malate complexes identified and calculated $\log\beta$ and ΔG° values	50
Table 3.4.2	Calculated ΔH° and $T\Delta S^\circ$ values for the formation of some Mo(VI)-malate complexes	56
Table 3.4.3	Tungstate(VI)-malate complexes identified and calculated $\log\beta$ and ΔG° values	58
Table 3.4.4	Calculated ΔH° and $T\Delta S^\circ$ values for the formation of some W(VI)-malate complexes	61
Table 3.5.1	Molybdate(VI)-citrate complexes identified and calculated $\log\beta$ and ΔG° values	63
Table 3.5.2	Concentrations of Mo(VI) and citrate, the pH and temperature of different solutions investigated by differential pulse polarography	68
Table 3.5.3	Calculated ΔH° and $T\Delta S^\circ$ values for the formation of some Mo(VI)-citrate complexes	76

Table 3.5.4	Tungstate(VI)-citrate complexes identified and calculated $\log\beta$ and ΔG° values	78
Table 3.5.5	Calculated ΔH° and $T\Delta S^\circ$ values for the formation of some W(VI)-citrate complexes	79
Table 3.6.1	Molybdate(VI)-tartrate complexes identified and calculated $\log\beta$ and ΔG° values	81
Table 3.6.2	Calculated ΔH° and $T\Delta S^\circ$ values for the formation of some Mo(VI)-tartrate complexes	84
Table 3.6.3	Tungstate(VI)-tartrate complexes identified and calculated $\log\beta$ and ΔG° values	86
Table 3.6.4	Calculated ΔH° and $T\Delta S^\circ$ values for the formation of some W(VI)-tartrate complexes	89
Table 3.7.1	Molybdate(VI)-aspartate complexes identified and calculated $\log\beta$ and ΔG° values	92
Table 3.7.2	Results of some model test with SUPERQUAD. Improvement in fit indicated by decreasing σ value (X : species rejected in a particular model-testing)	92
Table 3.7.3	Calculated ΔH° and $T\Delta S^\circ$ values for the formation of some Mo(VI)-aspartate complexes	96
Table 3.7.4	Tungstate(VI)-aspartate complexes identified and calculated $\log\beta$ and ΔG° values	98
Table 3.7.5	Calculated ΔH° and $T\Delta S^\circ$ values for the formation of some W(VI)-aspartate complexes	103
Table 3.8.1	Molybdate(VI)-nta complexes identified and calculated $\log\beta$ and ΔG° values	105
Table 3.8.2	Calculated ΔH° and $T\Delta S^\circ$ values for the formation of some Mo(VI)-nta complexes	110
Table 3.8.3	Tungstate(VI)-nta complexes identified in the system 1 day after preparation of the solutions, and calculated $\log\beta$ and ΔG° values	113
Table 3.8.4	Different calculations of ΔH° and $T\Delta S^\circ$ values for the formation of some W(VI)-nta complexes using the non-equilibrium model	118
Table 3.8.5	Calculated ΔH° and $T\Delta S^\circ$ values for the formation of some W(VI)-nta complexes (Approximate values based on non-equilibrium model)	119
Table 3.8.6	Proposed ΔH° and $T\Delta S^\circ$ values for the formation of some W(VI)-nta complexes at equilibrium	119
Table 4.1	Summary of all the complexes identified in all the complex systems investigated	124
Table 4.2.1	Proposed structures of the [1,2,r] complexes	135
Table 4.2.2	Proposed structures of the [1,1,r] complexes	137
Table 4.2.3	Proposed structures of the [2,2,r] complexes	139
Table 4.2.4	Proposed structures of the [2,1,r] complexes	142
Table 4.2.5	Proposed structures of the [4,2,r] complexes	146
Table 4.2.6	Proposed structures of the [4,4,r] complexes	147
Table 4.2.7	Proposed structures of the [2,4asp,r] , [3,4tart,r], [4,3tart,r] and [4,5tart,r] complexes	149

List of figures

Fig. 2.1	A schematic representation of the experimental set-up for potentiometric titrations	7
<u>Molybdate(VI)-oxalate</u>		
Fig. 3.1.1	Function F versus pH_c for some representative potentiometric titrations of the molybdate(VI)-oxalate system.	21
Fig. 3.1.2	Concentration of molybdate-oxalate complexes, expressed as a percentage of the total molybdenum(VI) concentration, as a function of pH_c . The total concentrations of molybdate(VI) and oxalate are both 0.01 M.	24
Fig. 3.1.3	Concentration of molybdate-oxalate complexes, expressed as a percentage of the total molybdenum(VI) concentration, as a function of pH_c . The total concentrations of molybdate(VI) and oxalate are 0.005 M and 0.05 M, respectively.	24
Fig. 3.1.4	Measured heat, Q , as a function of the molar ratio of acid to molybdate(VI) for a titration of 0.05 M molybdate(VI) and 0.05 M oxalate.	25
Fig. 3.1.5	Concentration of molybdate(VI)-oxalate complexes, expressed as a percentage of the total molybdenum(VI) concentration, as a function of the molar ratio of acid to molybdate(VI) for a titration of 0.05 M molybdate(VI) and 0.05 M oxalate.	26
<u>Tungstate(VI)-oxalate</u>		
Fig. 3.1.6.	Function F versus pH_c for some representative potentiometric titrations of the tungstate(VI)-oxalate system.	27
Fig. 3.1.7	Concentration of tungstate(VI)-oxalate complexes and uncomplexed polytungstates, expressed as a percentage of the total tungsten(VI) concentration, as a function of pH_c . The total concentrations of tungstate(VI) and oxalate are 0.01 M and 0.025 M, respectively.	29
Fig. 3.1.8	Concentration of tungstate(VI)-oxalate complexes and uncomplexed polytungstates, expressed as a percentage of the total tungsten(VI) concentration, as a function of pH_c . The total concentrations of tungstate(VI) and oxalate are both 0.005 M.	29
Fig. 3.1.9	Measured heat, Q , as a function of the molar ratio of acid to tungstate(VI) for a titration of 0.01 M tungstate(VI) and 0.025 M oxalate.	30
<u>Molybdate(VI)-lactate</u>		
Fig. 3.2.1.	Function F versus pH_c for some representative potentiometric titrations of the molybdate(VI)-lactate system.	33
Fig. 3.2.2	Concentration of molybdate(VI)-lactate complexes, expressed as a percentage of the total molybdenum(VI) concentration, as a function of pH_c . The total concentrations of molybdate(VI) and lactate are 0.05 M and 0.1 M, respectively.	35

- Fig. 3.2.3** Measured heat, Q , as a function of the molar ratio of acid to molybdate(VI) for a titration of 0.01 M molybdate(VI) and 0.05 M lactate. (A similar titration of tungstate(VI) and lactate is also shown for comparison.) 36

Tungstate(VI)-lactate

- Fig.3.2.4** Function F versus pH_c for some representative potentiometric titrations of the tungstate(VI)-lactate system. 37
- Fig. 3.2.5** Concentration of tungstate(VI)-lactate complexes, expressed as a percentage of the total tungsten(VI) concentration, as a function of pH_c . The total concentrations of tungstate(VI) and lactate are 0.001 M and 0.003 M, respectively. 38
- Fig. 3.2.6** Measured heat, Q , as a function of the molar ratio of acid to tungstate(VI) for a titration of 0.01 M tungstate(VI) and 0.0497 M lactate. (A similar titration of molybdate(VI) and lactate is also shown for comparison.) 39

Molybdate(VI)-mandelate

- Fig 3.3.1** Function F versus pH_c for some representative potentiometric titrations of the molybdate(VI)-mandelate system. 40
- Fig. 3.3.2** Concentration of molybdate(VI)-mandelate complexes, expressed as a percentage of the total molybdenum(VI) concentration, as a function of pH_c . The total concentrations of molybdate(VI) and mandelate are 0.05 M and 0.1 M, respectively. 41
- Fig. 3.3.3.1** Change in absorption spectra with pH_c ranging from 4.7 to 2.1. The total mandelate concentration is 0.0008 M. 42
- Fig. 3.3.3.2** Change in absorption spectra with pH_c ranging from 6.0 to 3.4. The total molybdate(VI) and mandelate concentrations are 0.0002 M and 0.001 M, respectively. 42
- Fig. 3.3.4** Calculated molar absorption spectra of mandelic acid and mandelate. 43
- Fig. 3.3.5** Calculated molar absorption spectra of various species of the molybdenum(VI)-mandelate system. 44
- Fig. 3.3.6** Measured heat, Q , as a function of the molar ratio of acid to molybdate(VI) for a titration of 0.02 M molybdate(VI) and 0.1 M mandelate. (A similar titration of tungstate(VI) and mandelate is also shown for comparison). 45

Tungstate(VI)-mandelate

- Fig. 3.3.7** Function F versus pH_c for some representative potentiometric titrations of the tungstate(VI)-mandelate system. 46
- Fig. 3.3.8** Concentration of tungstate(VI)-mandelate complexes, expressed as a percentage of the total tungsten(VI) concentration, as a function of pH_c . The total concentrations of tungstate(VI) and mandelate are 0.001 M and 0.003 M, respectively. 47

- Fig. 3.3.9** Measured heat, Q , as a function of the molar ratio of acid to tungstate(VI) for a titration of 0.02 M tungstate(VI) and 0.1 M mandelate. 48
- Molybdate(VI)-malate**
- Fig. 3.4.1** Function F versus pH_c for some representative potentiometric titrations of the molybdate(VI)-malate system. 49
- Fig. 3.4.2** Concentration of molybdate(VI)-malate complexes, expressed as a percentage of the total molybdenum(VI) concentration, as a function of pH_c . The total concentrations of molybdate(VI) and malate are 0.05 M and 0.2 M, respectively. 51
- Fig. 3.4.3** Concentration of molybdate(VI)-malate complexes, expressed as a percentage of the total molybdenum(VI) concentration, as a function of pH_c . The total concentrations of molybdate(VI) and malate are both 0.05 M. 51
- Fig. 3.4.4.1** Change in absorption spectra with pH_c ranging from 5.7 to 1.7. The total malate concentration is 0.0016 M. 52
- Fig. 3.4.4.2** Change in absorption spectra with pH_c ranging from 5.6 to 1.6. The total molybdate(VI) and malate concentrations are both 0.0001 M. 52
- Fig. 3.4.5.** Calculated molar absorption spectra of malate and its protonated forms. 53
- Fig. 3.4.6** Calculated molar absorption spectra of various species in the molybdate(VI)-malate system. 54
- Fig. 3.4.7** Measured heat, Q , as a function of the molar ratio of acid to molybdate(VI) for the four titrations used. (Concentrations of molybdate(VI) and malate shown on graph). 54
- Fig. 3.4.8** Concentration of molybdate(VI)-malate complexes, expressed as a percentage of the total molybdenum(VI) concentration, as a function of the molar ratio of acid to molybdate(VI) for a titration of 0.03 M molybdate(VI) and 0.05 M malate. 55
- Fig. 3.4.9** Concentration of molybdate(VI)-malate complexes, expressed as a percentage of the total molybdenum(VI) concentration, as a function of the molar ratio of acid to molybdate(VI) for a titration of 0.03 M molybdate(VI) and 0.03 M malate. 56
- Tungstate(VI)-malate**
- Fig. 3.4.10** Function F versus pH_c for some representative potentiometric titrations of the tungstate(VI)-malate system. 57
- Fig. 3.4.11** Concentration of tungstate(VI)-malate complexes, expressed as a percentage of the total tungsten(VI) concentration, as a function of pH_c . The total concentrations of tungstate(VI) and malate are 0.02 M and 0.15 M, respectively. 58
- Fig. 3.4.12** Concentration of tungstate(VI)-malate complexes, expressed as a percentage of the total tungsten(VI) concentration, as a function of pH_c . The total concentrations of tungstate(VI) and malate are 0.02 M and 0.04 M, respectively. 59

- Fig. 3.4.13** Measured heat, Q , as a function of the molar ratio of acid to tungstate(VI) for a the two titrations used. (Concentrations of tungstate(VI) and malate shown on graph.) 60
- Molybdate(VI)-citrate**
- Fig. 3.5.1** Function F versus pH_c for some representative potentiometric titrations of the molybdate(VI)-citrate system. 62
- Fig. 3.5.2** Concentration of molybdate(VI)-citrate complexes, expressed as a percentage of the total molybdenum(VI) concentration, as a function of pH_c . The total concentrations of molybdate(VI) and citrate are both 0.04 M. 64
- Fig. 3.5.3.1** Change in absorption spectra with pH_c ranging from 6.0 to 1.4. The total citrate concentration is 0.0016 M. 64
- Fig. 3.5.3.2** Change in absorption spectra with pH_c ranging from 5.6 to 1.0. Total molybdate(VI) and citrate concentration are 0.0001 M and 0.00012 M, respectively. 65
- Fig. 3.5.4.** Calculated molar absorption spectra of citrate and its protonated forms. 66
- Fig. 3.5.5** Concentration of molybdate(VI)-citrate complexes, expressed as a percentage of the total molybdenum(VI) concentration, as a function of pH_c . Concentration of citrate species, expressed as a percentage of the total citrate concentration, as a function of pH_c . The total concentrations of molybdate(VI) and citrate are 0.0001 M and 0.00012 M, respectively. 66
- Fig. 3.5.6** Calculated molar absorption spectra of various species in the molybdate(VI)-citrate system 67
- Fig. 3.5.7** Differential pulse polarograms of the solutions, A ([Mo(VI)]=0.001 M, [cit]=0.1 M, pH=8.9) and B ([Mo(VI)]=0.001 M, [cit]=0.1 M, pH=7.2). 69
- Fig. 3.5.8** Peak currents ($E=-1.78 \text{ V}$) obtained from differential pulse polarograms at various pH_c values for an equimolar solution of molybdate(VI) and citrate (0.00400 M) compared with the percentage of the monomeric complexes. 70
- Fig. 3.5.9** Differential pulse polarograms of equimolar solutions of molybdate(VI) and citrate (0.00400 M) at $\text{pH}_c = 4.7, 5.7$ and 6.7 , respectively. 71
- Fig. 3.5.10** Concentration of molybdate(VI)-citrate complexes, expressed as a percentage of the total molybdenum(VI) concentration, as a function of pH_c . The total concentrations of molybdate(VI) and citrate are both 0.00400 M. 71
- Fig. 3.5.11** Differential pulse polarograms of the solutions, D ([Mo(VI)]=0.004 M, [cit]=0.004 M, pH=5.7) and E ([Mo(VI)]=0.008 M, [cit]=0.008 M, pH=5.7). 72
- Fig. 3.5.12** Differential pulse polarograms of the solution F ([Mo(VI)]=0.001 M, [cit]=0.4 M, pH=1.4). 73
- Fig. 3.5.13** Differential pulse polarograms of the solutions, J ([Mo(VI)]=0.004 M, [cit]=0.002 M, pH=3) and H ([Mo(VI)]=0.004 M, [cit]=0.004 M, pH=3). 74
- Fig. 3.5.14** Differential pulse polarograms of the solutions, K ([Mo(VI)]=0.004 M, [cit]=0.002 M, pH=3.7) and L ([Mo(VI)]=0.004 M, [cit]=0.004 M, pH=3.7). 74

- Fig. 3.5.15** Measured heat, Q , as a function of the molar ratio of acid to molybdate(VI) for two titrations. (Concentrations of molybdate(VI) and citrate shown on graph.) 75
- Tungstate(VI)-citrate**
- Fig. 3.5.16** Function F versus pH_c for some representative potentiometric titrations of the tungstate(VI)-citrate system. 77
- Fig. 3.5.17** Concentration of tungstate(VI)-citrate complexes, expressed as a percentage of the total tungsten(VI) concentration, as a function of pH_c . The total concentrations of tungstate(VI) and citrate are 0.05 M and 0.075 M, respectively. 78
- Fig. 3.5.18** Measured heat, Q , as a function of the molar ratio of acid to tungstate(VI) for two titrations. (Concentrations of tungstate(VI) and citrate are shown on the graph.) 79
- Molybdate(VI)-tartrate**
- Fig. 3.6.1** Function F versus pH_c for some representative potentiometric titrations of the molybdate(VI)-tartrate system. 80
- Fig. 3.6.2** Concentration of molybdate(VI)-tartrate complexes, expressed as a percentage of the total molybdenum(VI) concentration, as a function of pH_c . The total concentrations of molybdate(VI) and tartrate are both 0.05 M. 82
- Fig. 3.6.3** Concentration of molybdate(VI)-tartrate complexes, expressed as a percentage of the total molybdenum(VI) concentration, as a function of pH_c . The total concentrations of molybdate(VI) and tartrate are 0.025 M and 0.05 M, respectively. 83
- Fig. 3.6.4** Measured heat, Q , as a function of the molar ratio of acid to molybdate(VI) for two titrations. (Concentrations of tungstate(VI) and tartrate are shown on the graph.) 83
- Tungstate(VI)-tartrate**
- Fig. 3.6.5** Function F versus pH_c for some representative potentiometric titrations of the tungstate(VI)-tartrate system. 85
- Fig. 3.6.6** Concentration of tungstate(VI)-tartrate complexes, expressed as a percentage of the total tungsten(VI) concentration, as a function of pH_c . The total concentrations of tungstate(VI) and tartrate are 0.02 M and 0.04 M, respectively. 87
- Fig. 3.6.7** Concentration of tungstate(VI)-tartrate complexes, expressed as a percentage of the total tungsten(VI) concentration, as a function of pH_c . The total concentrations of tungstate(VI) and tartrate are both 0.01 M. 87
- Fig. 3.6.8** Measured heat, Q , as a function of the molar ratio of acid to tungstate(VI) for two titrations. (Concentrations of tungstate(VI) and tartrate are shown on the graph.) 88
- Molybdate(VI)-aspartate**
- Fig. 3.7.1** Function F versus pH_c for some representative potentiometric titrations of the molybdate(VI)-aspartate system. 90

- Fig. 3.7.2** Concentration of molybdate(VI)-aspartate complexes, expressed as a percentage of the total molybdenum(VI) concentration, as a function of pH_c . The total concentrations of molybdate(VI) and aspartate are 0.005 M and 0.1 M, respectively. 93
- Fig. 3.7.3** Change in absorption spectra with pH_c from 6.9 to 2.3. The total concentrations of molybdate(VI) and aspartate are 0.005 M and 0.1 M, respectively. 93
- Fig. 3.7.4** Measured heat, Q , as a function of the pH_c for a titration of 0.01 M molybdate(VI) and 0.1 M aspartate. 95
- Fig. 3.7.5** Function F versus pH_c for some representative potentiometric titrations of the tungstate(VI)-aspartate system. 97
- Fig. 3.7.6** Concentration of tungstate(VI)-aspartate complexes and uncomplexed tungstate(VI) species, expressed as a percentage of the total tungsten(VI) concentration, as a function of pH_c . The total concentrations of tungstate(VI) and aspartate are 0.01 M and 0.02 M, respectively. 99
- Fig. 3.7.7** Measured heat, Q , as a function of the volume of titrant added for a titration of 0.01 M tungstate(VI) and 0.02 M aspartate. 100
- Fig. 3.7.8.** Concentration of uncomplexed tungstate(VI) species and tungstate(VI)-aspartate complexes, expressed as a fraction of the total tungsten(VI) concentration, as a function of volume HCl added to 25 ml of solution with total concentrations of tungstate(VI) and aspartate are 0.01 M and 0.02 M, respectively. 102
- Molybdate(VI)-nitrilotriacetate**
- Fig. 3.8.1** Function F versus pH_c for some representative potentiometric titrations of the molybdate(VI)-nta system. 104
- Fig. 3.8.2** Concentration of molybdate(VI)-nta complexes, expressed as a percentage of the total molybdenum(VI) concentration, as a function of pH_c . The total concentrations of molybdate(VI) and nta are both 0.05 M. 105
- Fig. 3.8.3** Concentration of molybdate(VI)-nta complexes, expressed as a percentage of the total molybdenum(VI) concentration, as a function of pH_c . The total concentrations of molybdate(VI) and nta are 0.0002 M and 0.00025 M, respectively. 106
- Fig. 3.8.4.1** Change in absorption spectra with pH_c ranging from 5.1 to 1.3. The total nta concentration is 0.00025 M. 106
- Fig. 3.8.4.2** Change in absorption spectra with pH_c ranging from 5.7 to 2.7. The total concentrations of molybdate(VI) and nta are 0.0002 M and 0.00025 M, respectively. 107
- Fig. 3.8.5** Calculated molar absorption spectra of two nta species, of molybdate(VI) and of two molybdate(VI)-nta complexes. 108
- Fig. 3.8.6.** Measured heat, Q , as a function of the molar ratio of acid to molybdate(VI) for a titration of 0.01 M molybdate(VI) and 0.01 M nta. 109

Tungstate(VI)-nitrilotriacetate

- Fig. 3.8.7** Function F versus pH_c for some representative standard potentiometric titrations of the tungstate(VI)-nta system. 111
- Fig. 3.8.8** Function F versus pH_c for some representative potentiometric point titrations of the tungstate(VI)-nta system. 111
- Fig. 3.8.9** Function F versus pH_c for the standard titration and the point titration of one particular solution. ($[\text{W(VI)}] = 0.0025 \text{ M}$, $[\text{nta}] = 0.025 \text{ M}$) 112
- Fig. 3.8.10** Concentration of tungstate(VI)-nta complexes at equilibrium, expressed as a percentage of the total tungsten(VI) concentration, as a function of pH_c . The total concentrations of tungstate(VI) and nta are 0.01 M and 0.1 M, respectively. 114
- Fig. 3.8.11** Concentration of tungstate(VI)-nta complexes *before equilibrium*, expressed as a percentage of the total tungsten(VI) concentration, as a function of titrant volume added to a 25 ml solution, with the total concentrations of tungstate(VI) and nta 0.01 M and 0.1 M, respectively. 115
- Fig. 3.8.12** Concentration of tungstate(VI)-nta complexes *at equilibrium*, expressed as a percentage of the total tungsten(VI) concentration, as a function of titrant volume added to a 25 ml solution, with the total concentrations of tungstate(VI) and nta 0.01 M and 0.1 M, respectively. 116
- Fig. 3.8.13** Measured heat, Q , as a function of the volume of titrant added to 25 ml of a solution of 0.01 M tungstate(VI) and 0.1 M nta. 116
- Fig. 4.1.1** The ΔG° (per metal) for the formation of Mo(VI) and W(VI) $[1,2,r]$ complexes. 125
- Fig. 4.1.2** The ΔG° (per metal) for the formation of Mo(VI) and W(VI) $[1,1,r]$ complexes. 125
- Fig. 4.1.3** The ΔG° (per metal) for the formation of Mo(VI) and W(VI) $[2,2,r]$ complexes. 126
- Fig. 4.1.4** The ΔG° (per metal) for the formation of Mo(VI) and W(VI) $[2,1,r]$ complexes. 126
- Fig. 4.1.5** The ΔG° (per metal) for the formation of Mo(VI) and W(VI) $[4,q,r]$, $[3,4,r]$ and $[2,4,r]$ complexes. 127
- Fig. 4.2.1** Comparison of $\Delta G^\circ/\text{Mo}$ and $\Delta H^\circ/\text{Mo}$ for the $[1,2,r]$ molybdate(VI) complexes. 127
- Fig. 4.2.2** Comparison of $\Delta G^\circ/\text{Mo}$ and $\Delta H^\circ/\text{Mo}$ for the $[1,1,r]$ molybdate(VI) complexes. 128
- Fig. 4.2.3** Comparison of $\Delta G^\circ/\text{Mo}$ and $\Delta H^\circ/\text{Mo}$ for the $[2,2,r]$ molybdate(VI) complexes. 128
- Fig. 4.2.4** Comparison of $\Delta G^\circ/\text{Mo}$ and $\Delta H^\circ/\text{Mo}$ for the $[2,1,r]$ molybdate(VI) complexes. 129
- Fig. 4.2.5** Comparison of $\Delta G^\circ/\text{Mo}$ and $\Delta H^\circ/\text{Mo}$ for the $[4,q,r]$, $[3,4,r]$, $[2,4,r]$ molybdate(VI) complexes. 129

Fig. 4.3.	The difference in the values of ΔG° , ΔH° and $T\Delta S^\circ$ (per metal) for the formation of tungstate(VI) and molybdate(VI) complexes of the same stoichiometry $[p,q,r]$.	130
Fig. 4.4.1	The ΔG° , ΔH° and $T\Delta S^\circ$ values for the protonation of the ligands and the $[1,1,r]$ and $[4,q,r]$ complexes.	131
Fig. 4.4.2	The ΔG° , ΔH° and $T\Delta S^\circ$ values for the protonation of the $[1,2,r]$, $[2,2,r]$ and $[2,1,r]$ complexes.	132
Fig. 4.5	The ΔG° , ΔH° and $T\Delta S^\circ$ values for the dimerization of some complexes.	133
Fig. 4.6	Proposed structures for the $[1,2,r]$ complexes.	136
Fig. 4.7	Proposed structures for the $[1,1,r]$ complexes.	138
Fig. 4.8.1	Proposed structures for the $[2,2,r]$ complexes.	140
Fig. 4.8.2	Proposed structures for the $[2,2,r]$ complexes.	141
Fig. 4.9.1.1	Proposed structures for the $[2,1,r]$ complexes	143
Fig. 4.9.1.2	Relationship between proposed structures for $[2,1,r]$ complexes of type A (Fig. 4.9.1) and the proposed structures for $[2,2,r]$ complexes of type B (Fig. 4.8.1).	143
Fig. 4.9.2	Proposed structures for didentate(A) and tridentate $[2,1,r]$ complexes of malate, citrate, aspartate and nta.	144
Fig. 4.9.3	Proposed structures for $[2,1,r]$ complexes of tartrate.	145
Fig. 4.10	Proposed structures for the $[4,2,r]$ complexes.	146
Fig. 4.11.1	Proposed structures for the $[4,4,r]$ tartrate and oxalate complexes.	148
Fig. 4.11.2	Proposed ring or chain structures for the $[4,4,r]$ citrate, malate and aspartate complexes.	148
Fig. 4.12	Proposed structure for the $[2,4,r]$ aspartate complex.	149
Fig. 4.13	Proposed structures for some polymeric $[3,4,r]$, $[4,3,r]$ and $[4,5,r]$ tartrate complexes.	149
Fig. 4.14	Possible relationship between $[1,1man,1]$, $[1,1man,2]$, $[1,2man,1]$ and $[1,2man,2]$.	153
Fig. 4.15	Thermodynamic values for the addition of a ligand to $[1,1,r]$ complexes.	168
Fig. 4.16	Thermodynamic values for the addition of a ligand to $[2,1,r]$ complexes.	170

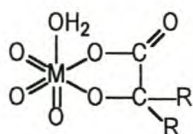
- Fig. 4.17.1** Distribution of molybdate(VI)-malate complexes at pH=5 as a function of the fraction of total malate concentration to the total concentration of complexing species (Mo+mal), which equals 1 M. 175
- Fig. 4.17.2** Distribution of molybdate(VI)-malate complexes at pH=5.5 as a function of the fraction of total malate concentration to the total concentration of complexing species (Mo+mal), which equals 1 M. 175
- Fig. 4.18.1** Distribution of molybdate(VI)-malate complexes at pH=4 and for [Mo(VI)]=0.005 M, expressed as a percentage of the total molybdenum(VI) concentration as a function of [mal]/[molybdate]. 176
- Fig. 4.18.2** Distribution of molybdate(VI)-malate complexes at pH=3 and for [Mo(VI)]=0.005 M, expressed as a percentage of the total molybdenum(VI) concentration as a function of [mal]/[molybdate]. 176
- Fig. 4.19** Concentration of tungstate(VI)-malate complexes at pH 5.5, 4.3, 3.0, expressed as a percentage of the total malate concentration, as a function of the fraction of total malate concentration to the total concentration of complexing species (W+mal), which equals 1M. 177
- Fig. 4.20** Concentration of tungstate(VI)-malate complexes, expressed as a percentage of the total molybdenum(VI) concentration, as a function of pH_e. The total concentrations of tungstate(VI) and malate are 0.01 M and 0.25 M, respectively. 177
- Appendix 2** Distribution of the ligand species. 195

Chapter 1

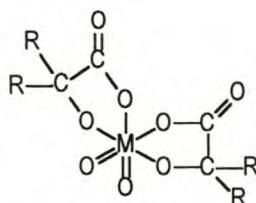
Introduction

The chemistry in aqueous solutions is important as water is the principle medium for living systems and in the soil. The knowledge of metal complexation in aqueous solution is important in understanding the transport and function of metals, for instance, the working of enzymes with active metal sites. Chelation is achieved by a host of ligands available in soil solutions as well as in plant or animal cell solutions and depends on the ligands present, competing metals, the formation constants of complexes, relative concentration of the reactants and the pH.

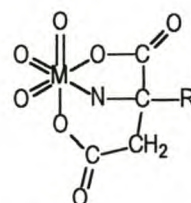
The Group 6 transition metals, molybdenum and tungsten, are important trace elements in living organisms, but relatively little is known about the processes in which they are involved [1]. Various investigations were previously undertaken to identify the complexes of these metals with specific ligands in aqueous medium [2-105], but the experimental conditions (pH or concentration of metal ion and ligand) were usually rather limited in order to simplify the systems. The results, even if correct, cannot necessarily be extrapolated to other conditions. On the other hand, studies undertaken under a broader range of conditions were often flawed to some extent as the plethora of uncomplexed molybdenum(VI) or tungsten(VI) species present in the system was ignored or misrepresented. Because of these difficulties, the results of previous studies are often inconsistent regarding the identity of the complexes and only very few formation constants and hardly any values for the change in enthalpy and entropy associated with the complex formation are known. Relatively little success has been achieved in attempts to isolate molybdate(VI)-ligand and tungstate(VI)-ligand crystals as polymerization often takes place upon evaporation, but a few crystalline structures of molybdate(VI) or tungstate(VI) complexes with the ligands used in this investigation have been determined by X-ray crystallographic analysis [75-90]. Knowledge of a crystal structure of a complex, however, is no proof that the complex exists in solution, or that it has the same structure as in a solid crystal lattice, since different energies come into play during crystallization of a complex from a solution, for example the heat of crystallization. Some studies have shown that the structures of complexes in solids may be essentially the same as in solution [102,92,106]. Structural trends have been established for some simple complexes: Whereas the reactants, molybdate (MoO_4^{2-}) and tungstate (WO_4^{2-}) have tetrahedral conformations, the complexes of molybdate(VI) and tungstate(VI) typically have octahedral structures as shown below. The ligands often bind didentate or tridentate to a MO_2 or MO_3 centre ($\text{M} = \text{Mo}, \text{W}$). Water molecules or OH groups may bind to these centres, where needed, in order to achieve octahedral conformation [108-110].



MO_3 centre,
five membered ring



MO_2 centre,
two five membered rings



MO_3 centre,
five and six membered rings

The aim of this investigation is to study the complex formation of Mo(VI) and W(VI) with some relatively simple and common organic ligands, lactate, mandelate, malate, citrate, tartrate, oxalate, nitrilotriacetic acid and aspartate, over a wide pH range in a 1 M NaCl medium at 25°C in order to identify the complexes and to gather quantitative thermodynamic values which would be useful as a model for further investigations of even more complex systems. Computer analysis of reliable potentiometric data has proved to be a powerful technique in identifying complexes in complicated aqueous systems and for calculating their formation constants, based on the known relationship between the formation constant and the concentration of the reactants and products at any given point during the titration (Eq. 2.3, Section. 2.6.1). This method is, therefore, chosen to model the molybdate(VI) and tungstate(VI) complexation during this investigation (*cf.* Section 2.2 and 2.6.1). The protonation and polymerization equilibria of uncomplexed molybdate(VI) or tungstate(VI) in the complex system are represented by good models of the molybdate(VI)-proton and tungstate(VI)-proton systems, which have been developed in the last years (*cf.* Section 2.6.1.1). Models for the protonation of the different (uncomplexed) ligands are refined in this investigation (*cf.* Section 2.6.1.2).

Computer analysis of good spectrophotometric data has also proved to be useful in characterizing species present in solution, to calculate their formation constants and their molar absorption spectra (*cf.* Section 2.3 and 2.6.2). However, because fewer experimental conditions are suitable for these complicated systems (compared to potentiometric investigations) the identification of only a few species is possible. (Owing to the very small part of the UV spectrum of tungstate(VI) that is available for absorption measurements, a similar spectrophotometric study of tungsten(VI)-ligand complex formation is not feasible). If the spectrophotometrically determined formation constants of these few species are similar to the constants determined by potentiometry (under different experimental conditions) it is regarded as confirmation of the potentiometric model as a whole.

The modelling of these systems is followed by enthalpimetric analysis in order to obtain the values for the change of enthalpy for the formation of the complexes identified (*cf.* Section 2.4 and 2.6.3). This analysis is based on the fact that the heat produced in a complexation reaction is the sum of the heat produced by all the species present at any point in the titration. The known relationship between the formation constant and the change in free energy (Eq. 2.4, Section. 2.6.1.1) enables the calculation of the free energy associated with the formation of all the identified species. The change in entropy associated with the formation of the complexes can be obtained using the known relationship between the change in enthalpy and entropy (Eq. 2.5, Section 2.6.1.1) and the calculated ΔH° and ΔG° values. These thermodynamic values are used to identify the main driving force for complex formation in the systems investigated and can be very useful in discriminating between various possible structures.

Although analysis of accurate potentiometric data produces models for the complex systems, it is desirable to gather other evidence in support of the existence of these calculated species, especially in cases where the model comprises a variety of complexes. A known polarographic method for the determination of molybdenum(VI) is based on the reduction of a molybdate(VI)-citrate complex (*cf.* Section 2.5). Since it can be assumed that complexes with different structures will show different redox behaviour an investigation by differential pulse polarography (DPP) can be expected to provide some independent evidence in support of the proposed reaction model. However, since molybdenum(VI) can be reduced to various lower oxidation

states as well as mixed-valence species, it is expected that the polarograms of already complicated complex systems might be difficult to analyze. It is attempted in one of the systems (Mo-citrate) to correlate the appearance and height of the reduction peaks in every polarogram with the complexes predicted by the potentiometric model (*cf.* 2.5).

The common feature of the ligands chosen for this investigation is the presence of at least one carboxylic acid group and at least one further oxygen or nitrogen donor on the α -carbon.

oxalic acid	HOOC-COOH	dicarboxylic acid
lactic acid	CH₃-CH(OH)-COOH	α -hydroxy-carboxylic acid
mandelic acid	Ph-CH(OH)-COOH	α -hydroxy-carboxylic acid
malic acid	HOOC-CH₂-CH(OH)-COOH	α -hydroxy-carboxylic acid
citric acid	(HOOC-CH₂)₂-C(OH)-COOH	α -hydroxy-carboxylic acid
tartaric acid	HOOC-CH(OH)-C(OH)-COOH	α -hydroxy-carboxylic acid
aspartic acid	⁻OOC-CH₂-CH(N(+)₃)-COOH	amino acid
nitrilotriacetic acid	N(CH₂-COOH)₃	amino acid

Five of these ligands, namely lactic, mandelic, malic, citric and tartaric acid are relatively simple α -hydroxycarboxylic acids. It has been established that α -hydroxycarboxylic acids usually bind didentate to molybdenum(VI) and tungsten(VI), forming a thermodynamically stable five-membered chelate ring via the hydroxylic and carboxylic oxygens, especially if the ligands contain no other carboxy or hydroxy groups, as in the case of lactic and mandelic acid. It has furthermore been established that the metal:ligand ratio of such molybdenum(VI) or tungsten(VI) complexes is often 1:2, the two ligands adopting *cis* arrangement around the MO₂ core [107-110]. The α -hydroxycarboxylic acids which contain further hydroxy or carboxy groups (malic and citric acid) may also bind tridentate by using the additional oxygen donors to form further metal-ligand bonds; a β -carboxylate, for example, might be involved in the formation of an additional stable six-membered chelate ring. The extra oxygen donors can also be used in the stabilization of dimeric complexes by binding didentate to one metal and monodentate to the other metal. Bridging of two metals can possibly be achieved via ligands such as tartrate which could bind didentate to two otherwise separate metal centres due to its two, chemically equivalent, vicinal α -hydroxycarboxylic groups. The variety of coordination possibilities is clearly considerable. Many types of complexes must, therefore, be considered in the search of a model which would fully describe each molybdenum(VI)- and tungsten(VI)-ligand system over as wide a pH range as possible.

For oxalic acid (the simplest dicarboxylic acid occurring naturally) the mode of chelation via the two vicinal carboxylate groups can be compared with that of the vicinal C-OH and COOH groups in the α -hydroxycarboxylic acids. The stronger bound hydroxy-proton of the latter ligands, compared to the carboxylate proton of the oxalic acid, is bound to influence the thermodynamics of complexation.

Aspartic acid, one of the important naturally occurring amino acids, was chosen as another ligand in this investigation as its similarity to the α -hydroxycarboxylic acid, malic acid, would lead to interesting comparisons in their chelating modes. (Malic acid and aspartic acid differ only in that the hydroxy group of malic acid is in the position of the amino group of aspartic acid). The different donating properties of N and O are expected to play a role in the stabilities of the respective complexes with molybdenum(VI) and tungsten(VI). (The similarity would be emphasized if the amino acid were to be called an α -amino-carboxylic acid.)

Since it was first synthesized by Heintz in 1862, nitrilotriacetic acid (nta) has become a widely used chelating agent in analytical and industrial chemistry (detergent, water softening, plant nutrition, pulp and paper manufacture, industrial and boiler cleaning) [69]. It is one of the simplest aminopolycarboxylic acids and has one central nitrogen donor to which three acetic acid groups are attached, thus rendering three additional carboxylic oxygen donors when fully deprotonated. All four donors are utilized in the complexation of some metal ions, forming three equivalent five-membered chelate rings. (Although, strictly speaking, nta is not a homologue of aspartic acid, the N donor of nta can also be regarded as an amino group on an α -carbon in relation to a carboxylic group as in the case of aspartic acid.) Nta was selected for this study of complexation with molybdenum(VI) and tungsten(VI) because of its general use as a chelating agent, but also because nta is seen as a possible pollutant and a carcinogenic suspect. Knowledge about the speciation and thermodynamic values for the formation of nta-complexes would be useful in narrowing the search for possible alternative chelating agents.

Chapter 2

Experimental and methods of analysis

2.1 REAGENTS, SOLUTIONS, STANDARDIZATIONS

All reagents were of analytical grade (Merck, BDH and Aldrich) and solutions were prepared with de-ionised water obtained from a Millipore Milli-Q system.

The percent error of all the concentrations mentioned in this thesis is less than 0.2%, even if all the significant digits are not shown in the text, captions or figures. For brevity the symbol, M, is used for mol dm⁻³ in the text.

Table 2.1 Reagents used in the investigation

Na ₂ MoO ₄ ·2H ₂ O	Merck	purified
Na ₂ WO ₄ ·2H ₂ O	Merck	purified
NaCl	Merck	purified/used as received
HCl	Merck	used as received
NaOH	Merck	purified
KHphthalate	Merck	used as received
Phenolphthalein	Merck	used as received
Methyl red	Merck	used as received
Bromophenol blue	Merck	used as received
TRIS	Merck	used as received
sodium oxalate	Merck	used as received
sodium lactate	Riedel de Haen	used as received
mandelic acid	Merck or BDH	used as received
DL-malic acid	Aldrich	used as received
sodium citrate	Aldrich	used as received
L-(+)-tartaric acid	Riedel-De Haën	purified
L-aspartic acid	BDH	used as received
Sodium nitrilotriacetate (nta)	Aldrich	used as received

All solutions were made 1 M with respect to chloride ions by addition of the appropriate amount of sodium chloride to ensure that a constant medium is maintained throughout the titrations.

A saturated solution of **NaCl** was allowed to stand for a week and then filtered. The filtrate was allowed to evaporate slowly at ca 25°C for several weeks. The recrystallized salt was used to prepare a stock solution which was standardized by evaporating known volumes to dryness and heating at 160°C to constant weight.

It was found that the alkalinity of the NaCl solution due to minor amounts of impurities persists even after recrystallization. Consequently NaCl was used directly from the source and the alkalinity determined (equivalent to $1.5 \cdot 10^{-5}$ M OH⁻) was included in calculations.

Sodium molybdate and sodium tungstate stock solutions were prepared from the recrystallized salts, $\text{Na}_2[\text{MoO}_4] \cdot 2\text{H}_2\text{O}$ and $\text{Na}_2[\text{WO}_4] \cdot 2\text{H}_2\text{O}$ and standardized. Accurately measured volumes of stock solution were pipetted into crucibles and evaporated at 80°C. The residue was heated for three hours at 160°C to ensure that the water of crystallization was completely expelled. The concentration of the original stock solution was calculated on the assumption that all the weighed crystals were anhydrous molybdate or tungstate.

Carbonate free sodium hydroxide solutions were prepared using filtered, supersaturated NaOH and were standardized against potassium hydrogenphthalate using methyl red as indicator.

Hydrochloric acid was standardized against TRIS, using bromophenol blue as indicator, or indirectly against potassium hydrogenphthalate by titration against a standardized sodium hydroxide solution.

Most ligands were used directly, without purification, but the purity of the ligands was verified by refinement of the concentration of the ligand during data analysis with SUPERQUAD (*cf.* 2.6.1.3). A **sodium oxalate** solution was standardized by titration with potassium permanganate solution. **Sodium lactate** was used as received; the concentration of the stock solution ($\approx 50\%$ w/w) was determined using the endpoint (not particularly sharp) given by automatic titration with hydrochloric acid, but could be verified by refinement during SUPERQUAD calculation (*cf.* 2.6.1.3). **Mandelic, malic and aspartic acid** were used as received but the purity of each acid was checked by a potentiometric titration with sodium hydroxide. Mandelate, malate and aspartate solutions were prepared by accurate neutralization of the respective acids. **Sodium citrate and sodium nitrilotriacetate** were used as received and standardized by potentiometry. **Tartaric acid** was recrystallized and dried in a vacuum oven. Solutions of tartaric acid were standardized by potentiometry. Tartrate solutions were prepared by accurate neutralization of the acid.

2.2 POTENTIOMETRY

Typically 70 - 90 ml of a ligand or metalate-ligand solution was titrated potentiometrically with hydrochloric acid or sodium hydroxide at 25°C using a Metrohm 636 Titroprocessor whenever the reaction rate was sufficient for automatic addition of titrant. For slower reactions this instrument was also used as a potentiometer, but the titrant additions were done manually (using a Metrohm Dosimat) only when the observed drift in the mV-reading had become insignificant. In some cases "point titrations" were carried out instead of continuous titrations in order to acquire equilibrium data. A point titration is a set of solutions

acidified to varying degrees which mimic a continuous titration. The pH of the different solutions is only measured after equilibrium has been reached, typically a day after preparation.

The experimental set-up used for the potentiometric titrations is shown in the following figure.

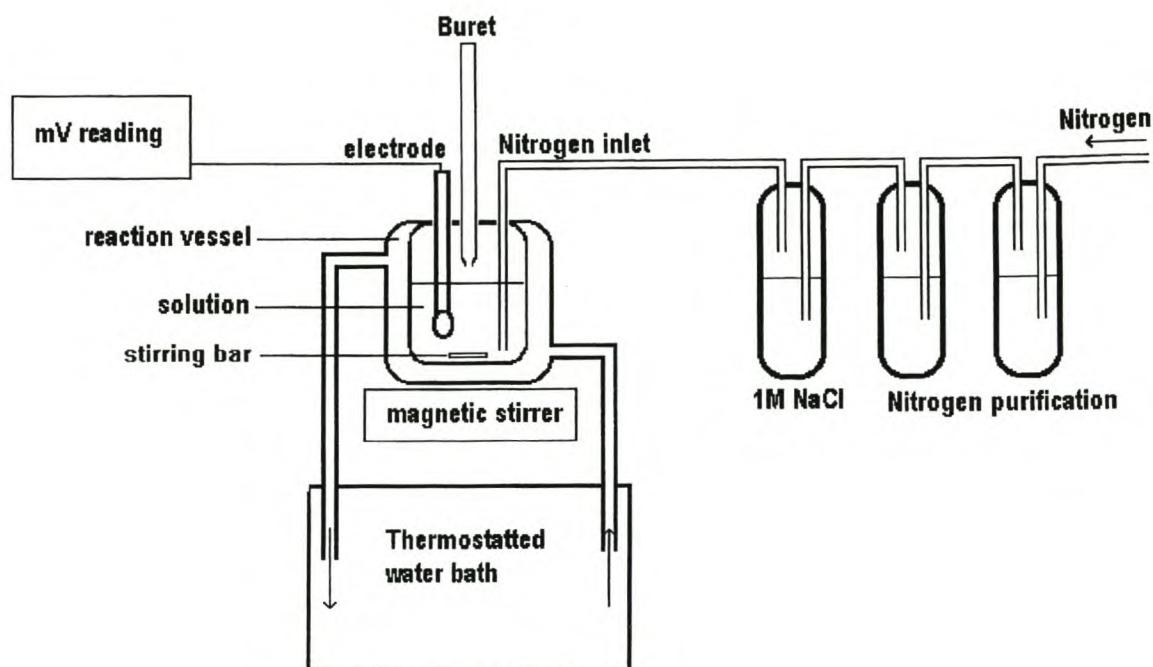


Fig. 2.1 A schematic representation of the experimental set-up for potentiometric titrations

Solutions were titrated in a water-jacketed titration cell, which was kept at constant temperature by circulating water from a thermostatted water bath at 25°C or 2°C. To exclude carbon dioxide from the system a stream of purified nitrogen was passed through 1 M NaCl and then bubbled slowly through the titration solution.

Solutions of ligand were titrated for the determination of the protonation constants. For each complex system investigated a wide range of solutions were titrated (or attempted) in order to acquire data representing a variety of types of complexes. Typically a number of solutions with equal concentrations of molybdate and ligand were titrated, as well as solutions with an excess of either the ligand or the metal. A wide range of tungstate-ligand titrations was attempted, but usually only the titrations of solutions with excess ligand and relatively low tungstate concentration proved to produce equilibrium data (*cf.* 2.6.1.1). Most titrations were done in duplicate to check for reproducibility.

The potential of the solution, E , was measured after each addition of titrant to ± 0.2 mV using a Ross combination electrode (Orion) with a 3 M KCl bridge solution supplied by Orion.

Equation 2.1 was used to calculate the free hydrogen concentration, h , from the measured potential at each titration point.

$$E = E^{\circ} + 0.1985 T \log h + E_j \quad [2.1]$$

where

E° = standard cell potential (mV)

T = temperature (Kelvin)

h = concentration of the free protons

$E_j = k h$ = liquid junction potential

Values for E° and k were determined from titrations of 1 M NaCl with HCl as described by Rossotti [111]. For two different electrodes used, k was determined to be -24.5 and -16 respectively.

For brevity $-\log h$ is denoted by pH_c . (The subscript "c" indicates concentration).

The complexation of citrate with molybdate was also studied potentiometrically at 2°C. Appropriate values for E° and k were determined in the same way as described above and substituted in Equation 2.1 for the calculation of h .

This electrode system was tested for reliability and stability before starting experiments and at regular intervals. Contamination by small amounts of potassium ions through bridge leakage during a titration could be ignored, because of relatively large volumes used in the experiments.

The exact concentrations of the reactants in the solutions which were titrated successfully are shown in Appendix 1. (Difficulties in measuring the pH accurately, particularly in the tungstate-ligand systems where slow reactions occur, are also briefly discussed). The large amount of titration data could not be included in this thesis but is available on request; some representative titrations are presented graphically.

2.3 SPECTROPHOTOMETRY

For the earlier work a Varian Cary 210 spectrophotometer in conjunction with an Apple IIe computer was used for absorption measurements and data collection. Cuvette holders were water-jacketed [112] to maintain the temperature at 25°C by circulation of water from a thermostatted water bath. Later a GBC 920 UV/VIS double beam spectrophotometer equipped with a Peltier thermocell was used for absorption measurements.

Solutions of ligand or molybdate and ligand were titrated with HCl in a water jacketed titration cell, which was kept at constant temperature by circulating water from a thermostatted water-bath at 25°C. The hydrogen ion concentration was measured as described for the potentiometric experiments. At regular pH-intervals samples of the solution were transferred to the cuvettes at 25°C and the absorbance was

measured over a suitable wavelength range, typically 206-320 nm, at 2-3 nm intervals. The reference solution was simply the ionic medium, 1.0 M (Na)Cl. Quartz cuvettes of different path lengths were used, depending on the concentration of the solution.

The experimental conditions (the concentration of reactants, wavelengths measured, path lengths) and the number of spectra acquired per titration are shown in Appendix 1. The large amount of spectral data could not be included in this thesis but is available on request. Most spectra are shown graphically.

In order to simplify calculations, the number of non-complexing species had to be as low as possible. It was also crucial not to have many complexes present in small percentage concentrations only. Suitable conditions were identified by calculating distribution of species under specific conditions using the potentiometric model and the program KON3PH (written in FORTRAN for an IBM compatible PC) [113]. Very few conditions were suitable for the identification of complexes; mainly those with low concentration of molybdate and with an excess of ligand, which favours complexation. Owing to the very small part of the UV spectrum of tungstate that is available for absorption measurements, a similar spectrophotometric study of tungsten-ligand was not feasible.

2.4 CALORIMETRY

An isothermal titration calorimeter, Tronac model 550, was used for the first enthalpy measurements. Later, data were collected with a Tronac model 1250 [114,115]. Solutions (20 or 25 ml) containing molybdate (or tungstate) and ligand, or ligand alone, were titrated with hydrochloric acid from a precision microburette (2.5 ml). All titrations were done in duplicate and the data (heat evolved vs. volume added) were collected automatically by means of a personal computer using software supplied by Tronac.

The total heat evolved during the titration of a mixture of molybdate (or tungstate) and ligand with hydrochloric acid is the sum of the heats of the formation of the complexes, the formation of polymolybdates or polytungstates, the protonation of ligand *and* the heat of dilution. The heat of dilution was therefore subtracted from the total heat in order to get data which represents the heat evolved due only to the formation of the species. (Where the heat is plotted in the figures of this thesis, the heat of dilution has already been subtracted).

The heat of dilution was determined by analysing calorimetric data collected from a "blank" titration of 1 M HCl into 1 M NaCl solution. This dilution reaction is slightly endothermic.

Some enthalpies for the formation of polymolybdates and polytungstates were determined previously and could be used in the calculations [116,117]. The enthalpies for the formation of the protonated ligands were, determined by separate titrations of a ligand solution with 1 M HCl, unless they were already known from previous investigations.

Suitable conditions for calorimetric titrations, where concentrations are low enough to ensure a significant pH change during the titration with 1 M HCl, yet high enough to produce enough heat to measure accurately, were determined with the program KONPH based on the potentiometric models. For the purpose of calculation of enthalpies, conditions with fewer species were more suitable than with many minor species. Conditions where no (or few) polymolybdate or polytungstate species existed were preferred to avoid errors due to possible shortcomings in the molybdate-proton or tungstate-proton model or approximate enthalpies of those species. Such ideal experimental conditions could, however, not always be identified (particularly in the W-aspartate and W-nta systems). Furthermore, for some systems, regions of slow equilibria could not be avoided. Instead of aborting the calculation of enthalpies for those systems, such titrations were done to collect calorimetric data, well knowing it to be flawed, but in the hope of calculating good *estimates* of the enthalpies of some complexes. The successful and useful titrations are listed in Appendix 1.

2.5 DIFFERENTIAL PULSE POLAROGRAPHY

In their investigation of the polarographic reduction of molybdenum(VI) in the presence of citrate at pH~8.2, Creager *et al.* [43] have shown that a very low temperature is required to suppress the kinetic portion of the limiting current. At 2°C the rate of formation of the electroactive Mo(VI) citrate species is so small that on the polarographic time-scale the limiting current is controlled virtually entirely by diffusion of the complex from the bulk solution. For the purpose of the present investigation it has been assumed that the limiting current is diffusion controlled at all potentials and under all conditions. Most of the differential pulse polarograms were therefore recorded at 2°C and the results examined in terms of the postulated reaction model and species distribution curves pertaining to 2°C. Some preliminary differential pulse polarograms were recorded at 25°C.

A Metrohm Polarecord E506 with an E505 polarographic stand was used for recording the differential pulse polarograms. A thermostatted Metrohm cell with a three-electrode system was used: a dropping mercury electrode with a drop time of 0.4 s at 86.2 cm mercury height as the working electrode, a silver-silver chloride (3 M KCl) reference electrode and a platinum wire auxiliary electrode. The solutions were deaerated with purified nitrogen for at least 30 min before polarograms were recorded at 2°C (or at 25°C). The scan rate was 5 mV s⁻¹ and the pulse amplitude 52 mV.

Individual solutions of molybdate, citrate and HCl were prepared and analyzed polarographically. Usually polarograms were measured of sets of solutions (same molybdate to citrate ratio but acidified to different degrees) in order to get a series of polarograms which could be correlated with an ordinary distribution curve.

The composition and pH of the solutions of which polarograms were recorded are shown in Section 3.5.1.3. Some polarograms are shown in Section 3.5.1.3.

2.6 METHODS OF DATA ANALYSIS

2.6.1 Potentiometric analysis

The computer speciation program, SUPERQUAD [118], was mostly used for the analysis of the data. This ensured consistent treatment of data and interpretation of results, particularly with respect to the inclusion or exclusion of minor species. (The programs SIRKO [119] and HYPERQUAD [120] were used occasionally as a check, for instance for the calibration of electrodes). The consistency of duplicate titrations could be checked by comparing SUPERQUAD residual plots. SUPERQUAD can accommodate only 600 experimental data points. If more than 600 data points were collected, duplicates were ignored in final data sets. (The actual number of titrations used in the final data set for calculation is shown in Appendix 1). The model is restricted to 24 species only.

Speciation programs like SUPERQUAD are used to find the best model (species and their formation constants) to describe the system represented by the titration data given. Different models can be compared by their so-called "fit". In the case of SUPERQUAD the fit is indicated by the parameters σ (sample standard deviation) and χ^2 . A small value for σ , in particular, indicates that the pH calculated using a particular model, generally differs very little from the actual experimentally determined pH.

A model representing a system in which complex formation takes place consists of a set of chemical species (which are the products of various equilibria between two or more reactants) and their formation constants.

The reactants in the present investigations of Mo(or W)- ligand-proton systems are:

- a) molybdate (or tungstate)
- b) ligand (a suitably chosen (de)protonated form, cf. 2.6.1.2)
- c) protons

The possible chemical equilibria to be considered are:

- 1) protonation and condensation reactions of uncomplexed molybdate (or tungstate)
- 2) protonation reactions of the ligand
- 3) complexation reactions between molybdate (or tungstate), ligand and protons.

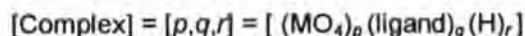
These three possible types of reactions can all be represented by the general Equation (2.2)



where $M = \text{Mo or W}$ and
 $n = \text{magnitude of charge on the ligand}$

(For the reactions of Mo (or W) and protons, $q = 0$, and for the protonation reactions of ligand, $p = 0$)

A complex species is denoted by $[p,q,r]$ or $[p,q,r]^{p-}$, notations derived from the unique stoichiometric coefficients of the reactants in a particular complex formation reaction and the charge of the resulting complex.



The overall formation constant of each complex is denoted by β_{pqr} , where

$$\beta_{pqr} = [\text{Complex}] / ([\text{MO}_4^{2-}]^p [\text{ligand}^{2-}]^q [\text{H}^+]^r) \quad [2.3]$$

In the search for a model of a three-component (ternary) system, all three types of reactions mentioned above must be considered simultaneously as (at least, initially) complete complexation cannot be assumed to occur. Uncomplexed Mo (or W) or free ligand species must be included in the initial models, especially when data from titrations with an excess of either ligand or metalate are treated, until inclusion of these species proves to be unnecessary. The overall model of a metal-ligand-proton system is thus a combination of three sub-models, namely the Mo(VI)- or W(VI)-proton model, the ligand-proton model, and the Mo(VI) or W(VI)-ligand-proton model. These sub-models (and the equilibria they represent) are described and discussed in greater detail in the following paragraphs.

2.6.1.1 Molybdenum(VI)- and Tungsten(VI)-proton model

The relevant reactions can be represented by the simplified Equation 2.2:



The chemistry of molybdenum(VI) and tungsten(VI) in acidic aqueous solution is very complicated and has been studied in depth [116,117, 121-125]. Potentiometric studies, aided by computer modelling, have contributed largely in solving the systems, but absolute certainty as to the existence of all proposed species, particularly those occurring in small percentage concentrations, has not been attained. However, models have been obtained which describe the potentiometric data for the molybdate-proton-system very accurately. These models agree well regarding the major species (which are also confirmed by other experimental methods) and usually differ only in the minor species. One such model (pertaining to 1 M (Na)Cl and 25°C) was chosen to represent the molybdate-proton side reactions in this study of molybdate-ligand-proton systems for pH and is shown in Table 2.2 [116].

No molybdate-proton model has ever been calculated from experimental data at 2°C for the molybdate-proton system. For the purpose of modelling possible uncomplexed molybdate species present in the Mo-citrate system at 2°C, it is *assumed* that the same molybdate species exist at 2°C as at 25°C, furthermore, that the ΔH° and ΔS° pertaining to 25°C, which have been determined previously (Table 2.5) are similar to the values pertaining to 2°C. These assumptions allow the calculation of approximate formation constants using Equations 2.4 and 2.5. These values are also shown in Table 2.2.

$$\Delta G^\circ = -2.303 R T \log K \quad (\text{for } T = 298.15 \text{ and } 275.15 \text{ K, respectively}) \quad [2.4]$$

$$\Delta G^\circ = \Delta H^\circ - T\Delta S^\circ \quad [2.5]$$

Table 2.2 Molybdenum(VI)-proton model for 25°C and 2°C used in calculations [116].

chemical species	[p,q,r]	log $\beta_{p,q,r}$ Temp = 25°C	log $\beta_{p,q,r}$ Temp = 2°C
[MoO ₄] ²⁻ chosen as "reactant"	[1,0,0]	log $\beta_{1,0,0}$ = 0.00	log $\beta_{1,0,0}$ = 0.00
[HMoO ₄] ⁻	[1,0,1]	log $\beta_{1,0,1}$ = 3.45	log $\beta_{1,0,1}$ = 3.1
[MoO ₃ (OH) ₂] ₃	[1,0,2]	log $\beta_{1,0,2}$ = 7.12	log $\beta_{1,0,2}$ = 7.5
[MoO ₂ (OH)(OH ₂) ₃] ⁺	[1,0,3]	log $\beta_{1,0,3}$ = 8.05	log $\beta_{1,0,3}$ = 8.6
[HMo ₂ O ₇] ⁻	[2,0,3]	log $\beta_{2,0,3}$ = 14.48	log $\beta_{2,0,3}$ = 15.9
[HMo ₂ O ₆] ⁺	[2,0,5]	log $\beta_{2,0,5}$ = 18.24	log $\beta_{2,0,5}$ = 19.6
[Mo ₇ O ₂₄] ⁶⁻	[7,0,8]	log $\beta_{7,0,8}$ = 52.87	log $\beta_{7,0,8}$ = 56.62
[HMo ₇ O ₂₄] ⁵⁻	[7,0,9]	log $\beta_{7,0,9}$ = 57.39	log $\beta_{7,0,9}$ = 61.02
[H ₂ Mo ₇ O ₂₄] ⁴⁻	[7,0,10]	log $\beta_{7,0,10}$ = 60.71	log $\beta_{7,0,10}$ = 64.2
[H ₃ Mo ₇ O ₂₄] ³⁻	[7,0,11]	log $\beta_{7,0,11}$ = 62.94	log $\beta_{7,0,11}$ = 66.6
[Mo ₈ O ₂₆] ⁴⁻	[8,0,12]	log $\beta_{8,0,12}$ = 71.22	log $\beta_{8,0,12}$ = 75.1

The above model is not necessarily believed to be absolutely correct, but it predicts the pH of molybdate-proton-systems at a wide variety of molybdenum(VI) concentrations very well, and can, therefore, be used with confidence as a working model. Furthermore, when working with systems where strong complexation occurs (and therefore little uncomplexed molybdate is present) the exact identity of the minor species is not important. In this study, only aspartate complexation is so weak that the minor molybdate-proton equilibria seems very important. However, under such conditions the search for a molybdate-ligand model is extremely difficult and entirely unambiguous characterization is not possible. The most valuable data pertaining to the Mo-aspartate system is the data representing conditions of excess aspartate, which favour complexation of molybdate, avoiding once again the necessity of a perfect molybdate-proton model.

The same method and care was taken in the search for a good tungsten-proton model as with molybdenum-proton model. When tungstate is acidified, equilibrium is established quickly until ~ 60% of the negative charge (WO₄²⁻) has been neutralized by protons, after which slow equilibria occur (where the degree of protonation, $F > 0.6$). The model for the tungstate-proton system, which is shown in Table 2.3, is only valid for equilibrium conditions and not for the region of slow equilibria [117].

As a consequence of the limited applicability of the model, the experimental conditions for the study of tungsten complexation is also limited. Slow reactions of tungstate have to be avoided by ensuring complete complexation of tungstate. Usually this means that the concentration of tungstate has to be low, and the ligand in excess. The accuracy of potentiometry, however, decreases if the concentration of tungstate is too

low. These two factors are weighed against each other, and usually result in only a few suitable titration conditions (which are tabulated in Appendix 1).

The necessary precautions could be taken to avoid slow reactions for some tungstate-ligand systems. For other tungstate-ligand systems, however, almost all attempted titrations had regions of slow equilibria. In the case where the equilibrium was established within a few minutes, readings were taken, but where equilibration took too long, the particular "slow region" was skipped by simply adding titrant until pH measurements could once again be taken. Instead of aborting the investigation completely, an attempt was made to model the system, using the above tungstate-proton model, well knowing it to be only the best approximation available.

Table 2.3 Tungsten(VI)-proton model used in calculations (25°C) [117].

chemical species	[p,q,r]	log $\beta_{p,q,r}$
[WO ₄] ²⁻ chosen as "reactant"	[1,0,0]	log $\beta_{1,0,0}$ = 0.00
([HWO ₄] ⁻)	[1,0,1]	log $\beta_{1,0,1}$ = 3.4
[W ₆ O ₂₀ (OH) ₂] ⁶⁻	[6,0,6]	log $\beta_{6,0,6}$ = 49.01
[W ₇ O ₂₄] ⁶⁻	[7,0,8]	log $\beta_{7,0,8}$ = 65.19
[HW ₇ O ₂₄] ⁵⁻	[7,0,9]	log $\beta_{7,0,9}$ = 69.96
[H ₂ W ₁₂ O ₂₄] ¹⁰⁻	[12,0,14]	log $\beta_{12,0,14}$ = 115.4

2.6.1.2 Ligand-proton model

The relevant reactions can be represented by the simplified Equation 2.2:



The protonation reactions of most of the ligands used have previously been studied, but sometimes in media other than 1 M NaCl. All the protonation constants were determined (or verified) by potentiometry (and sometimes by spectrophotometry) for 1 M (Na)Cl medium. The general ligand proton model is:

Table 2.4 General ligand-proton model

general chemical species	[p,q,r]	log $\beta_{p,q,r}$
[L] ⁿ⁻ chosen as "reactant"	[0,1,0]	log $\beta_{0,1,0}$ = 0.00
[HL] ⁿ⁻⁺¹	[0,1,1]	log $\beta_{0,1,1}$
[H ₂ L] ⁿ⁻⁺²	[0,1,2]	log $\beta_{0,1,2}$
etc. (depending on the number of protonations that can take place)		

A convenient (de)protonated form of each ligand had to be chosen to be used as "reactant" (species [0,1,0]) in the reaction Equation 2.2. Although it is common practice in analytical chemistry to write the ligand in its fully deprotonated form, the ligand-species which was present at the highest pH where complexation started was regarded as "reactant" in this investigation (Table 2.4). This species was identified by comparing the pH at which complexation started with the species distribution of the respective ligand (figures, Appendix 2).

Table 2.5 Ligand-species used as "reactants" in this investigation

ligand	[0,1,0] , chosen "reactant"	abbreviation
oxalic acid	OOC-COO^-	ox^{2-}
lactic acid	$\text{CH}_3\text{-CH(OH)-COO}^-$	Hlac^-
mandelic acid	Ph-CH(OH)-COO^-	Hman^-
malic acid	$\text{OOC-CH}_2\text{-CH(OH)-COO}^-$	Hmal^{2-}
citric acid	$(\text{OOC-CH}_2)_2\text{-C(OH)-COO}^-$	Hcit^{3-}
tartaric acid	$\text{OOC-CH(OH)-C(OH)-COO}^-$	$\text{H}_2\text{tar}^{2-}$
aspartic acid	$\text{OOC-CH}_2\text{-CH(N(+)H}_3\text{)-COO}^-$	Hasp^-
nitrilotriacetic acid	$\text{N(CH}_2\text{-COO}^-)_3$	nta^{3-}

It can be seen that the carboxylic acid groups of the species used as "reactant" are all deprotonated, whereas the hydroxy groups are not deprotonated. The abbreviation, HL^n , emphasizes the presence of the hydroxy proton in some ligands. Both carboxylic protons of the singly deprotonated aspartic acid which was used as "reactant" are deprotonated, but one of the protons has protonated the amino group within the molecule.

2.6.1.3 Model search strategy with SUPERQUAD

SUPERQUAD is able to incorporate 24 species (representing chemical reactions) in its calculations. For initial model testing, the possible molybdate-proton (or tungstate-proton) species and the ligand-proton species must be incorporated with their formation constants ($\log \beta_{\text{pqr}}$) fixed. Complex species can then be added as test species, and their formation constants allowed to be refined. The species with the greatest standard deviation in the value of the formation constant (if above 33%) is first rejected by the program. The calculation is repeated, with one less species every time, until the formation constants of all species are acceptable to the program (standard deviation in the value of the formation constant $< 33\%$ or $3\sigma < 0.43$ log units). Different species are then tested against the last acquired model. Repeated calculations lead to models with better overall fits, indicated by the parameters σ , the sample standard deviation, and χ^2 . For these investigations the sample standard deviation, σ , is based on estimated errors of 0.01 ml in the volume and 0.002 in the pH.

Rejection of a certain test species at almost any stage, is not a proof that it does not exist. It has often been shown, that species once rejected, might be accepted in another model. The search for the best model thus is an almost never ending process. The decision to accept a certain model as the "best model" for the system has to be taken with great care.

The program SUPERQUAD allows refinement of other parameters such as concentrations, but the danger exists that such refinements might "absorb" faults in the model. Rather than using this facility, much effort has gone into every experimental aspect to ensure accurate data. This facility was, however, used to verify

the concentrations of the ligand in the ligand-titrations where the risk, mentioned above, is minimal, as no real uncertainties exist regarding the ligand model. In all cases the concentrations refined to the expected values, without affecting the $\log \beta_{\text{per}}$ -values significantly. This was regarded as sufficient check of the ligand concentrations.

The search of the models for each particular system is described briefly in Chapter 3. Although it is not always explicitly mentioned, the models which were finally proposed had undergone the following type of tests of consistency:

1) Subsets of data (cutting of data)

If models had been obtained from a large data set, titrations which were the only ones representing a certain minor species would be removed and the model recalculated. If a minor species was then rejected and the rest of the model, especially the major species, remained, it was seen as evidence for a good original model.

2) Refinement of ligand and metalate formation constants

Formation constants of ligand-species or of molybdate or tungstate-species, which were normally fixed, were allowed to refine. If the refinement did not affect the complex-species, the background ligand and metalate models were shown to be valid models. It also showed that the complex-species were not simply mathematical artefacts to compensate for wrong ligand or metalate species in the model.

3) Concentration refinement

The concentrations of molybdate, tungstate, ligand or protons, which were normally fixed, were allowed to refine while calculating the final model to check for consistency.

2.6.2 Spectrophotometric analysis

The programs SPECFIT [126,127] and SQUAD [128,129] were used to calculate the model (species, their formation constants and molar absorbances) which best explained the experimental absorbances of the ligand or the molybdate-ligand systems. If the solutions contained uncomplexed molybdate or free ligand species, these needed to be included in the model. To simplify the calculation of the complex model, the formation constants of these uncomplexed species were fixed. The program SQUAD, unlike SPECFIT, has the facility to *also* fix known molar absorbances of species. Using the program SQUAD, calculations of systems where uncomplexed molybdenum(VI) monomers (molybdate [1,0,0] and its protonated monomers, [1,0,1] and [1,0,2]) needed to be considered, were simplified by fixing their known spectra. A test of the final model would, however, be to allow these spectra to be refined as well. If they agreed well with the known spectra, the complex model was accepted with confidence.

2.6.3 Calorimetric analysis

The values for the total heat evolved during titrations were corrected for the heat of dilution of hydrochloric acid in 1 M NaCl.

$$Q = (\text{total amount of heat measured} - \text{heat of dilution}) \quad [2.6]$$

Graphical representation of the titrations are usually given by plotting Q vs molar ratio of acid added to molybdate or tungstate (Chapter 3). This enables easier comparison of the heat evolved during different titrations. These curves sometimes show distinct breaks at certain mole ratios in accordance with the stoichiometry of the major complex identified from the potentiometric measurements.

The enthalpy changes for the formation of the different complexes were calculated from the measured heat corrected for dilution effects, Q .

$$Q = \sum n_{pqr} \Delta H_{pqr}^{\circ} \quad [2.7]$$

where n_{pqr} is the number of moles formed and ΔH_{pqr}° the molar enthalpy change of a given species $[p, q, r]$ at 25°C in 1 M (Na)Cl medium. The set of linear equations obtained from corresponding Q and n_{pqr} values were solved for the unknown ΔH_{pqr}° parameters using a BMDP least squares program [130]. The n_{pqr} values at each titration point were calculated (based on a proposed model) by a subroutine supplied to the BMDP. The program SIRKO [119], designed for the analysis of different types of data, including calorimetric data, was also used. The program also first calculates the concentrations of the species based on a given model by simultaneous solution of the three mass-balance equations (2.8.1-3) to enable the equations represented by 2.7 to be solved for the unknown ΔH_{pqr}° parameters :

$$B = b + \sum p \beta_{pqr} b^p c^q h^r \quad [2.8.1]$$

$$C = c + \sum q \beta_{pqr} b^p c^q h^r \quad [2.8.2]$$

$$H = h + \sum r \beta_{pqr} b^p c^q h^r \quad [2.8.3]$$

where b = equilibrium concentration of $[\text{MoO}_4]^{2-}$ (or $[\text{WO}_4]^{2-}$),
 c = equilibrium concentration of ligandⁿ⁻
 h = equilibrium concentration of H^+ .

The values for the enthalpy change for the formation of the protonated ligand species (ΔH_{01r}°) were calculated first from the heat (corrected for the heat of dilution) developed during the titration of the ligand alone. These values were fixed in the calculations of the ΔH° values for the formation of the complexes using data from the titration of molybdate (or tungstate) and ligand.

Conditions for calorimetric titrations pertaining to molybdate-ligand systems were chosen such as to ensure that all (or most) of the molybdate is complexed. Therefore, most of the enthalpy calculations could be

done by considering only ligand and Mo-ligand species. However, despite the ten-fold excess of ligand in the calorimetric titration of a molybdate-aspartate solution, uncomplexed molybdate species, [1,0,2], [7,0,9], [7,0,10], [7,0,11] and [8,0,12] were present in 0.5 to 5 percentage concentrations. During the calculation of the ΔH° values for the formation of the Mo-aspartate complexes, the formation constants and ΔH° values for these molybdenum(VI) species had to be fixed. These approximate preliminary values, which were determined previously [116], are shown in the Table 2.6.

Table 2.6 Values for ΔH° for the formation of molybdenum(VI) species [116].

chemical species	[p,q,r]	$\Delta H^\circ_{p,q,r}$ (kJ mol ⁻¹)
[MoO ₄] ²⁻ chosen as "reactant"	[1,0,0]	0
[HMoO ₄] ⁻	[1,0,1]	+21
[MoO ₃ (OH ₂) ₃]	[1,0,2]	-29
[MoO ₂ (OH)(OH ₂) ₃] ⁺	[1,0,3]	-23
[HMo ₂ O ₇] ⁻	[2,0,3]	-84
[HMo ₂ O ₆] ⁺	[2,0,5]	-92
[Mo ₇ O ₂₄] ⁶⁻	[7,0,8]	-257
[HMo ₇ O ₂₄] ⁵⁻	[7,0,9]	-248
[H ₂ Mo ₇ O ₂₄] ⁴⁻	[7,0,10]	-249
[H ₃ Mo ₇ O ₂₄] ³⁻	[7,0,11]	-266
[Mo ₈ O ₂₆] ⁴⁻	[8,0,12]	-274

These approximate ΔH° values are good enough for the calculation of thermodynamic values of complex formation.

Conditions of excess ligand for calorimetric titrations pertaining to tungstate-ligand systems usually ensured that all of the tungstate was complexed. Therefore, most of the enthalpy calculations could be done by considering only ligand and W-ligand species. However, despite the excess of ligand in the calorimetric titration of the tungstate-aspartate and tungstate-nta solutions, uncomplexed tungstate species, [6,0,6], [7,0,8], [7,0,9] and [12,0,14] were present in substantial percentage concentrations. During the calculation of the ΔH° values for the formation of the W-aspartate and W-nta complexes, the formation constants and ΔH° values for these tungsten(VI) species had to be fixed. These values, which were determined previously [117], are shown in the Table 2.7.

Table 2.7 Values for ΔH° for the formation of tungsten(VI) species [117].

chemical species	[p,q,r]	$\Delta H^\circ_{p,q,r}$ (kJ mol ⁻¹)
[WO ₄] ²⁻ chosen as "reactant"	[1,0,0]	0
[HWO ₄] ⁻	[1,0,1]	-
[W ₆ O ₂₀ (OH) ₂] ⁶⁻	[6,0,6]	-231
[W ₇ O ₂₄] ⁶⁻	[7,0,8]	-333
[HW ₇ O ₂₄] ⁵⁻	[7,0,9]	-328
[H ₂ W ₁₂ O ₂₄] ¹⁰⁻	[12,0,14]	-542

The value for the change in free energy (ΔG°) for the formation of each complex species was calculated from the formation constants, $\log\beta_{\text{par}}$, using Equation 2.4. For those species for which ΔH° could be determined, the entropy term $T\Delta S^\circ$, could be calculated from the Equation 2.5. (The entropy term, $T\Delta S^\circ$, is usually shown instead of the ΔS° , since ΔH° and $T\Delta S^\circ$ are both energies and can be compared directly).

Indirect calculation of ΔH°

In the case of the molybdate-citrate-proton system an additional, indirect, calculation of enthalpy values could be done, as two sets of species and their formation constants were obtained by potentiometric analysis, one describing the system at 2°C and one at 25°C.

Since Equation 2.4 = Equation 2.5

$$\log K = \Delta H^\circ / 2.303RT - \Delta S^\circ / 2.303R \quad [2.9]$$

If it is assumed that the values for ΔH° and ΔS° are constant over the temperature range in question, ΔH° and ΔS° can be calculated from the gradient ($\Delta H^\circ / 2.303R$) and the y-intercept ($\Delta S^\circ / 2.303$), respectively, of the function, $\log K$ vs $1/T$ (cf. 3.5.1.1).

Chapter 3

Experimental Results and Data Analysis

Presentation of experimental data

The conditions of the potentiometric, spectrophotometric, calorimetric and polarographic measurements are tabulated in Appendix 1 but the data collected are presented graphically in this chapter.

To give an overview of the collected potentiometric data the titrations for each system are presented as a function F vs pH, where

$$F = (H - h + K_w / h) / (2B + nC) \quad [3.1]$$

and

H , B and C = analytical concentrations of acid, Mo(VI) or W(VI) and ligand, respectively

h = concentration of free H^+

n = charge on ligand

$K_w = 10^{-13.71}$ (for this medium, 1 M NaCl)

The function F (Equation 3.1) represents the fraction of the total negative charge neutralized due to protonation. (Further explanatory notes on F curves are given in Appendix 5.)

For each system the protonation curve of the ligand alone is also shown in order to illustrate how protonation of the system is affected by complexation. If only a slight difference occurs between the F curves of a particular complex system and the F curve of the ligand weak complexation is indicated. Pronounced inflexions of the curves indicate the formation of species $[p,q,r]$ of which the ratio $r/(2p + nq)$ corresponds to the F value at the inflexion.

The experimental spectra are shown as plots of absorbance vs wavelength. The heat developed during the titrations (corrected for the heat of dilution) is usually shown as a function of volume added or the ratio of acid to metal.

Model-search

The search for a best model representing the potentiometric and/or spectrophotometric data is described for each system investigated. The identified species, their formation constants and the value for the change in free energy (ΔG°) associated with their formation are tabulated in the following sections. The ΔG° for each complex is calculated from the formation constant, using Equation 2.4 ($\Delta G^\circ = 2.303RT \log \beta$).

Calorimetric data analysis

The calculation of the ΔH° values from the calorimetric data is discussed and tabulated. The entropy term, $T\Delta S^\circ$, for the formation of some of the complexes is calculated from the ΔG° and ΔH° values, using Equation 2.5 ($\Delta G^\circ = \Delta H^\circ - T\Delta S^\circ$).

3.1 COMPLEXATION WITH OXALATE

3.1.1 Molybdenum(VI)-oxalate system

3.1.1.1 Potentiometric data and analysis

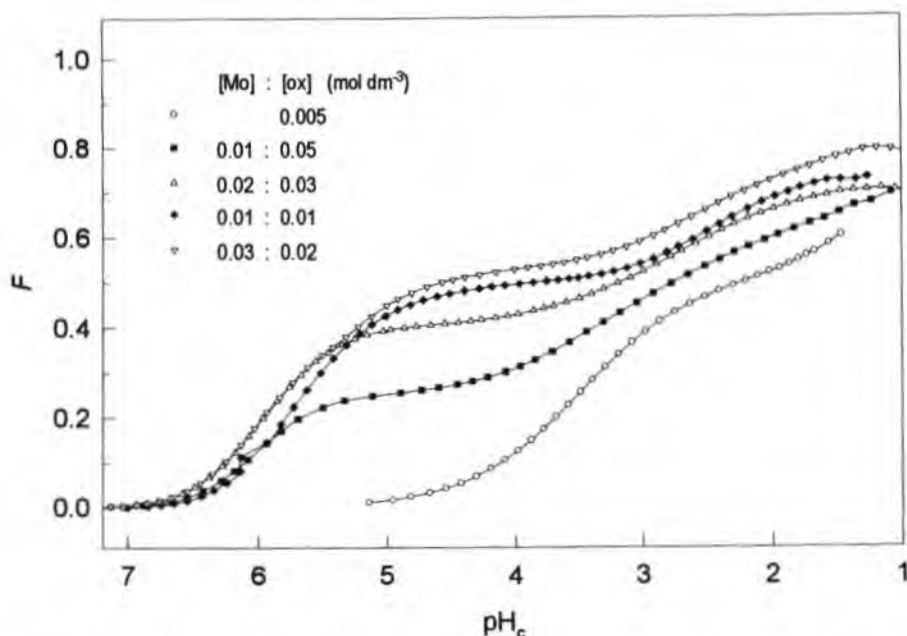


Fig.3.1.1 Function F versus pH_c for some representative potentiometric titrations of the molybdate(VI)-oxalate system.

F curves

Figure 3.1.1 shows that complex formation results in the uptake of protons at much higher pH than in the case of oxalate alone. The inflexion at $F=0.5$ ($\text{pH} \sim 4$) exhibited by the curves pertaining to equimolar solution (01:01) corresponds with the formation of the major complex in that pH region, [1,1,2], for which $r / (2p+2q) = 0.5$.

Modelling of the oxalate and Mo-oxalate systems (species, $\log\beta$, ΔG°)

Previously determined protonation constants of oxalate (shown in Table 3.1.1) were used in calculations and to produce a species distribution diagram of the oxalate system (Appendix 2) [2].

Recalculation of the previous data pertaining to the Mo-oxalate system [2] over the pH range 7-2 led to the inclusion of the [1,1,3] complex, but its percentage concentration was very low. Calculation of the new experimental data, which extended to $\text{pH} \sim 1$, showed that the inclusion of the [1,1,3] complex improved the

model significantly. The model consisting of the complexes, [1,1,2], [1,1,3], [2,2,5] and [2,2,6] was accepted with a good fit (model A : $\sigma = 1.20$, $\chi^2 = 80$). A further significant improvement of fit could be attained with the inclusion of the [2,1,5] complex ($\sigma = 0.69$). The complex [2,1,5] can only compete with the [2,2,6] as a major species under conditions of excess molybdate. Calculations show that even for the titration of the solution of 0.03 M molybdate : 0.02 M oxalate, the maximum percentage concentration of the [2,2,6] complex (~45%) is greater than that of the [2,1,5] complex (~35%). Nevertheless, the [2,1,5] complex is an interesting and important addition to the complexes previously identified as it is the first complex in the model for which $p > q$.

A few other species could be added to the model with almost insignificant improvement of fit. These always turned out to be very minor complexes. The [1,2,4] complex, for instance, reaches a maximum percentage concentration of ~ 8% in the titration pertaining to a three-fold excess of oxalate (model B : $\sigma = 0.61$, $\chi^2 = 55$). This complex is accepted, not only on the grounds of a slightly better fit, but because its relative standard deviation (14%) is the same as that of the fully accepted [1,1,3] complex. The importance of this species lies in the fact that (possibly) molybdate-oxalate species $[p,q,r]$ exist for which $p < q$. This is not of great consequence for the experimental conditions of this investigation, but it could be very significant under conditions of great excess of oxalate, for instance where $[Mo]=0.001M$ and $[ox]=0.1M$ at low pH (~1.5). (Its inclusion in the model does not alter the formation constants of the other complexes by more than 0.1 log unit, so that the model can be used with or without [1,2,4].)

Table 3.1.1 Molybdate(VI)-oxalate complexes identified and calculated $\log\beta$ and ΔG° values.
1 M (Na)Cl at 298.15 K

COMPLEX	new model (B)		previous model (D) [2]	
	$\log\beta_{pqr} \pm 3\sigma$	ΔG° (kJ mol ⁻¹)	$\log\beta_{pqr} \pm 3\sigma$	ΔG° (kJ mol ⁻¹)
[0,1,1] ⁻	3.52 ± 0.02	-20.1	3.52 ± 0.02	-20.1
[0,1,2]	4.41 ± 0.02	-25.2	4.41 ± 0.02	-25.2
[1,1,2] ²⁻	13.65 ± 0.01	-77.9	13.62 ± 0.01	-77.8
[1,1,3] ⁻	15.32 ± 0.19	-87.46		
[2,2,5] ³⁻	31.19 ± 0.08	-178.1	31.19 ± 0.08	-178.1
[2,2,6] ²⁻	34.10 ± 0.05	-194.7	34.10 ± 0.05	-194.7
[2,1,5] ⁻	25.88 ± 0.05	-147.7		
[1,2,4] ²⁻	20.50 ± 0.19	-117.0		

The chosen model (B) does not differ much from the model previously published (D). The inclusion of [2,1,5] and the minor complex [1,2,4] are mainly due to the extended pH region covered by the titrations.

In addition to the above-mentioned complexes, the [4,2,8] and [4,4,10] complexes were also accepted at times. If included in the model, these complexes appeared in the same pH range as the [2,2,5] complex and, in fact, at the expense of the [2,2,5] complex. (The formation constant of [2,2,5], and therefore its maximum percentage concentration, was reduced in the presence of [4,2,8] and [4,4,10].) Interestingly, the

formation constants of the species [1,1,3], [2,1,5] and [1,2,4] were increased, and their standard deviations reduced, implying a better individual fit. (model C : $\sigma = 0.56$, $\chi^2 = 34$).

Using this data, it was impossible to attain certainty about these tetramers to an extent that would justify their inclusion in the model for general use. It is believed that the model (B) (Table 3.1.1), consisting of the simpler complexes [1,1,*r*], [2,2,*r*] [2,1,5] and [1,2,4], is adequate to predict the formation of complexes of the correct *p:q* ratios, and that it is of no great consequence whether the true complex has a Mo:ox ratio of 2:2 or 4:4 or whether both exist.

Further titrations could possibly enable a better distinction between the 2:2 and 4:4 or 2:1 and 4:2 complexes, but they were not carried out, as the main purpose of this investigation was to establish the complexes in the very low pH region, and not particularly at very high molybdate concentrations.

Some reaction models, their respective fits, and formation constants for the complexes are shown to summarize the development of the model as discussed above:

(r.s.d. = relative standard deviation)

	model A		model B		model C	
χ^2	80		55		34	
σ	1.20		0.61		0.56	
		r.s.d		r.s.d		r.s.d
$\log\beta_{112}$	13.65	1%	13.65	1%	13.65	1%
$\log\beta_{113}$	15.32	30%	15.32	14%	15.58	8%
$\log\beta_{225}$	31.19	11%	31.19	6%	30.71	27%
$\log\beta_{226}$	34.10	6%	34.10	4%	34.01	4%
$\log\beta_{215}$	-		25.88	4%	25.93	3%
$\log\beta_{124}$	-		20.50	14%	20.61	10%
$\log\beta_{4410}$	-		-		64.63	18%
$\log\beta_{428}$	-		-		49.40	16%

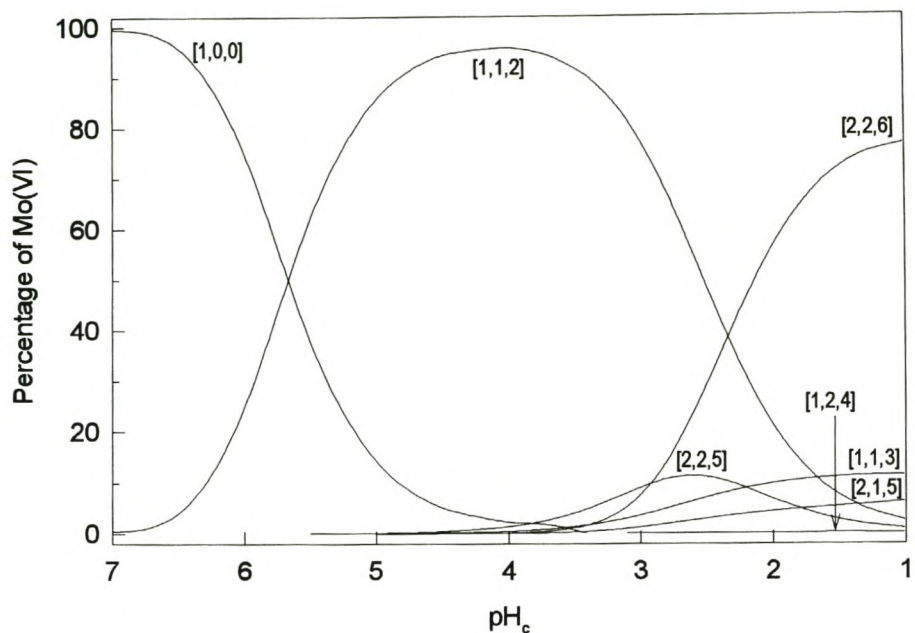
Distribution of species

Fig. 3.1.2 Concentration of molybdate(VI)-oxalate complexes, expressed as a percentage of the total molybdenum(VI) concentration, as a function of pH_c. The total concentrations of molybdate(VI) and oxalate are both 0.01 M and 0.01 M.

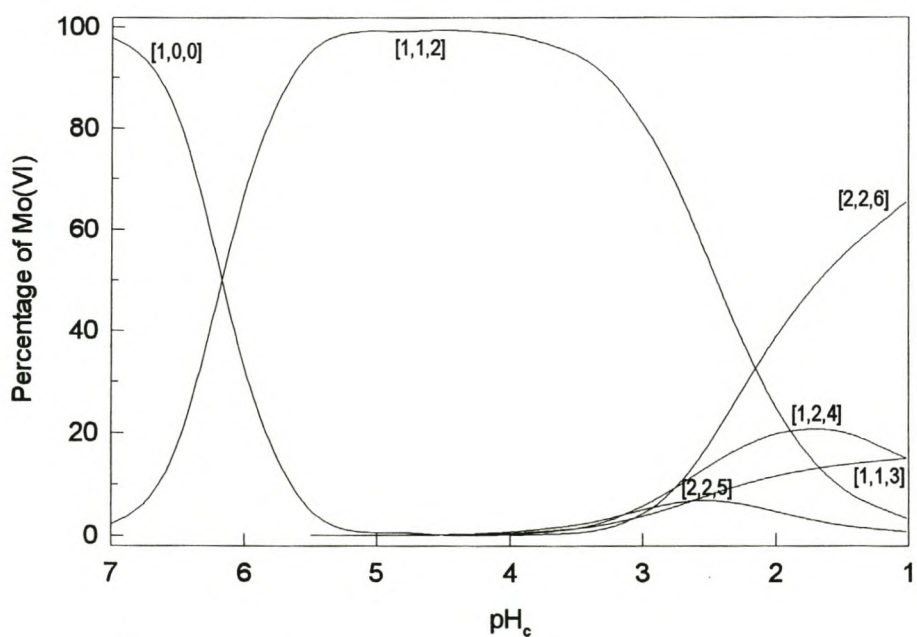


Fig. 3.1.3 Concentration of molybdate(VI)-oxalate complexes, expressed as a percentage of the total molybdenum(VI) concentration, as a function of pH_c. The total concentrations of molybdate(VI) and oxalate are 0.005 M and 0.05 M, respectively.

3.1.1.2 Enthalpimetric data and analysis

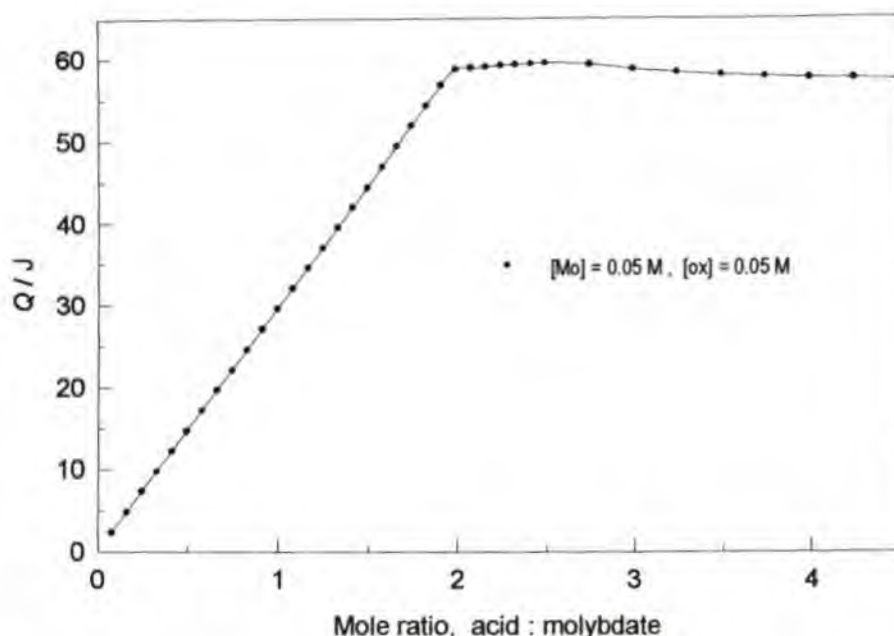


Fig. 3.1.4 Measured heat, Q , as a function of the molar ratio of acid to molybdate(VI) for a titration of 0.05 M molybdate(VI) and 0.05 M oxalate.

Calculation of enthalpy and entropy

The enthalpimetric data collected and used by Cruywagen [2] for the calculation of the value for the change of enthalpy for the formation of [1,1,2], [2,2,5] and [2,2,6] were used for recalculation. The data are represented by a plot of Q vs mole ratio of acid added to molybdate (Fig. 3.1.4). The first inflexion is in accordance with the stoichiometry of the major complex [1,1,2] (for which $r/p = 2$) and the second inflexion is in accordance with the stoichiometry of [2,2,5] (for which $r/p = 2.5$). The distribution of the species, also as a function of mole ratio of acid added to molybdate, for the same condition (0.05 M molybdate : 0.05 M oxalate) is also shown (Fig. 3.1.5). Comparison of these two plots, clearly shows that the first inflexion of the Q curve concurs with the point in the titration where [1,1,2] reaches its maximum percentage (ratio=2) and the second, at the point where [2,2,5] reaches a maximum percentage (ratio=2.5).

Since all of the oxalate is used in complexation during this particular titration, the values for the enthalpy change for the protonation of oxalate need not be taken into account. It is not possible to calculate the enthalpy change for the formation of either [2,1,5] or [1,2,4] accurately, as too little of these species is present under the experimental condition. Furthermore, the relative percentages of all the complexes change little for the mole ratio, acid: molybdate > 3 (Fig. 3.1.5), while the heat produced also changes minimally (Fig. 3.1.4). For the final calculations only the data for which the mole ratio, acid: molybdate < 3 were used. The values for the enthalpy change for the formation of the complexes [1,1,2], [1,1,3], [2,2,5]

and [2,2,6] were calculated using the new model (B) and are shown in Table 3.1.2. The values for the enthalpy change for the formation of these, as well as the [4,4,10], species were also calculated using the alternative model (C) and are also shown in Table 3.1.2. (The other complexes in model C do not occur under the experimental conditions.) The values calculated, based on model B and C, are very similar, and differ only slightly from the values obtained by a similar calculation, using the previously published model A. The fit of the enthalpimetric model is slightly better when using model B than model A, and is best when using model C, indicating that model C is certainly not to be disregarded completely. (A *very tentative value* for the enthalpy change for the formation of the complex [2,1,5] could be calculated using model B and C.)

Table 3.1.2 Calculated ΔH° and $T\Delta S^\circ$ values for the formation of some Mo(VI)-oxalate complexes. 1 M (Na)Cl at 298.15 K

COMPLEX	model B		model C		model A	
	ΔH° (kJ mol ⁻¹)	$T\Delta S^\circ$ (kJ mol ⁻¹)	ΔH° (kJ mol ⁻¹)	$T\Delta S^\circ$ (kJ mol ⁻¹)	ΔH° (kJ mol ⁻¹)	$T\Delta S^\circ$ (kJ mol ⁻¹)
[1,1,2] ²⁻	-59.4 ± 1.0	19	-59.4 ± 1.0	19	-59.3 ± 1.0	19
[1,1,3] ⁻	-57.9 ± 2.0	30	-57.0 ± 2.0	32	-	-
[2,2,5] ³⁻	-118.1 ± 4.0	60	-116.1 ± 3.0	59	-121.7 ± 4.0	56
[2,2,6] ²⁻	-118.9 ± 2.0	76	-117.2 ± 2.0	77	-114.7 ± 4.0	80
[4,4,10] ⁶⁻	-	-	-250 ± 10	119	-	-
[2,1,5] ⁻	-92 ± 15 #	56 #	-92 ± 15 #	56 #		
# very tentative values						

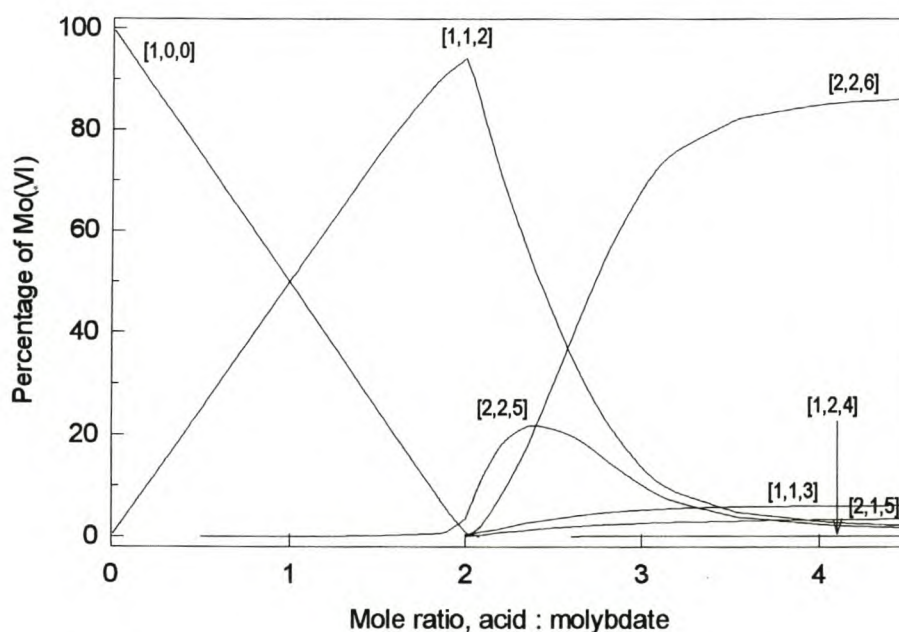


Fig. 3.1.5 Concentration of molybdate(VI)-oxalate complexes, expressed as a percentage of the total molybdenum(VI) concentration, as a function of the molar ratio of acid to molybdate(VI) for a titration of 0.05 M molybdate(VI) and 0.05 M oxalate.

3.1.2 Tungsten(VI)-oxalate system

3.1.2.1 Potentiometric data and analysis

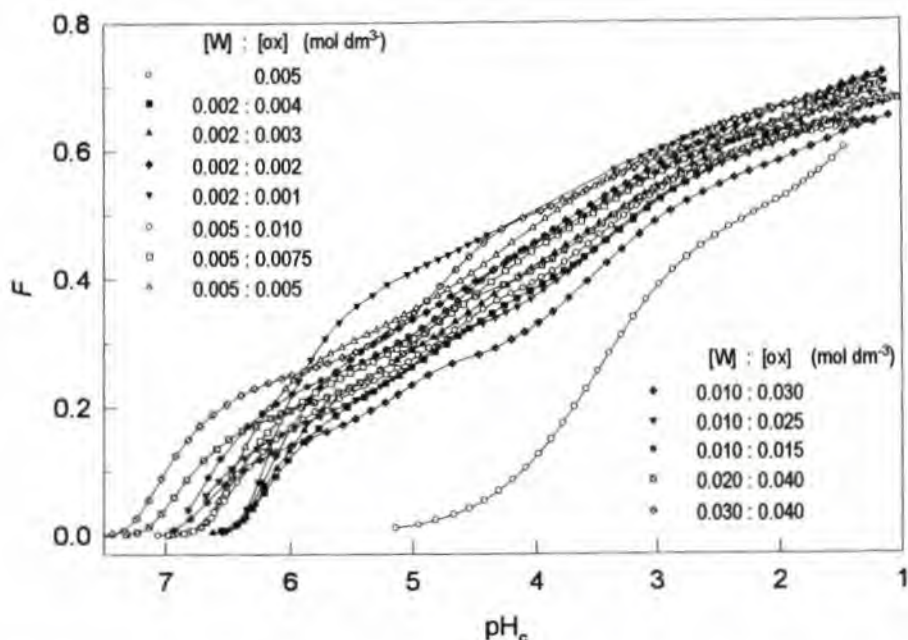


Fig. 3.1.6 Function F versus pH_c for some representative potentiometric titrations of the tungstate(VI)-oxalate system.

F curves

Most of the F curves are well defined, even in the region of slow equilibria (pH 4.5 to 3.2), except the curve pertaining to the titration of a solution with an excess of tungstate. The first parts of the F curves pertaining to the W-oxalate system (Fig. 3.1.6) are clearly quite different to the first parts of the F curves pertaining to the Mo-oxalate system (Fig. 3.1.1). If the F curves (Fig. 3.1.6) are compared with the distribution curve (Fig. 3.1.7+8) it can be seen that the clear inflexions of the W-oxalate curves at pH 6.5 to 5.5 coincide with the complete conversion of tungstate to the polytungstates, [7,0,8] and [12,0,14]. In both the W-oxalate and the Mo-oxalate systems the [1,1,2] complex is the first major complex formed upon acidification (Fig. 3.1.7, Fig. 3.1.2). Whereas the inflexion caused by the complete conversion of molybdate to [1Mo,1ox,2] is very clear (Fig. 3.1.1), the complete conversion of polytungstates to [1W,1ox,2] is barely noticeable since the polytungstates are already a product of protonation. The F curves pertaining to the equimolar solutions show an inflexion at $F \sim 0.63$ ($\text{pH} \sim 2.5$) which corresponds with the formation of the major complex in that pH region, [2,2,5], for which $r / (2p+2q) = 0.63$.

Modelling of the W-oxalate systems (species, $\log\beta$, ΔG°)

Preliminary calculations clearly showed that in order to attain a very good fit, complexes with the p:q ratio of 1:1, 2:2, 2:1 and 1:2 were needed in the model and, furthermore, that the complexes [1,1,2], [1,1,3], [2,2,5] and [1,2,4] could be regarded as certain. In addition, the complexes [2,1,5], [2,2,4] and [2,2,6] were accepted in the model easily (with improvement of fit). The complexes [4,2,8], [4,4,9] and [4,4,10] could at times be added to the model, but sometimes also replaced the complexes [2,1,5] and [2,2,6]. The fit, however, did not improve significantly, so that the simpler (more conservative) model, consisting of the complexes [1,1,2], [1,1,3], [2,2,4], [2,2,5], [2,2,6], [1,2,4] and [2,1,5] was accepted as a good working model (model A, $\sigma = 0.77$, $\chi^2 = 35$). The relative standard deviations of the complexes [1,1,3], [2,1,5] and [2,2,6], 21%, 24% and 21%, respectively, were rather high, but these species were accepted on the grounds that they also occurred in the corresponding molybdate-oxalate system.

The model in which [4,4,9] and [4,4,10] were added, and [2,1,5] was replaced by [4,2,8] was considered an interesting alternative to the simple model A (model B, $\sigma = 0.70$, $\chi^2 = 63$). Although the overall fit was not much better, it was interesting to note that the standard deviations of all the species, except the minor species [2,2,4], were $\leq 18\%$ in this model. In the molybdate-oxalate system the [4,4,r] and [4,2,8] complexes were also sometimes accepted as minor species, but it was decided to use the simpler model for further calculations. In the case of the tungstate-oxalate system, however, the percentage concentrations of these species were such that they could not simply be regarded as minor species if included in the model. Due to the greater uncertainties (possible inaccuracies of measurements) in the tungstate-ligand systems due to slow reactions it was decided not to choose between the models, but to present them as alternative models.

Table 3.1.3 Tungstate(VI)-oxalate complexes identified and calculated $\log\beta$ and ΔG° values.
1 M (Na)Cl at 298.15 K

COMPLEX	Simple model (model A, $\sigma = 0.77$, $\chi^2 = 35$)		Alternative model (model B, $\sigma = 0.70$, $\chi^2 = 63$)	
	$\log\beta_{pqr} \pm 3\sigma$	ΔG° (kJ mol ⁻¹)	$\log\beta_{pqr} \pm 3\sigma$	ΔG° (kJ mol ⁻¹)
[1,1,2] ²⁻	13.65 ± 0.02	-77.9	13.66 ± 0.02	-77.9
[1,1,3] ⁻	15.89 ± 0.32	-90.7	16.11 ± 0.13	-91.9
[2,2,4] ⁴⁻	28.43 ± 0.18	-162.0	28.18 ± 0.39	-160.8
[2,2,5] ³⁻	33.09 ± 0.04	-188.8	32.87 ± 0.11	-187.6
[2,2,6] ²⁻	34.52 ± 0.31	-197.0	34.57 ± 0.27	-197.3
[2,1,5] ⁻	28.24 ± 0.24	-161.1		
[1,2,4] ²⁻	21.53 ± 0.35	-122.9	21.50 ± 0.21	-122.7
[4,2,8] ⁴⁻			55.24 ± 0.25	-315.2
[4,4,9] ⁷⁻			64.10 ± 0.25	-365.8
[4,4,10] ⁶⁻			67.99 ± 0.25	-388.0

The similarity between these models A and B with the models B and C of the molybdate-oxalate system is striking. Just as in the case of the Mo-oxalate system the inclusion of the tetramers, [4,2,r] and [4,4,r], is achieved mostly at the cost of the dimers.

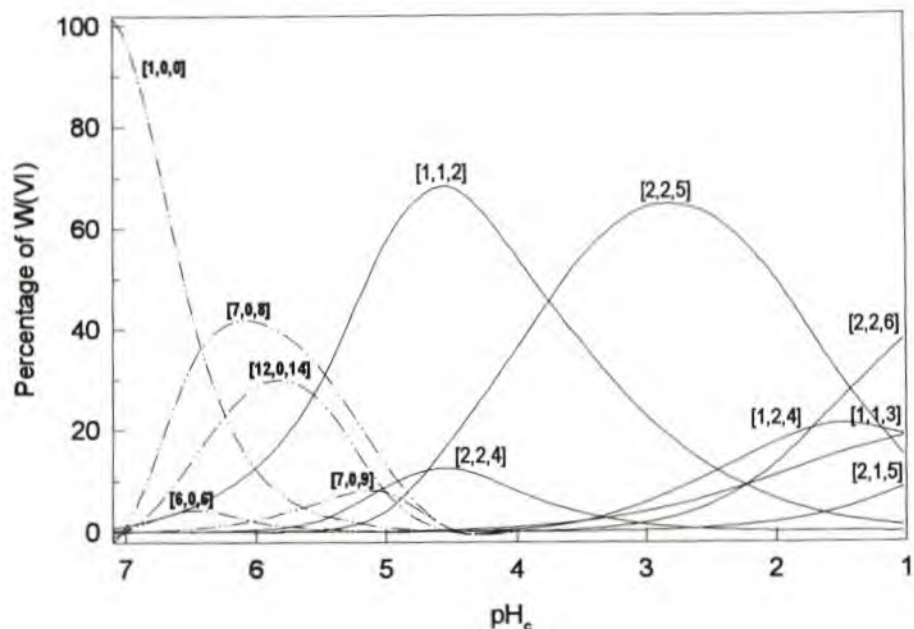
Distribution of species

Fig. 3.1.7 Concentration of tungstate(VI)-oxalate complexes and uncomplexed polytungstates, expressed as a percentage of the total tungsten(VI) concentration, as a function of pH_c . The total concentrations of tungstate(VI) and oxalate are 0.01 M and 0.025 M, respectively.

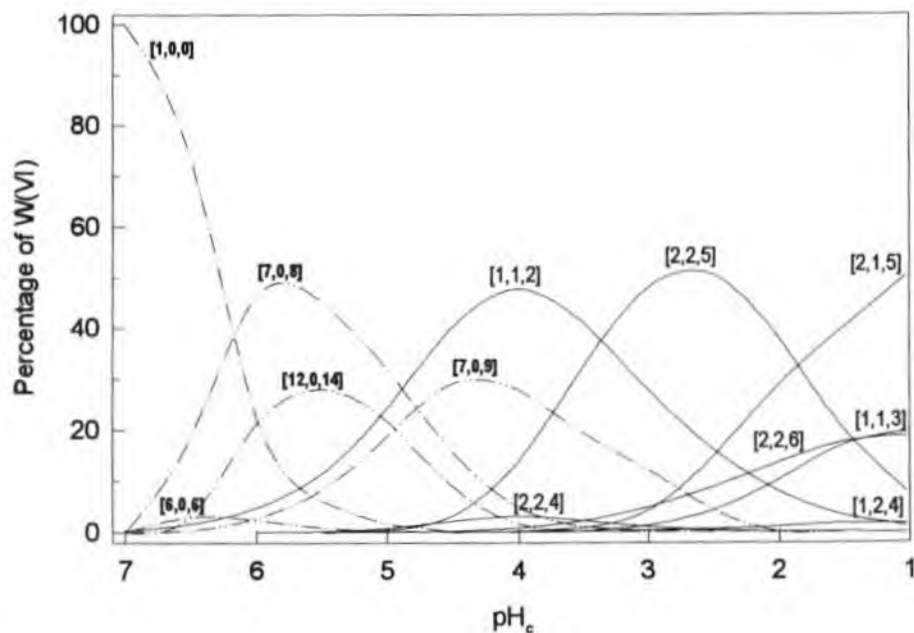


Fig. 3.1.8 Concentration of tungstate(VI)-oxalate complexes and uncomplexed polytungstates, expressed as a percentage of the total tungsten(VI) concentration, as a function of pH_c . The total concentrations of tungstate(VI) and oxalate are both 0.005 M.

The percentages of the uncomplexed polytungstates are also shown to explain the obvious difference in the F curves at $\text{pH} > 4$ of the molybdate-oxalate and tungstate-oxalate systems.

According to Fig. 3.1.8, the [7,0,9] tungstate species is the highest protonated polytungstate present, and exists in the pH range 6 to 2. The tungstate model is known not to be valid from $\text{pH} \sim 4.5$ and below. The [7,0,9] probably represents itself, as well as other, as yet unknown, tungstate species. Wherever this approximate tungstate model predicts [7,0,9] species as the major tungstate species, slow reactions occur, as has been shown in this tungstate-oxalate system (Appendix 1).

3.1.2.2 Enthalpimetric data and analysis

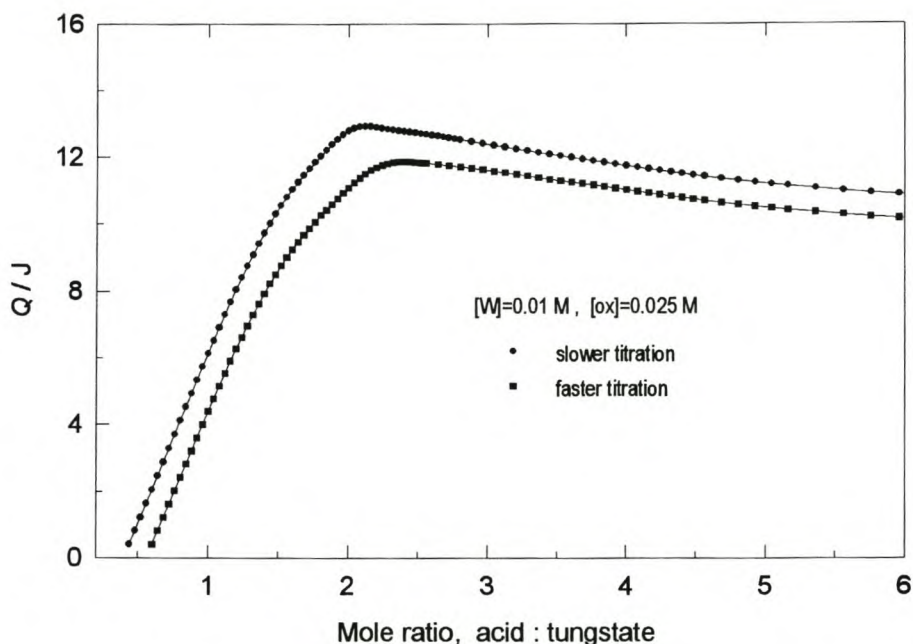


Fig. 3.1.9 Measured heat, Q , as a function of the molar ratio of acid to tungstate(VI) for a titration of 0.01 M tungstate(VI) and 0.025 M oxalate.

Calculation of enthalpy and entropy

The potentiometric model shows that the first important species which form upon acidification of tungstate-oxalate solutions are polytungstates. The first predominant complex, [1,1,2], does not form at high enough pH to avoid slow reactions of uncomplexed tungstate. The titration condition chosen is not ideal, but it was believed that it would be the best condition for calculating approximate enthalpy values for the predominant complexes. (The concentration of reactants should ideally be higher to ensure greater accuracy of the

measured heat, and lower, to minimize slow reactions.) An indication of the non-ideal conditions, in which slow reactions take place at pH 6-5, is the difference in the *shapes* of the curves of Q vs mole ratio of acid added to tungstate for the faster and the slower titration of the same solution (Fig. 3.1.9). (The difference in the *height* of the curves is mainly as the result of defining the first data point of each titration differently.) The Q curve pertaining to the slower titration shows a distinct break at a mole ratio of 2:1 in accordance with the stoichiometry of the major complex identified from the potentiometric measurements, [1,1,2], for which $r/p = 2$. The slight inflexion at a mole ratio of $\sim 1.2:1$ at higher pH is the result of the almost complete conversion of tungstate to a few polytungstates, for which the average r/p value is ~ 1.2 . The major inflexion of the Q curve pertaining to the faster titration is at a mole ratio of ~ 2.3 . This value does not agree with the formation of a major complex at equilibrium. This shift of the inflexion point (from 2 to 2.3 pertaining to the two titrations) is due to the slow reactions, the heat of which cannot be measured accurately during a relatively fast titration. It must be concluded that the measurements of the slower titrations are better, although also not quite representative of equilibrium conditions. The data from the slower titration was preferred and used to calculate approximate values for the change of enthalpy for the formation of the complexes. The data points pertaining to the region of slow equilibria were ignored. The polytungstates were included in the model and their ΔH° values fixed during calculations (Table 2.7).

The Q values change very little for the mole ratio, acid:tungstate > 4 (which coincides with a pH < 2.8). Furthermore, the percentage concentration of four complexes increases upon further acidification (Fig. 3.1.7). It was, therefore, difficult to calculate unique values for the enthalpy of these complexes and these lower pH data points were ignored in the final calculations.

Included in the measured heat is the contribution from the protonation of oxalate, which is in excess. To account for the heat involved in the protonation of free oxalate the values for the change in enthalpy for these reactions were determined in a separate titration. The values obtained after correcting for the endothermic heat of dilution were $\Delta H^\circ_{011} = + 3.17 \text{ kJ mol}^{-1}$ and $\Delta H^\circ_{012} = + 5.18 \text{ kJ mol}^{-1}$. Since the percentage concentration of the H_2Ox^- species $< 1\%$, its inclusion was not justified in the calculations.

Both models A and B (Table 3.1.3) were used to calculate the ΔH° values for the formation of the complexes listed in Table 3.1.4. The ΔH° values of the major complexes [1,1,2] and [2,2,5] as well as the minor complexes [1,1,3], [2,2,6] and [1,2,4] change very little with change in the model despite the very few data points which represent the latter species (Table 3.1.4). The ΔH° value of the [2,2,4] is, however, model dependent, being significantly greater when the calculation is based on model A. The species [4,4,9] and [4,4,10] compete with the [2,2,4] complex in the model B. This is indicated by the smaller formation constant for [2,2,4] in model B (Table 3.1.3) and by the smaller ΔH° value. The ΔH° values for [4,4,9] and [4,4,10] are very similar. The ΔH° values for the complexes [2,1,5] and [4,2,8] could not be calculated as their percentage concentrations were $< 1\%$. The fit of the enthalpimetric model is slightly better when model B is used, indicating that this model certainly must not to be disregarded. The better fit could, however, simply be the result of the greater number of species present, some of which could be used as adjustable parameters.

Table 3.1.4 Calculated ΔH° and $T\Delta S^\circ$ values for the formation of some W(VI)-oxalate complexes.
1 M (Na)Cl at 298.15 K

COMPLEX	model A		model B	
	ΔH° (kJ mol ⁻¹)	$T\Delta S^\circ$ (kJ mol ⁻¹)	ΔH° (kJ mol ⁻¹)	$T\Delta S^\circ$ (kJ mol ⁻¹)
[0,1,1] ⁻	+3.17 ± 0.5	23.3	+3.17 ± 2	23.3
[0,1,2]	+5.18 ± 0.5	30.4	+5.18 ± 0.5	30.4
[1,1,2] ²⁻	-70.8 ± 0.5	7.1	-70.4 ± 0.5	7.5
[1,1,3] ⁻	-66.7 ± 1.0	24.0	-66.9 ± 1.0	25.0
[2,2,4] ⁴⁻	-116 ± 5	46	-106 ± 8	55
[2,2,5] ³⁻	-137.7 ± 2.0	51.1	-139.7 ± 2.0	47.9
[2,2,6] ²⁻	-138 ± 4	59	-136 ± 4	61
[2,1,5] ⁻	-	-	-	-
[1,2,4] ²⁻	-86.5 ± 5	36	-88 ± 5	35
[4,4,9] ²⁻	-	-	-277 ± 5	89
[4,4,10] ²⁻	-	-	-279 ± 5	109
[4,2,8] ⁴⁻	-	-	-	-

Literature enthalpy values for oxalate pertaining to ionic strength 1 M are $\Delta H^\circ_{011} = + 2.71 \text{ kJ mol}^{-1}$ [131].

3.2 COMPLEXATION WITH LACTATE

3.2.1 Molybdenum(VI)-lactate system

3.2.1.1 Potentiometric data and analysis

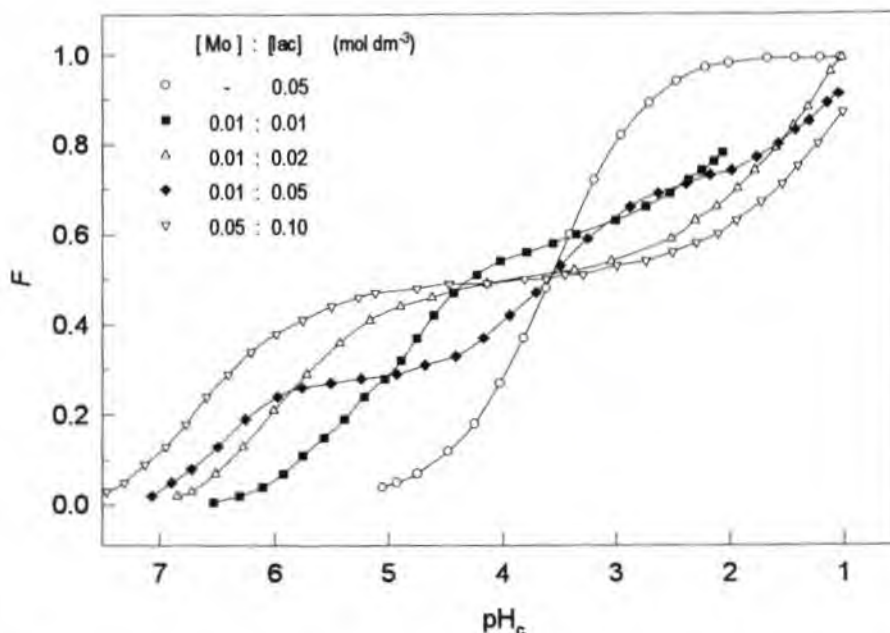


Fig 3.2.1. Function F versus pH_c for some representative potentiometric titrations of the molybdate(VI)-lactate system.

F curves

Figure 3.2.1 shows that complex formation results in the uptake of protons at much higher pH than in the case of lactate alone. At low pH on the other hand, protonation of the complexes is more difficult than protonation of lactate. The inflexions exhibited by the curves pertaining to excess of lactate show that after all molybdate has reacted very little protonation takes place until the pH is low enough ($\sim < 5$) for free lactate to become protonated and F then increases again. The inflexion at $F = 0.5$ (at pH 5-2) exhibited by the curves pertaining to the solutions with a two-fold excess of lactate corresponds with the formation of the major complex in that pH region, namely the [1,2,2] complex, for which $r / (2p+q) = 0.5$.

Modelling of the lactate and Mo-lactate systems (species, $\log \beta$, ΔG°)

The protonation constant of lactate, which was calculated from data obtained from the titration of lactate, is shown in Table 3.2.1 and was used to produce a species distribution diagram of the lactate system (Appendix 2).

Preliminary calculations of the data of the complex system showed that one species, namely the [1,2,2] complex, predominated in the range pH 2-7. The addition of the two dilactate species, [1,2,1] and [1,2,3], together with some other minor species, [1,1,*r*], [2,2,*r*] and [2,1,*r*], resulted in a very good fit between the experimental and calculated pH-values ($\sigma = 1.25$). Two of these species, [1,2,1] and [2,1,3], have relatively high standard deviations of 30% and 26%, respectively, which are very close to the rejection limit. Since the maximum percentage concentration of these species never exceeds 3% in any of the titrations, their inclusion in the model does not seem justified. Their inclusion in the model, however, does not affect the value of the formation constants of the important complexes significantly. Consequently they were retained in the best reaction model (Table 3.2.1) for the sake of completeness.

Table 3.2.1 Molybdate(VI)-lactate complexes identified and calculated $\log\beta$ and ΔG° values. 1 M (Na)Cl at 298.15 K

COMPLEX	$\log\beta_{pqr} \pm 3\sigma$	ΔG° (kJ mol ⁻¹)
[0,1,1] ⁻	3.60 ± 0.01 (3.63)	-20.53
[1,2,1] ³⁻	7.46 ± 0.46	-42.67
[1,2,2] ²⁻	15.71 ± 0.01	-89.67
[1,2,3] ⁻	16.78 ± 0.09	-95.75
[1,1,2] ⁻	11.76 ± 0.03	-67.10
[1,1,3]	12.66 ± 0.32	-72.24
[2,2,2] ⁴⁻	16.07 ± 0.14	-91.70
[2,2,3] ³⁻	21.70 ± 0.14	-123.8
[2,2,4] ²⁻	24.97 ± 0.30	-142.5
[2,1,3] ²⁻	18.44 ± 0.38	-105.2
[2,1,4] ⁻	21.53 ± 0.12	-122.9
[2,1,5]	23.12 ± 0.14	-132.0

Literature value pertaining to 1 M NaClO₄ medium in brackets [132].

Only the [1,2,2] and [2,2,4] complexes have been proposed in previous investigations [17-19, 92-93,104]. To check for consistency of this rather complicated model, the protonation constant of lactate was refined together with the constants of the complexes in the final computer run. The value obtained for $\log\beta_{011}$, namely 3.603, was in excellent agreement with that obtained from the separate titrations, namely 3.597.

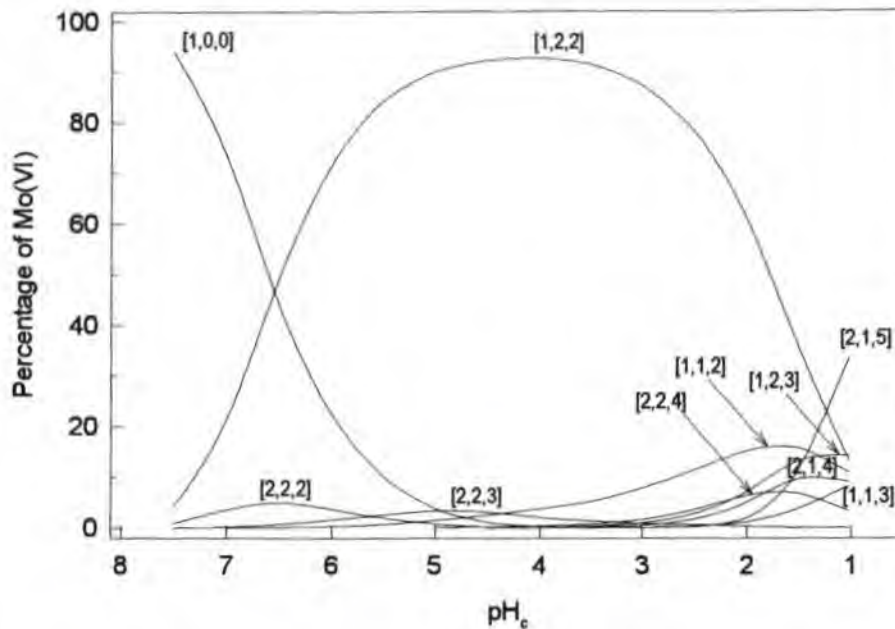
Distribution of species

Fig. 3.2.2 Concentration of molybdate(VI)-lactate complexes, expressed as a percentage of the total molybdenum(VI) concentration, as a function of pH_c . The total concentrations of molybdate(VI) and lactate are 0.05 M and 0.1 M, respectively.

3.2.1.2 Enthalpimetric data and analysis

Calculation of enthalpy and entropy

The plot of Q vs mole ratio of acid added to molybdate (Fig. 3.2.3) shows a break at a mole ratio of approximately 2:1 in accordance with the stoichiometry of the major complex identified from the potentiometric measurements, [1,2,2], for which $r/p=2$. Included in the measured heat is the contribution from the protonation of lactate, which is relatively small, despite the five-fold excess of lactate. (An excess of lactate is essential to ensure complete complexation of molybdate upon acidification, thereby excluding side-reactions involving polyanion formation.) To account for the heat involved in the protonation of free lactate the enthalpy change for the reaction was determined in a separate titration (Table 3.2.2).

Owing to the very small concentrations of the minor complexes under the conditions of the enthalpimetric titrations, calculation of their ΔH° values was not justified, especially at low pH where several equilibria overlap and very little heat is measured. The enthalpy change for the formation of the [1,2,2] complex was calculated from the data represented by the first straight-line segment of the curves (Fig. 3.2.3.) and for which the concentrations of the other complexes were less than 2%.

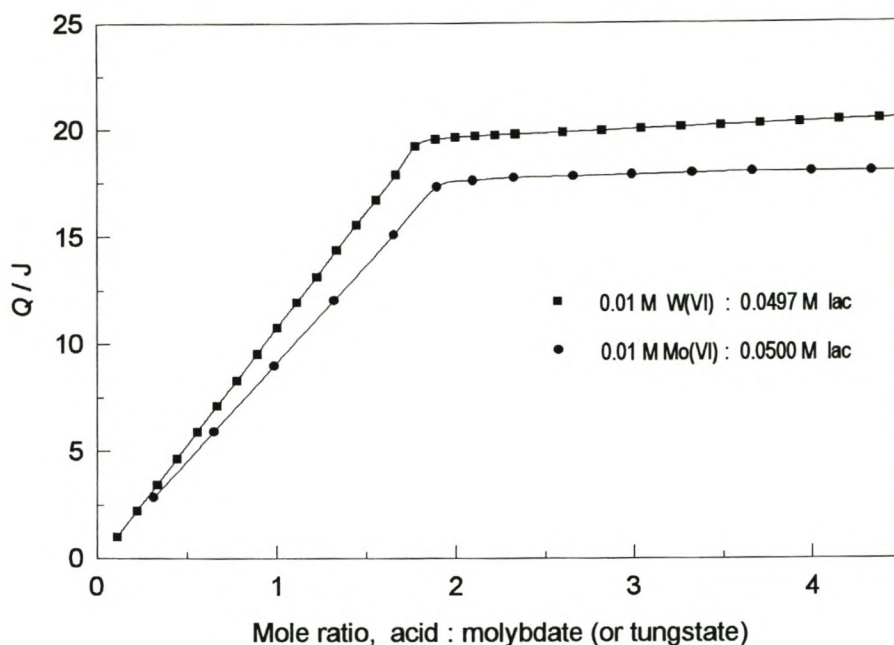


Fig. 3.2.3 Measured heat, Q , as a function of the molar ratio of acid to molybdate(VI) for a titration of 0.01 M molybdate(VI) and 0.05 M lactate. (A similar titration of tungstate(VI) and lactate is also shown for comparison.)

Table 3.2.2 Calculated ΔH° and $T\Delta S^\circ$ values for the formation of some Mo(VI)-lactate complexes. 1 M (Na)Cl at 298.15 K

COMPLEX	ΔH° (kJ mol ⁻¹)	$T\Delta S^\circ$ (kJ mol ⁻¹)
[0,1,1]	-1.7 ± 2	18.8
[1,2,2] ²⁻	-72 ± 2	18

The ΔH°_{011} value can be compared with those given by Smith and Martell [133], 0.33 and -7.1 kJ mol⁻¹ at ionic strengths $I = 0$ and 2.0 M respectively.

3.2.2 Tungsten(VI)-lactate system

3.2.2.1 Potentiometric data and analysis

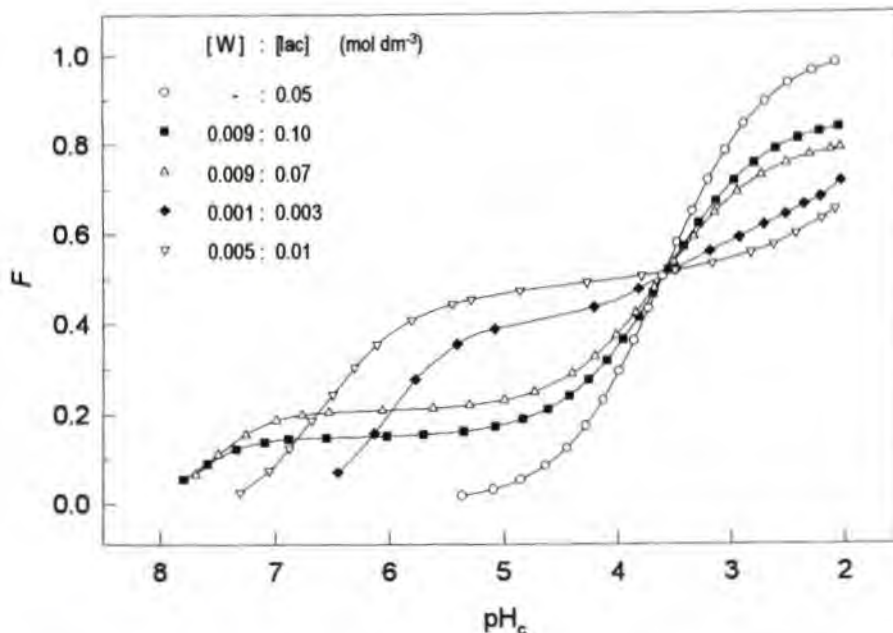


Fig.3.2.4 Function F versus pH_c for some representative potentiometric titrations of the tungstate(VI)-lactate system.

F curves

As in the case of the F curves for the Mo-lactate system, it is seen that complex formation results in the uptake of protons at much higher pH than in the case of lactate alone (Fig. 3.2.4). At low pH on the other hand, protonation of the complexes is more difficult than protonation of lactate. The inflexions exhibited by the curves pertaining to an excess of lactate show that after all tungstate has reacted very little protonation takes place until the pH is low enough ($\sim < 5$) for free lactate to become protonated and F then increases again. The inflexion at $F = 0.5$ (at pH 5-3) exhibited by the curves pertaining to solutions with a two-fold excess of lactate corresponds with the formation of the major complex in that pH region, the [1,2,2] complex, for which $r / (2p+q) = 0.5$.

Modelling of the W-lactate system (species, $\log\beta$, ΔG°)

Preliminary calculations showed that, as in the case with the Mo-lactate-system, the [1,2,2] complex predominated in the range pH 2-7 of the W-lactate system. Fewer minor species were identified than in the Mo-lactate-system because slow reactions necessitated restrictions on the experimental conditions. The species retained in the best model, however, all had analogues in the model for the Mo-lactate system and all the formation constants had relative standard deviations of less than 10%. Given the experimental

constraints, a satisfactory fit ($\sigma = 1.8$) was obtained. The value for the formation constants of the various complexes are listed in Table 3.2.3.

Table 3.2.3 Tungstate(VI)-lactate complexes identified and calculated $\log\beta$ and ΔG° values. 1 M (Na)Cl at 298.15 K

COMPLEX	$\log\beta_{\text{pqr}} \pm 3\sigma$	ΔG° (kJ mol ⁻¹)
[0,1,1] ⁻	3.60 ± 0.01	-20.53
[1,2,2] ²⁻	17.47 ± 0.01	-99.72
[1,2,3] ⁻	18.38 ± 0.11	-104.9
[1,1,2] ⁻	13.03 ± 0.07	-74.35
[1,1,3]	14.56 ± 0.13	-83.1
[2,2,3] ³⁻	25.47 ± 0.11	-145.3

Only the [1,2,2] complex has been previously determined with certainty [93]. Therefore the protonation constant of lactate was refined together with the constants of the complexes in the final computer run to check for consistency. The value obtained for $\log\beta_{011}$, 3.596, is in excellent agreement with that obtained from the separate titrations, 3.597. All the W-lactate complexes identified had Mo-lactate analogues.

Distribution of species

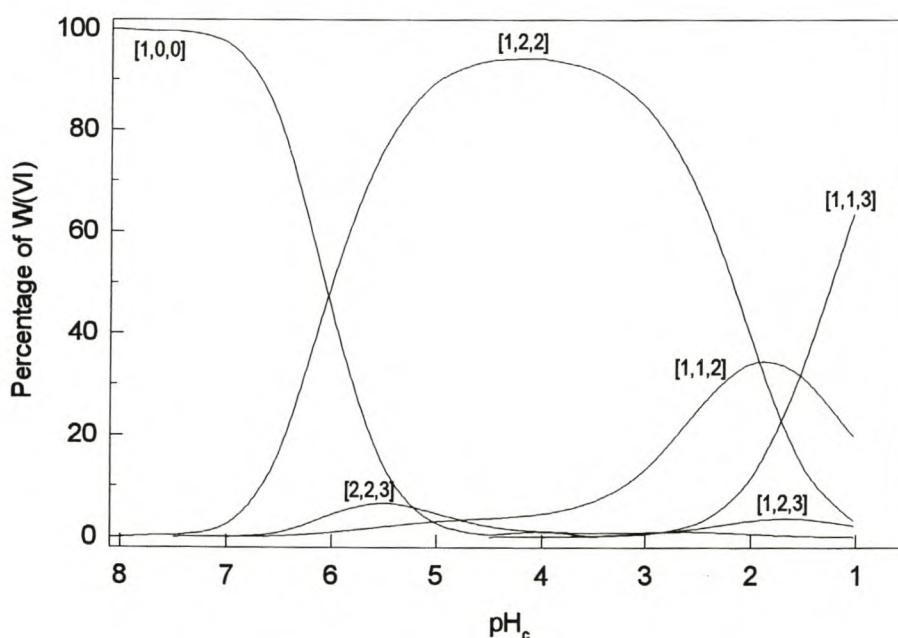


Fig. 3.2.5 Concentration of tungstate(VI)-lactate complexes, expressed as a percentage of the total tungsten(VI) concentration, as a function of pH_c . The total concentrations of tungstate(VI) and lactate are 0.001 M and 0.003 M, respectively.

3.2.2.2 Enthalpimetric data and analysis

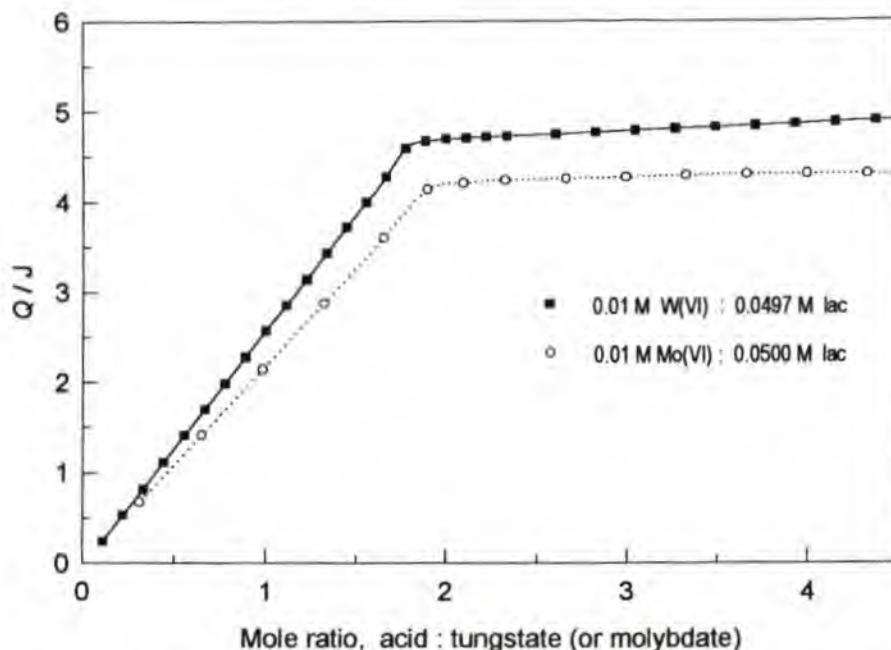


Fig. 3.2.6 Measured heat, Q , as a function of the molar ratio of acid to tungstate(VI) for a titration of 0.01 M tungstate(VI) and 0.0497 M lactate. (A similar titration of molybdate(VI) and lactate is also shown for comparison.)

The plot of Q vs mole ratio of acid added to tungstate (Fig. 3.2.6) shows a break at a mole ratio of approximately 2:1 in accordance with the stoichiometry of the major complex identified from the potentiometric measurements, namely [1,2,2]. Included in the measured heat is the contribution from the protonation of lactate which is relatively small despite the five-fold excess of lactate. (An excess of lactate is essential to ensure complete complexation of tungstate upon acidification, thereby excluding side-reactions involving polyanion formation.) To account for the heat involved in the protonation of free lactate, $\Delta H_{011}^{\circ} = -1.7 \text{ kJ mol}^{-1}$ was used in calculations (Table 3.2.2).

Owing to the very small concentrations of the minor complexes under the conditions of the enthalpimetric titrations, calculation of their ΔH° values was not justified, especially at low pH where several equilibria overlap and very little heat was measured. The enthalpy change for the formation of the [1,2,2] complex was calculated from the data represented by the first straight-line segment of the curves (Fig. 3.2.6) and for which the concentrations of the other complexes were less than 2%.

Table 3.2.4 Calculated ΔH° and $T\Delta S^{\circ}$ values for the formation of some W(VI)-lactate complexes. 1 M (Na)Cl at 298.15 K

COMPLEX	ΔH° (kJ mol ⁻¹)	$T\Delta S^{\circ}$ (kJ mol ⁻¹)
[0,1,1]	-1.7 ± 2	18.8
[1,2,2] ²⁻	-80 ± 2	20

3.3 COMPLEXATION WITH MANDELATE

3.3.1 Molybdenum(VI)-mandelate system

3.3.1.1 Potentiometric data and analysis

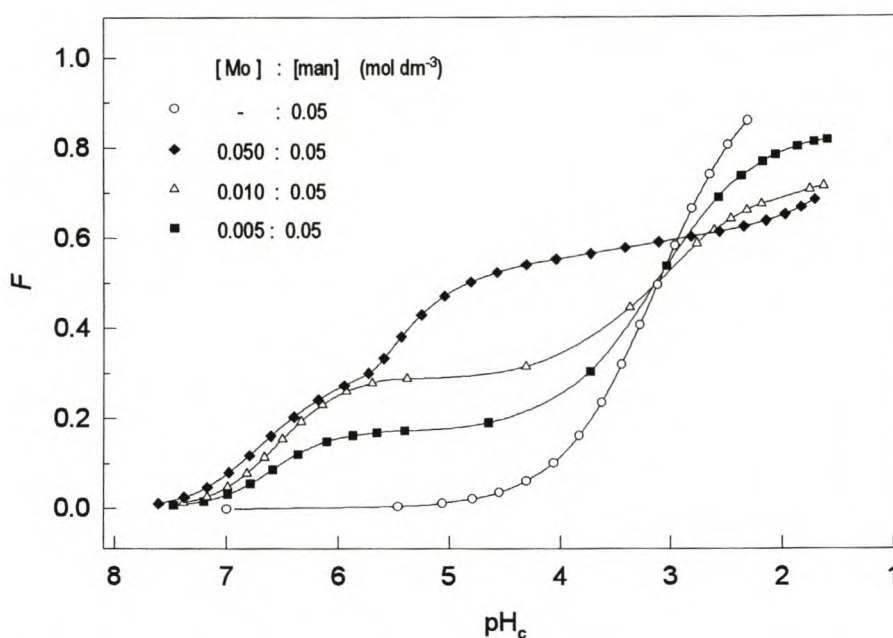


Fig 3.3.1 Function F versus pH_c for some representative potentiometric titrations of the molybdate(VI)-mandelate system.

F curves

The F curves (Fig 3.3.1) show that complexation starts at pH 7-8 resulting in a sharp increase in F values until at low pH the protonation of the complexes becomes more difficult than that of mandelate itself. The inflexions exhibited by the curves pertaining to an excess of mandelate show that after all the molybdate has reacted very little protonation takes place until the pH is low enough (~ 4.5) for free mandelate to become protonated and F increases again. The F value pertaining to the titrations with excess mandelate changes little in the pH region 6-4.5 which correlates with the existence of a predominant species [1,2,2] in this region, for which $r / (2q+q) = 0.5$ (Fig. 3.3.2).

Modelling of the mandelate and Mo-mandelate systems (species, $\log\beta$, ΔG°)

The protonation constant of mandelate, which was calculated from data obtained from the titration of mandelate, is shown in Table 3.3.1 and was used to produce a species distribution diagram of the mandelate system (Appendix 2).

The [1,2,2] complex predominates over a wide pH range in the Mo-mandelate system. A number of minor species also occur in the best model (Table 3.3.1) ($\sigma = 0.99$ and $\chi^2 = 1.21$). Except for the [1,2,1] and [1,2,3] complexes with relative standard deviations of ~20%, the relative standard deviations are all < 10%.

Table 3.3.1 Molybdate(VI)-mandelate complexes identified and calculated $\log\beta$ and ΔG° values.

1 M (Na)Cl at 298.15 K

COMPLEX	$\log\beta_{pqr} \pm 3\sigma$	ΔG° (kJ mol ⁻¹)
[0,1,1] ⁻	3.15 ± 0.01 (3.14)	-17.98
[1,2,1] ³⁻	7.80 ± 0.30	-44.5
[1,2,2] ²⁻	15.93 ± 0.01	-90.03
[1,2,3] ⁻	16.27 ± 0.29	-92.8
[1,1,1] ²⁻	6.83 ± 0.12	-39.0
[1,1,2] ⁻	11.57 ± 0.06	-66.0
[2,2,4] ²⁻	25.87 ± 0.03	-147.6
[2,2,5] ⁻	26.86 ± 0.12	-153.3
[2,1,3] ²⁻	19.00 ± 0.15	-108.4
[2,1,4] ⁻	21.18 ± 0.24	-120.9
[2,1,5]	23.00 ± 0.06	-131.2

Literature value pertaining to 1 M KNO₃ medium in brackets [134].

To check the model for consistency, the protonation constant of mandelate was refined together with the constants of the complexes in the final computer run. This extra refinement did not alter the model and the formation constants had the expected values.

Distribution of species

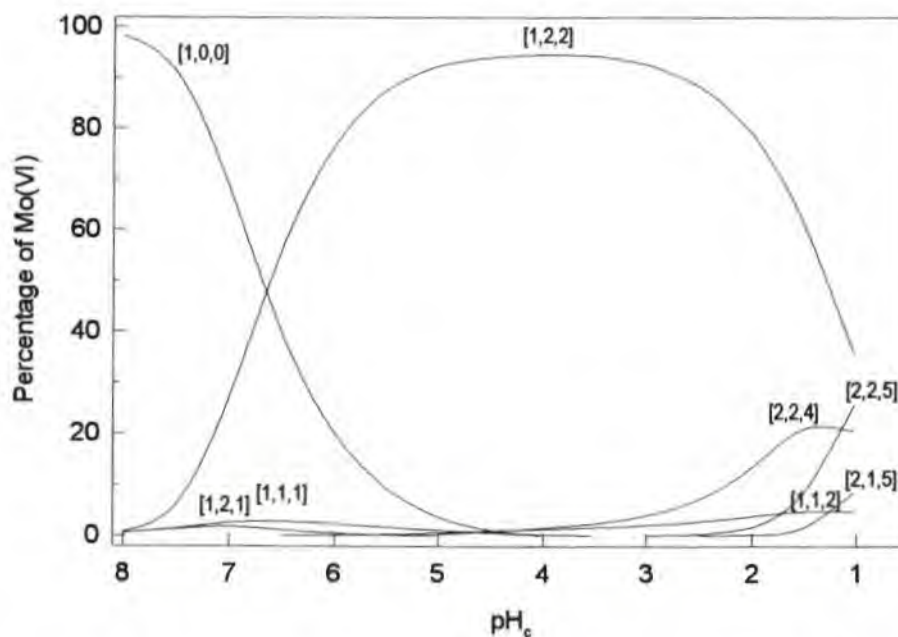


Fig. 3.3.2 Concentration of molybdate(VI)-mandelate complexes, expressed as a percentage of the total molybdenum(VI) concentration, as a function of pH_c . The total concentrations of molybdate(VI) and mandelate are 0.05 M and 0.1 M, respectively.

3.3.1.2 Spectrophotometric data and analysis

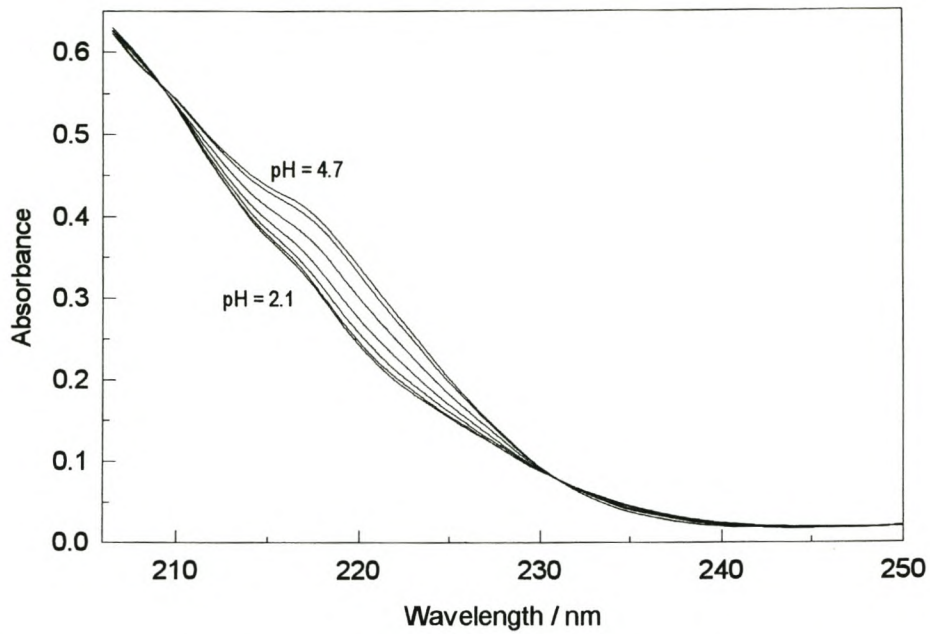


Fig. 3.3.3.1 Change in absorption spectra with pH_c ranging from 4.7 to 2.1. The total mandelate concentration is 0.0008 M.

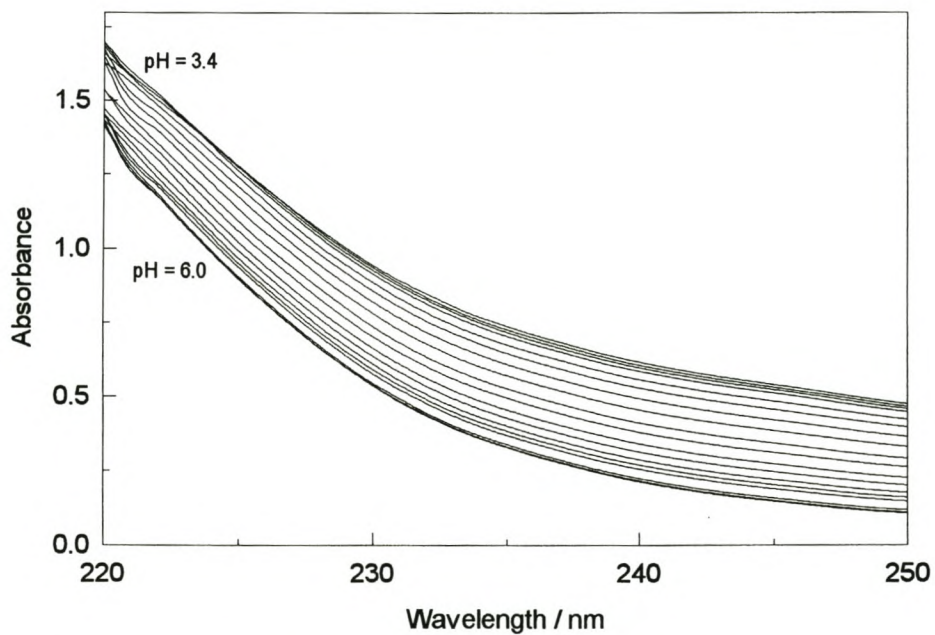


Fig. 3.3.3.2 Change in absorption spectra with pH_c ranging from 6.0 to 3.4. The total molybdate(VI) and mandelate concentration are 0.0002 M and 0.001 M, respectively.

Protonation constant and spectra of mandelate

The protonation constant of mandelate calculated with the program SQUAD from the experimental spectra, $\log/\beta_{011} = 3.16 \pm 0.01$, agrees very well with the value (3.15) obtained from the potentiometric data (Table 3.3.1). The spectra of mandelate [0,1,1] and mandelic acid [0,1,2] have been accurately determined and are shown in Fig. 3.3.4 below.

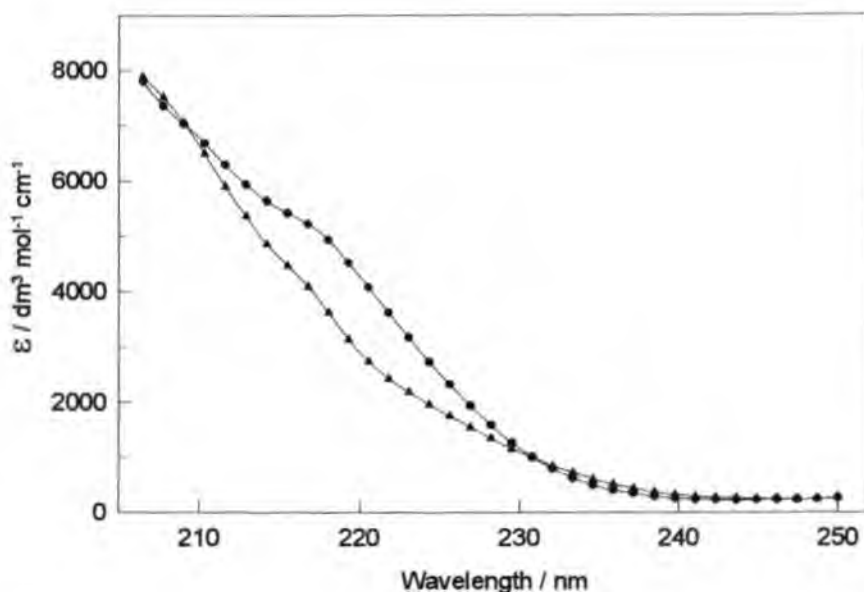


Fig. 3.3.4 Calculated molar absorption spectra of mandelic acid (▲) and mandelate (●).

Calculation of models (complexes, formation constants, absorption spectra)

The four- and five-fold excess of mandelate used in the spectrophotometric analysis (Appendix 1) was necessary to promote complex formation at the very low molybdate concentrations used. Because of this excess of ligand, its contribution to the total absorbance measured became comparable to that of molybdate. The spectra of mandelate and mandelic acid were therefore fixed during the calculations of the spectra and formation constants of the complexes.

Preliminary calculations, based on the potentiometric model, showed that under the conditions of the first titration (five-fold excess of mandelate) a maximum percentage concentration of about 90% of the [1,2,2] complex is present over the range pH 6-4, with less than 6% of the [1,1,2] species. Attempts to calculate the spectrum of [1,1,2] failed, so that in the final calculations this species had to be neglected. The data treated with SQUAD resulted in a good fit between experimental and calculated absorbances with the value of the formation constant of the [1,2,2] complex, $\log\beta_{122} = 16.01$, in very good agreement with that obtained by potentiometry (15.93), despite the simplified model used.

Preliminary calculations showed that under the conditions of the second titration (four-fold excess of mandelate) a maximum percentage concentration of about 25% of the [1,1,2] complex was present and that other minor complex species were negligible, but that a significant percentage of uncomplexed molybdate species, $[\text{HMoO}_4]^-$ ([1,0,1]) and in particular $[\text{MoO}_3(\text{H}_2\text{O})_3]$ ([1,0,2]) were present at $\text{pH} < 3$. The spectra and equilibrium constants of these two molybdenum species, known from previous work [125], were therefore also supplied to the program.

The data of the two titrations were then combined and the value calculated for the formation constant of the [1,1,2] complex, $\log \beta_{112} = 11.7$, agreed reasonably well with that obtained by potentiometry (11.57). The value now calculated for the formation constant of the [1,2,2] complex, $\log \beta_{122} = 16.03$, was practically the same as that obtained from the data of the first experiment alone. The spectra of the complexes are shown in Fig. 3.3.5.

Spectrophotometric analysis confirmed the two most important complex species and their formation constants calculated by potentiometry. Considering the big difference in the spectrophotometric and potentiometric conditions, and the limitations imposed particularly on the spectrophotometric experiments and the calculations, the confirmation of two species indicated the usefulness of the potentiometric method even for predicting species at low molybdate concentrations.

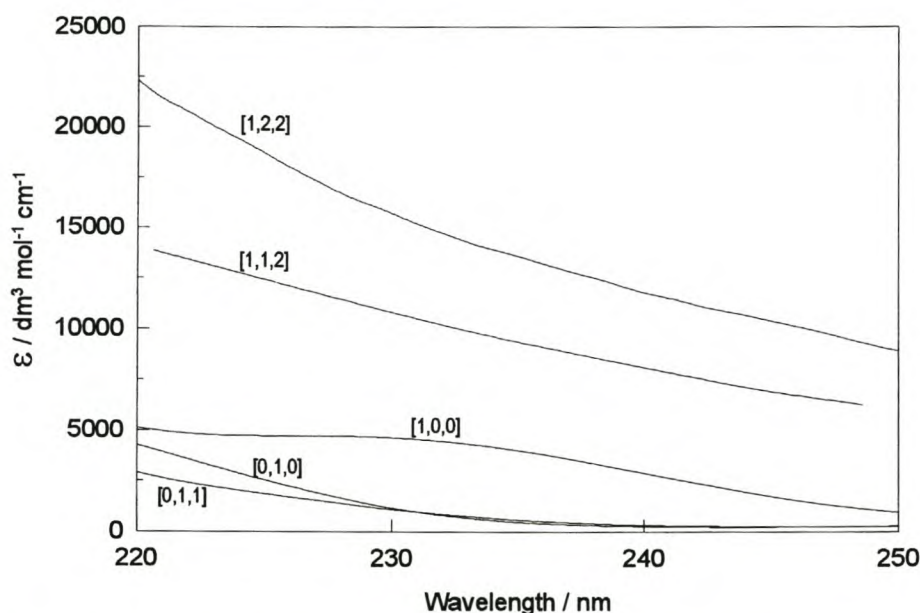


Fig. 3.3.5 Calculated molar absorption spectra of various species of the molybdenum(VI)-mandelate system.

3.3.1.3 Enthalpimetric data and analysis

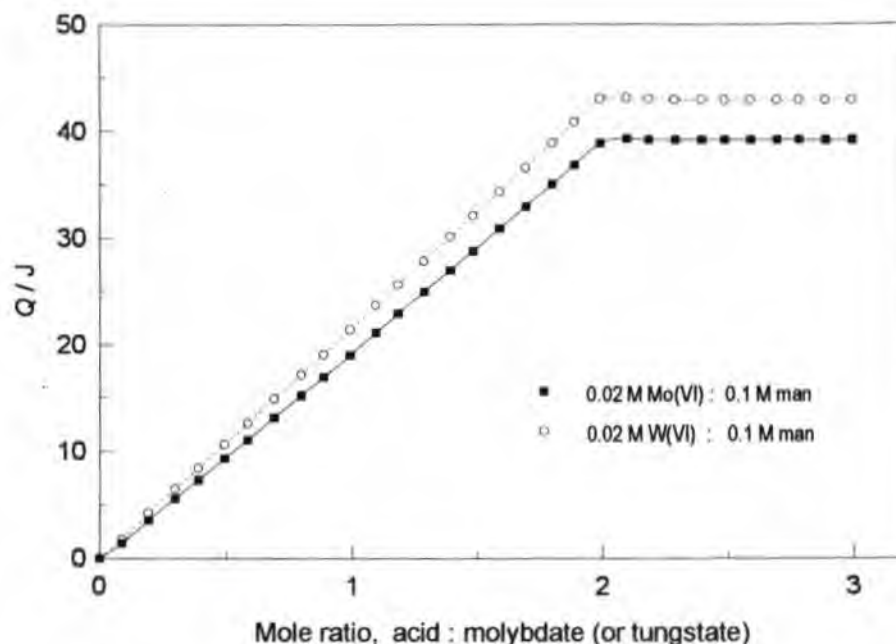


Fig. 3.3.6 Measured heat, Q , as a function of the molar ratio of acid to molybdate(VI) for a titration of 0.02 M molybdate(VI) and 0.1 M mandelate. (A similar titration of tungstate(VI) and mandelate is also shown for comparison.)

Calculation of enthalpy and entropy

The plot of Q vs mole ratio of acid added to molybdate (Fig. 3.3.6) shows a break at a mole ratio of approximately 2:1 in accordance with the stoichiometry of the major complex $[1,2,2]$, determined by potentiometry and spectrophotometry.

Included in the measured heat, is the contribution from the protonation of mandelate, which is relatively small despite the five-fold excess of mandelate. (An excess of mandelate was essential to ensure complete complexation of molybdate upon acidification, thereby excluding side-reactions involving polyanion formation.) To account for the heat involved in the protonation of free mandelate the enthalpy change for the reaction was determined in a separate titration (Table 3.3.2). The value obtained after correcting for the endothermic heat of dilution was $\Delta H_{011}^{\circ} = -0.5 \text{ kJ mol}^{-1}$, compared to the -1.7 kJ mol^{-1} determined for lactate under the same conditions (Table 3.2.2).

Under the chosen conditions minor complex species did not appear in measurable concentrations for most of the titration which simplified the calculation of the enthalpy changes.

Table 3.3.2 Calculated ΔH° and $T\Delta S^{\circ}$ values for the formation of some Mo(VI)-mandelate complexes. 1 M (Na)Cl at 298.15 K

COMPLEX	ΔH° (kJ mol ⁻¹)	$T\Delta S^{\circ}$ (kJ mol ⁻¹)
[0,1,1]	-0.5 ± 0.5	17.5
[1,2,2] ²⁻	-78.2 ± 0.5	12.7

3.3.2 Tungsten(VI)-mandelate system

3.3.2.1 Potentiometric data and analysis

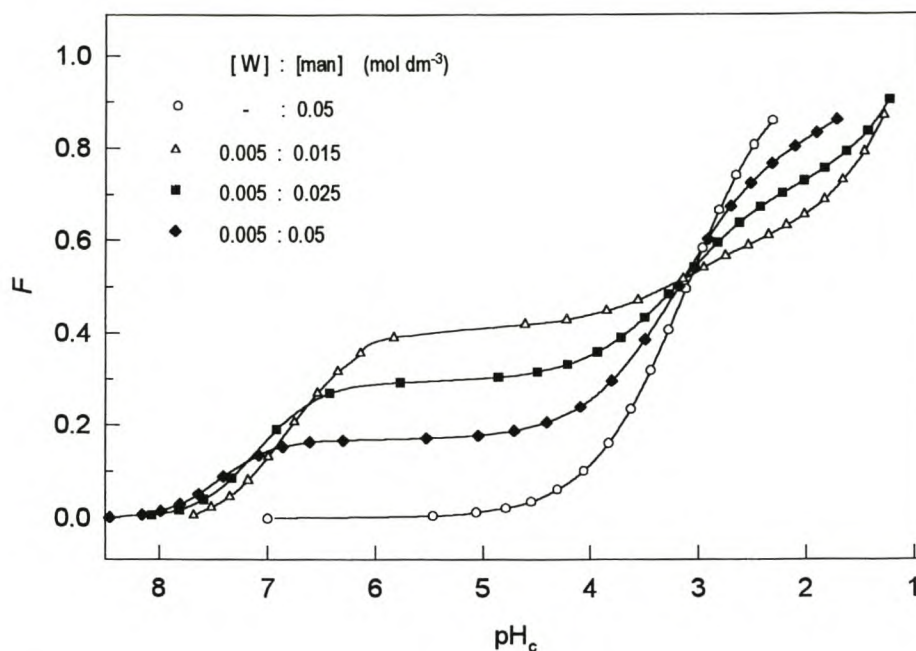


Fig. 3.3.7 Function F versus pH_c for some representative potentiometric titrations of the tungstate(VI)-mandelate system.

F curves

The F curves (Fig 3.3.7) show that complexation starts at $\text{pH} = 8$ resulting in a sharp increase in F values until at low pH the protonation of the complexes becomes more difficult than that of mandelate itself. The inflexions exhibited by the curves pertaining to an excess of mandelate show that, after all the tungstate has reacted, very little protonation takes place until the pH is low enough (~ 4.5) for free mandelate to become protonated and F increases again. The F value pertaining to the titrations with excess mandelate changes little in the pH region 6-4, which correlates with the existence of a predominant species, [1,2,2], in this region (Fig. 3.3.8).

Modelling of the W-mandelate systems (species, $\log\beta$, ΔG°)

Just as in the molybdate-mandelate system, the di-mandelate complex, [1,2,2], was identified as the predominant species in the pH region 7 - 2. In the region $\text{pH} < 2$ the mono-mandelates [1,1,2] and [1,1,3] proved to be important species as their inclusion in the model improved the fit between the experimental and calculated pH significantly. Fewer species were identified than in the molybdate-mandelate system

because slow reactions necessitated restrictions on the experimental conditions. The $[1,2,r]$ and $[1,1,r]$ were the only types of species identified. Except for the $[1,2,3]$ complex, with a relative standard deviation of 20%, the other complexes all had low relative standard deviations of $< 5\%$. Given the experimental constraints, a satisfactory fit ($\sigma = 1.48$ and $\chi^2 = 44$) was achieved. The value for the formation constants of the various complexes are shown in Table 3.3.3.

Table 3.3.3 Tungstate(VI)-mandelate complexes identified and calculated $\log\beta$ and ΔG° values. 1 M (Na)Cl at 298.15 K

COMPLEX	$\log\beta_{pqr} \pm 3\sigma$	ΔG° (kJ mol ⁻¹)
$[0,1,1]^-$	3.15 ± 0.01	-17.98
$[1,2,2]^{2-}$	17.59 ± 0.01	-100.4
$[1,2,3]^-$	18.09 ± 0.30	-103.2
$[1,1,2]^-$	13.78 ± 0.07	-78.6
$[1,1,3]$	15.33 ± 0.07	-87.5

All four species have molybdate-lactate and tungstate-lactate analogues, and barring $[1,1,3]$, also molybdate-mandelate analogues.

Distribution of species

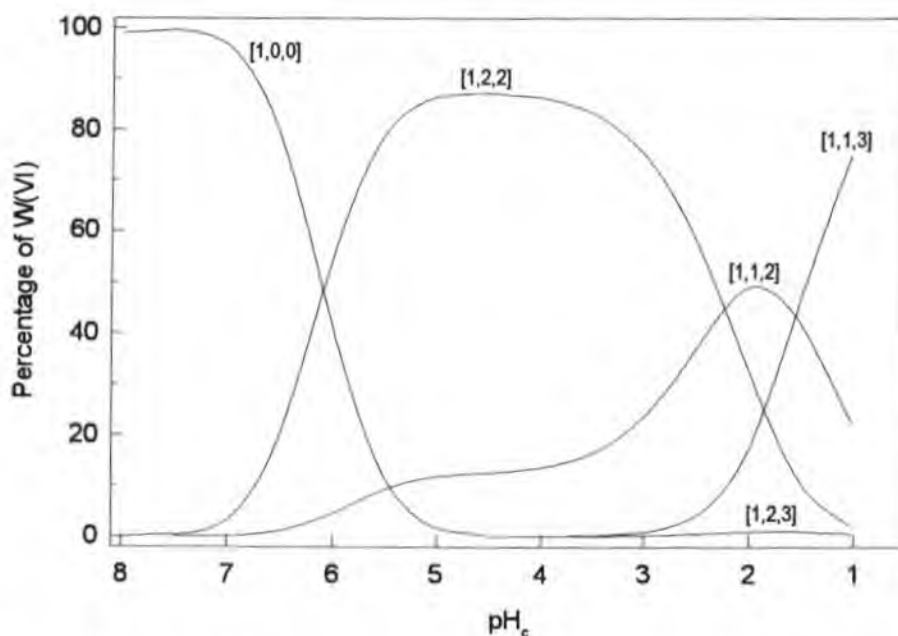


Fig. 3.3.8 Concentration of tungstate(VI)-mandelate complexes, expressed as a percentage of the total tungsten(VI) concentration, as a function of pH_c . The total concentrations of tungstate(VI) and mandelate are 0.001 M and 0.003 M, respectively.

3.3.2.2 Enthalpimetric data and analysis

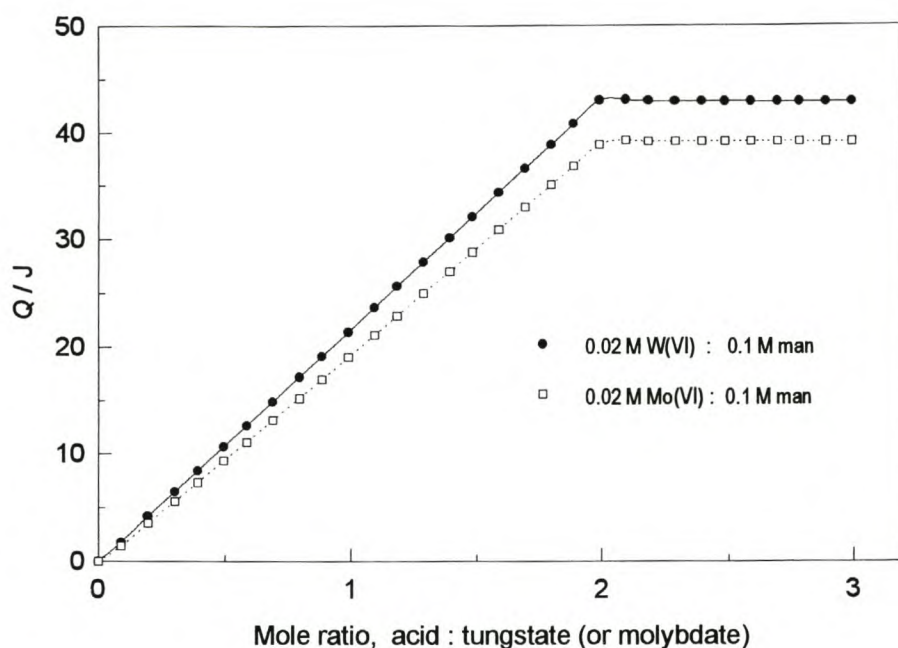


Fig. 3.3.9 Measured heat, Q , as a function of the molar ratio of acid to tungstate(VI) for a titration of 0.02 M tungstate(VI) and 0.1 M mandelate.

Calculation of enthalpy and entropy

The plot of Q vs mole ratio of acid added to molybdate (Fig. 3.3.9) shows a break at a mole ratio of approximately 2:1 in accordance with the stoichiometry of the major complex $[1,2,2]$, determined by potentiometry.

Included in the measured heat is the contribution from the protonation of mandelate which is relatively small despite the five-fold excess of mandelate. (An excess of mandelate is essential to ensure complete complexation of tungstate upon acidification thereby excluding side-reactions involving polyanion formation.) To account for the heat involved in the protonation of free mandelate $\Delta H_{011}^{\circ} = -0.5 \text{ kJ mol}^{-1}$ was used in the calculations (Table 3.3.2).

Under the chosen conditions minor complex species do not appear in measurable concentrations for most of the titration which simplifies the calculation of the enthalpy changes.

Table 3.3.4 Calculated ΔH° and $T\Delta S^{\circ}$ values for the formation of some W(VI)-mandelate complexes. 1 M (Na)Cl at 298.15 K

COMPLEX	ΔH° (kJ mol ⁻¹)	$T\Delta S^{\circ}$ (kJ mol ⁻¹)
[0,1,1]	-0.5 ± 0.5	17.5
[1,2,2] ²⁻	-86.3 ± 0.5	14.1

3.4 COMPLEXATION WITH MALATE

3.4.1 Molybdenum(VI)-malate system

3.4.1.1 Potentiometric data and analysis

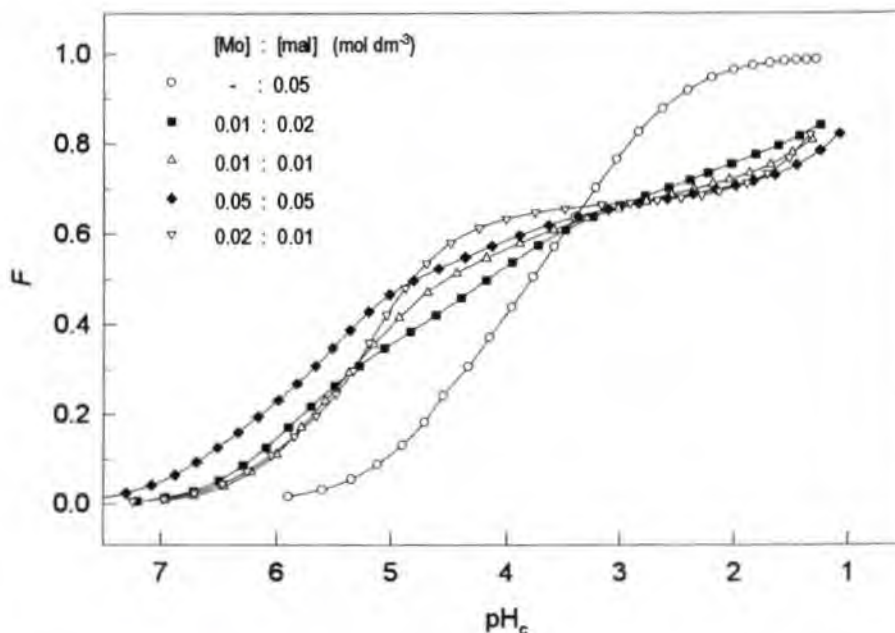


Fig. 3.4.1 Function F versus pH_c for some representative potentiometric titrations of the molybdate(VI)-malate system.

F curves

The curves (Fig. 3.4.1) show that complexation starts at pH 7 resulting in a sharp increase in F values until at low pH the protonation of the complexes becomes more difficult than that of malate itself. The values of the F curves pertaining to the titration of a solution with a two-fold excess of molybdate change little in the pH range 4-2. This can be ascribed to the dominant [4,2,8] complex under those conditions (Fig. 3.4.3). For the other curves the values of F increase fairly steadily, without sharp inflexions, because none of the many complexes predominates over a large pH range (Fig. 3.4.8).

Modelling of the malate and Mo-malate systems (species, $\log\beta$, ΔG°)

The protonation constants of malate, which were calculated from data obtained from the titration of malate, are shown in Table 3.4.1 and were used to produce a species distribution diagram of the malate system (Appendix 2).

The final model of the Mo-malate system comprises fourteen species, representing 6 different molybdate : malate ratios, protonated to various degrees: [1,2, r] , [1,1, r] , [2,2, r] , [4,4, r] , [2,1, r] and [4,2, r]

(Table 3.4.1). This model resulted in a very good fit ($\sigma = 0.97$, $\chi^2 = 27$). Except for the [2,1,4] complex, which has a standard deviation of 16%, all other species have a standard deviation of less than 7%. This makes [2,1,4] one of the least certain complexes, but it is retained in the model because it is the protonated form of a complex, [2,1,3], which has a very high degree of certainty (r.s.d ~ 3%). Although the fit could be improved marginally (σ lowered from 0.97 to 0.95) by the addition of some very minor species, such as [4,4,9] and [4,4,10], these species were not included in the best model, since their percentage concentrations were very small and their relative standard deviations (18%) quite large.

Table 3.4.1 Molybdate(VI)-malate complexes identified and calculated $\log\beta$ and ΔG° values.
1 M (Na)Cl at 298.15 K

COMPLEX	$\log\beta_{\text{pqr}} \pm 3 \sigma$	ΔG° (kJ mol ⁻¹)
[0,1,1] ⁻	4.44 ± 0.01 (4.44)	-25.3
[0,1,2]	7.57 ± 0.01 (7.57)	-43.2
[1,2,2] ⁴⁻	15.48 ± 0.01	-88.36
[1,2,3] ³⁻	20.13 ± 0.01	-114.9
[1,2,4] ²⁻	24.14 ± 0.01	-137.8
[1,1,1] ³⁻	7.47 ± 0.01	-42.64
[1,1,2] ²⁻	13.23 ± 0.01	-75.52
[1,1,3]	15.87 ± 0.08	-90.59
[2,2,4] ⁴⁻	28.06 ± 0.03	-160.2
[2,2,5] ³⁻	32.01 ± 0.07	-182.7
[2,1,3] ³⁻	20.10 ± 0.04	-114.7
[2,1,4] ²⁻	24.35 ± 0.24	-139.0
[4,2,8] ⁴⁻	52.92 ± 0.03	-302.1
[4,2,9] ³⁻	54.35 ± 0.05	-310.2
[4,2,10] ²⁻	55.27 ± 0.09	-315.5
[4,4,11] ⁵⁻	69.92 ± 0.09	-399.1

Literature value pertaining to a 1 M medium in brackets [133].

Only a few molybdenum species ([1,0,3], [7,0,8], [7,0,9] [7,0,11]) needed to be included in the final calculations, since complexation was strong, even without an excess of malate, due to the formation of complexes with 2:1 stoichiometry, like [4,2,*r*] and [2,1,*r*]. Titrations of solutions with an excess of molybdate could be used to good effect, unlike in the oxalate, lactate and mandelate systems, where the [1,1,*r*] and [1,2,*r*] complexes predominate.

The first of the two following distribution curves highlights the similarity between this system and the molybdate-lactate and molybdate-mandelate system under similar conditions (large excess of ligand) where the [1,2,*r*] complexes predominate. The distribution of species for equimolar solutions illustrates the complexity of the system better.

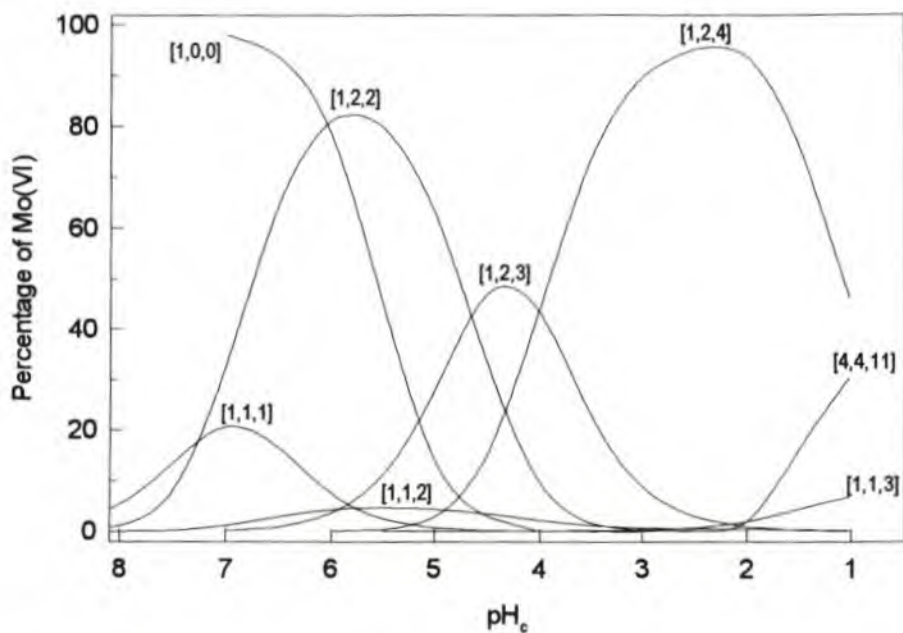
Distribution of species

Fig. 3.4.2 Concentration of molybdate(VI)-malate complexes, expressed as a percentage of the total molybdenum(VI) concentration, as a function of pH_c . The total concentrations of molybdate(VI) and malate are 0.05 M and 0.2 M, respectively.

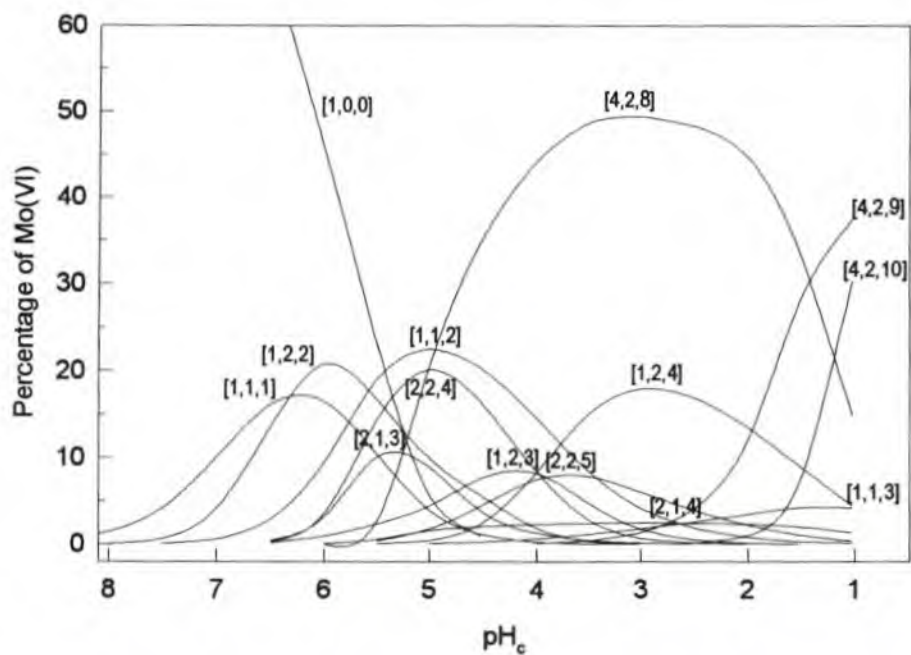


Fig. 3.4.3 Concentration of molybdate(VI)-malate complexes, expressed as a percentage of the total molybdenum(VI) concentration, as a function of pH_c . The total concentrations of molybdate(VI) and malate are both 0.05 M.

3.4.1.2 Spectrophotometric data and analysis

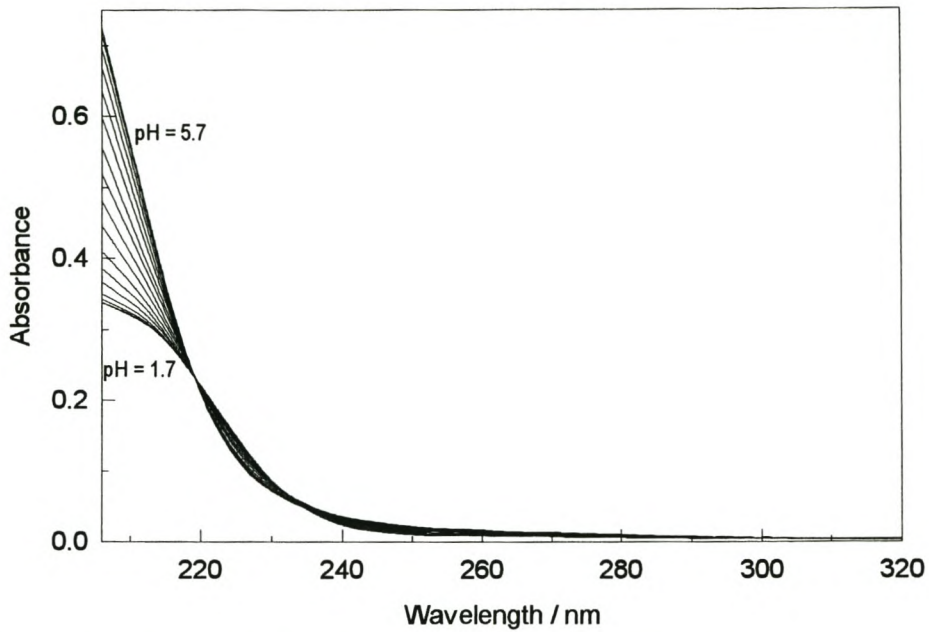


Fig. 3.4.4.1 Change in absorption spectra with pH_c ranging from 5.7 to 1.7.

The total malate concentration is 0.0016 M.

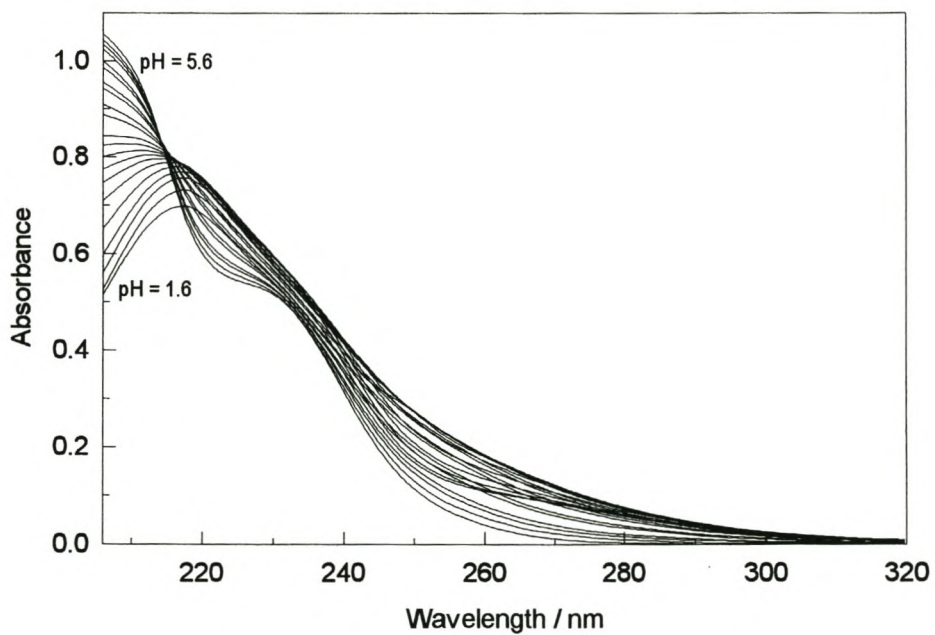


Fig. 3.4.4.2 Change in absorption spectra with pH_c ranging from 5.6 to 1.6.

The total molybdate(VI) and malate concentrations are both 0.0001 M.

Protonation constants and spectra of malate

The protonation constants of malate calculated with the program SQUAD from the 17 experimental spectra (Appendix 1), $\log\beta_{011} = 4.43 \pm 0.02$ and $\log\beta_{012} = 7.59 \pm 0.06$ agree very well with the values obtained from the potentiometric data (4.44 and 7.57). The spectra of malate $[1,0,0]^{2-}$, $[0,1,1]^-$ and malic acid $[0,1,2]$ have been accurately determined and are shown in Fig. 3.4.5.

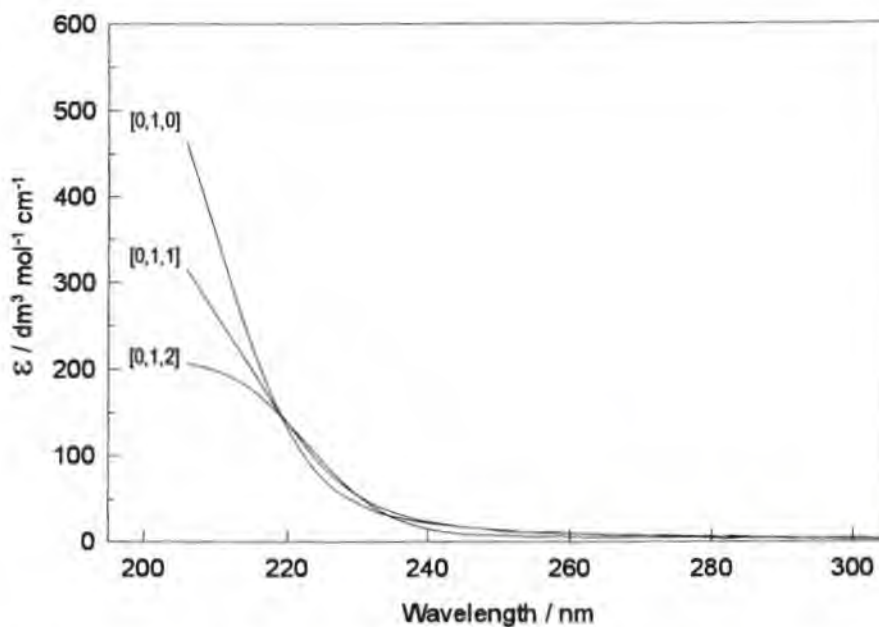


Fig. 3.4.5. Calculated molar absorption spectra of malate and its protonated forms.

Calculation of models (complexes, formation constants, absorption spectra)

Under the experimental conditions (Appendix 1) the system is simple enough to extract useful formation constants and absorption spectra of two complexes, namely $[1,1,2]$ and $[2,1,4]$. The expected maximum percentage concentrations of these complexes (based on the potentiometric results) were 50% and 20%, respectively. The $[1,1,3]$ complex reaches a maximum percentage concentration of only ~5%. Rather than neglecting it in the calculations its formation constant was supplied to the program and the calculations carried out on the basis that it has the same spectrum as the $[1,1,2]$ complex. The known protonation constants and spectra of the malate species were supplied to the program as well as the protonation constants of (uncomplexed) monomeric molybdate $[1,0,1]^-$, $[1,0,2]$ and $[1,0,3]^+$ and the spectrum of bimolybdate, $[1,0,1]$ [122-125]. The values obtained for the formation constants were, $\log\beta_{112} = 13.34$ (13.23) and $\log\beta_{214} = 24.33$ (24.35). The agreement with the values determined by potentiometry, given in brackets, is better than one would expect considering the approximations in the calculations. Reassuring also, is the good agreement between the spectra now calculated for the $[1,0,1]^-$ and $[1,0,3]^+$ species and those previously determined [122-125]. Of all the complexes identified by potentiometry the $[2,1,4]$ complex was the most uncertain (Section 3.4.1.1). Having provided additional evidence for its existence and also verifying the value of the formation constant of the $[1,1,2]$ complex, the reaction model determined by potentiometry could be accepted with confidence to be used as a basis for an enthalpimetric study.

The calculated spectra of the complexes are shown in Fig. 3.4.6. The relative insignificance of the absorption of the uncomplexed malate species can be seen clearly.

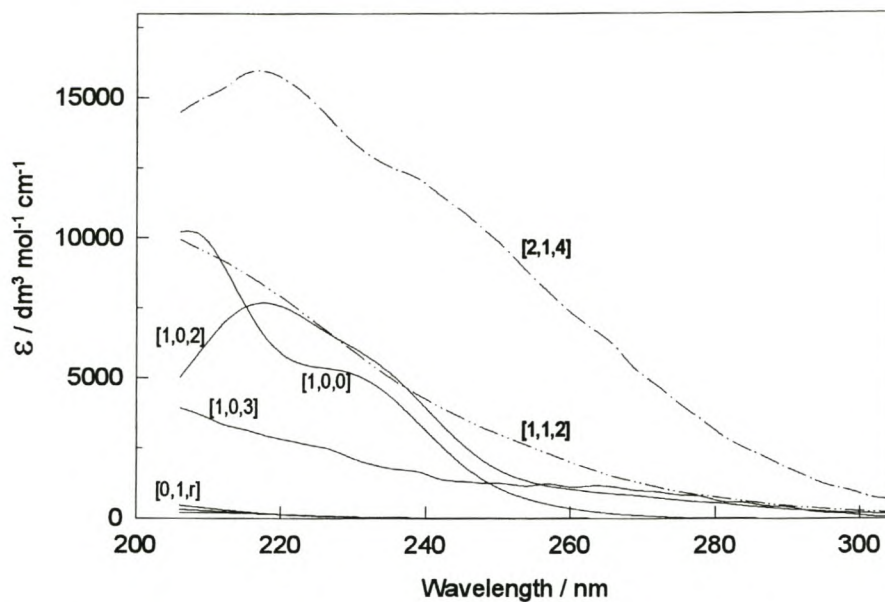


Fig. 3.4.6 Calculated molar absorption spectra of various species in the molybdate(VI)-malate system.

3.4.1.3 Enthalpimetric data and analysis

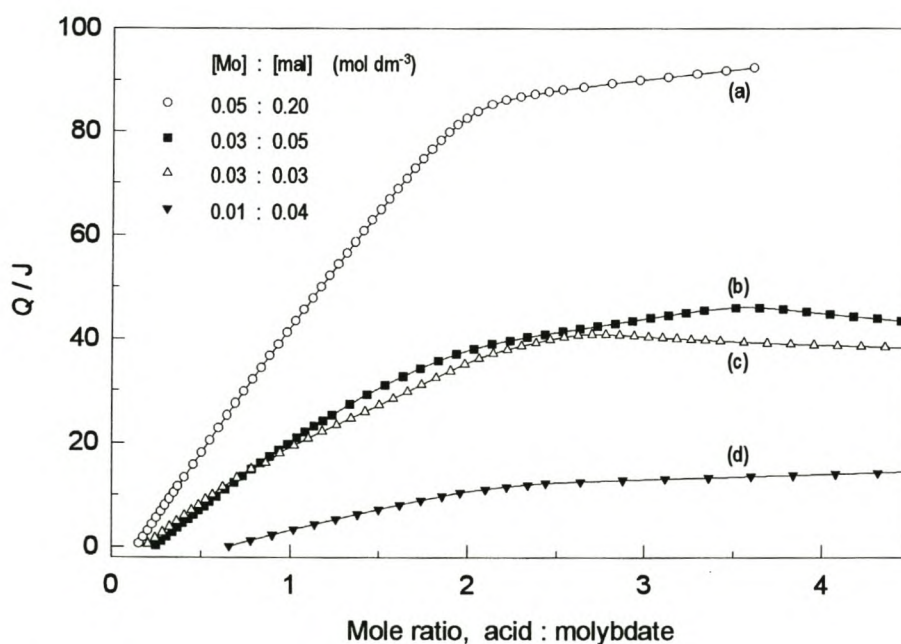


Fig. 3.4.7 Measured heat, Q , as a function of the molar ratio of acid to molybdate(VI) for the four titrations used. (Concentrations of molybdate(VI) and malate shown on graph.)

The plots of Q vs mole ratio of acid added to molybdate for all four enthalpimetric titrations of molybdate-malate solutions are shown in Fig. 3.4.7. Only the Q plots pertaining to the conditions of four-fold excess of malate (a and d) show a fairly distinct inflexion at a mole ratio of acid added to molybdate of approximately (2:1), indicating the formation of the [1,2,2] complex (for which $r/p = 2$). This is very similar to the fairly simple molybdate-lactate and molybdate-mandelate systems, where [1,2, r] complexes predominate throughout.

The different shapes of the two curves (b) and (c) at the same molybdate concentration but with different malate concentrations reflect the change in relative concentrations of the complexes. Distribution curves (Fig 3.4.8 and 3.4.9) are shown as a function of the molar ratio of acid to molybdate for these titrations for easy comparison with Fig. 3.4.7.

Except at the very beginning of the titration, more heat is developed for the solution having an excess of malate (b) because of the higher percentage of [1,2, r] complexes, which develop more heat per molybdenum on formation than the other complexes (Table 3.4.2). This is further illustrated by the inflexion (highest Q value) of curve (b) at the mole ratio of 3.5, and of curve (c) at the mole ratio of about 2.7 which in both cases coincide with the formation of the maximum percentage concentration of the highest protonated [1,2, r] species.

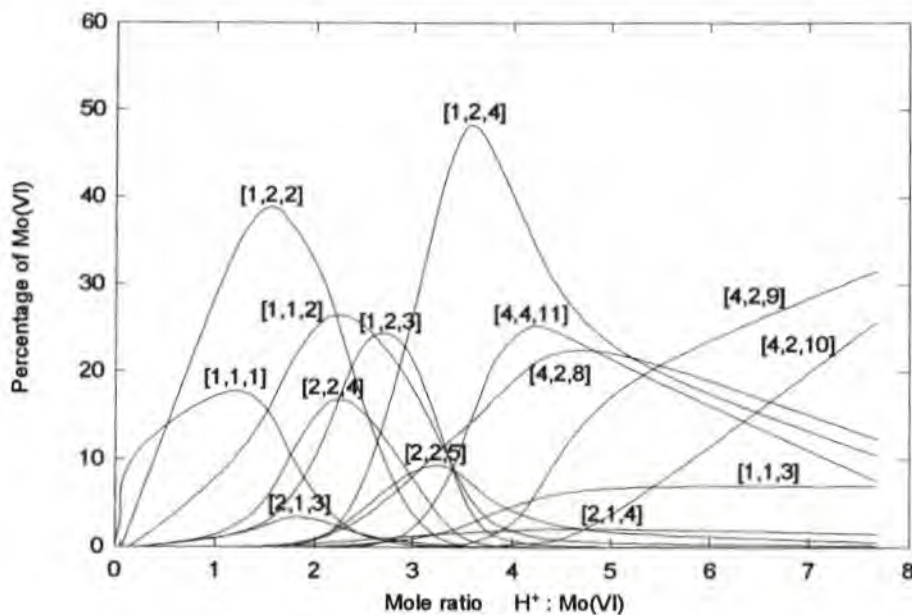


Fig. 3.4.8 Concentration of molybdate(VI)-malate complexes, expressed as a percentage of the total molybdenum(VI) concentration, as a function of the molar ratio of acid to molybdate(VI) for a titration of 0.03 M molybdate(VI) and 0.05 M malate (titration (b) in Fig. 3.4.7).

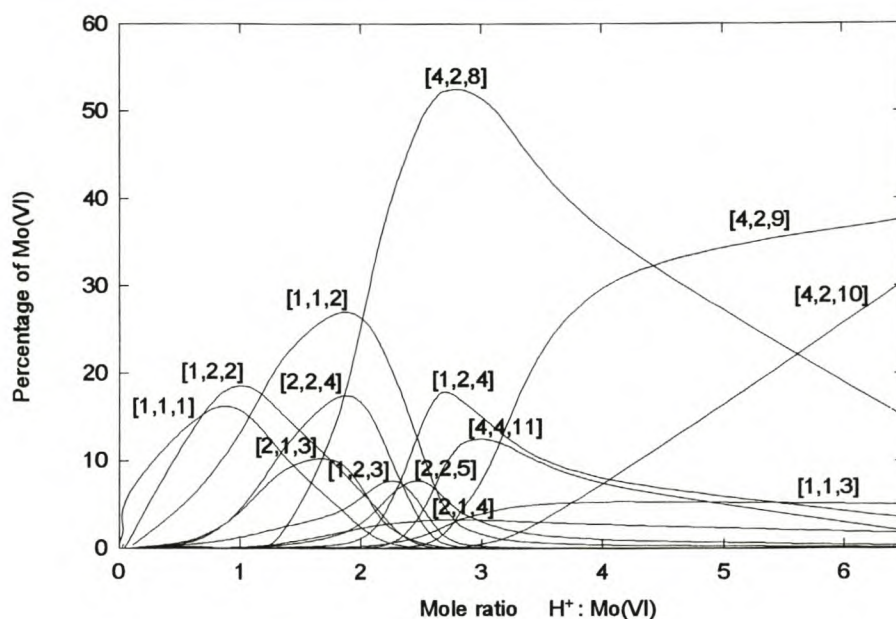


Fig. 3.4.9 Concentration of molybdate(VI)-malate complexes, expressed as a percentage of the total molybdenum(VI) concentration, as a function of the molar ratio of acid to molybdate(VI) for a titration of 0.03 M molybdate(VI) and 0.03 M malate (titration (c) in Fig. 3.4.7).

To account for the heat involved in the protonation of free malate the values for the change in enthalpy for these reactions were determined in a separate titration (Table 3.4.2). The values obtained after correcting for the endothermic heat of dilution were $\Delta H_{011}^{\circ} = -2.0 \text{ kJ mol}^{-1}$ and $\Delta H_{012}^{\circ} = -6.5 \text{ kJ mol}^{-1}$.

Table 3.4.2. Calculated ΔH° and $T\Delta S^{\circ}$ values for the formation of some Mo(VI)-malate complexes. 1 M (Na)Cl at 298.15 K

COMPLEX	ΔH° (kJ mol ⁻¹)	$T\Delta S^{\circ}$ (kJ mol ⁻¹)	COMPLEX	ΔH° (kJ mol ⁻¹)	$T\Delta S^{\circ}$ (kJ mol ⁻¹)
[0,1,1] ⁻	-2.0 ± 0.1	23.3	-	-	-
[0,1,2]	-6.5 ± 0.1	36.7	-	-	-
[1,2,2] ⁴⁻	-76.2 ± 0.5	12	[2,1,3] ³⁻	-82 ± 5	32
[1,2,3] ³⁻	-82.3 ± 0.5	33	[2,1,4] ²⁻	-112 ± 5	27
[1,2,4] ²⁻	-83.7 ± 0.5	54	[4,2,8] ⁴⁻	-233 ± 5	69
[1,1,1] ³⁻	-50.1 ± 1.0	-8	[4,2,9] ³⁻	-226 ± 5	84
[1,1,2] ²⁻	-49.2 ± 0.5	26	[4,2,10] ²⁻	-197 ± 10	125
[1,1,3] ⁻	-49.6 ± 0.5	41	[4,4,11] ⁵⁻	-239 ± 15	160
[2,2,4] ⁴⁻	-115 ± 5	46	-	-	-
[2,2,5] ³⁻	-119 ± 5	64	-	-	-

Literature enthalpy values for malate pertaining to ionic strength 0.1 M are $\Delta H_{011}^{\circ} = -0.59 \text{ kJ mol}^{-1}$ and $\Delta H_{012}^{\circ} = -2.84 \text{ kJ mol}^{-1}$ [133].

3.4.2 Tungsten(VI)-malate system

3.4.2.1 Potentiometric data and analysis

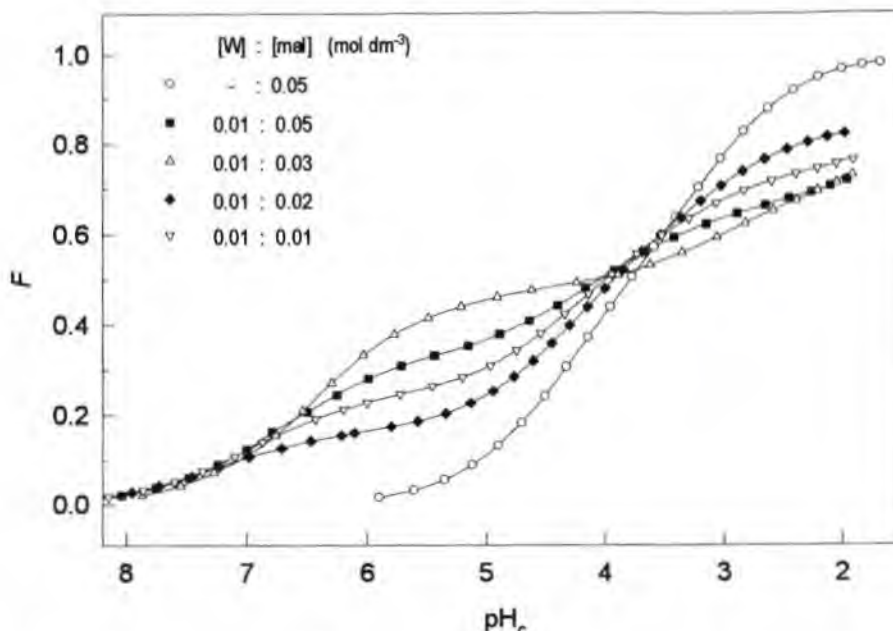


Fig. 3.4.10 Function F versus pH_c for some representative potentiometric titrations of the tungstate(VI)-malate system.

F curves

The curves (Fig. 3.4.10) show that complexation starts at pH 8 resulting in a sharp increase in F values until, at low pH, the protonation of the complexes becomes more difficult than that of malate itself. The F values for the curve pertaining to the equimolar solution change little ($F \sim 0.5$) in the region $\text{pH} \sim 4$. This can be ascribed to the predominance of the complexes [1,1,2] and [2,2,4] (Table 3.4.3), for which $r/(2p+2q)=0.5$ in both cases. Similarly, the F values for the curve pertaining to the solution with a two-fold excess of malate change little ($F \sim 0.3$) in the region $\text{pH} \sim 6$. This can be ascribed to the predominance of the complex [1,2,2] (Fig. 3.4.11) for which $r/(2p+2q)=0.33$.

Modelling of the W-malate system (species, $\log \beta$, ΔG°)

Due to slow reactions, no titrations of solutions with an excess of tungstate were feasible. Even for solutions with equal concentrations of tungstate and malate the concentrations had to be as low as 0.01 M to exclude these slow reactions. As described in Section 2.6.1.1 the presence of uncomplexed tungstate species can be accounted for by the tungstate-proton model if the degree of protonation (F) < 0.6. Preliminary calculations showed that, for the equimolar solution, the percentage concentration of tungstate present as polyanions increases from about 7% to more than 50% in the pH region 4-2, a region for which $F > 0.6$. Therefore, data pertaining to $\text{pH} < 4$ for the equimolar titration had to be ignored in the calculations.

The final model comprises eleven species, representing 5 different tungstate:malate ratios protonated to various degrees: $[1,2,r]$, $[1,1,r]$, $[2,2,r]$, $[4,4,r]$ and $[2,1,r]$ (Table 3.4.3). A value for the sample standard deviation, $\sigma = 1.24$, implies a very good fit. Only the species $[2,1,3]$ and $[4,4,11]$ have standard deviations of greater than 8%, actually 23% and 12%, respectively. These species occur in very low percentage concentrations under the conditions employed. Higher concentrations of the reagents and also an excess of tungstate, as required by the stoichiometry of $[2,1,3]$, would however not be feasible.

Table 3.4.3 Tungstate(VI)-malate complexes identified and calculated $\log\beta$ and ΔG° values.
1 M (Na)Cl at 298.15 K

COMPLEX	$\log\beta_{\text{pqr}} \pm 3\sigma$	ΔG° (kJ mol ⁻¹)
$[0,1,1]^-$	4.44 ± 0.01	-25.3
$[0,1,2]$	7.57 ± 0.01	-43.2
$[1,2,2]^{4-}$	17.20 ± 0.01	-98.2
$[1,2,3]^{3-}$	21.70 ± 0.02	-123.9
$[1,2,4]^{2-}$	25.60 ± 0.01	-146.2
$[1,1,1]^{3-}$	8.85 ± 0.01	-50.5
$[1,1,2]^{2-}$	14.78 ± 0.06	-84.4
$[1,1,3]^-$	17.26 ± 0.03	-98.5
$[2,2,2]^{6-}$	18.87 ± 0.06	-107.7
$[2,2,3]^{5-}$	25.72 ± 0.10	-146.8
$[2,2,4]^{4-}$	31.88 ± 0.07	-182.0
$[2,1,3]^{3-}$	23.07 ± 0.33	-131.7
$[4,4,11]^{5-}$	73.60 ± 0.15	-420.1

Distribution of species

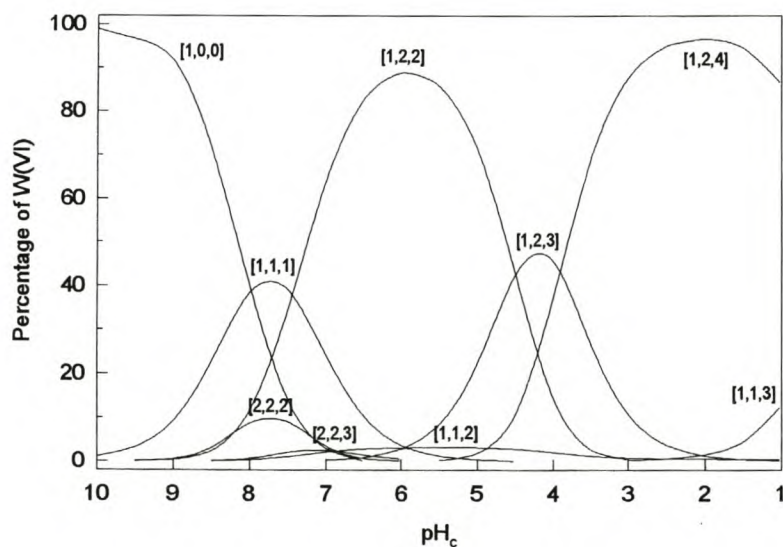


Fig. 3.4.11 Concentration of tungstate(VI)-malate complexes, expressed as a percentage of the total tungsten(VI) concentration, as a function of pH_c . The total concentrations of tungstate(VI) and malate are 0.02 M and 0.15 M, respectively.

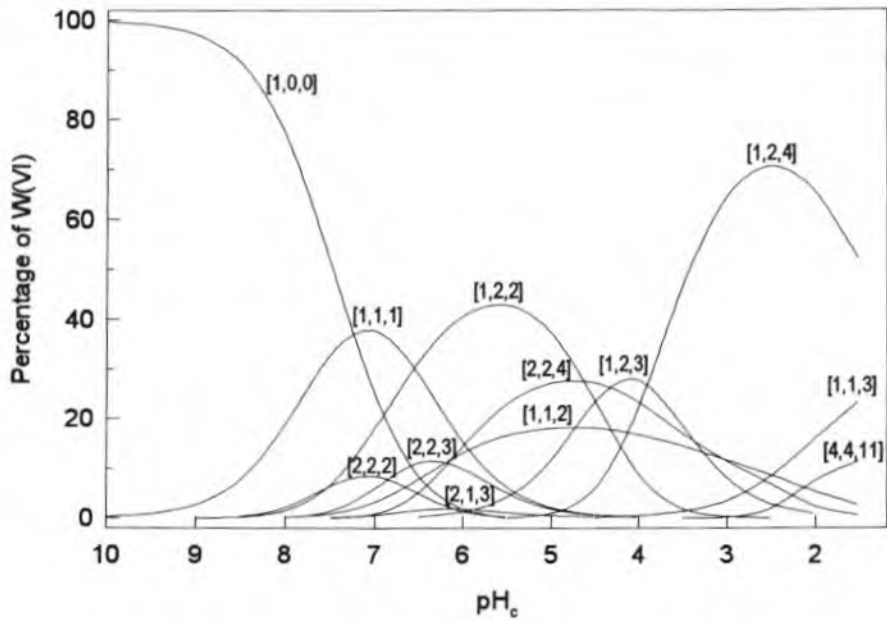


Fig. 3.4.12 Concentration of tungstate(VI)-malate complexes, expressed as a percentage of the total tungsten(VI) concentration, as a function of pH_e. The total concentrations of tungstate(VI) and malate are 0.02 M and 0.04 M, respectively.

The first of the distribution curves (Fig. 3.4.11) highlights the similarity between malate complexation and complexation with monohydroxycarboxylates such as lactate and mandelate, where the [1,2,*r*] complexes predominate. The second species distribution (Fig. 3.4.12) illustrates the complexity of the system better.

3.4.2.2 Enthalpimetric data and analysis

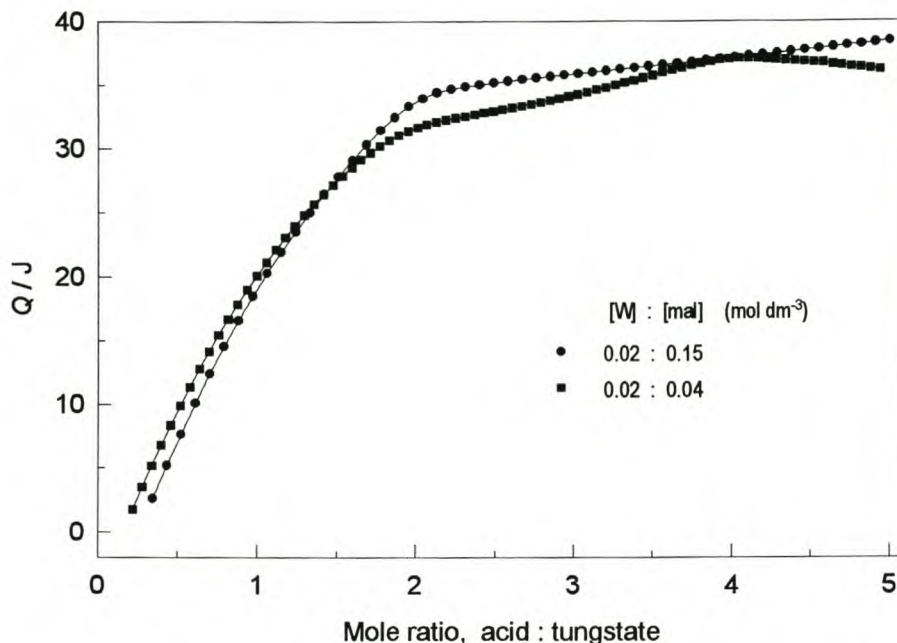


Fig. 3.4.13 Measured heat, Q , as a function of the molar ratio of acid to tungstate(VI) for the two titrations used. (Concentrations of tungstate(VI) and malate shown on graph)

The plots of Q vs mole ratio of acid added to tungstate for two different titrations are shown in Fig. 3.4.13. The different shapes of the two curves at the same tungstate concentration, but with different malate concentrations, reflect the change in relative concentrations of the complexes. For the solution with the greater (7.5-fold) excess of malate the $[1,2,r]$ species dominate (Fig. 3.4.11). The complete conversion into the $[1,2,2]$ complex is indicated by the distinct break in the curve occurring at the acid : tungstate mole ratio of 2:1 (Fig. 3.4.13). Unlike the Q curves for the tungstate-mandelate and -lactate titrations, the Q curve for this titration up to the 2:1 inflexion is not a straight line, but shows a slight inflexion at the mole ratio 1:1. This is due to the formation of significant amounts of $[1,1,1]$ complex in this system.

The first section of the Q curve (up to the mole ratio 1:1) of the titration of a solution with a two-fold excess of malate is very similar to the other Q curve, as the $[1,1,1]$ complex is also the dominant complex in this region (Fig. 3.4.12). A clear inflexion also appears at the mole ratio 2:1, which coincides with the complete conversion to the $[1,2,2]$ complex. If the two curves are compared, a further, slight inflexion at the mole ratio 1.5 :1 can be identified in the curve pertaining to the solution with a two-fold excess of malate. This can be ascribed to the complete conversion to the $[2,2,3]$ complex, for which $r/p = 1.5$ (Fig. 3.4.12).

The greater heat development during the titration of the solution with 7.5-fold excess of malate, is an indication that more heat is developed in the formation of $[1,2,r]$ complexes than other complexes. This is confirmed by calculations (Table 3.4.4) and is also illustrated by the highest Q value of the titration with

two-fold excess of malate which is attained at a mole ratio of ~4:1 (which corresponds to a pH~2.4) where the [1,2,4] complex predominates clearly (Fig. 3.4.11). The conversion of the [1,2,4] complex to the [1,1,3] and [4,4,11] complexes is clearly an endothermic process (which is confirmed by the calculations).

To account for the heat involved in the protonation of free malate the values for the change of enthalpy for these reactions were determined in a separate titration (Table 3.4.4). The values obtained after correcting for the endothermic heat of dilution were $\Delta H_{011}^{\circ} = -2.0 \text{ kJ mol}^{-1}$ and $\Delta H_{012}^{\circ} = -6.5 \text{ kJ mol}^{-1}$.

Table 3.4.4 Calculated ΔH° and $T\Delta S^{\circ}$ values for the formation of some W(VI)-malate complexes. 1 M (Na)Cl at 298.15 K

COMPLEX	ΔH° (kJ mol ⁻¹)	$T\Delta S^{\circ}$ (kJ mol ⁻¹)
[0,1,1] ⁻	-2.0 ± 0.1	23.3
[0,1,2]	-6.5 ± 0.1	36.7
[1,2,2] ⁴⁻	-82.5 ± 0.5	15.7
[1,2,3] ³⁻	-88.2 ± 0.5	35.7
[1,2,4] ²⁻	-91.8 ± 0.6	54.4
[1,1,1] ³⁻	-62.8 ± 0.5	-12.3
[1,1,2] ²⁻	-59.8 ± 0.5	24.6
[1,1,3] ⁻	-63.0 ± 2.0	36
[2,2,2] ⁶⁻	-119 ± 3	-11
[2,2,3] ⁵⁻	-114 ± 5	33
[2,2,4] ⁴⁻	-142 ± 3	40
[2,1,3] ³⁻	-106 ± 20	26
[4,4,11] ⁵⁻	-341 ± 30	79

The percentage concentrations of the complexes [2,1,3] and [4,4,11] are small under the experimental conditions (Fig. 3.4.12). Understandably the ΔH° values for these complexes are the least certain.

3.5 COMPLEXATION WITH CITRATE

3.5.1 Molybdenum(VI)-citrate system

3.5.1.1 Potentiometric data and analysis

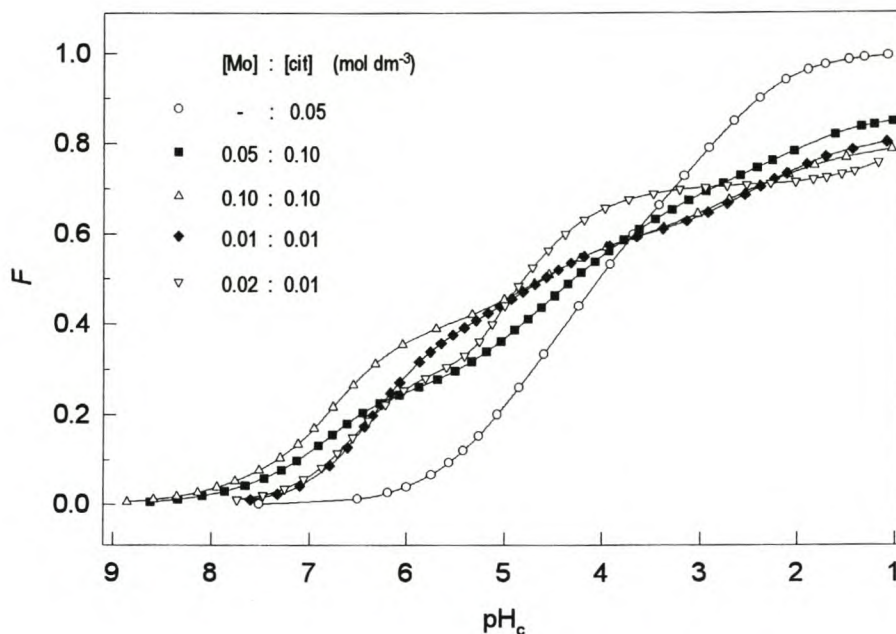


Fig. 3.5.1 Function F versus pH_c for some representative potentiometric titrations of the molybdate(VI)-citrate system.

F curves

The curves (Fig. 3.5.1) show that complexation starts at pH 9 resulting in a sharp increase in F values until at low pH the protonation of the complexes becomes more difficult than that of citrate itself. For solutions of equal concentrations of citrate and molybdate, inflexions at $F = 0.4, 0.6$ and 0.8 correspond to complexes $[1,1,2], [1,1,3]$ and $[1,1,4]$, respectively, for which $r/(2p+3q) = 0.4, 0.6$ and 0.8 respectively (Fig. 3.5.2).

Modelling of the citrate and Mo-citrate systems (species, $\log\beta$, ΔG°)

Previously determined protonation constants of citrate pertaining to 25°C (shown in Table 3.5.1) were used in calculations and to produce a species distribution diagram of the citrate system (Appendix 2). The protonation constants of citrate pertaining to 2°C, which were calculated from data obtained from the titration of citrate at 2°C, are also shown in Table 3.5.1.

Final models for the Mo-citrate system pertaining to 25° and 2°C are very similar and differ only in respect of some of the minor complexes. Both models comprise species representing the six molybdate:citrate ratios, 1:2, 1:1, 2:2, 4:4, 2:1 and 4:2 (Table 3.5.1). The only difference is that the relatively minor species $[1,1,4]$ and $[2,1,4]$ are included in the model pertaining to 25°C, without analogues at 2°C, and that the

relatively minor species [4,2,8] and [4,4,12] are included in the model pertaining to 2°C without analogues at 25°C. Good fits were attained for both models ($\sigma = 1.7$, $\chi^2 = 28$ at 25° and $\sigma = 1.72$, $\chi^2 = 50.2$ at 2°C).

Due to the formation of complexes with 2:1 stoichiometry at $\text{pH} < 3$, the percentage of uncomplexed molybdate is so small that some of the polyoxomolybdate ions, e.g. [7,0,11] and [8,0,12], could be neglected in the final calculations. For the calculations using data collected at 2°C a background molybdate-model was needed. It was assumed that the same molybdate species exist as at 25°C. The values for the formation constants of these molybdate species were estimated by using the known ΔH° and ΔS° values (cf. 2.6.1.1).

Table 3.5.1 Molybdate(VI)-citrate complexes identified and calculated $\log\beta$ and ΔG° values.
1 M (Na)Cl at 298.15 K

COMPLEX	Temp = 25°C		Temp = 2°C	
	$\log\beta_{\text{pqr}} \pm 3\sigma$	ΔG° (kJ mol ⁻¹)	$\log\beta_{\text{pqr}} \pm 3\sigma$	ΔG° (kJ mol ⁻¹)
[0,1,1] ²⁻	5.12 ± 0.01	-29.2	3.14 ± 0.01	-27.1
[0,1,2] ⁻	9.17 ± 0.01	-52.4	9.27 ± 0.02	-48.8
[0,1,2]	11.94 ± 0.02	-68.2	12.10 ± 0.03	-63.7
[1,1,1] ⁴⁻	8.34 ± 0.01	-47.7	9.10 ± 0.01	-47.9
[1,1,2] ³⁻	15.00 ± 0.01	-85.6	15.78 ± 0.02	-83.1
[1,1,3] ²⁻	19.62 ± 0.01	-112.0	20.56 ± 0.03	-108.3
[1,1,4] ⁻	21.12 ± 0.11	-120.5		
[2,2,4] ⁶⁻	31.02 ± 0.03	-177.1	33.08 ± 0.03	-174.2
[2,2,5] ⁵⁻	35.86 ± 0.05	-204.7	37.99 ± 0.04	-200.1
[2,2,6] ⁴⁻	40.08 ± 0.07	-228.8	42.15 ± 0.17	-222.0
[1,2,4] ⁴⁻	25.34 ± 0.18	-144.6	26.46 ± 0.15	-139.4
[1,2,5] ³⁻	29.54 ± 0.11	-168.6	30.75 ± 0.10	-162.0
[1,2,6] ²⁻	33.34 ± 0.02	-190.3	34.74 ± 0.02	-183.0
[2,1,3] ⁴⁻	21.73 ± 0.09	-124.0	22.92 ± 0.17	-120.7
[2,1,4] ³⁻	26.90 ± 0.06	-153.5		
[2,1,5] ²⁻	31.53 ± 0.03	-180.0	33.32 ± 0.05	-175.5
[4,2,8] ⁶⁻	-	-	59.76 ± 0.11	-314.7
[4,2,9] ⁵⁻	60.76 ± 0.15	-346.8	64.45 ± 0.15	-339.4
[4,2,10] ⁴⁻	64.69 ± 0.11	-369.2	68.39 ± 0.10	-360.2
[4,4,11] ³⁻	77.45 ± 0.24	-442.1	81.67 ± 0.20	-430.1
[4,4,12] ²⁻	(81.33) #	(-464) #	85.72 ± 0.36	-451.5

If [4,4,12] is included in the test-model, it is rejected because its relative standard deviation is 39%, which is just higher than the rejection limit of 33%. As it is highly likely that this complex also exists at 25°C, the value of the formation constant, calculated by the program just before rejection, is also shown in Table 3.5.1.

The relative standard deviations of the formation constants for the [4,4,11] and [4,4,12] complexes at 2°C are 14% and 24%, respectively, and 17% for the [4,4,11] complex at 25°C. These deviations are significantly greater than those for most other complexes, but they are well within the rejection limit of 33%.

Distribution of species

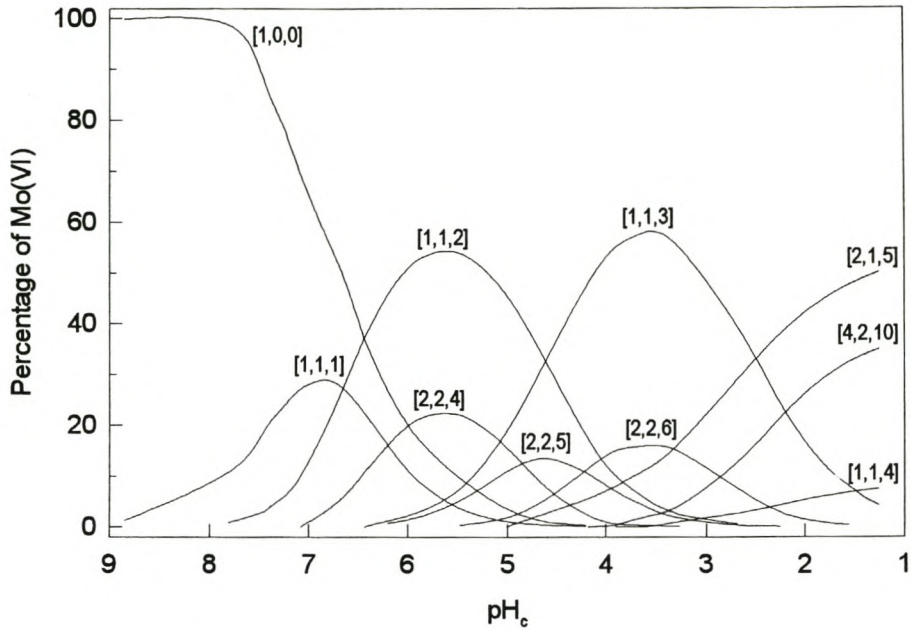


Fig. 3.5.2 Concentration of molybdate(VI)-citrate complexes, expressed as a percentage of the total molybdenum(VI) concentration, as a function of pH_c . The total concentrations of molybdate(VI) and citrate are both 0.04 M.

3.5.1.2 Spectrophotometric data and analysis

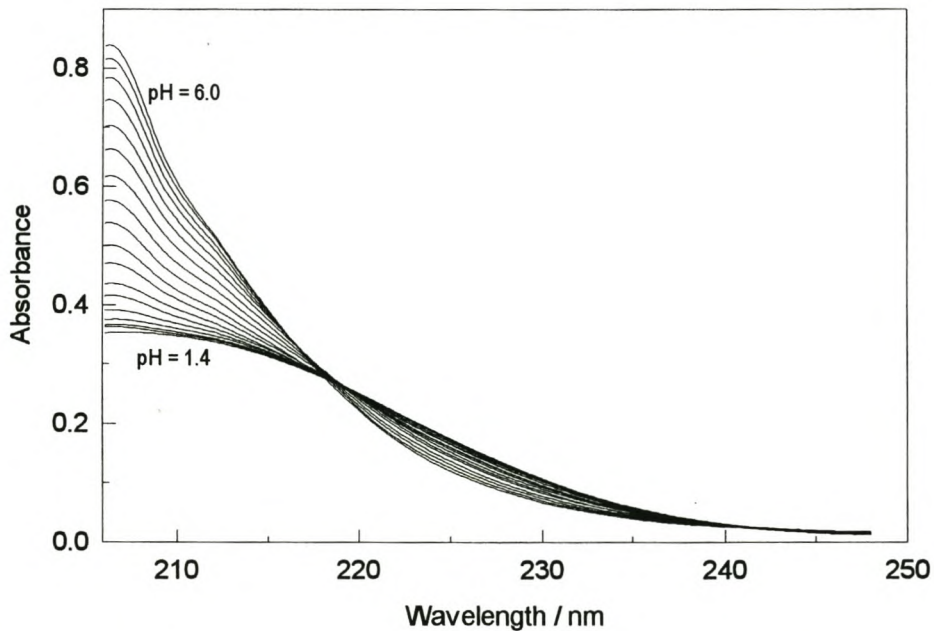


Fig. 3.5.3.1 Change in absorption spectra with pH_c ranging from 6.0 to 1.4. The total citrate concentration is 0.0016 M.

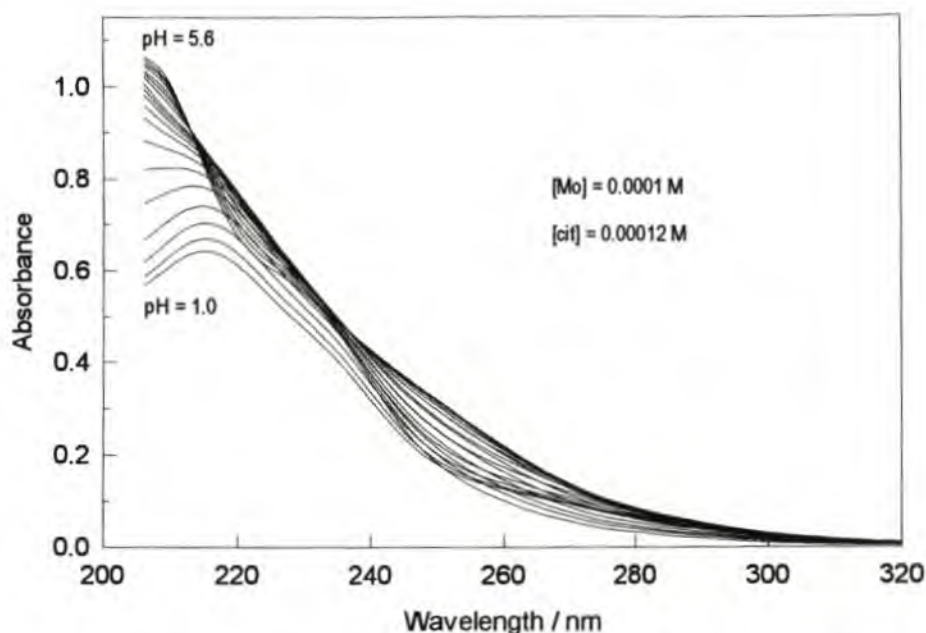


Fig. 3.5.3.2 Change in absorption spectra with pH_e ranging from 5.6 to 1.0. The total molybdate(VI) and citrate concentrations are 0.0001 M and 0.00012 M, respectively.

Protonation constants and spectra of citrate

The protonation constants of citrate calculated with the program SPECFIT using the experimental spectra (Appendix 1), $\log \beta_{011} = 5.09$, $\log \beta_{012} = 9.13$ and $\log \beta_{013} = 11.95$ agree very well with the values (5.12, 9.17 and 11.94) obtained from the potentiometric data. The spectra of citrate $[0,1,0]^{3-}$ and its protonated forms $[0,1,1]^{2-}$, $[0,1,2]^{-}$ and $[0,1,3]$ have been accurately determined and are shown in Fig. 3.5.4.

Calculation of models (complexes, formation constants, absorption spectra)

The experimental spectra representing the titration of a solution of 0.0001 M molybdate and 0.00012 M citrate in the pH range 5.6 - 1 are shown in Fig. 3.5.3. Under these experimental conditions (Appendix 1) the system is simple enough to extract useful formation constants and absorption spectra of three complexes, namely $[1,1,2]$, $[1,1,3]$ and $[2,1,5]$ (Fig. 3.5.5).

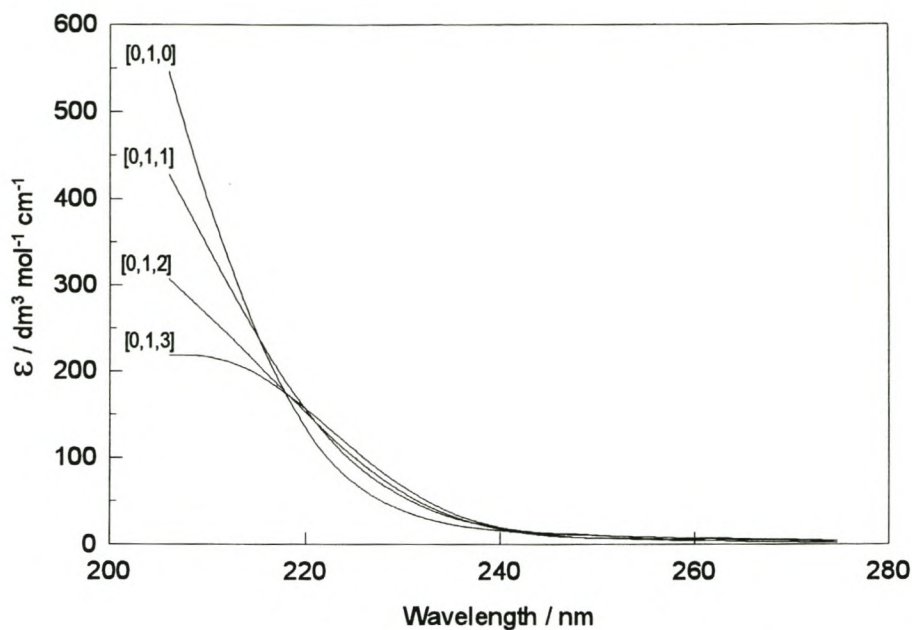


Fig. 3.5.4. Calculated molar absorption spectra of citrate and its protonated forms.

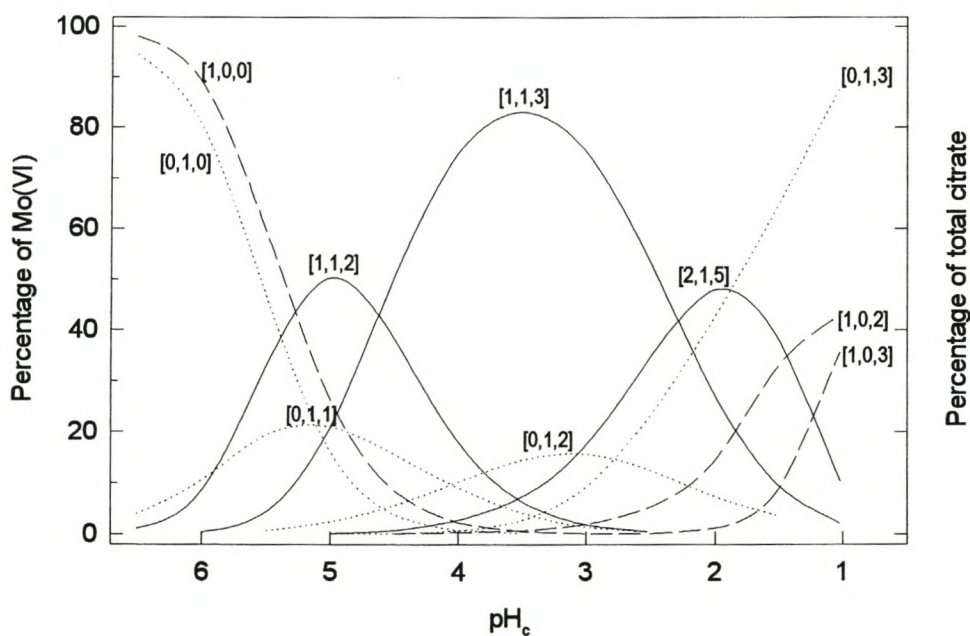


Fig. 3.5.5 Concentration of molybdate(VI)-citrate complexes, expressed as a percentage of the total molybdenum(VI) concentration, as a function of pH_c . Concentration of citrate species, expressed as a percentage of the total citrate concentration, as a function of pH_c . The total concentrations of molybdate(VI) and citrate are 0.0001 M and 0.00012 M, respectively.

The calculated protonation constants and spectra of the citrate species (Fig. 3.5.4) were supplied to the program SQUAD. The protonation constants and spectra of (uncomplexed) monomeric molybdate species [1,0,2] and [1,0,3]⁺ were also given, as calculations predicted the presence of these species at pH < 2.5 [122-125]. The values obtained for the formation constants were as follows: $\log\beta_{112} = 14.99$ (15.00), $\log\beta_{113} = 19.67$ (19.62) and $\log\beta_{215} = 31.77$ (31.53). The agreement with the values determined by potentiometry, given in brackets, is excellent given the uncertainties involved in the method and the similarity of the spectra of [1,1,2] and [1,1,3]. To check for consistency the spectrum of either of the [1,0,2] or [1,0,3]⁺ was calculated in some runs. These spectra were in good agreement with the spectra previously determined [122-125] and which were usually fixed. The calculated and known spectra are shown in Fig. 3.5.6.

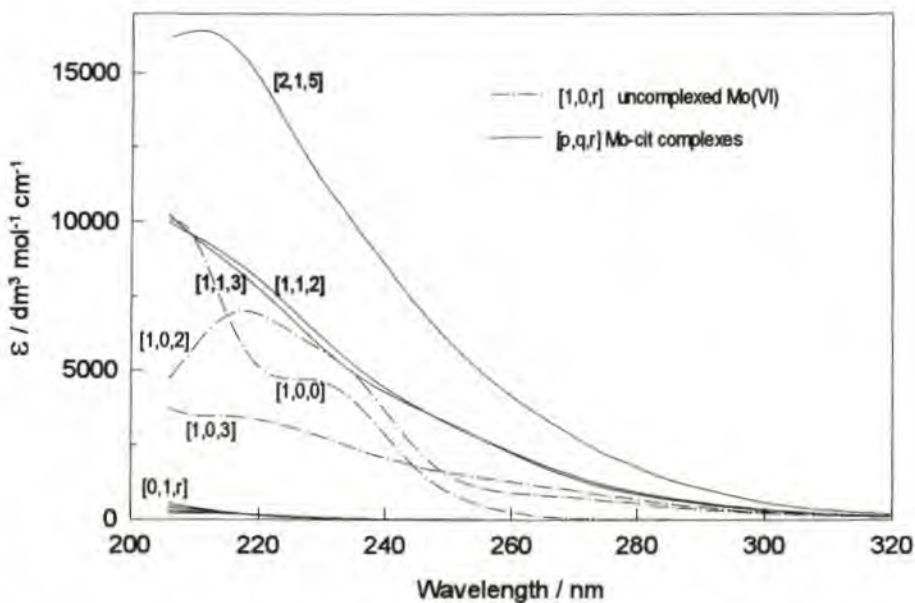


Fig. 3.5.6 Calculated molar absorption spectra of various species in the molybdate(VI)-citrate system.

Characterization of the other complexes was not attempted because of the large number of equilibria (and spectra) to be considered for a relatively small change in absorption with pH.

3.5.1.3 Analysis of Differential Pulse Polarograms

Table 3.5.2 Concentrations of Mo(VI) and citrate, the pH and temperature of different solutions investigated by differential pulse polarography.

[Mo]	[cit ³⁻]	Temp	pH of different solutions	
0.004	0.004	2°C	6.7, 5.7, 5.2, 4.7, 3.7, 3.0, 2.5, 1.3	
0.04	0.20	25°C	7.5, 7.0, 6.5, 6.0, 5.5, 5.23, 5.0, 4.5, 4.27, 4.0, 3.5, 3.0, 2.5, 2.0	
0.04	0.04	25°C	6.0, 5.5, 5.0, 4.5, 4.0, 3.5, 3.0, 2.5	
0.04	0.04	2°C	8.2, 7.5, 6.9, 6.4, 5.7, 5.5, 5.1, 4.6, 4.1, 3.5, 3.0, 2.5	
0.001	0.001	25°C	7.0, 6.7, 5.8, 5.5, 5.0, 4.0	
0.001	0.1	2°C	8.9, 7.2	A,B
0.001	0.01	2°C	5.5	C
0.004	0.004	2°C	5.7, 3.7, 3.0	D,H,I
0.008	0.008	2°C	5.7	E
0.004	0.4	2°C	1.4	F
0.004	0.04	2°C	3.0	G
0.004	0.002	2°C	3.7, 3.0	J,K
0.001	0.256	25°C ?	5.0	
0.004	0.016	25°C ?	2.5	
0.001	0.004	2°C		

Peak identification

The following paragraphs describe how the peaks have been correlated with the complexes, in particular using certain polarograms (A to K), some of which are also shown in the following figures. (The exact scale of the current-axis is not shown as it is not necessary for this qualitative investigation.)

Mononuclear complexes, [1,1,1]

A differential pulse polarogram A (Fig. 3.5.7) of a molybdenum-citrate solution (0.001:0.1) at pH=8.9, shows a strong reduction peak at -1.78 V and a much weaker peak at -1.25 V. Only the [1,1,1] complex occurs in significant amounts in this solution (percentage concentration = 13%) and the two peaks can therefore be associated with the stepwise reduction of this complex to form two lower oxidation states of molybdenum.

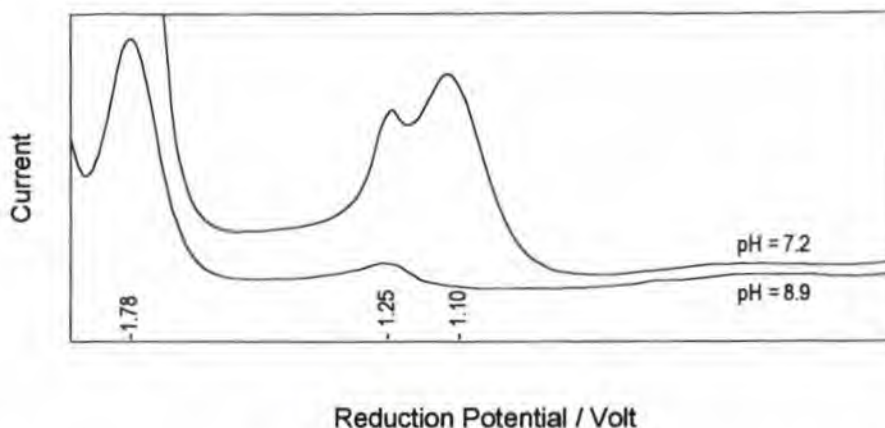


Fig. 3.5.7 Differential pulse polarograms of the solutions:
 A ([Mo(VI)]=0.001 M, [cit]=0.1 M, pH=8.9) and B ([Mo(VI)]=0.001 M, [cit]=0.1 M, pH=7.2).

When the pH of the solution is lowered to 7.2, the polarogram **B** (Fig. 3.5.7) shows an increase in the peak currents due to the increase in the percentage concentration of the [1,1,1] complex from 13.5% to 69.4%. However, at this pH the protonated form of the [1,1,1] complex, namely the [1,1,2] complex, also occurs in the solution at a concentration of 21.2%, which explains the appearance of a new peak at -1.1 V.

A fourth reduction peak occurs at -0.85 V when the concentration of the [1,1,3] complex reaches a sufficient level, for example in the solution with a molybdate and citrate concentration of 0.001 M and 0.01 M, respectively, at pH=5.5 (Polarogram C, not shown). Under these conditions the two mononuclear complexes [1,1,2] and [1,1,3] are the major components in the solution (percentage concentration of [1,2,*r*] < 2%).

The appearance and growth of the four peaks at potentials -1.78, -1.25, -1.1 and -0.85 V therefore clearly serve to verify the existence of the three [1,1,*r*] complexes. However the peak heights do not necessarily correlate with the concentrations of the individual complexes *over the whole pH range*. For example, the height of the reduction peak at -1.78 V is not determined only by the concentration of the [1,1,1] complex, but also by the [1,1,2] and [1,1,3] complexes in keeping with their formation with decreasing pH. This can be inferred from the curves in Fig. 3.5.8, where both the distribution of these species and the peak current are plotted as a function of pH.

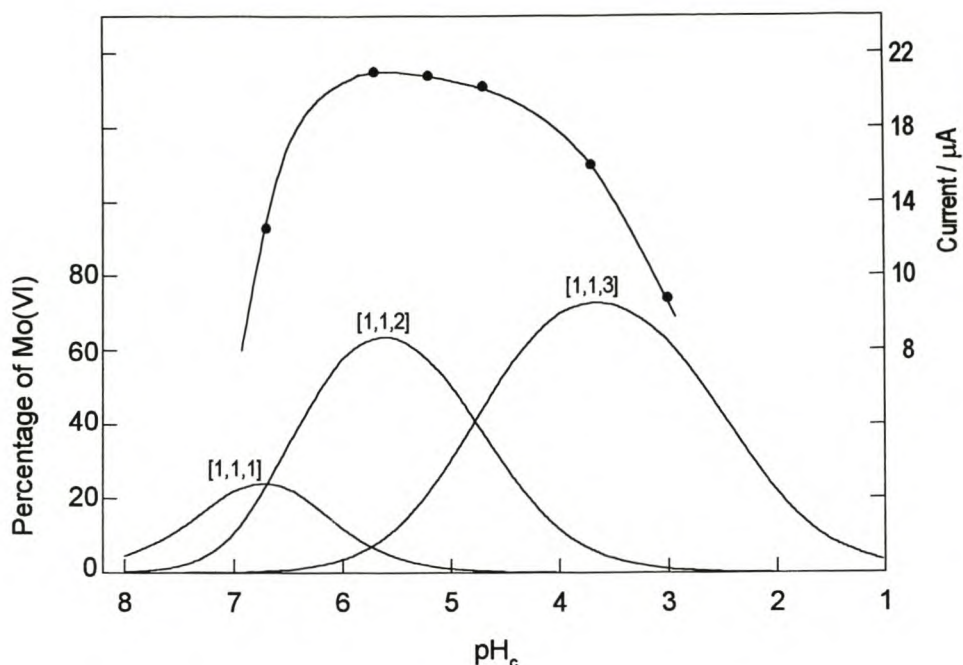


Fig. 3.5.8 Peak currents ($E = -1.78$ V) obtained from differential pulse polarograms at various pH_c values for an equimolar solution of molybdate(VI) and citrate (0.004 M) compared with the percentage of the monomeric complexes.

This behaviour can be understood in terms of the stepwise reduction of molybdenum(VI) to lower oxidation states. The first reduction step of the $[1,1,r]$ complexes occurs at increasingly lower negative potential with successive protonation, namely -1.25 , -1.1 and -0.85 V for the $[1,1,1]$, $[1,1,2]$ and $[1,1,3]$ complexes, respectively. Further reduction to the next oxidation state seems to be less dependent on the degree of protonation of the complexes and then takes place, for all complexed molybdenum, at -1.78 V; the greatest contribution to the peak current comes from the $[1,1,2]$ complex (**Fig. 3.5.8**). Therefore, although the $[1,1,1]$ complex would not be present at low pH the second step in the reduction of the $[1,1,2]$ and $[1,1,3]$ complexes accounts for the peak current at -1.78 V.

Dinuclear complexes $[2,2,r]$

The redox behaviour of the dinuclear complexes is expected to be different from that of the mononuclear complexes. This is indeed what is observed. Solutions containing $[2,2,r]$ complexes in addition to the $[1,1,r]$ complexes have polarograms with two extra peaks at -1.48 and -0.5 V. The differential pulse polarograms of an equimolar solution of molybdate and citrate (0.004:0.004) at different pH values in the range 6.7-4.7 are shown in **Fig. 3.5.9** and can be compared with the species distribution diagram (**Fig. 3.5.10**). The

polarogram pertaining to $\text{pH}=6.7$ shows the peaks at -1.78 , -1.25 and -1.05 V associated with the $[1,1,1]$ and $[1,1,2]$ complexes, which are predominant complexes at this pH. At $\text{pH}=5.7$ both the $[1,1,3]$ and $[2,2,4]$ complexes also occur in the solution and in addition to the reduction peak of the $[1,1,3]$ complex at -0.85 V the two new peaks associated with the dinuclear complex at -1.48 and -0.5 V can be seen on the polarogram.

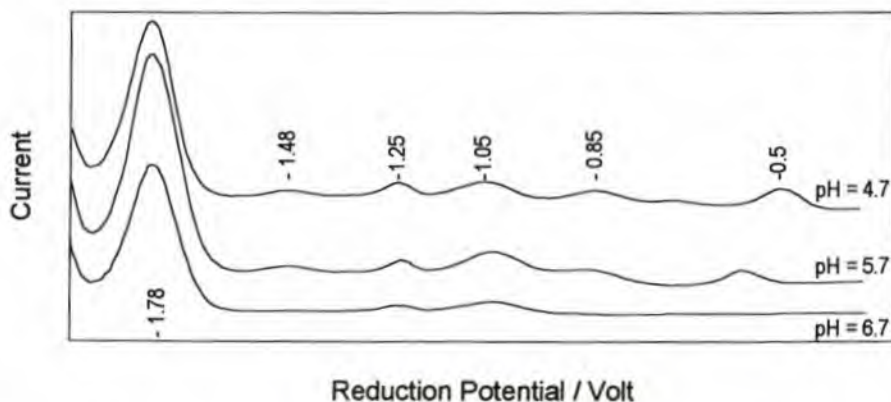


Fig. 3.5.9 Differential pulse polarograms of equimolar solutions of molybdate(VI) and citrate (0.004 M) at $\text{pH}_c = 4.7, 5.7$ and 6.7 , respectively.

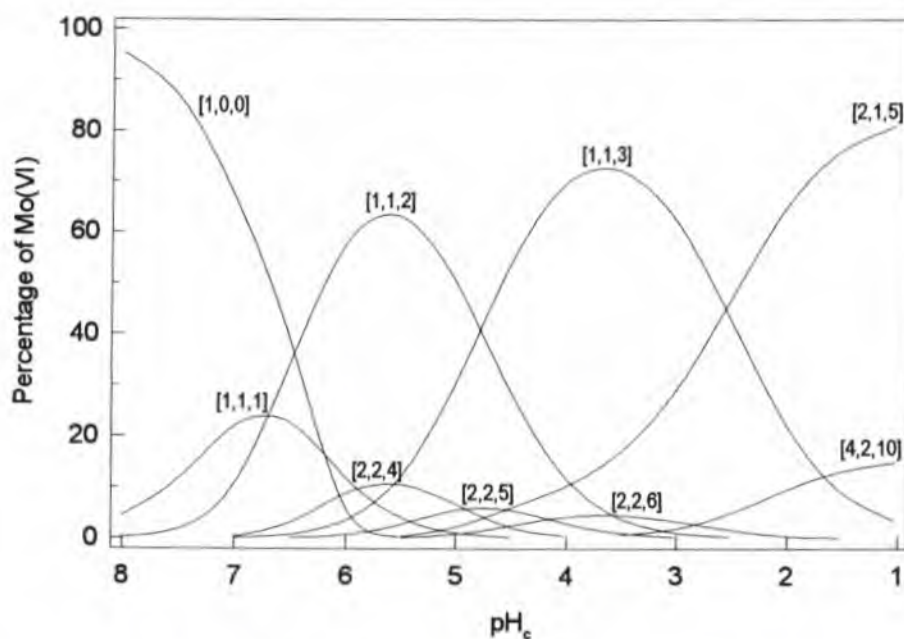


Fig. 3.5.10 Concentration of molybdate(VI)-citrate complexes, expressed as a percentage of the total molybdenum(VI) concentration, as a function of pH_c . The total concentrations of molybdate(VI) and citrate are both 0.004 M.

Further evidence for the assignment of the peaks at -1.48 and -0.5 V to the reduction of dinuclear complexes is obtained by comparing the polarograms of equimolar solutions of molybdate and citrate 0.004 M (D) and 0.008 M (E) at the same pH=5.7 (Fig. 3.5.11). Doubling of the concentration has the effect of increasing the concentrations of the dimeric complexes [2,2,4] and [2,2,5] by a factor of 3.4, while the ratio of their concentrations remains about the same. In agreement with this change the height of the peak at -1.48 V increases by a factor of ca. 3.6. For the peak at -0.5 V the factor is only ca. 2.6, which might indicate that a small amount of some mononuclear complex is also reduced at this potential (or that some other process is taking place simultaneously). In fact, for some solutions containing only mononuclear complexes (polarogram A, Fig. 3.5.7, pH=8.9), a weak peak can be seen at ca. -0.54 V when the polarogram is run at a much greater sensitivity. Doubling of the concentrations causes the concentration of the [1,1,*r*] complex to increase by a factor of ca. 1.85 and in accordance with this the peak heights at -1.25, -1.05 and -0.85 V increase by factors of 1.83, 1.84 and 1.9, respectively, confirming reduction of the mononuclear complexes at these potentials.

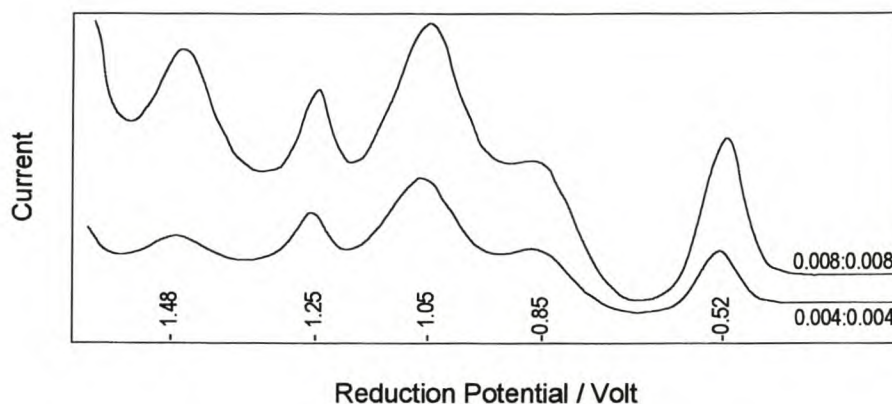


Fig. 3.5.11 Differential pulse polarograms of the solutions:

D ([Mo(VI)]=0.004 M, [cit]=0.004 M, pH=5.7) and E ([Mo(VI)]=0.008 M, [cit]=0.008 M, pH=5.7).

[1,2,*r*] complexes

At very low pH, on the other hand, conditions can be chosen for which the [1,2,6] complex is the predominant species. For example, at pH=1.4 the percentage concentration of the [1,2,6] complex is 98% in a solution with large excess of citrate (0.001:0.400). From the polarogram (F) shown in Fig. 3.5.12 it is seen that new reduction peaks occur at -1.26, -0.64 and -0.31 V. The potential of these peaks change somewhat when the conditions are changed, (G) for example, at pH=3 and higher molybdenum concentration (0.004:0.04) the reduction peaks occur at -1.22, -0.69 and -0.38 V. An additional strong reduction peak is also observed at -1.6 V, which might be due to the reduction of a [1,2,*r*] complex to a lower valent complex which is stable only under these conditions. In addition to the [1,1,3] complex (ca. 36%) the solution in question contains only the [1,2,5] and [1,2,6] complexes (6% and 56%) as major components.

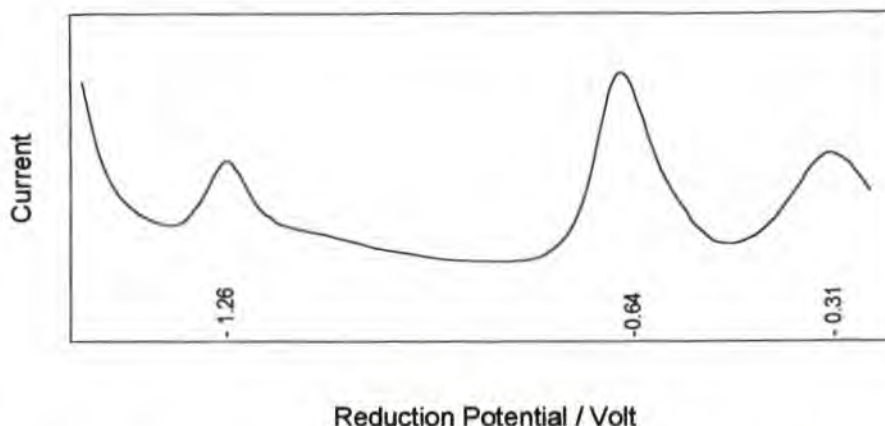


Fig. 3.5.12 Differential pulse polarograms of the solution F ($[\text{Mo(VI)}]=0.001 \text{ M}$, $[\text{cit}]=0.4 \text{ M}$, $\text{pH}=1.4$).

[2,1,r] and [4,2,r] complexes

Conditions favourable for the formation of the [2,1,5] and [4,2,r] complexes are relatively low pH and some excess of molybdate, but not so much that free molybdenum species would be comparable to the concentration of the complexes in question. By comparing polarograms (H,I) of an equimolar solution of molybdate and citrate (0.004:0.004) and polarograms (J,K) of a solution with molybdate in excess (0.004:0.002) at two suitable pH values, namely 3 (**Fig. 3.5.13**) and 3.7 (**Fig. 3.5.14**), two new reduction peaks are observed for the solutions containing an excess of molybdate. From the polarogram in **Fig. 3.5.13** it is seen that the reduction peaks occur at -1.4 and -0.66 V. The former peak can be ascribed to the reduction of the [4,2,10] complex, of which the concentration in the two solutions is 0.4% and 12.7%, respectively. The latter peak is not so well defined, but it is most likely due to the reduction of the [2,1,5] complex because it is exhibited by both solutions and stronger in the solution with the highest concentration, but not in direct proportion to the percentage concentrations (29% and 82%). However, the growth of this peak correlates well with the increase in concentration of the [2,1,5] complex with pH in the range 4.6-2.5 for equimolar solutions of molybdate and citrate (0.004:0.004).

Differential pulse polarography of various other solutions have been recorded to check the agreement between a particular complex and the associated reduction peak. Although due to great overlap of equilibria, peaks are not necessarily well defined or clearly separated under prevailing conditions, their presence in the polarograms always corresponded with the occurrence of the particular complexes in the solutions investigated.

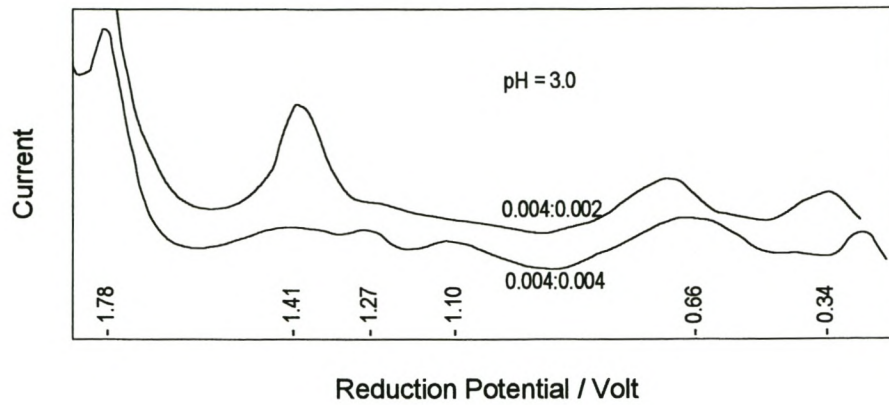


Fig. 3.5.13 Differential pulse polarograms of the solutions:

J ([Mo(VI)]=0.004 M, [cit]=0.002 M, pH=3) and H ([Mo(VI)]=0.004 M, [cit]=0.004 M , pH=3).

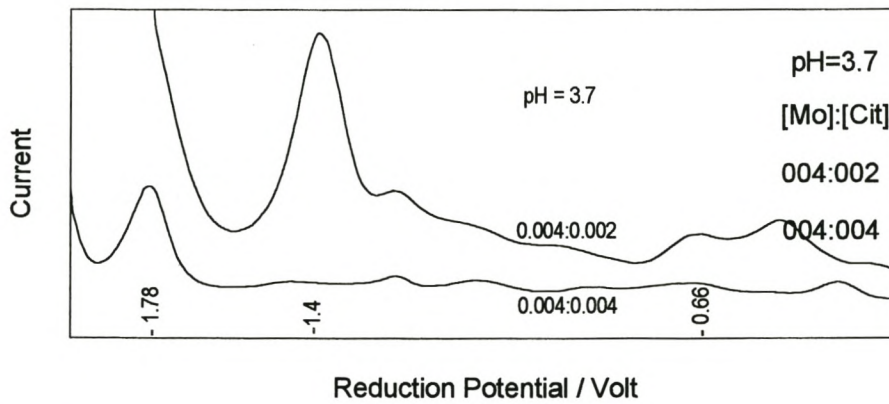


Fig. 3.5.14 Differential pulse polarograms of the solutions:

K ([Mo(VI)]=0.004 M, [cit]=0.002 M , pH=3.7) and L ([Mo(VI)]=0.004 M, [cit]=0.004 M , pH=3.7).

3.5.1.4 Enthalpimetric data and analysis

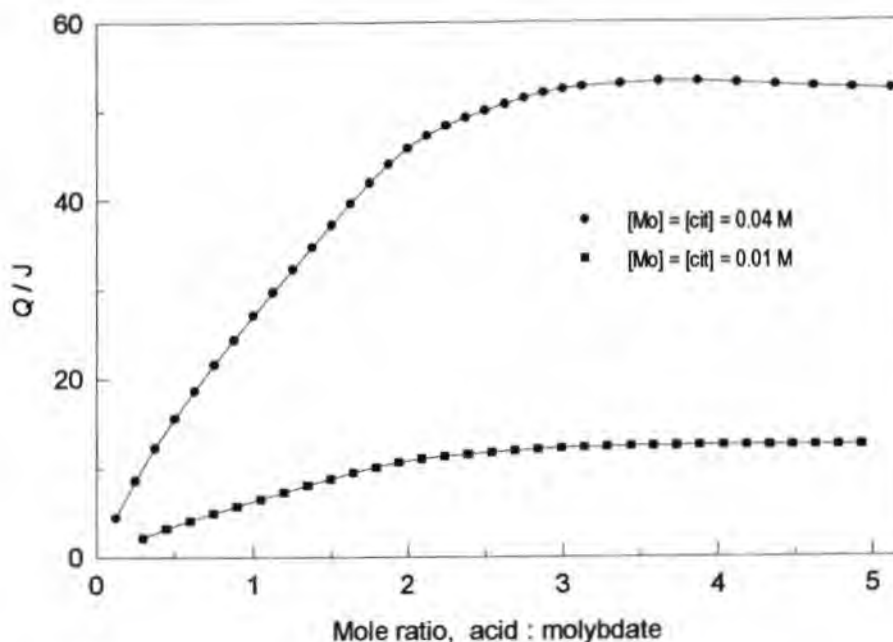


Fig. 3.5.15 Measured heat, Q , as a function of the molar ratio of acid to molybdate(VI) for two titrations. (Concentrations of molybdate(VI) and citrate shown on graph.)

The plot of Q vs mole ratio of acid added to molybdate during two enthalpimetric titrations of equimolar solutions of molybdate and citrate are shown in Fig. 3.5.15. Both plots show distinct inflexions at mole ratio acid to molybdate of 2:1 and a less obvious inflexion at the mole ratio 3:1. These inflexions are in agreement with the formation of large amounts of complexes having 1:1:2 and 1:1:3 stoichiometries (Fig. 3.5.2). The species distribution of the 0.01 M equimolar solution is very similar to that of the 0.04 M equimolar solution, except that, for the lower concentration, less than 10% of the molybdenum is present as $[2,2,r]$ complexes. From the two Q plots it can be seen that the Q value of the 0.04 M solution at a particular mole ratio is usually more than four times the value of the corresponding Q value of the 0.01 M solution. This is an indication that more heat is developed by the formation of $[2,2,r]$ complexes (per Mo) than of $[1,1,r]$ complexes, which is confirmed by the values obtained (Table 3.5.2).

To account for the rather small amount of heat involved in the protonation of free citrate, previously determined enthalpy values, $\Delta H_{011}^{\circ} = -1.3 \text{ kJ mol}^{-1}$, $\Delta H_{012}^{\circ} = -5.8 \text{ kJ mol}^{-1}$ and $\Delta H_{013}^{\circ} = -10.1 \text{ kJ mol}^{-1}$, were used as fixed parameters in the treatment of the data [135].

The values for the change in enthalpy were also calculated from the formation constants of the complexes pertaining to 2° and 25°C using the equation 2.9 (Chapter 2). These enthalpy values are denoted by ΔH_{temp}° to distinguish them from the values determined using calorimetric data.

Table 3.5.3 Calculated ΔH° and $T\Delta S^\circ$ values for the formation of some Mo(VI)-citrate complexes. 1 M (Na)Cl at 298.15 K

COMPLEX	ΔH° (kJ mol ⁻¹)	$T\Delta S^\circ$ (kJ mol ⁻¹)	ΔH°_{temp} (kJ mol ⁻¹)
[0,1,1]	-1.3 ± 0.1	28	-1.4 ± 0.4
[0,1,2]	-5.8 ± 0.1	47	-6.9 ± 0.4
[0,1,2]	-10.1 ± 0.1	58	-11.1 ± 1.0
[1,1,1] ⁴⁻	-49.9 ± 0.5	-2.2	-51 ± 3
[1,1,2] ³⁻	-56.4 ± 0.5	29.2	-53 ± 3
[1,1,3] ²⁻	-69 ± 2	42.7	-64 ± 3
[1,1,4] ⁻	-73 ± 2	47.6	
[2,2,4] ⁶⁻	-142 ± 2	36	-141 ± 4
[2,2,5] ⁵⁻	-138 ± 3	67	-146 ± 6
[2,2,6] ⁴⁻	-135 ± 4	94	-142 ± 17
[1,2,4] ⁴⁻	-86	# 59	# -77 ± 23
[1,2,5] ³⁻	-90	# 79	# -83 ± 15
[1,2,6] ²⁻	-93.2 ± 5	97	-96 ± 3
[2,1,3] ⁴⁻	-82	# 42	# -81 ± 18
[2,1,4] ³⁻	-82 ± 10	72	-
[2,1,5] ²⁻	-123 ± 2	57	-122 ± 6
[4,2,8] ⁶⁻			
[4,2,9] ⁵⁻	-242	# 105	# -252 ± 21
[4,2,10] ⁴⁻	-242 ± 8	127	-253 ± 15
[4,4,11] ⁹⁻	-308 ± 10	134	-289 ± 31
[4,4,12] ⁸⁻			
# approximate values			

Despite the respective shortcomings of the methods, the agreement between the enthalpies calculated from enthalpimetric titration data and those calculated using the difference in formation constants at different temperatures is good, particularly regarding the major species [1,1,1], [1,1,2], [1,1,3], [2,2,4], [2,1,5] and [4,2,10]. The ΔH°_{temp} values for the minor complexes for which enthalpy changes could not be calculated from experimental data could therefore be used as guidelines in allocating approximate values. Under the experimental conditions no [1,2,4] complex was present, and the percentage concentration of [1,2,5] [2,1,3] and [4,2,9] were so small that they could be ignored in the model. However, if these species were included in the model, the mentioned approximate values were fixed during the calculation of the other enthalpy values.

Evaluation of reliable ΔH° values for all the species in the pH region < 2.5, especially for the minor species, is problematical because of the great overlap of the equilibria and the little heat produced at low pH. To check for consistency of the final values (Table 3.5.2) many different combinations of titrations were used in the calculations. In all the cases the final values resulted in a good fit of the calculated heat to the measured heat.

3.5.2 Tungsten(VI)-citrate system

3.5.2.1 Potentiometric data and analysis

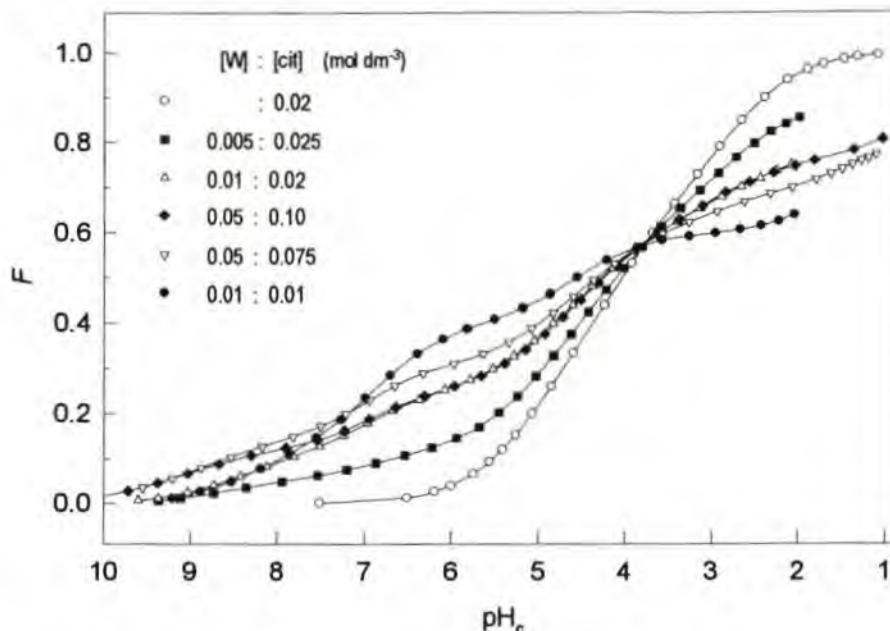


Fig. 3.5.16 Function F versus pH_c for some representative potentiometric titrations of the tungstate(VI)-citrate system

F curves

The curves (Fig. 3.5.16) show that complexation starts at pH 10 resulting in an increase in F values until at low pH the protonation of the complexes becomes more difficult than that of citrate itself. The inflexions exhibited by the curves at $\text{pH} \sim 6$ and ~ 3.0 indicate the presence of major complexes. For solutions of equal concentrations of citrate and molybdate, inflexions at 0.4 and 0.6 ($\text{pH} \sim 6$ and ~ 3) correspond to complexes $[1,1,2]$ and $[1,1,3]$.

Modelling of the W-citrate systems (species, $\log \beta$, ΔG°)

The usual tungsten(VI) species that might occur at $F < 0.6$ were included in preliminary calculations (Section 2.6.1.1), but it was found that the stability of the complexes under the experimental conditions were such that only negligible amounts ($< 0.1\%$) of these tungstate species were present. It was therefore assumed that the formation of other tungstate polyanions at $F > 0.6$ could also be neglected.

Model testing revealed that the $[1,1,r]$ were clearly the predominant species, but that several minor species also had to be included to obtain a satisfactory description of the data. A good fit ($\sigma = 1.92$, $\chi^2 = 30$) was

obtained for the final model which comprised eight species, representing 4 different tungstate: citrate ratios, protonated to various degrees: [1,1,*r*], [2,2,*r*], [1,2,6] and [2,1,4] (Table 3.5.3).

Table 3.5.4 Tungstate(VI)-citrate complexes identified and calculated $\log\beta$ and ΔG° values.
1 M (Na)Cl at 298.15 K

COMPLEX	$\log\beta_{pqr} \pm 3\sigma$	ΔG° (kJ mol ⁻¹)
[1,1,1] ⁴⁻	10.21 ± 0.01	-58.3
[1,1,2] ³⁻	17.03 ± 0.01	-97.2
[1,1,3] ²⁻	21.67 ± 0.01	-123.7
[1,1,4] ⁻	22.82 ± 0.03	-130.2
[2,2,4] ⁶⁻	34.89 ± 0.06	-199.1
[2,2,5] ⁵⁻	39.33 ± 0.12	-224.5
[1,2,6] ²⁻	35.00 ± 0.03	-199.7
[2,1,4] ³⁻	31.68 ± 0.27	-180.8

The relative standard deviations of the formation constants of only two complexes, [2,2,5] and [2,1,4], were greater than 4% (namely 9% and 19%, respectively). The existence of [2,1,4] could not be proved more conclusively because conditions favourable for its existence, *i.e.* an excess of tungstate, had to be avoided because of slow reactions and concomitant unstable potentials. It is, however, significant that all the species have molybdate analogues, even to the degree of protonation.

Distribution of species

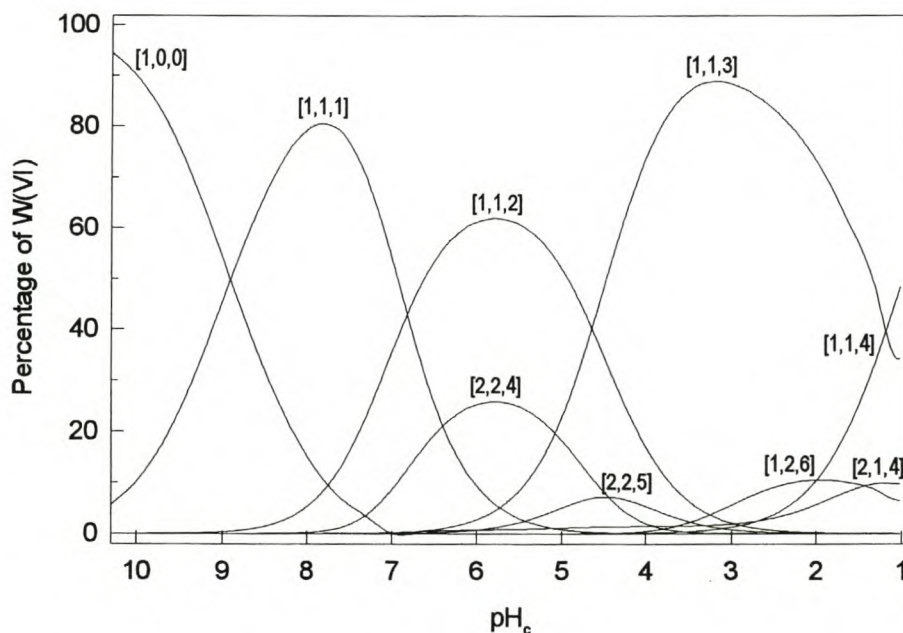


Fig. 3.5.17 Concentration of tungstate(VI)-citrate complexes, expressed as a percentage of the total tungsten(VI) concentration, as a function of pH_c . The total concentrations of tungstate(VI) and citrate are 0.05 M and 0.075 M, respectively.

3.5.2.2 Enthalpimetric data and analysis

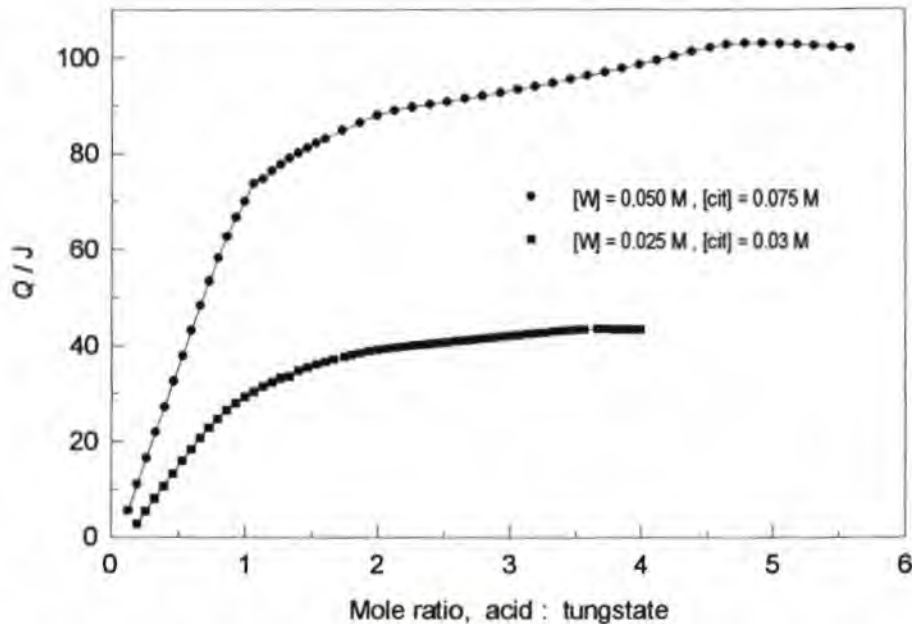


Fig. 3.5.18 Measured heat, Q , as a function of the molar ratio of acid to tungstate(VI) for two titrations. (Concentrations of tungstate and citrate are shown on the graph.)

The plot of Q vs mole ratio of acid added to tungstate during two enthalpimetric titrations of solutions with a slight excess of citrate are shown in Fig. 3.5.18. Both plots show inflexions at mole ratio acid to tungstate of 1:1 in accordance with the formation of the $[1,1,1]$ complex for which $r/p = 1$. A relatively small increase in the heat evolved is observed upon further addition of acid which results in successive protonation of the $[1,1,1]$ complex (and also of free citrate) and its conversion into the other minor species.

To account for the rather small amount of heat involved in the protonation of free citrate, previously determined enthalpy values, $\Delta H_{011}^\circ = -1.3 \text{ kJ mol}^{-1}$, $\Delta H_{012}^\circ = -5.8 \text{ kJ mol}^{-1}$ and $\Delta H_{013}^\circ = -10.1 \text{ kJ mol}^{-1}$, were used as fixed parameters in the treatment of the data [135]. Under the conditions chosen for the enthalpimetric titrations, protonation and condensation of free tungstate could be neglected.

Table 3.5.5 Calculated ΔH° and $T\Delta S^\circ$ values for the formation of some W(VI)-citrate complexes. 1 M (Na)Cl at 298.15 K.

COMPLEX	ΔH° (kJ mol ⁻¹)	$T\Delta S^\circ$ (kJ mol ⁻¹)	COMPLEX	ΔH° (kJ mol ⁻¹)	$T\Delta S^\circ$ (kJ mol ⁻¹)
$[1,1,1]^{4-}$	-63.1 ± 2.0	-5	$[2,2,4]^{6-}$	-165 ± 10	34
$[1,1,2]^{3-}$	-66.5 ± 2.0	31	$[2,2,5]^{5-}$	-187 ± 10	38
$[1,1,3]^{2-}$	-74.5 ± 2.0	49	$[1,2,6]^{2-}$	-102 ± 15	98
$[1,1,4]^-$	-74.3 ± 2.0	56	$[2,1,4]^{3-}$	-118 ± 20	63

Because of the considerable overlap of equilibria, particularly of the minor complexes, the enthalpy changes for the minor complexes could be calculated with limited accuracy only. At worst the values could be regarded only as adjustable parameters in the calculation of the ΔH° values of the predominant complexes.

3.6 COMPLEXATION WITH TARTRATE

3.6.1 Molybdenum(VI)-tartrate system

3.6.1.1 Potentiometric data and analysis

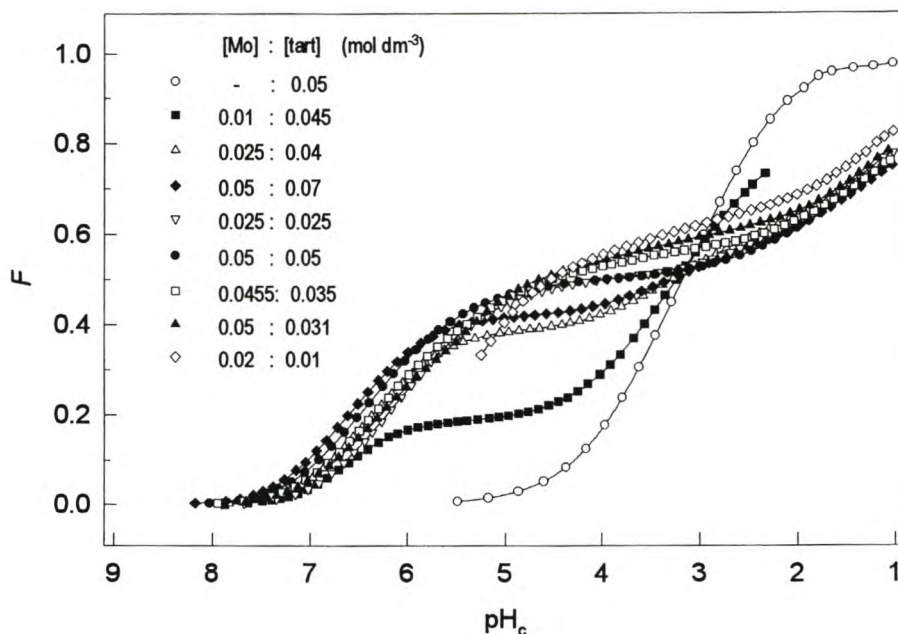


Fig. 3.6.1 Function F versus pH_c for some representative potentiometric titrations of the molybdate(VI)-tartrate system.

F curves

The curves (Fig. 3.6.1) show that complexation starts at pH 8 resulting in a sharp increase in F values until at low pH the protonation of the complexes becomes more difficult than that of tartrate itself. The very distinct inflexion of the curves of both equimolar titrations at $F = 0.5$ at pH 4.5 - 3.5 can be ascribed to the very predominant complex [4,4,8] for which $r/(2p+2q) = 0.5$ (Fig. 3.6.2). The inflexions of the other curves cannot be ascribed to single complexes because under those conditions more than one complex is important throughout the titration. The inflexion at $F = 0.2$ (at pH 6) for the titration with a four-fold excess of tartrate is the result of the complete complexation of molybdate.

Modelling of the tartrate and Mo-tartrate systems (species, $\log\beta$, ΔG°)

The protonation constants of tartrate, which were calculated from data obtained from the titration of tartrate, are shown in Table 3.6.1 and were used to produce a species distribution diagram of the tartrate system (Appendix 2).

A wider range of data were collected for this investigation than for the previous investigation [142]. Analysis of the new data led to the identification of the same major species as before, namely the complexes [1,2,2], [1,2,3], [1,2,4], [2,1,4], [2,1,5], [4,4,8], but some other, unusual types of minor species in the place of the previously proposed [4,2,6], [4,2,7], [4,4,7] and [4,4,9] complexes. The addition of combinations of different minor species improves the fit of the model containing the major species, and it is not easy to decide which combination is the best to use. It seems that possibly more of these minor complexes exist than can be accommodated in the model due to a restriction on the number of complexes which SUPERQUAD can calculate, as well as the rejection limit of 33%. After testing the model containing the minor species [2,1,2], [3,4,8], [4,3,7], [4,3,8], [4,3,9], [4,5,8] and [4,5,9] on different sets of data, and testing many other complexes against it, it is proposed that this model is very useful and that it gives a good indication of the type of complexes that exist. The overall fit of the model is good ($\sigma = 2.5$, $\chi^2 = 42$) and even the relative standard deviations of all the complexes are less than 7%, with the exception of the [4,3,9] complex with a relative standard deviation of 14%.

Table 3.6.1 Molybdate(VI)-tartrate complexes identified and calculated $\log\beta$ and ΔG° values. 1 M (Na)Cl at 298.15 K

New model			Previous Model [142]	
COMPLEX	$\log\beta_{\text{pqr}} \pm 3\sigma$	ΔG° (kJ mol ⁻¹)	$\log\beta_{\text{pqr}} \pm 3\sigma$	ΔG° (kJ mol ⁻¹)
[0,1,1] ⁻	3.660 ± 0.005 (3.72)	-20.9	-	-
[0,1,2]	6.374 ± 0.005 (6.48)	-36.4	-	-
[1,2,2] ⁴⁻	16.18 ± 0.01	-92.32	16.33 ± 0.02	-93.2
[1,2,3] ³⁻	19.85 ± 0.03	-113.3	19.99 ± 0.03	-114.1
[1,2,4] ²⁻	22.83 ± 0.03	-130.3	22.92 ± 0.03	-130.8
[2,1,2] ⁴⁻	15.33 ± 0.04	-87.47	-	-
[2,1,3] ³⁻	20.39 ± 0.12	-116.3	-	-
[2,1,4] ²⁻	24.70 ± 0.04	-140.9	24.81 ± 0.03	-141.6
[2,1,5]	25.97 ± 0.04	-148.2	26.16 ± 0.04	-149.3
[2,2,5] ³⁻	31.59 ± 0.15	-180.3	-	-
[3,4,6] ⁶⁻	47.54 ± 0.39	-271.4	-	-
[3,4,8] ⁶⁻	54.56 ± 0.11	-311.3	-	-
[4,3,8] ⁶⁻	56.35 ± 0.09	-321.5	-	-
[4,4,7] ⁹⁻	-	-	56.23 ± 0.05	-320.8
[4,4,8] ⁸⁻	61.41 ± 0.04	-350.4	61.53 ± 0.05	-351.1
[4,4,9] ⁷⁻	63.40 ± 0.33	-361.8	63.98 ± 0.08	-365.1
[4,5,8] ¹⁰⁻	64.04 ± 0.12	-365.4	-	-
[4,5,9] ⁹⁻	67.70 ± 0.09	-386.3	-	-
[4,2,6] ⁶⁻	-	-	43.41 ± 0.33	-247.7
[4,2,7] ⁵⁻	-	-	48.17 ± 0.15	-274.9

Literature value pertaining to 1 M NaClO₄ medium in brackets [62].

The previous model is also shown for comparison with the new model. It shows that the formation constants of the major complexes in the two models are very similar (not affected greatly by the minor species) and that the major difference lies in the type of minor complexes. It is interesting that the relative standard

deviation on the formation constants of the [4,2,6] and [4,2,7] complexes in the previous model are larger than in the new model, despite the many more minor species present. It is obvious now, that the [4,2,*r*] complexes were, most likely, imaginary species representing many other minor complexes in the calculations. The identification of complexes with the ratio molybdate:tartrate of 3:4, 4:3 and 4:5 during this investigation is mainly due to the inclusion of titrations of solutions which favour complexes with ratios other than the usual 1:1, 2:1 and 1:2.

Distribution of species

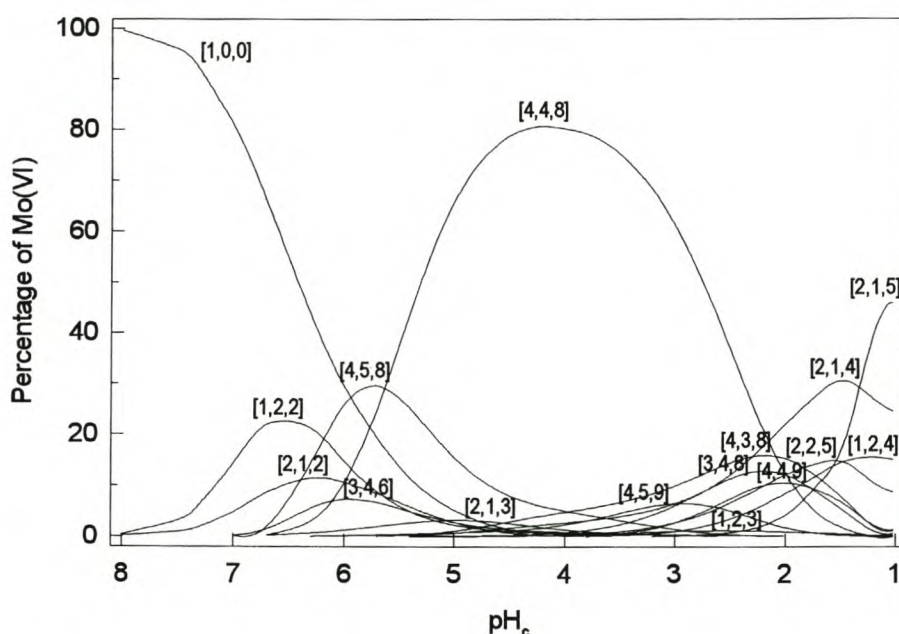


Fig. 3.6.2 Concentration of molybdate(VI)-tartrate complexes, expressed as a percentage of the total molybdenum(VI) concentration, as a function of pH_c . The total concentrations of molybdate(VI) and tartrate are both 0.05 M.

The predominance of the [4,4,8] complex in the pH range 5 - 2 in the 0.05 M equimolar solution of molybdate and tartrate and the plethora of minor complexes at $\text{pH} > 5$ and $\text{pH} < 3$ is striking (Fig. 3.6.2). If the molybdate concentration is halved, the conditions favour the complexes [*p*,*q*,*r*] for which the $q > p$, such as the [1,2,*r*], [4,5,8], [4,5,9], [3,4,6] and [3,4,8] complexes and then the [4,4,8] complex is a relatively minor species (Fig. 3.6.3).

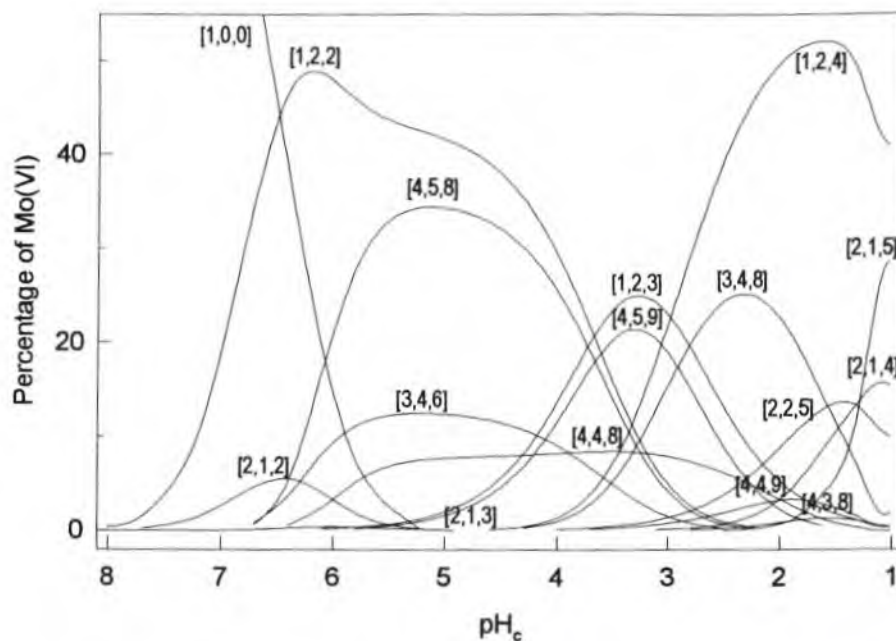


Fig. 3.6.3 Concentration of molybdate(VI)-tartrate complexes, expressed as a percentage of the total molybdenum(VI) concentration, as a function of pH_c . The total concentrations of molybdate(VI) and tartrate are 0.025 M and 0.05 M, respectively.

3.6.1.2 Enthalpimetric data and analysis

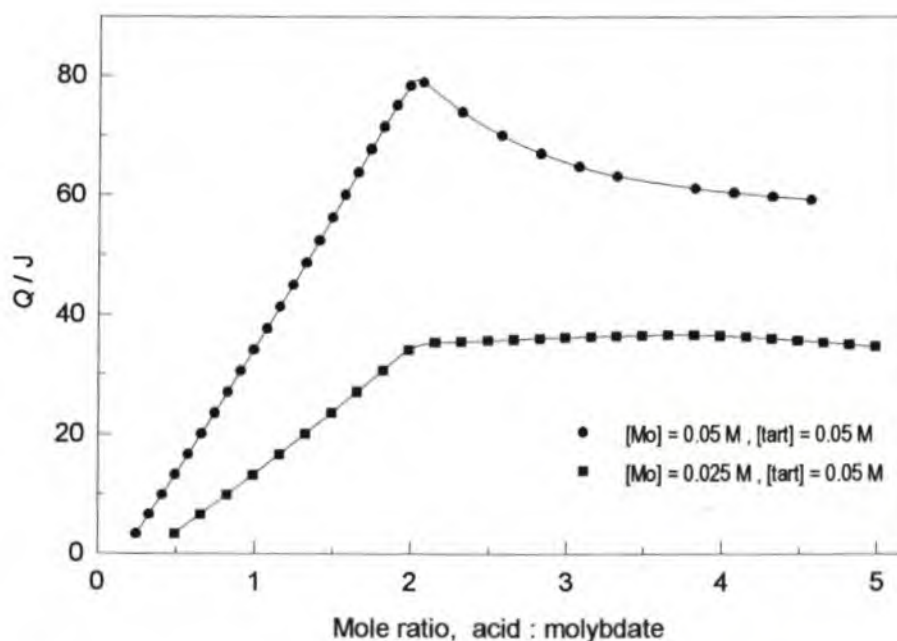


Fig. 3.6.4 Measured heat, Q , as a function of the molar ratio of acid to molybdate(VI) for two titrations. (Concentrations of molybdate and tartrate are shown on the graph.)

The plots of Q vs mole ratio of acid added to molybdate for two enthalpimetric titrations are shown in Fig. 3.6.4. Both Q plots show a distinct inflexion at a mole ratio of acid added to molybdate of approximately 2:1, indicating that the formation of a predominant complex with a [1, q ,2] stoichiometry has been completed at that point. As can be seen from the distribution curves (Fig. 3.6.2+3), both the [1,2,2] and [4,4,8] complexes reach their maximum percentages at pH values which coincide with the mole ratio indicated by the enthalpy curves. The Q value for the equimolar titration at this point is *more* than double that of the solution pertaining to a two-fold excess of tartrate, although the molybdate concentration of the equimolar solution is only double the molybdate concentration of the other solution. This is an indication that the enthalpy for the formation of the [4,4,8] complex is greater (per Mo) than for the [1,2,2] complex, which has been confirmed by the calculated values (Table 3.6.2).

To account for the heat involved in the protonation of free tartrate, the previously determined values for the change in enthalpy for these reactions were used in the calculations ($\Delta H_{011}^{\circ} = -3.1 \text{ kJ mol}^{-1}$ and $\Delta H_{012}^{\circ} = -7.0 \text{ kJ mol}^{-1}$). Under the conditions chosen for the enthalpimetric titrations, protonation and condensation of free molybdate could be neglected.

Table 3.6.2 Calculated ΔH° and $T\Delta S^{\circ}$ values for the formation of some Mo(VI)-tartrate complexes. 1 M (Na)Cl at 298.15 K .

COMPLEX	ΔH° (kJ mol ⁻¹)	$T\Delta S^{\circ}$ (kJ mol ⁻¹)
[0,1,1] ⁻	-3.1 ± 0.1	17.8
[0,1,2]	-7.0 ± 0.1	29.4
[1,2,2] ⁴⁻	-79.8 ± 1.0	12
[1,2,3] ³⁻	-80.0 ± 1.0	33
[1,2,4] ²⁻	-80.0 ± 1.0	50
[2,1,2] ⁴⁻	-80 ± 5	8
[2,1,3] ³⁻	-93 ± 12	23
[2,1,4] ²⁻	-120 ± 4	21
[2,1,5] ⁻	-117.8 ± 3.0	30
[2,2,5] ³⁻	-152 ± 10	28
[3,4,6] ⁸⁻	-239 ± 40	33
[3,4,8] ⁶⁻	-224 ± 30	87
[4,3,8] ⁶⁻	-310 ± 40	12
[4,4,8] ⁸⁻	-350 ± 30	0
[4,4,9] ⁷⁻	-353 ± 40	9
[4,5,8] ¹⁰⁻	-345 ± 50	21
[4,5,9] ⁹⁻	-408 ± 50	-22

The enthalpy values for the minor species are, understandably, less certain than for the values pertaining to the major complexes.

3.6.2 Tungsten(VI)-tartrate system

3.6.2.1 Potentiometric data and analysis

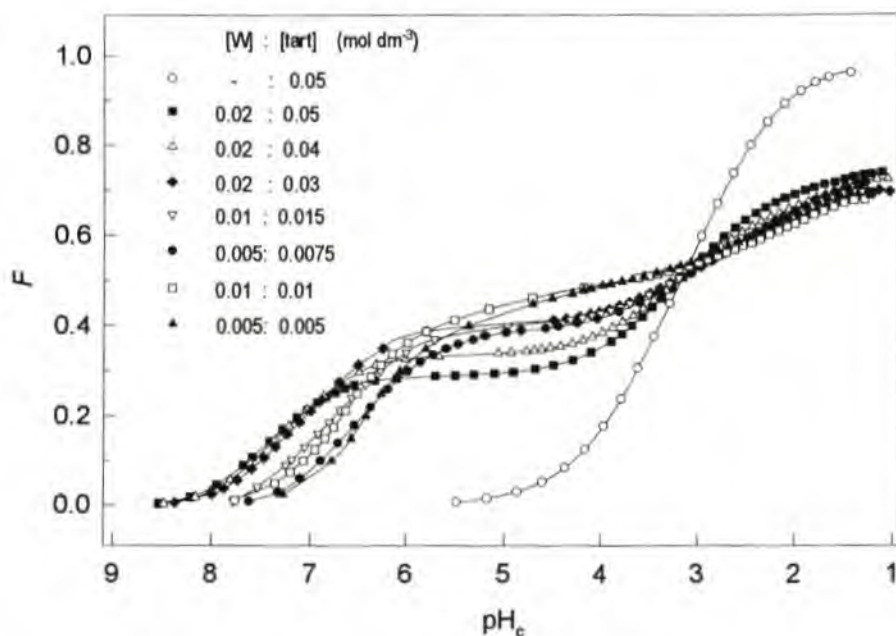


Fig. 3.6.5 Function F versus pH_e for some representative potentiometric titrations of the tungstate(VI)-tartrate system.

F curves

The curves (Fig. 3.6.5) show that complexation starts at $\text{pH} \approx 8$ resulting in a sharp increase in F values until at low pH the protonation of the complexes becomes more difficult than that of tartrate itself. The sharp inflexion pertaining to the solution with two-fold excess of tartrate at $\text{pH} \approx 6$ ($F \approx 0.3$) can be ascribed to the formation of the $[1,2,2]$ complex for which $r / (2p+2q) = 0.33$ (Fig. 3.6.6). The inflexions of the other curves cannot be ascribed easily to single complexes because more than one complex is present in significant amounts at every pH . The F values pertaining to the equimolar titrations change relatively little at $\text{pH} 3.5 - 4.5$ due to the formation of the $[4,4,8]$ complex ($F \approx 0.5$), but the resulting inflexion is not so distinct as in F curves pertaining to the molybdate-tartrate equimolar titrations where the $[4,4,8]$ predominated clearly. (Higher concentrations could be used in the molybdate-tartrate investigations which favoured the formation of such species as $[4,4,8]$.)

Modelling of the W-tartrate system (species, $\log\beta$, ΔG°)

Preliminary calculations showed that the [1,2,2], [1,2,3], [1,2,4] complexes were important and predominate under conditions of excess of tartrate, and that the complex [4,4,8] predominates at pH~4 in equimolar solutions. The very common [1,1,*r*] and [2,2,*r*] complexes were not accepted in the final models. A variety of more unusual species ([3,4,*r*], [4,5,*r*], [4,3,*r*], etc.) were tested and their inclusion proved to be the only way of improving the fit of the model significantly. The model shown below (Table 3.6.3) is proposed as the best representation of the tungstate-tartrate system on the grounds of the good overall fit ($\sigma = 0.83$, $\chi^2 = 69$) as well as its similarity to the model of the molybdate-tartrate system.

Table 3.6.3 Tungstate(VI)-tartrate complexes identified and calculated $\log\beta$ and ΔG° values.
1 M (Na)Cl at 298.15 K

COMPLEX	$\log\beta_{\text{pqr}} \pm 3 \sigma$	ΔG° (kJ mol ⁻¹)
[0,1,1] ⁻	3.660 ± 0.01	-20.9
[0,1,2]	6.374 ± 0.01	-36.4
[1,2,2] ⁴⁻	17.85 ± 0.04	-101.9
[1,2,3] ³⁻	21.38 ± 0.05	-122.0
[1,2,4] ²⁻	24.29 ± 0.05	-138.6
[2,1,2] ⁴⁻	16.94 ± 0.48	-96.66
[2,1,3] ³⁻	23.64 ± 0.09	-134.9
[2,1,4] ²⁻	27.38 ± 0.09	-156.2
[3,4,6] ⁸⁻	52.65 ± 0.11	-300.4
[3,4,8] ⁶⁻	58.86 ± 0.26	-335.9
[4,3,8] ⁶⁻	62.46 ± 0.12	-356.4
[4,4,8] ⁸⁻	66.79 ± 0.09	-381.1
[4,5,9] ⁹⁻	73.68 ± 0.13	-420.4

The relative standard deviations of most species are < 9%. The exceptions are the [2,1,2] and [3,4,8] complexes with relative standard deviations of 31% and 18%, respectively. The experimental conditions are not very favourable for the formation of the [2,1,*r*], [3,4,*r*], [4,3,*r*] and [4,5,*r*] or other similar complexes. It is therefore difficult to discriminate between complexes (e.g. [3,4,8], [4,5,10] and [5,6,13]) based on calculations of these data. The unusual complexes [3,4,*r*], [4,3,8] and [4,5,9] might be polymeric, tungstate-tartrate chains (Chapter 4). If so, it is possible that tungstate or tartrate or tungstate-tartrate units can be added to, or subtracted from them to form other polymeric species. It is therefore conceivable that many more (or other) complexes exist in solution than are accommodated in the model.

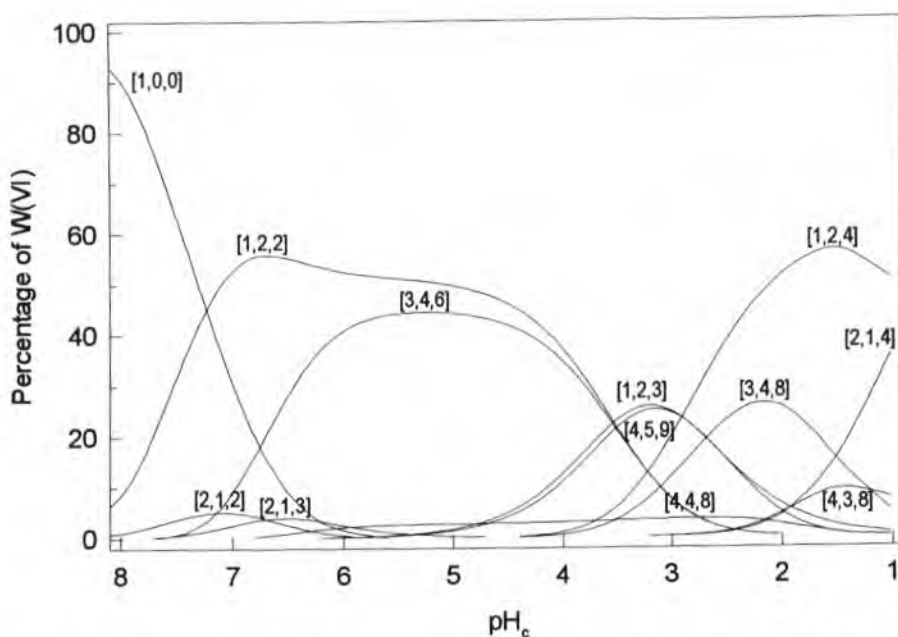
Distribution of species

Fig. 3.6.6 Concentration of tungstate(VI)-tartrate complexes, expressed as a percentage of the total tungsten(VI) concentration, as a function of pH_c . The total concentrations of tungstate(VI) and tartrate are 0.02 M and 0.04 M, respectively.

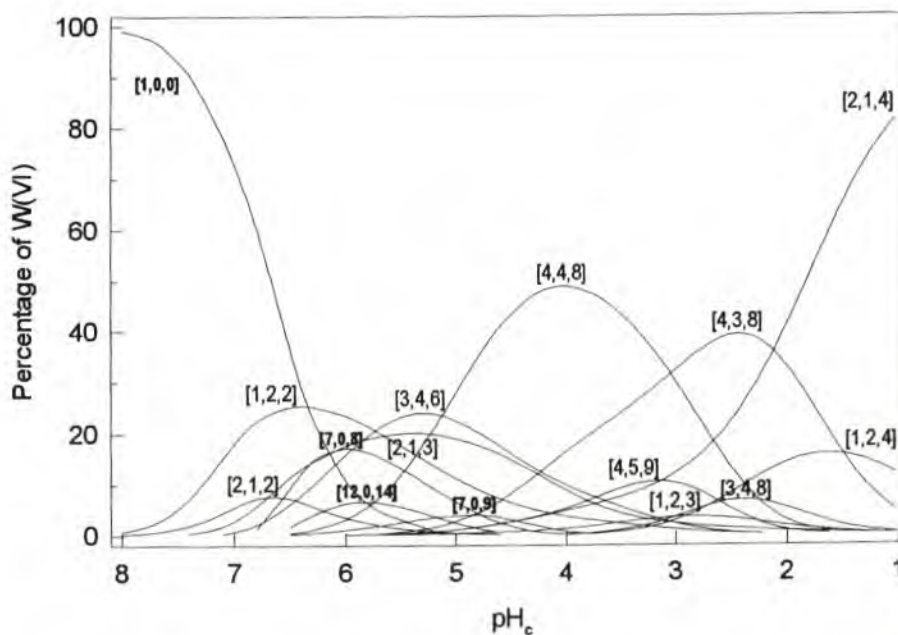


Fig. 3.6.7 Concentration of tungstate(VI)-tartrate complexes, expressed as a percentage of the total tungsten(VI) concentration, as a function of pH_c . The total concentrations of tungstate(VI) and tartrate are both 0.01 M. (Uncomplexed polytungstates are also shown.)

3.6.2.2 Enthalpimetric data and analysis

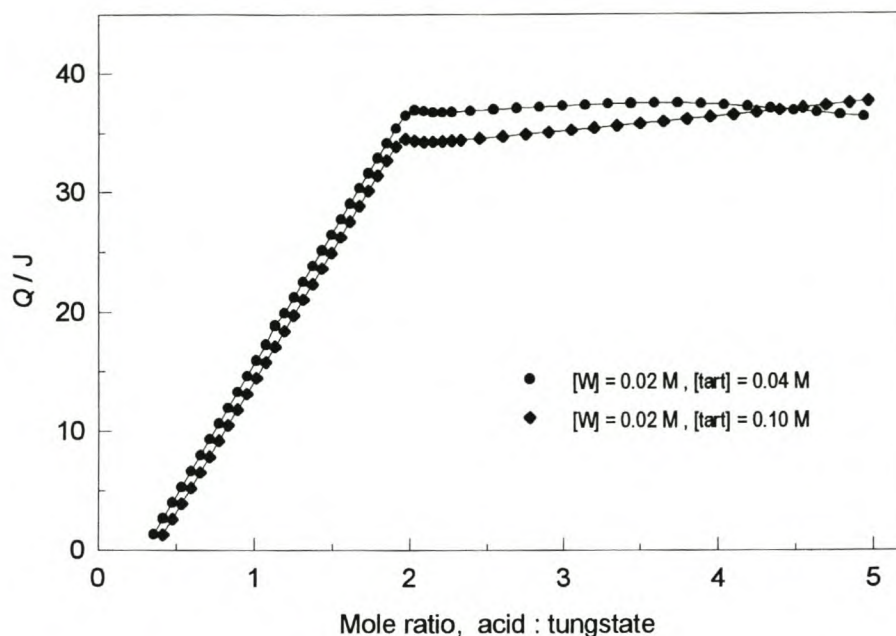


Fig. 3.6.8 Measured heat, Q , as a function of the molar ratio of acid to tungstate(VI) for two titrations. (Concentrations of tungstate(VI) and tartrate are shown on the graph.)

The plots of Q vs mole ratio of acid added to tungstate for two enthalpimetric titrations are shown in Fig. 3.6.8. Both Q plots show a distinct inflexion at a mole ratio of acid added to tungstate of approximately 2:1, indicating that the formation of a predominant complex with a $[1,q,2]$ stoichiometry has been completed at that point. As can be seen from the distribution curves, both the $[1,2,2]$ and $[3,4,6]$ complexes reach their maximum percentages at pH values which coincide with the mole ratio indicated by the enthalpy curves. A relatively small increase in the heat evolved is observed upon further addition of acid which results in the successive protonation of the monomeric complex (and also of free tartrate) and its conversion to the other minor species.

To account for the heat involved in the protonation of free tartrate, the previously determined values for the change in enthalpy for these reactions were used in the calculations ($\Delta H_{011}^{\circ} = -3.1 \text{ kJ mol}^{-1}$ and $\Delta H_{012}^{\circ} = -7.0 \text{ kJ mol}^{-1}$). Under the conditions chosen for the enthalpimetric titrations, protonation and condensation of free tungstate could be neglected.

Table 3.6.4 Calculated ΔH° and $T\Delta S^\circ$ values for the formation of some W(VI)-tartrate complexes. 1 M (Na)Cl at 298.15 K .

COMPLEX	ΔH° (kJ mol ⁻¹)	$T\Delta S^\circ$ (kJ mol ⁻¹)
[0,1,1] ⁻	-3.1 ± 0.1	17.8
[0,1,2]	-7.0 ± 0.1	29.4
[1,2,2] ⁴⁻	-83.8 ± 2.0	18
[1,2,3] ³⁻	-84.3 ± 1.0	38
[1,2,4] ²⁻	-83.3 ± 2.0	55
[2,1,2] ⁴⁻	-121 ± 10	-24
[2,1,3] ³⁻	-144 ± 5	-10
[2,1,4] ²⁻	-141 ± 4	15
[3,4,6] ⁶⁻	-263 ± 10	37
[3,4,8] ⁶⁻	-261 ± 10	75
[4,3,8] ⁶⁻	-275 ± 40	81
[4,4,8] ⁸⁻	-334 ± 40	47
[4,5,9] ⁹⁻	-351 ± 40	70

The uncertainty of the enthalpy values for the minor species are, understandably, greater than for the major complexes.

3.7 COMPLEXATION WITH ASPARTATE

3.7.1 Molybdenum(VI)-aspartate system

3.7.1.1 Potentiometric data and analysis

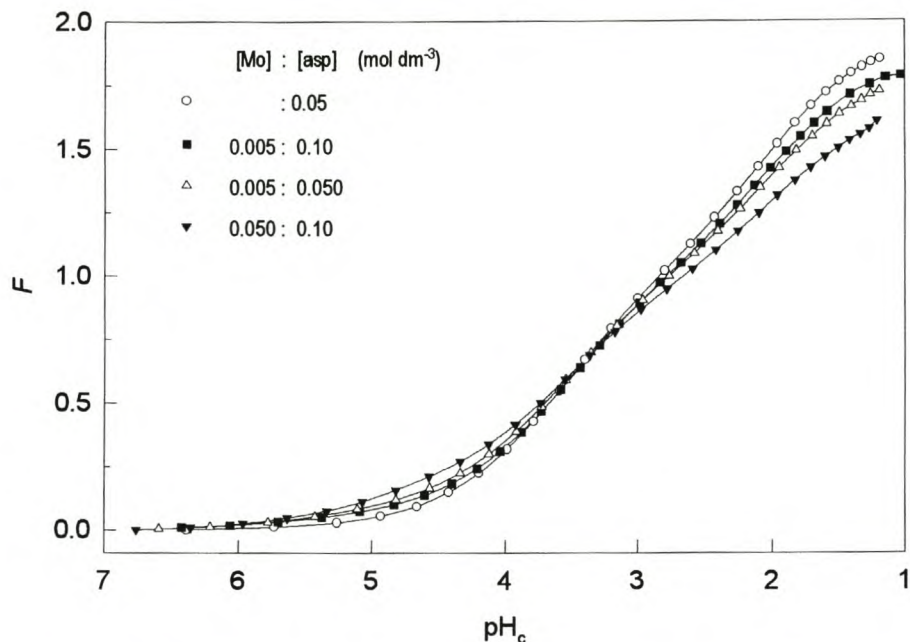


Fig. 3.7.1 Function F versus pH_c for some representative potentiometric titrations of the molybdate(VI)-aspartate system.

F curves

The curves (Fig. 3.7.1) show that complexation starts at $\text{pH} \sim 7$. An F value of 1.0 indicates an average charge of zero for the species in solution. This is the case at $\text{pH} \sim 3$ where H_2asp (aspartic acid) is the major species. A decrease in pH causes further protonation of aspartic acid until at $\text{pH} \sim 1$ more than 80% is in the form of H_3asp^+ . At low pH protonation of the complex species is more difficult than that of aspartate whereas the opposite is true at high pH ; the crossover point is at $\text{pH} \sim 3.4$. The small difference between the F curves of titrations of the molybdate-aspartate mixtures and aspartate alone is indicative of weak complexation.

Modelling of the aspartate and Mo-aspartate systems (species, $\log\beta$, ΔG°)

The protonation constants of aspartate, which were calculated from data obtained from the titration of aspartate, are shown in Table 3.7.1 and were used to produce a species distribution diagram of the aspartate system (Appendix 2).

Preliminary calculation of the data of this complex system showed that using data collected from titrations of solutions without an excess of aspartate would be meaningless as very little complexation would occur. Even in a titration of a solution with a ten-fold excess of aspartate, 7% of the molybdate was still uncomplexed in the pH range investigated.

The [1,1,1] complex could be identified easily as the first major complex that forms upon acidification of a mixture of molybdate and aspartate. Its inclusion in a particular model invariably caused a considerable improvement in the fit while the standard deviation of its formation constant was significantly smaller than that of any other species considered. Selection of the other complexes was not straightforward.

As mentioned above, an excess of ligand is a prerequisite for substantial complexation, but it turned out that some of the most likely complexes in the model, [2,1,4] and [2,1,5], have a stoichiometry for which the optimum conditions would be equal concentrations of molybdate and aspartate or even an excess of molybdate. After some extensive model testing, several different combinations of species were found which resulted in practically the same fit. For example, alternative (preliminary) models in which either the [1,1,2] or [2,2,4] species were retained had σ values of 2.31 and 2.37, respectively. The only hope of better discrimination between different models was to collect additional data, which would enable the speciation program to distinguish between certain complexes. A preliminary model was used in the calculations of the program KON3PH [113] to find suitable experimental conditions. Various additional titrations were then carried out and all the data used in the further calculations (Appendix 1).

The best model obtained comprised nine complexes representing 5 different molybdate:aspartate ratios protonated to various degrees: [1,1,*r*], [1,2,*r*], [2,1,*r*], [4,4,*r*] and [2,4,*r*] (Table 3.7.1). Of these species only the [1,2,1] complex was a very minor species (<10%) under all conditions. The major species, occurring in relative concentrations greater than 40%, are the [1,1,1], [2,1,4] and [2,1,5] complexes. In the final computer run two titrations (pertaining to a two- and five-fold excess of ligand respectively) for which the uncomplexed molybdate species were at their highest concentrations were omitted. The fit improved slightly but the model was not affected and practically identical values for the formation constants were obtained. Also, the values calculated for the protonation constants of aspartate were in excellent agreement with those determined independently.

A value for the sample standard deviation, $\sigma = 1.44$ ($\chi^2 = 38$), implies a very good fit. The only species for which the relative standard deviation of the formation constant is greater than 10%, is the [4,4,10] with a 23% deviation; for most titrations its concentration was rather small and still on the increase at the lowest pH which precludes satisfactory characterization.

Table 3.7.1 Molybdate(VI)-aspartate complexes identified and calculated $\log\beta$ and ΔG° values.

1 M (Na)Cl at 298.15 K

COMPLEX	$\log\beta_{\text{pqr}} \pm 3 \sigma$	ΔG° (kJ mol ⁻¹)
[0,1,1]	3.64 ± 0.01 (3.69)	-20.8
[0,1,2] ⁺	5.65 ± 0.01 (5.80)	-32.3
[1,1,1] ²⁻	6.54 ± 0.01	-37.3
[1,1,2] ⁻	9.84 ± 0.12	-56.2
[1,2,1] ³⁻	6.57 ± 0.10	-37.5
[1,2,2] ²⁻	11.47 ± 0.04	-65.5
[2,1,4] ⁻	21.20 ± 0.05	-121.0
[2,1,5]	23.50 ± 0.05	-134.1
[4,4,9] ³⁻	50.86 ± 0.11	-290.3
[4,4,10] ²⁻	53.48 ± 0.34	-305.2
[2,4,8]	37.74 ± 0.10	-215.4

Literature value pertaining to 1 M NaClO₄ medium in brackets [136].

Except for the well known [1,1,1] complex the rest of the model proposed does not agree with a recently reported model [66] consisting of the complexes [1,1,1], [2,2,4], [2,2,5] and [2,2,6], which pertains to a different ionic medium, *i.e.*, 0.1 M NaNO₃. This model was based on three potentiometric titrations with molybdate to aspartate ratios of 1:4, 1:5 and 1:10 for an initial molybdate concentration of 0.002 - 0.003 M. For our data the model now proposed (Table 3.7.1) resulted in a much better fit ($\sigma = 1.44$) than for the model mentioned above ($\sigma = 4.36$). The improvement in the fit upon the addition of species to a model comprising initially only four complexes and subsequent rejection of [2,2,*r*] species is illustrated in Table 3.7.2. The final model can be arrived at *via* different routes, for example, by starting with a series of four mononuclear species.

Table 3.7.2 Results of some model tests with SUPERQUAD. Improvement in fit is indicated by a decreasing σ value. (X : species rejected in a particular model-testing.)

$\sigma = 4.36$	$\sigma = 2.87$	$\sigma = 2.07$	$\sigma = 1.61$	$\sigma = 1.44$
[1,1,1] ²⁻	[1,1,1] ²⁻	[1,1,1] ²⁻	[1,1,1] ²⁻	[1,1,1] ²⁻
	[1,1,2] ⁻	[1,1,2] ⁻	[1,1,2] ⁻	[1,1,2] ⁻
[2,2,4] ²⁻	[2,2,4] ²⁻	[2,2,4] ²⁻	X	X
[2,2,5] ⁻	[2,2,5] ⁻	[2,2,5] ⁻	X	X
[2,2,6]	[2,2,6]	[2,2,6]	[2,2,6]	X
		[1,2,1] ³⁻	[1,2,1] ³⁻	[1,2,1] ³⁻
		[1,2,2] ²⁻	[1,2,2] ²⁻	[1,2,2] ²⁻
			[2,1,4] ⁻	[2,1,4] ⁻
			[2,1,5]	[2,1,5]
			[4,4,9] ³⁻	[4,4,9] ³⁻
			[4,4,10] ²⁻	[4,4,10] ²⁻
				[2,4,8]

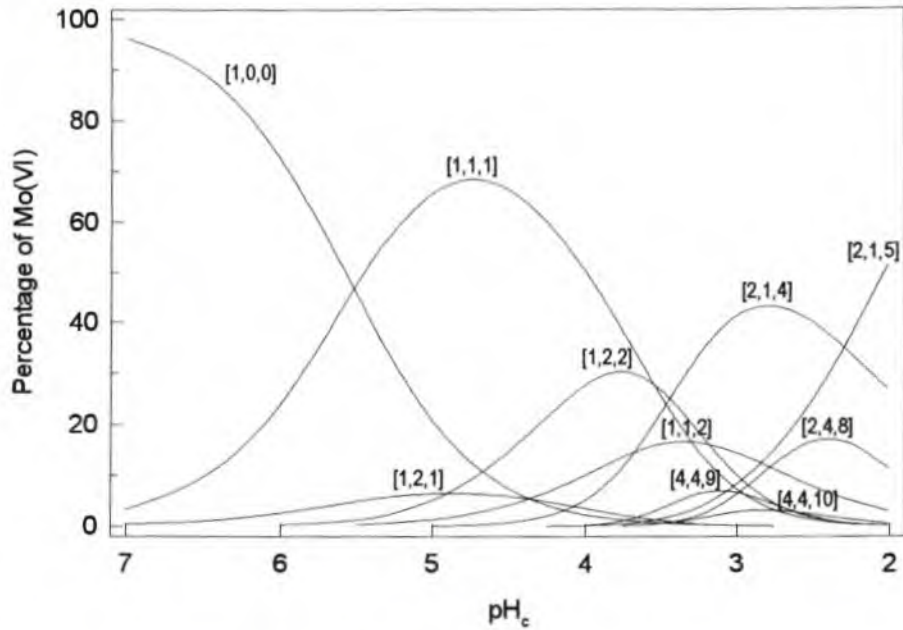
Distribution of species

Fig. 3.7.2 Concentration of molybdate(VI)-aspartate complexes, expressed as a percentage of the total molybdenum(VI) concentration, as a function of pH_c . The total concentrations of molybdate(VI) and aspartate are 0.005 M and 0.1 M, respectively.

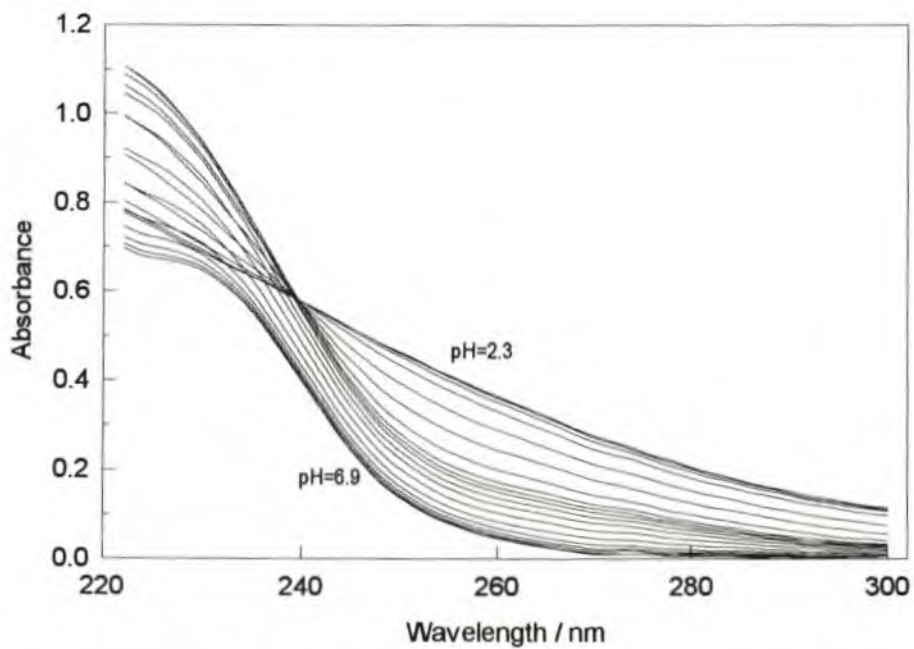
3.7.1.2 Spectrophotometric data and analysis

Fig. 3.7.3 Change in absorption spectra with pH_c from 6.9 to 2.3. The total concentrations of molybdate(VI) and aspartate are 0.005 M and 0.1 M, respectively.

The absorbance of the aspartate species at the chosen path length is small and shows only a small dependence on pH below 230 nm. (The absorbance increases rapidly, only below 220 nm.) An aspartate spectrum measured against air could therefore simply be subtracted from the molybdate-aspartate spectra measured against air in order to get spectra representing complexation. There was no need to determine the spectra of the individual aspartate species. (The formation constants were therefore also not determined spectrophotometrically.)

Calculation of models (complexes, formation constants, absorption spectra)

Under the experimental conditions (10 and 20-fold excess of aspartate), molybdenum side equilibria could be neglected as a first approximation. Calculations based on the potentiometric model showed that in the case of aspartate in ten-fold excess a maximum of only about 5% of the molybdate is present in the form of heptamolybdates at pH=4. Despite the rather limited wavelength range available for investigating complex formation, the variation in absorption with pH at a number of wavelengths is sufficient to be useful for quantitative treatment (Fig. 3.7.3).

The two sets of data were treated separately using the program SPECFIT [127]. By application of model-free evolving factor analysis (EFA), concentration profiles with at least four complexes could be constructed. For the data pertaining to twenty-fold excess of aspartate, for instance, the concentration profiles show maxima at pH 4.8, 3.8 and 3.4 while the concentration of the last component(s) still increases at pH 2.3. It can be seen from Fig. 3.7.2 that the maxima at pH 4.8 and 3.8 correspond with the [1,1,1] and [1,2,2] complexes. Because of the great overlap of equilibria the maximum of the concentration profile at pH=3.4 cannot be assigned unambiguously to the [1,1,2] complex.

When EFA is carried out with one more complex, the additional concentration profile has a maximum at pH 2.9 which concurs approximately with the distribution curve of the [2,1,4] complex. However, the concentration profile with maximum at pH 3.4 is then defined by only one experimental curve. Although this analysis supports the potentiometric results, it shows that the change in absorption with pH in the measurable wavelength range is not sufficient to evaluate equilibrium constants for all the complexes in the system. Apparently the spectra of some of the species show very little or no change at all in the wavelength range 222-300 nm. Although reasonable values for the formation constants of some of the species could be calculated (while fixing the formation constants of some others) the spectra obtained were often unsatisfactory with very large or even negative molar absorptivities for some species at certain wavelengths. However, by using only the first ten spectra of each data set (pH 7.0 - 4.9) the formation constant for the [1,1,1] complex could be calculated with the value $\log \beta_{111} = 6.52 \pm 0.02$, which is in very good agreement with that obtained by potentiometry (6.54).

3.7.1.3 Enthalpimetric data and analysis

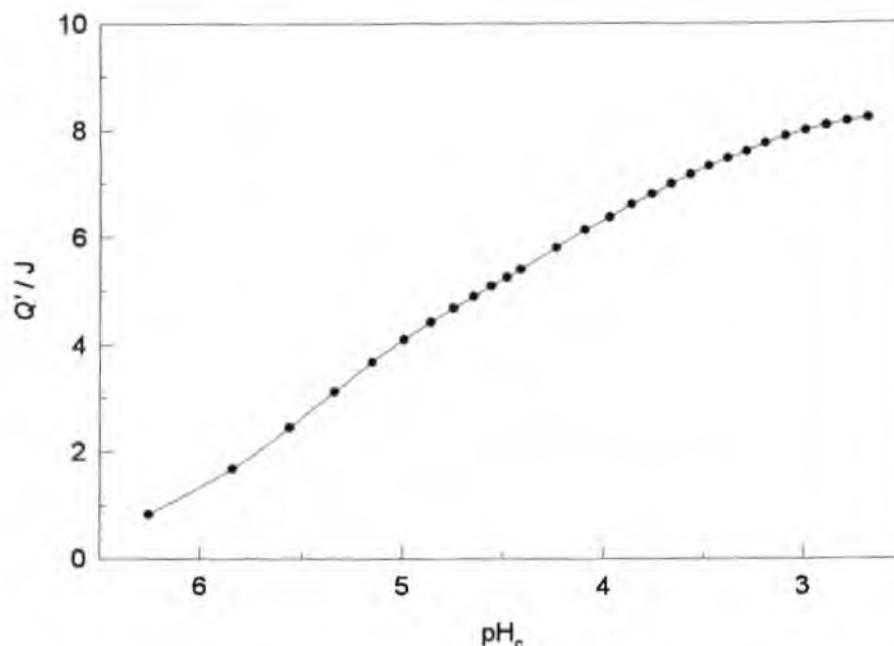


Fig. 3.7.4 Measured heat of complexation, Q' , as a function of the pH_c for a titration of 0.01 M molybdate(VI) and 0.1 M aspartate.

The plot of the heat of complexation, Q' , vs calculated pH is shown in Fig 3.7.4. The heat of complexation, Q' , is obtained by subtracting the heat evolved by protonation of the free aspartate (in ten-fold excess) from the total measured heat. The curve shows only a slight inflexion at $\text{pH} \sim 5$ where the [1,1,1] complex reaches a maximum. At this pH about 90% of the molybdate is complexed and the further substantial increase in heat observed with decrease in pH implies more favourable enthalpy changes for successive complex formation. This is confirmed by the greater values (per molybdate) for the ΔH° for the formation of the important complexes [2,1,4], [2,1,5] and [1,2,2] which are present at lower pH (Table 3.7.3).

To account for the heat involved in the protonation of free aspartate the values for the change in enthalpy for these reactions were determined in a separate titration (Appendix 1). The values obtained after correcting for the endothermic heat of dilution were $\Delta H_{011}^\circ = -5.8 \text{ kJ mol}^{-1}$ and $\Delta H_{012}^\circ = -10.2 \text{ kJ mol}^{-1}$. The very small amount of heat (< 3.4% at any titration point) contributed by the side reactions of molybdate with hydrogen ions has also been taken into account in the calculations using known ΔH° values of molybdate species (Table 2.5) which are present in concentrations ranging from 0.5 to 5% (*cf.* 2.6.3).

Table 3.7.3 Calculated ΔH° and $T\Delta S^\circ$ values for the formation of some Mo(VI)-aspartate complexes, 1 M (Na)Cl at 298.15 K

COMPLEX	ΔH° (kJ mol ⁻¹)	$T\Delta S^\circ$ (kJ mol ⁻¹)
[0,1,1]	-5.8 ± 0.2	15.0
[0,1,2] ⁺	-10.2 ± 0.6	22.1
[1,1,1] ²⁻	-27.4 ± 0.6	10
[1,1,2] ⁻	-20 ± 7	36
[1,2,1] ³⁻	-34 ± 8	4
[1,2,2] ²⁻	-43 ± 3	23
[2,1,4] ⁻	-96 ± 2	25
[2,1,5]	-99 ± 8	35
[4,4,9] ³⁻	-119 ± 10	171
[4,4,10] ²⁻	-122 ± 15	183
[2,4,8]	-69 ± 10	146

Literature values for formation of the aspartate species are $\Delta H_{011}^\circ = -5.0 \text{ kJ mol}^{-1}$ and $\Delta H_{012}^\circ = -13.4 \text{ kJ mol}^{-1}$ [133].

Under the experimental conditions the complexes [1,1,1], [1,2,2] and [2,1,4] predominate and many other complexes, particularly the [1,2,1], [2,4,8], [4,4,9] and [4,4,10], are present at very low percentage concentrations only. The ΔH° values for these species are obviously rather uncertain.

3.7.2 Tungsten(VI)-aspartate system

3.7.2.1 Potentiometric data and analysis

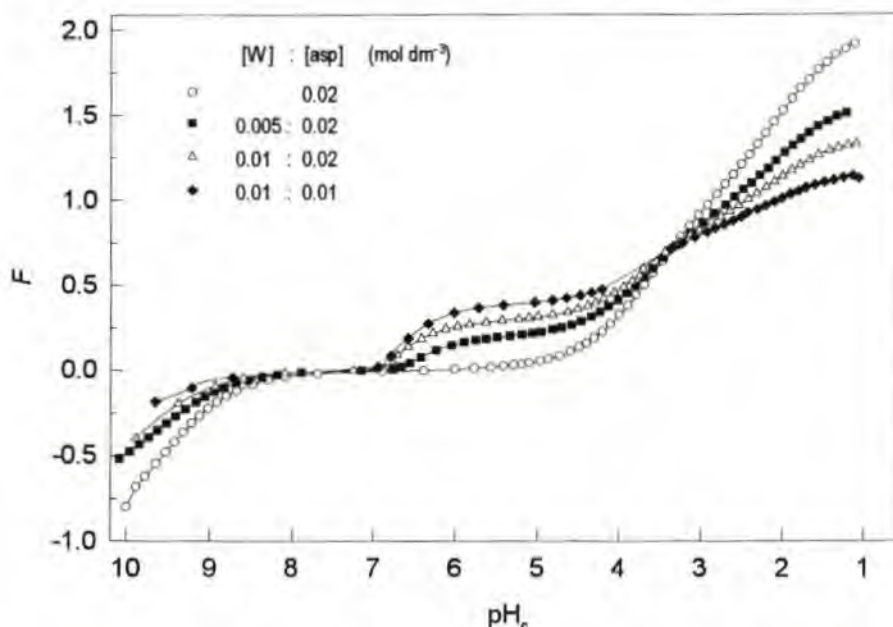


Fig. 3.7.5 Function F versus pH_c for some representative potentiometric titrations of the tungstate(VI)-aspartate system.

F curves

If the F curves (Fig. 3.7.5) and the distribution curves (Fig. 3.7.6) are compared, it can be seen that the F curves in the pH range 10 - 7 represent only the protonation of aspartate to Hasp^- . At pH 7 - 5 the shapes of the F curves are strongly dictated by the protonation of uncomplexed tungstate. In the region pH 3.5 - 1 the protonation of the $[2,1,r]$ complexes is more difficult than the protonation of aspartate alone.

Modelling of the W-aspartate system (species, $\log\beta$, ΔG°)

Preliminary calculations showed that complexation only takes place at $\text{pH} < 4$, whether complexation has been "encouraged" by an excess of aspartate or not. This means that, before complexation starts during a titration, uncomplexed tungstate is acidified to the extent ($F > 0.6$) that slow equilibria cannot be avoided completely under the experimental conditions. Preliminary models also indicated that complexes such as $[1,2,r]$ are not present in solution and that $[2,1,r]$ are the most likely species. Further titrations of solutions with an excess of aspartate would therefore not contribute significantly to finding the "best" complex model and it was decided not to extend the titrations to more conditions. Many species were then tested again, and in different combinations, but only the two species, $[2,1,4]$ and $[2,1,5]$, were accepted in the model, which form at $\text{pH} < 4$ (Table 3.7.4).

Table 3.7.4 Tungstate(VI)-aspartate complexes identified and calculated $\log\beta$ and ΔG° values. 1 M (Na)Cl at 298.15 K

COMPLEX	$\log\beta_{pqr} \pm 3 \sigma$	ΔG° (kJ mol ⁻¹)
[0,1,-1]	-9.55 ± 0.03	+54.52
[0,1asp,1]	3.64 ± 0.01	-20.8
[0,1asp,2] ⁺	5.65 ± 0.01	-32.3
[2,1,4] ⁻	24.88 ± 0.50	-142.0
[2,1,5]	27.43 ± 0.50	-156.6

A value for the sample standard deviation, $\sigma = 0.90$ implies a very good fit. The relative standard deviation of the species [2,1,4] and [2,1,5] are 14% and 8% , respectively, which is a higher percentage than usual for predominant species (in this case, predominant over a small pH region). This is indicative of the greater uncertainties in the data for the W-aspartate system: First, the tungsten(VI) equilibrium model holds true only in the region $F < 0.6$ and does not describe the species in the region of slow equilibria $F > 0.6$. It had to be used, however, as the best approximation in the region $F > 0.6$. The [7,0,9] species is, according to this approximate model, the predominant tungsten species in the slow equilibria region, but it must be borne in mind that some other, unknown, tungsten species might exist below pH 5. Second, although care has been taken to establish equilibrium after every addition and before taking a mV reading, the data pertaining to the slow equilibria region might not be absolutely representative of equilibrium conditions. (Every apparently stable mV reading could not be checked to ensure complete stability; the titration would take too long, resulting in other uncertainties like change in volume due to evaporation.) This possible error in procedure might have led to data being less accurate than usual, especially for the titration of the equimolar solution.

Despite the uncertainties and experimental limitations the identified [2,1,4] and [2,1,5] complexes seem very probable as their analogues also predominate in the related molybdate-aspartate system at pH < 4. The [1,1,*r*] complexes of the molybdate-aspartate system are not present in the tungstate-aspartate system in the pH region 7 - 4, where only uncomplexed tungstate (and aspartate) occur. This is probably due to the greater stability of tungstate polyanions compared to the molybdate polyanions. (The molybdate-aspartate complexes are already weak, but can only just compete with the molybdate species in the region pH 7-4.)

Distribution of species

The different uncomplexed tungstate and aspartate species are also shown, as they are of great significance in this weakly complexed system.

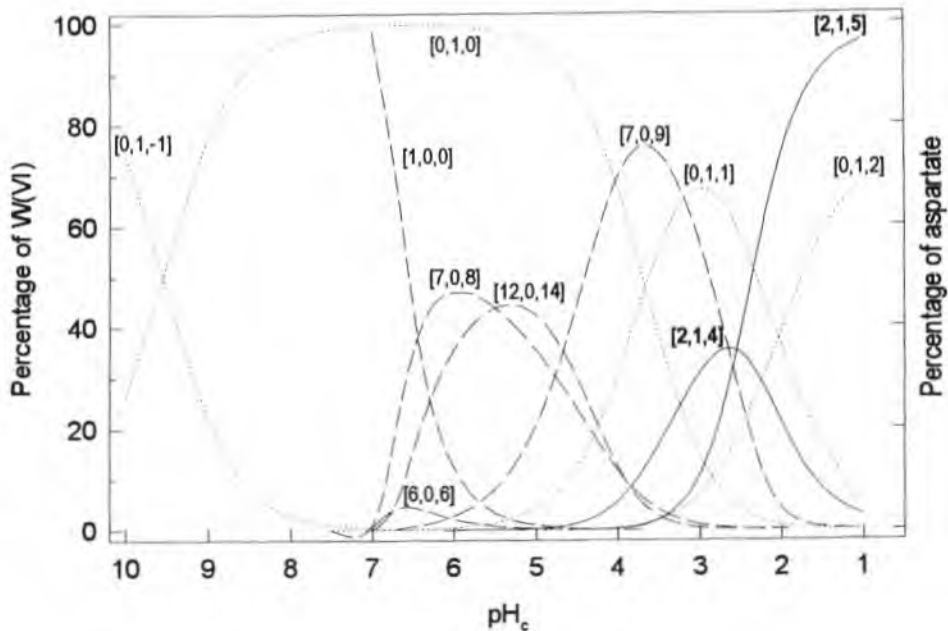


Fig. 3.7.6 Concentration of tungstate(VI)-aspartate and uncomplexed tungstate species, expressed as a percentage of the total tungsten(VI) concentration, as a function of pH_c. The total concentrations of tungstate(VI) and aspartate are 0.01 M and 0.02 M, respectively.

Right ordinate and dotted lines: Concentration of uncomplexed aspartate species expressed as a percentage of total aspartate concentration.

The species distribution shows that complexation with aspartate at pH ~2.8 is the reason for the system to reach equilibrium faster at pH ~2.8 than in the immediately preceding pH range of 4 - 2.8 where slow tungstate reactions occur (Appendix 1). In the region of slow equilibria, the large polymeric tungstate species, [7,0,9] (and maybe some other, unidentified species), breaks up into smaller units which are available for complex formation.

3.7.2.2 Enthalpimetric data and analysis

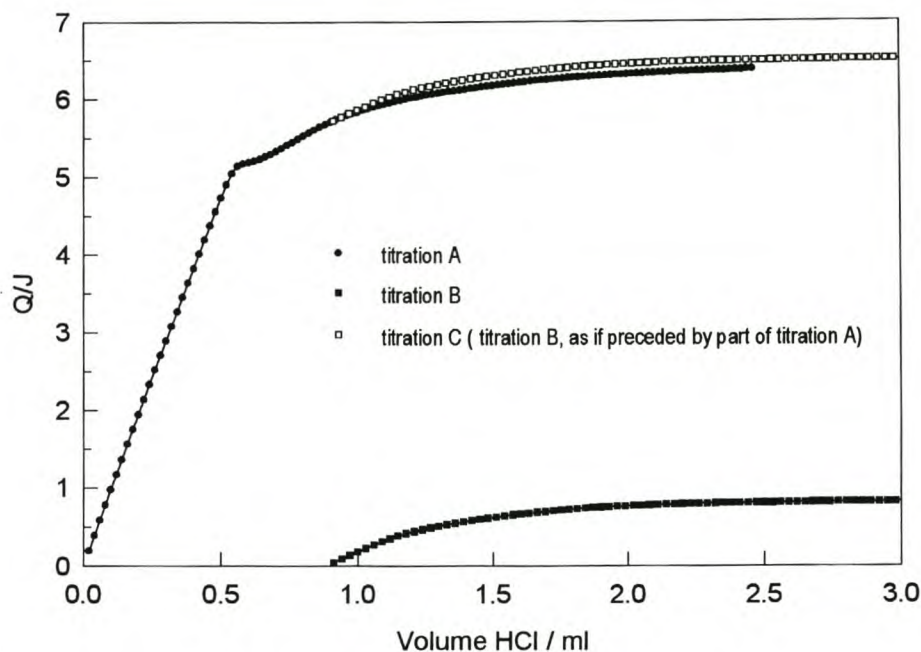


Fig. 3.7.7 Measured heat, Q , as a function of the volume of titrant added for a titration of 0.01 M tungstate(VI) and 0.02 M aspartate. (Titrations A, B and C are discussed in the text.)

The potentiometric model predicted that the region of slow equilibria could not be avoided by promoting complexation of tungstate through the addition of a large excess of aspartate. Whereas this problem could, to some extent, be dealt with during potentiometric titrations (by waiting for mV readings to stabilize after addition of titrant or simply by jumping unfavourable pH regions), it was not possible to get accurate enthalpimetric data as the titrations were executed automatically and continuously. Nevertheless, two titrations (Appendix 1) were carried out in the hope of calculating rough estimates for the values for the change of enthalpies. The two solutions titrated differed only in the amount of acid present at the beginning of the titration. During the first titration (A) 25 ml of a particular solution ($[W] = 0.01$, $[asp] = 0.02$, $[H^+] = -0.01629$ M) was titrated with ~ 2.5 ml of 1 M HCl. For the second titration (B) 25 ml of the same solution was first acidified with 0.88 ml of 1 M HCl (to $pH \sim 4$) and allowed to stand for a while before the automatic calorimetric titration started. The actual volume at the beginning of this titration was thus 25.88 ml. Titration (B) was executed three times faster than titration (A) in order to produce more heat per time unit. For better comparison of the heat developed in these related titrations, the values of Q were plotted against the *volume HCl added* and the results of titration (B) were plotted *as if the initial volume were 25 ml* (Fig. 3.7.7). For both titrations the plotted Q values were corrected for dilution. The volume added before the start of titration (B), 0.88 ml, was carefully selected; it was deduced from the potentiometric titration of the same solution, that 0.88 ml is the highest volume which would acidify the solution without bringing it to the region of slow equilibria.

Both titrations were not truly representative of equilibrium conditions at each data point because both covered the pH range 4 - 2.9 which had been identified as a region of slow equilibria during potentiometric titration of the same solution.

The second titration (B) started just before entering the pH region of slow reactions. An imaginary titration (C) in which the first part of titration (A) (volume < 0.88 ml) is followed by titration (B) (volume > 0.88) was plotted in Fig. 3.7.7. (This is acceptable because the state of the solutions for titration (A) and (B) were the same at 0.88 ml.) The Q values for this imaginary titration (C) is increasingly higher than the values of the corresponding Q values of titration (A) for the addition of 0.88 - 1.3 ml of titrant. For the rest of the titration (> 1.3 ml) the shape of the curves are the same, although the Q values differ. This indicates that heat is involved in the conversion of species. In this region the faster titration (B,C) registers Q values different (higher) than for the slower titration (A). It can be reasoned that, had it been possible to get true equilibrium calorimetric data in this region, the Q values would have been even lower than in the case of the slower titration (A). It seems, therefore, that the enthalpy for the formation of the first species that form upon acidification at $\text{pH} < 4$ is higher than for the species that exist at equilibrium.

This is evidence enough that titration (A) is the better titration to use to obtain a rough estimate of the enthalpy of formation of complexes in the lower pH region and that the true enthalpy values are probably lower than the calculated values.

In order to interpret the shape of the Q curve of titration (A) it was compared with the distribution curves pertaining to titration (A) (Fig. 3.7.7). The distribution curves were also replotted against "volume added" instead of pH (Fig. 3.7.8) so that the x-axis was the same as for the Q curve.

Up to the addition of ~0.6 ml of titrant the heat development increases almost linearly due to the first protonation of asp^{2-} to form Hasp^- ($\text{pH} > 7$) and later ($\text{pH} < 7$) the polymerization of uncomplexed tungstate. The distinct inflexion (at $\text{pH} \sim 5.5$) coincides with the complete polymerization of tungstate. Most of the heat developed during the titration is thus *not* due to complexation of tungstate and aspartate. There is further heat development after the distinct inflexion due to the formation of [7,0,9] and later also of unknown polymeric tungstates and of tungstate-aspartate complexes.

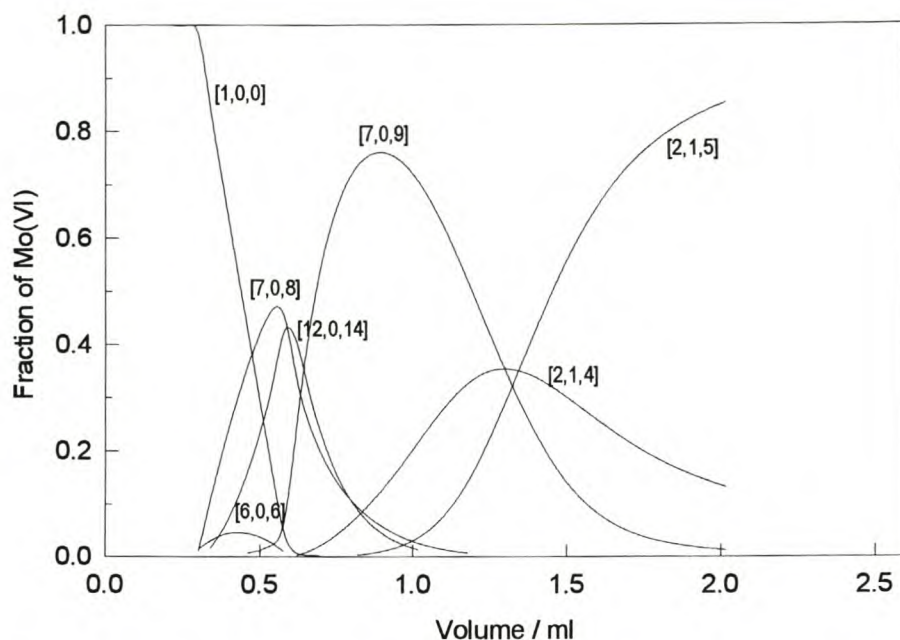


Fig. 3.7.8. Concentration of uncomplexed(VI) tungstate species and tungstate(VI)-aspartate complexes, expressed as a fraction of the total tungsten(VI) concentration, as a function of volume HCl added to 25 ml of solution with total concentrations of tungstate(VI) and aspartate 0.01 M and 0.02 M, respectively.

During preliminary attempts to calculate ΔH_{214}° and ΔH_{215}° from titration (A), ΔH_{011}° , ΔH_{012}° (aspartate species), ΔH_{708}° , ΔH_{709}° , ΔH_{606}° and ΔH_{12014}° (tungstate species) were fixed at values previously determined (Section 2.6.1.1). The ΔH_{214}° and ΔH_{215}° as well as the ΔH_{01-1}° (deprotonated aspartate species) were calculated ($\Delta H_{01-1}^{\circ} = -40.17 \text{ kJ mol}^{-1}$, $\Delta H_{214}^{\circ} = -82.4 \text{ kJ mol}^{-1}$ and $\Delta H_{215}^{\circ} = -97.1 \text{ kJ mol}^{-1}$). The fit was poor because the calculated heat differed substantially from the experimental heat for the addition of 0.6 to 1.3 ml of titrant. This was to be expected as, firstly, the experimental data just after the complete polymerization of tungstate (maximum percentage of [7,0,8] and [12,0,14]) showed condition of non-steady state, due to the sudden drop of heat output during the formation of further tungstate species. Secondly, as soon as steady state conditions were again prevailing, the titration entered the region of slow equilibria (titrant volume > 0.88 ml), for which the tungstate model was insufficient.

When the enthalpies of the uncomplexed tungstate species were allowed to be refined, absolutely unrealistic values were obtained for them, but the fit was excellent in the slow-equilibrium region, and therefore also for the titration as a whole. For complexation, however, reasonable values were obtained: $\Delta H_{214}^{\circ} = -89.2 \text{ kJ mol}^{-1}$ and $\Delta H_{215}^{\circ} = -89.2 \text{ kJ mol}^{-1}$.

An equally good fit was acquired by using a scientifically more sound approach, that is, by ignoring the data ranging from the first onset of tungstate polymerization till just after the maximum percentage of [7,0,9] is

reached, which (more or less) coincides with the start of complexation with aspartate (volume additions 0.3 - 0.8 ml ignored). This reduced the influence of the flawed tungstate model. To obtain a good fit, ΔH_{709}° had to be allowed to refine, but unlike the previous calculation, the value was more realistic (286.2 kJ mol⁻¹). The values of $\Delta H_{214}^{\circ} = -87.8$ kJ mol⁻¹ and $\Delta H_{215}^{\circ} = -89.2$ kJ mol⁻¹ (Table 3.7.5) were very similar to the previous calculated values, showing that if the fit in the tungstate polymerization region was good (by hook or by crook) the enthalpies of both complexes remain in the vicinity of -89 kJ mol⁻¹ (Table 16.4)

For the final calculations of the titration (A), the very first data pertaining to the protonation of [0,1,-1] were also ignored, in other words, only the data from the addition of 0.88 ml titrant onwards were used. A good fit could be achieved even with the value for the enthalpy for the formation of [7,0,9] fixed at $\Delta H_{709}^{\circ} = -328.0$ kJ mol⁻¹. The calculated values $\Delta H_{214}^{\circ} = -97.7$ kJ mol⁻¹ and $\Delta H_{215}^{\circ} = -100.2$ kJ mol⁻¹ were surprisingly higher than before. The fact that a good fit was attained by using known values for ΔH_{por}° unfortunately is no proof of accuracy of the H_{214}° and ΔH_{215}° values, as particularly the [7,0,9] species is somewhat dubious as a sole representative of the tungsten equilibria in the region where it occurs.

Due to the many restrictions in calculating the true enthalpies, no further conclusion is possible, other than to accept that the values of both ΔH_{214}° and ΔH_{215}° are probably in the range -89 to -100 kJ mol⁻¹. As discussed before, the true values are most probably even smaller than the values obtained from the calculation of the experimentally flawed titration. For the purpose of calculating an approximate change of entropy for the complexes, the smaller values were used (Table 3.7.5).

Table 3.7.5 Calculated ΔH° and $T\Delta S^{\circ}$ values for the formation of some W(VI)-aspartate complexes. 1 M (Na)Cl at 298.15 K

COMPLEX	$\log\beta_{pqr} \pm 3\sigma$	ΔG° (kJ mol ⁻¹)	ΔH° (kJ mol ⁻¹)	$T\Delta S^{\circ}$ (kJ mol ⁻¹)
[0,1,-1]	-9.55 ± 0.03	+54.52	+40.3	-14.2
[0,1,1]	3.64 ± 0.01	-20.8	-5.8 ± 0.1	15.0
[0,1,2]	5.65 ± 0.01	-32.3	-10.2 ± 0.1	22.1
[2,1,4]	24.88 ± 0.50	-142.0	-88 ± 10	54
[2,1,5]	27.43 ± 0.50	-156.6	-89 ± 10	67

Although it had been decided to use the results of titration (A) as the best estimate for the enthalpies, the enthalpies were also calculated using data from titration (B). The following enthalpy values for complexation were obtained during a calculation in which the enthalpy values for the formation of tungstate species were fixed, and for the formation of aspartate species were calculated: $\Delta H_{214}^{\circ} = -107.7$ kJ mol⁻¹ and $\Delta H_{215}^{\circ} = -104.4$ kJ mol⁻¹. The fit could be improved insignificantly by refining ΔH_{709}° to the value of -326.4 kJ mol⁻¹. The higher values for ΔH_{214}° and ΔH_{215}° for titration (B) were predicted from the comparison of the Q curves of titration (A) and (B), as discussed previously (Fig. 3.7.7).

3.8 COMPLEXATION WITH NITRILOTRIACETATE (NTA)

3.8.1 Molybdenum(VI)-nta system

3.8.1.1 Potentiometric data and analysis

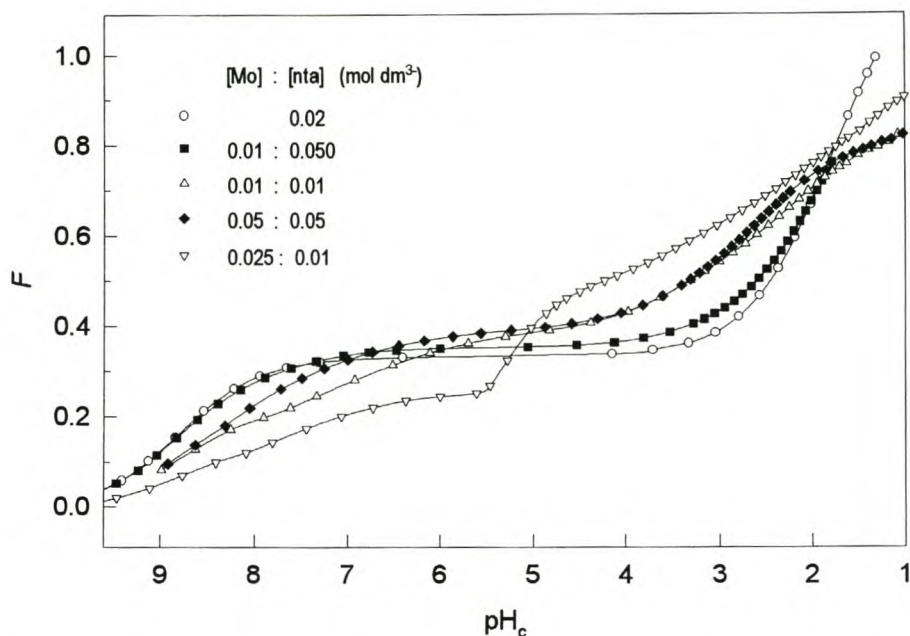


Fig. 3.8.1 Function F versus pH_c for some representative potentiometric titrations of the molybdate(VI)-nta system.

F curves

A prominent inflexion at $F=0.33$ over the pH range 6.5–4.5 by the F curve for the titration of can nta only be explained by the predominance of the Hnta^{2-} species (Appendix 2), for which the degree of protonation $r/3q = 1/3$. (At this point a third of the negative charges of nta^{3-} have been neutralized.) A decrease in pH causes further protonation of nta until at $\text{pH} \sim 1$ about 40% is in the form of H_4nta^+ . The distinct inflexion at $F = 0.4$ and $F = 0.8$ for the titrations of equimolar solutions correspond with the formation of the predominant [1,1,2] complex, for which $r/(2p+3q) = 2/5$, and the [2,2,8] complex, for which $r/(2p+3q) = 8/10$, respectively (Table 3.8.1).

Modelling of the nta and Mo-nta systems (species, $\log\beta$, ΔG°)

The protonation constants of nta, which were calculated from data obtained from the titration of nta, are shown in Table 3.8.1 and were used to produce a species distribution diagram of the nta system shown in Appendix 2. For the calculation of the protonation constants, $\text{pK}_w = 13.71$ (valid for 1 M NaCl) was included in the model.

The well characterized [1,1,2] complex [69-74,88,102] could easily be identified as the first major complex which forms upon acidification of a mixture of molybdate and nta. With decrease in pH this complex is further protonated to form the [1,1,3] and [1,1,4] species. The other species included in the best-fit model are dinuclear complexes, [2,1,5], [2,1,6], [2,2,7] and [2,2,8]. A value for the sample standard deviation, $\sigma = 1.05$ ($\chi^2 = 40$), implies a very good fit. The only species for which the relative standard deviation of the formation constant is greater than 5%, is [2,1,5] with a 9% deviation. The only minor species which has a maximum percentage concentration < 10% for all the conditions investigated, is the [2,1,5] complex.

Table 3.8.1 Molybdate(VI)-nta complexes identified and calculated $\log\beta$ and ΔG° values. 1 M (Na)Cl at 298.15 K

COMPLEX	$\log\beta_{pqr} \pm 3\sigma$	ΔG° (kJ mol ⁻¹)
[0,1,1] ²⁻	8.78 ± 0.01 (8.92)	-50.1
[0,1,2] ⁻	11.04 ± 0.01 (11.33)	-63.0
[0,1,3]	12.73 ± 0.01 (13.14)	-72.7
[0,1,4] ⁺	13.69 ± 0.05 (14.53)	-78.1
[1,1,2] ³⁻	17.78 ± 0.02	-101.5
[1,1,3] ²⁻	21.02 ± 0.02	-120.0
[1,1,4] ⁻	22.57 ± 0.07	-128.8
[2,2,7] ³⁻	45.16 ± 0.04	-257.8
[2,2,8] ²⁻	47.95 ± 0.02	-273.7
[2,1,5] ²⁻	30.74 ± 0.12	-175.5
[2,1,6] ⁻	33.09 ± 0.04	-188.9

Literature value pertaining to 1 M NaClO₄ medium in brackets [137]

Distribution of species

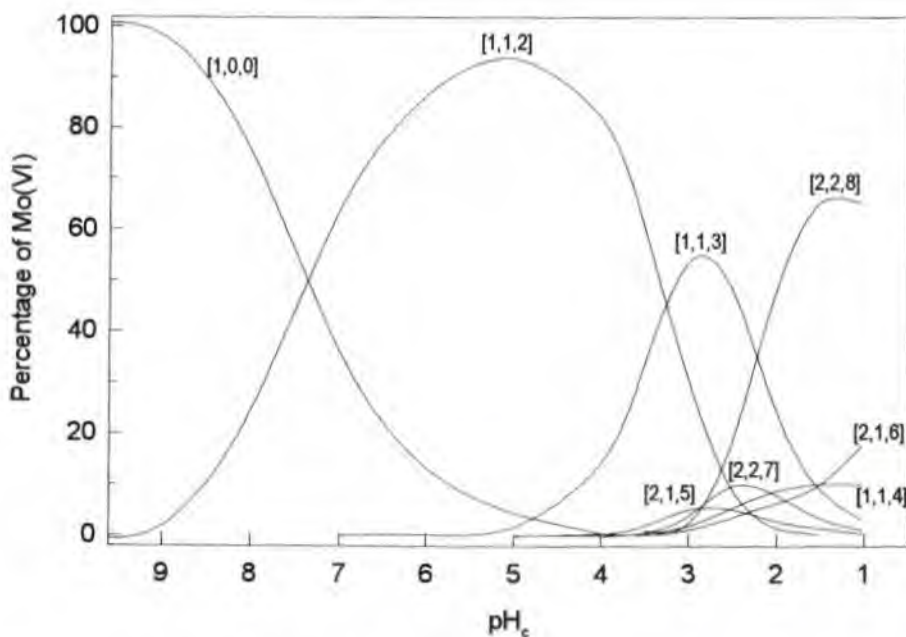


Fig. 3.8.2 Concentration of molybdate(VI)-nta complexes, expressed as a percentage of the total molybdenum(VI) concentration, as a function of pH_c . The total concentrations of molybdate(VI) and nta are both 0.05 M.

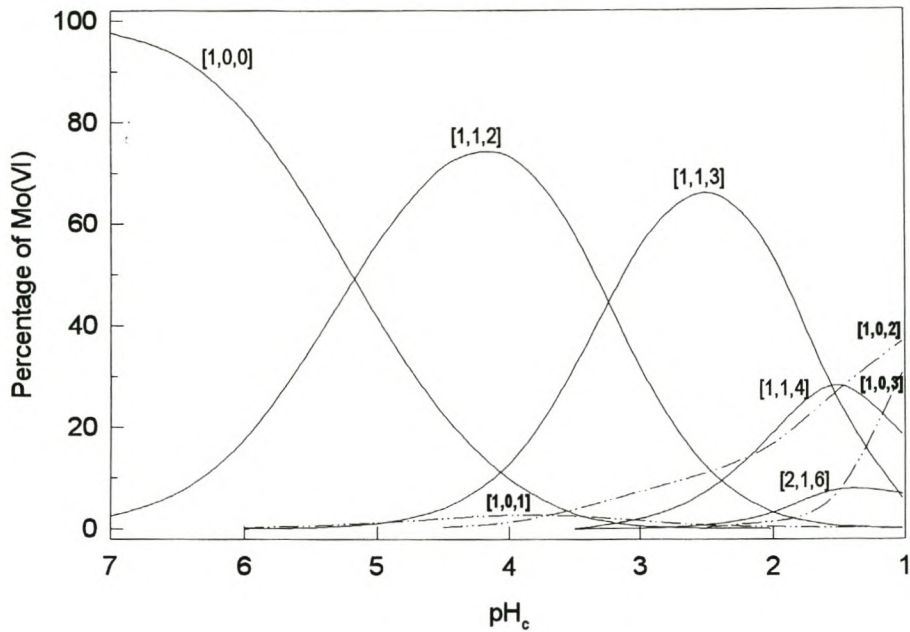


Fig. 3.8.3 Concentration of molybdate(VI)-nta complexes, expressed as a percentage of the total molybdenum(VI) concentration, as a function of pH_c . The total concentrations of molybdate(VI) and nta are 0.0002 M and 0.00025 M, respectively.

3.8.1.2 Spectrophotometric data and analysis

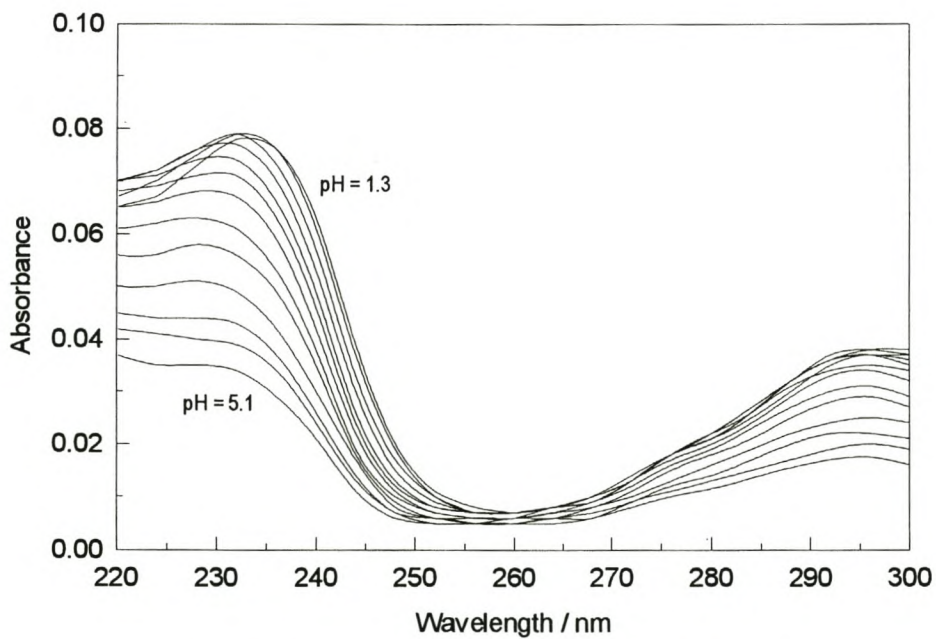


Fig. 3.8.4.1 Change in absorption spectra with pH_c ranging from 5.1 to 1.3. The total nta concentration is 0.00025 M.

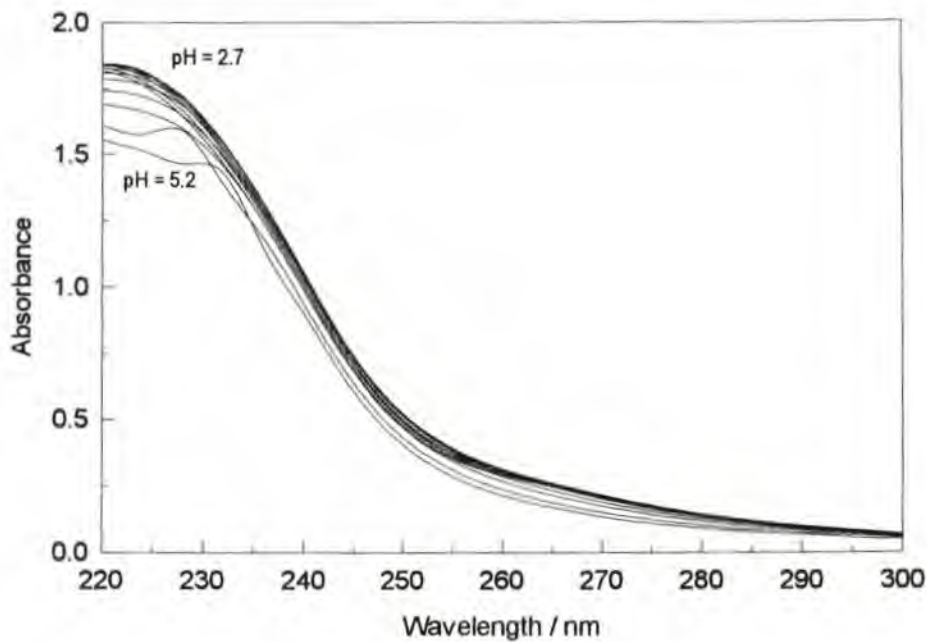


Fig. 3.8.4.2 Change in absorption spectra with pH_c ranging from 5.7 to 2.7. The total concentrations of molybdate(VI) and nta are 0.0002 M and 0.00025 M, respectively.

Spectra of nta species

Formation constants (potentiometrically determined) were fixed for the calculation of the molar absorption spectra of the different nta species using the experimental spectra from the titration of nta alone. The calculated molar absorption spectra of Hnta^{2-} and H_2nta^- ([0,1,1] and [0,1,2]) which were used in further calculations are shown in Fig 3.8.5.

Calculation of models (complexes, formation constants, absorption spectra)

The spectrophotometric titration of a 0.0002 M molybdate and 0.00025 M nta solution (Appendix 1) was started at $\text{pH} \sim 5$ where about 50% of the ligand is in the form of Hnta^{2-} and about 50% is complexed (Appendix 2 and Fig. 3.8.3). The formation constants and spectra of Hnta^{2-} and H_2nta^- were fixed during calculation. Under the conditions chosen for the experiment, calculations showed that all molybdate side-reactions, except the formation of monomeric molybdic acid, [1,0,2], could be neglected. The percentage concentration of [1,0,2] was, however, relatively small, reaching a maximum of only $\sim 9\%$ in the solution at the lowest pH measured ($\text{pH} = 2.7$). The spectrum and formation constant of this species as well as the spectrum of molybdate, [1,0,0], had been determined previously and were supplied to the program as known quantities [122-125].

The unknowns to be calculated were the formation constants and spectra of the [1,1,2] and [1,1,3] complexes. The values for the formation constants obtained, $\log \beta_{112} = 17.84$ and $\log \beta_{113} = 20.90$, agreed

very well with those obtained by potentiometry, namely $\log\beta_{112} = 17.78$ and $\log\beta_{113} = 21.03$. The slightly greater difference between the constants of the [1,1,3] complex (perhaps not significant) can be ascribed to the incipient formation of the [1,1,4] complex ($\sim 3\%$ at $\text{pH}=2.7$) which was neglected in the calculations (Fig. 3.8.3). The calculated molar absorption spectra of the [1,1,2] and [1,1,3] complexes are also shown in Fig. 3.8.5. Although the differences in the absorbances of the [1,1,2] and [1,1,3] complexes in the wavelength range 212-300 nm are rather small, a quite satisfactory value of $\log\beta_{113}$ could be calculated because of the difference in the shapes of the spectral curves and the large number of wavelengths used. Characterization of the other complexes by spectrophotometry was not attempted, mainly because of the great overlap of equilibria and the relatively small change in absorption with pH. The good agreement between the spectrophotometric and potentiometric results for the [1,1,2] and [1,1,3] complexes, however, can be regarded as indirect support for the other species in the model derived from the potentiometric data.

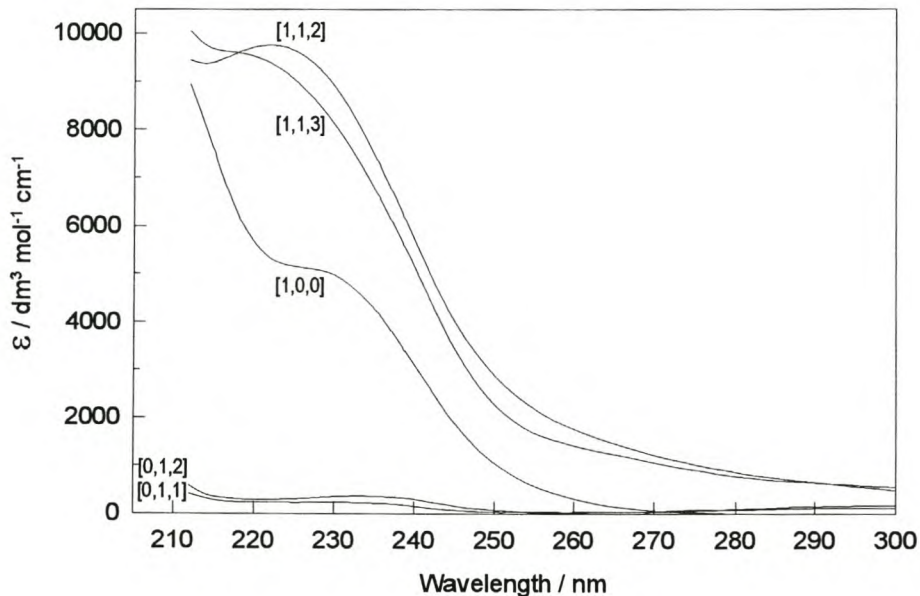


Fig. 3.8.5 Calculated molar absorption spectra of two nta species, of molybdate(VI) and of two molybdate(VI)-nta complexes.

3.8.1.3 Enthalpimetric data and analysis

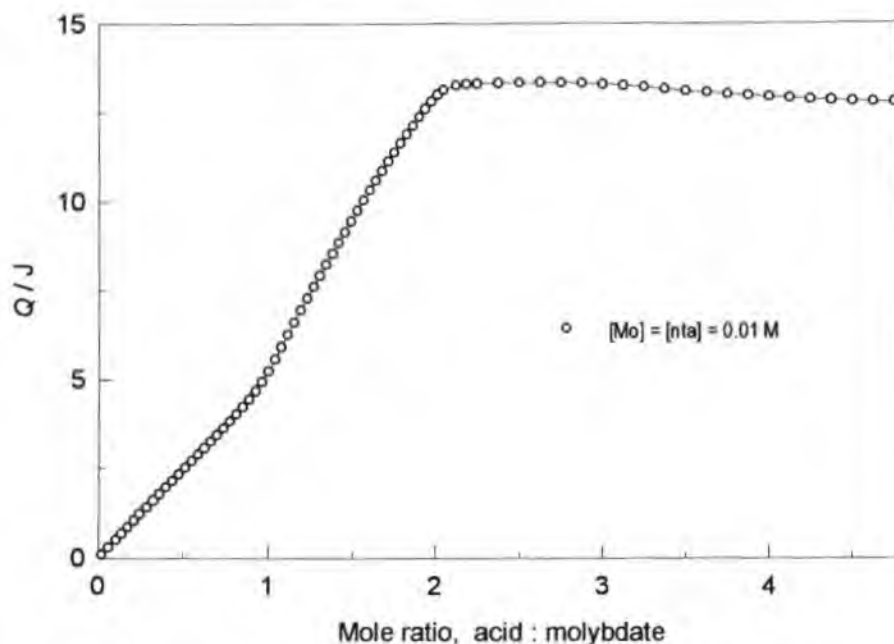


Fig. 3.8.6. Measured heat, Q , as a function of the molar ratio of acid to molybdate(VI) for a titration of 0.01 M molybdate(VI) and 0.01 M nta.

The plot of Q vs mole ratio of acid added to molybdate (Fig. 3.8.6) shows a break at a mole ratio of 1:1 where the first protonation of nta is almost complete and complex formation becomes significant. The second break occurs at a mole ratio of 2:1 indicating that the formation of the first complex [1,1,2] has been completed at that point. The very slight inflexion at mole ratio 3:1 and even slighter inflexion at 4:1 correspond to the formation of [1,1,3] and [1,1,4] complexes, respectively.

The enthalpy changes for the protonation of nta^{3-} in 1 M NaCl, $\Delta H_{011}^{\circ} = -24.2 \text{ kJ mol}^{-1}$, $\Delta H_{012}^{\circ} = -24.4 \text{ kJ mol}^{-1}$ and $\Delta H_{013}^{\circ} = -26.6 \text{ kJ mol}^{-1}$, were determined in separate titrations (Appendix 1) and treated as fixed parameters in the calculation of the $\Delta H_{\text{pqr}}^{\circ}$ values of the complexes. The relatively large enthalpy change for the first protonation of nta is in agreement with the view that the nitrogen atom accepts the first proton. The small enthalpy changes for the second and third protonations are typical for these types of protonation reactions which are normally entropy driven [138].

Evaluation of reliable ΔH° values for all the species in the pH region < 4.0 and especially for the minor species is problematic considering the great overlap of the equilibria. Conditions were therefore chosen for which the [2,1,5] and [2,1,6] complexes could be neglected, *i.e.* an excess of ligand was used (Appendix 1). Also, by increasing the concentrations of both the molybdate and nta the percentage concentrations of the [2,2,7] and [2,2,8] complexes were increased. However, because the maximum percentage concentration

of the [1,1,4] complex was only about 10% and still on the increase at pH ~ 1 a realistic value for its enthalpy change could not be evaluated from the data. Rather than neglecting this complex, the quite reasonable approximation (based on the results of the other investigations) was made that the enthalpy changes for a complex and its protonated form are about the same. The data were therefore treated on the assumption that $\Delta H_{114}^{\circ} = \Delta H_{113}^{\circ}$. Since ΔH_{113}° could be calculated with sufficient accuracy the approximation only affected the value of ΔH_{114}° .

Table 3.8.2 Calculated ΔH° and $T\Delta S^{\circ}$ values for the formation of some Mo(VI)-nta complexes. 1 M (Na)Cl at 298.15 K

COMPLEX	ΔH° (kJ mol ⁻¹)	$T\Delta S^{\circ}$ (kJ mol ⁻¹)
[0,1,1] ²⁻	-24.2 ± 0.5	26
[0,1,2] ⁻	-24.4 ± 1.0	39
[0,1,3]	-26.6 ± 1.0	46
[0,1,4] ⁺	-	
[1,1,2] ³⁻	-69.0 ± 1.0	32
[1,1,3] ²⁻	-71.2 ± 2.0	49
[1,1,4] ⁻	-71.2 #	58 #
[2,2,7] ³⁻	-123 ± 4	135
[2,2,8] ²⁻	-132 ± 2	142
[2,1,5] ²⁻		
[2,1,6] ⁻		
# approximate		

Literature values for the formation of the nta species pertaining to 0.1 M ionic strength are, $\Delta H_{011}^{\circ} = -19.7$, $\Delta H_{012}^{\circ} = -18.4$ and $\Delta H_{013}^{\circ} = -16.7$ kJ mol⁻¹ [133].

3.8.2 Tungsten(VI)-nta system

3.8.2.1 Potentiometric data and analysis

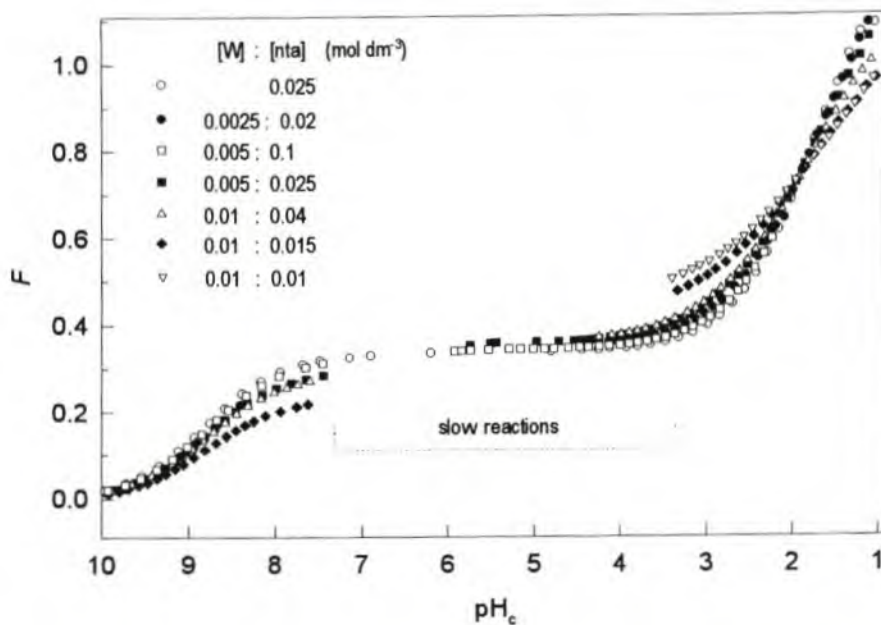


Fig. 3.8.7 Function F versus pH_c for some representative standard potentiometric titrations of the tungstate(VI)-nta system.

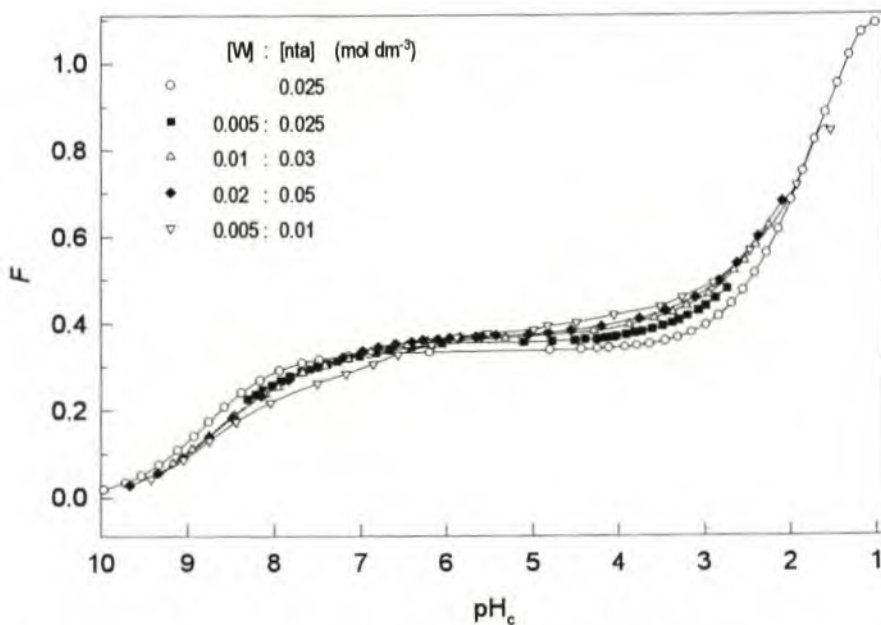


Fig. 3.8.8 Function F versus pH_c for some representative potentiometric point titrations of the tungstate(VI)-nta system.

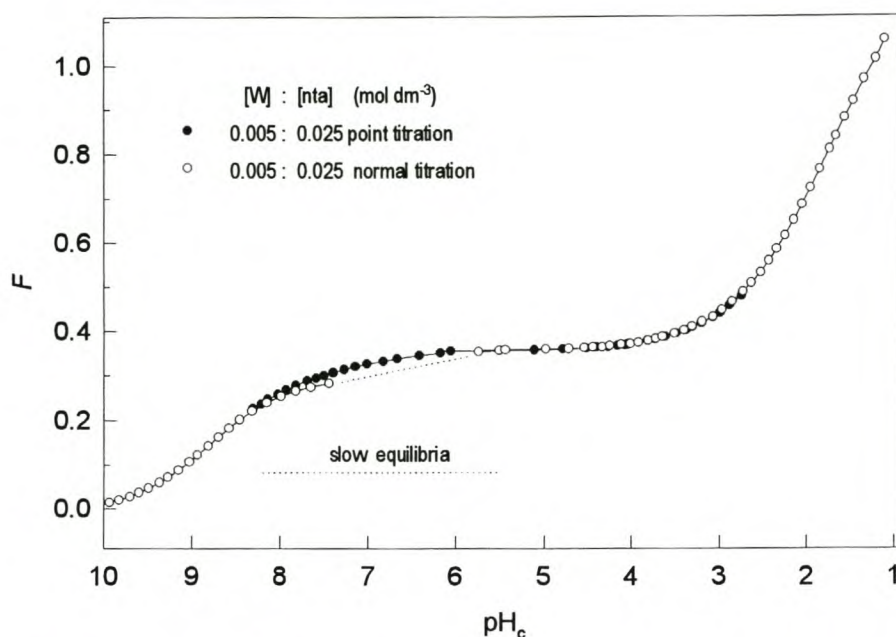


Fig. 3.8.9 Function F versus pH_c for the standard titration and the point titration of one particular solution. ($[W(\text{VI})] = 0.0025 \text{ M}$, $[nta] = 0.025 \text{ M}$)

F curves

The F curves pertaining to the standard and to the point titrations are shown in Fig. 3.8.7 and Fig. 3.8.8, respectively. The break in the F curves of the standard titrations represent the region of slow equilibria, where pH could not be measured accurately.

From the F curves of the point titrations, it can be seen that the region of slow equilibria was well defined by the different solutions constituting the so-called point titration.

To compare the two types of titrations, the F curves calculated for the normal and point titrations of the solutions with $[W(\text{VI})] = 0.005 \text{ M}$ and $[nta] = 0.025 \text{ M}$ are shown in Fig. 3.8.9. For these conditions slow equilibria clearly exist in the pH range 8 - 5.5. After the addition of a certain volume of HCl , some of the free protons are slowly used in complexation, thereby increasing the F value and increasing the pH , until equilibrium is reached.

The calculations (below) reveal that the difference in F curves can possibly be ascribed mainly to the slow formation of the $[1,1,2]$ complex.

Modelling of the W - nta system (species, $\log\beta$, ΔG°)

Due to the difficulties with the pH measurements in both the standard and the point titrations (Appendix 1), the data were not of the usual quality. Instead of discarding the potentiometric investigation, the data from the standard and the point titrations were used in separate calculations hoping to find two models which

would, at least, agree for data pertaining to $\text{pH} > 8$ and $\text{pH} < 4$, but perhaps differing in the pH region 8 - 4 and thus leading to an explanation for the slow equilibria.

In both calculations, the models for the subsystems nta and tungstate were used as usual. Preliminary calculations of both data sets showed that complexation only takes place at $\text{pH} < 8.7$. For later calculations the data not representing complexation ($\text{pH} > 8.7$) were ignored.

Despite the difficulty in getting stable mV readings in the point titration (due to drifts in the electrode readings which could not be ascribed to slow complexation), these data points were regarded as more representative of the tungstate-nta system at equilibrium than the standard titration data.

Model obtained from the point titrations (equilibrium data)

The best model comprises the complexes [1,1,2], [2,1,3], [2,1,4], [2,1,5] and [2,2,8]. A value for the sample standard deviation, $\sigma = 0.62$, implies a very good fit. The values for the formation constants are listed in Table 3.8.3.

The [1,1,2] complex predominates in the pH region 8.5 - 4.5, whereas the [2,1, r] species predominate in the pH region 4.5 - 1.9 (Fig. 3.8.10). The [2,2,8] is only important at $\text{pH} < 1.8$ and is the most uncertain species, its relative standard deviation being the highest (26%). This uncertainty is understandable as this species is only represented by a very few data points. The complexes [1,1,2], [2,1,4] and [2,1,5] fit the data well, their respective relative standard deviations being 4%, 5% and 8%. The very minor species [2,1,3] has the second poorest fit (r.s.d = 23%) and is only accepted in the model, because of the importance of its protonated forms. Despite the problems with the investigation, a model was acquired which has a striking resemblance to the model of the related molybdate-nta system, which also contains species [1,1, r], [2,1, r] and [2,2, r].

According to this tungstate-nta model, relatively little uncomplexed tungstate polymeric species remain in solution after equilibrium has been established. For the titration pertaining to the two-fold excess of nta, about 10 % of the tungsten(VI) is uncomplexed at $\text{pH} \sim 4.5$. In the other titrations almost 100% of the tungsten is complexed upon acidification. The accuracy of the tungstate model is, therefore, not very crucial to the outcome of the model search.

Table 3.8.3 Tungstate(VI)-nta complexes identified in the system 1 day after preparation of the solutions, and calculated $\log\beta$ and ΔG° values. (1 M (Na)Cl at 298.15 K)

COMPLEX	$\log\beta_{\text{pqr}} \pm 3\sigma$	ΔG° (kJ mol ⁻¹)
[0,1,1] ²⁻	8.78 ± 0.01	-50.1
[0,1,2] ⁻	11.04 ± 0.01	-63.0
[0,1,3]	12.73 ± 0.01	-72.7
[0,1,4] ⁺	13.69 ± 0.05	-78.1
[1,1,2] ³⁻	17.67 ± 0.05	-100.8
[2,1,3] ⁴⁺	25.99 ± 0.03	-148.3
[2,1,4] ³⁻	30.92 ± 0.07	-176.4
[2,1,5] ²⁻	33.84 ± 0.10	-193.1
[2,2,8] ²⁻	48.72 ± 0.05	-278.0

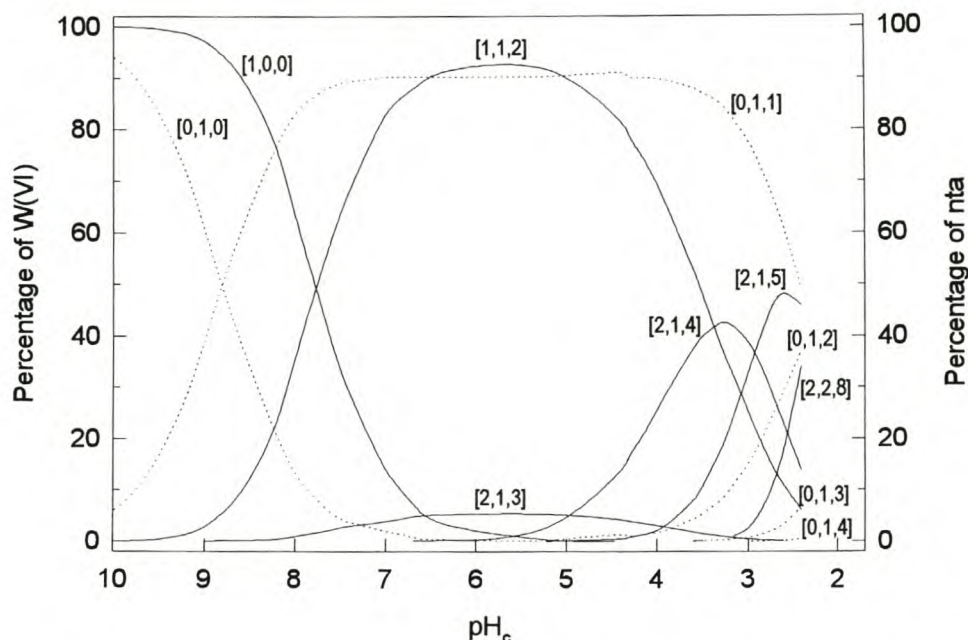
Distribution of species at equilibrium (model from Table 3.8.3)

Fig. 3.8.10 Concentration of tungstate(VI)-nta complexes at equilibrium, expressed as a percentage of the total tungsten(VI) concentration, as a function of pH_c. The total concentrations of tungstate(VI) and nta are 0.01 M and 0.1 M, respectively.

Right ordinate and dotted lines: Concentration of uncomplexed nta species expressed as a percentage of total nta concentration.

Model obtained from the standard titration (non-equilibrium data)

The best model for the non-equilibrium data, obtained from the standard titrations, comprises only the species [1,1,2] and [2,1,5]. A value for the sample standard deviation, $\sigma = 1.4$, implies a poorer fit than for the model pertaining to the point titrations (as can be expected with non-equilibrium data). Still, the individual complexes fit the data relatively well, their relative standard deviations being 6% and 5%, respectively.

The apparent "formation constants" (not true equilibrium constants), $\log \beta_{112} = 16.9$ and $\log \beta_{215} = 33.2$, are smaller than the formation constants calculated from equilibrium data (point titration) and describe a (non-equilibrium) system in which complexation has proceeded to a lesser degree than at true equilibrium. According to this model, between 50% and 85% of tungsten is present in the uncomplexed polymeric forms in the pH region 4.5 - 3.5 in the different titrations. In this pH region the currently used model for the subsystem tungstate is not considered accurate (*cf.* 2.6.1.1), but for lack of a better model, the best to use.

In the course of the calculations it was decided to ignore the data for which $\text{pH} < 2$ since, particularly in the titrations with smaller excess of nta, the [7,0,9] species "reappeared" at $\text{pH} < 2$ after the [2,1,5] had reached its maximum percentage concentration at $\text{pH} \sim 2$. It is highly unlikely that the [7,0,9] truly exists at this pH. (Its "presence" is most likely a result of the inadequate model, the [7,0,9] species being the highest

protonated tungstate species "available" in the model to "stand in" for true tungstate species.) However, its apparent existence seems to indicate that at this low pH complexation might, once again, be poor (at least before equilibrium is established).

Comparison of equilibrium and non-equilibrium models

The non-equilibrium and equilibrium models were used to calculate distribution curves pertaining to a (calorimetric) titration of 25 ml of a tungstate-nta solution (0.01 M W(VI) and 0.1 M nta) with 4.5 ml of 1 M HCl. These distribution curves which are shown in Fig. 3.8.11-12, respectively, enable easier comparison of the system before and at equilibrium, and are used in the discussion of the enthalpimetric data.

The main and most obvious difference in Fig. 3.8.11-12 is the greater predominance of [1,1,2] after equilibrium is reached and the presence of significant amounts of [7,0,9] (or other unknown poly-tungstate species represented by it) before equilibrium is reached in the pH region 8.5 - 4.5. Comparison of the equilibrium and non-equilibrium models and the respective distribution curves seem to indicate that complexation equilibria are established fairly quickly in the pH region 3.5 - 2.0, but that at higher pH, and maybe at lower pH, complexation equilibria are established relatively slowly. At pH > 3.5 polymeric tungstates seem to form with greater ease compared to the [1,1,2] complex despite the fact that [1,1,2] is thermodynamically more stable and predominates in the W-nta-system in the long run. The [2,1,5] predominates completely at low pH before equilibrium, but at equilibrium a significant amount of the complex [2,2,8] is present at low pH. At this low pH some uncomplexed H₃nta ([0,1,3]) is present. Possibly the addition of a further H₃nta -ligand to a [2,1,5] complex, to form [2,2,8], is a slow process.

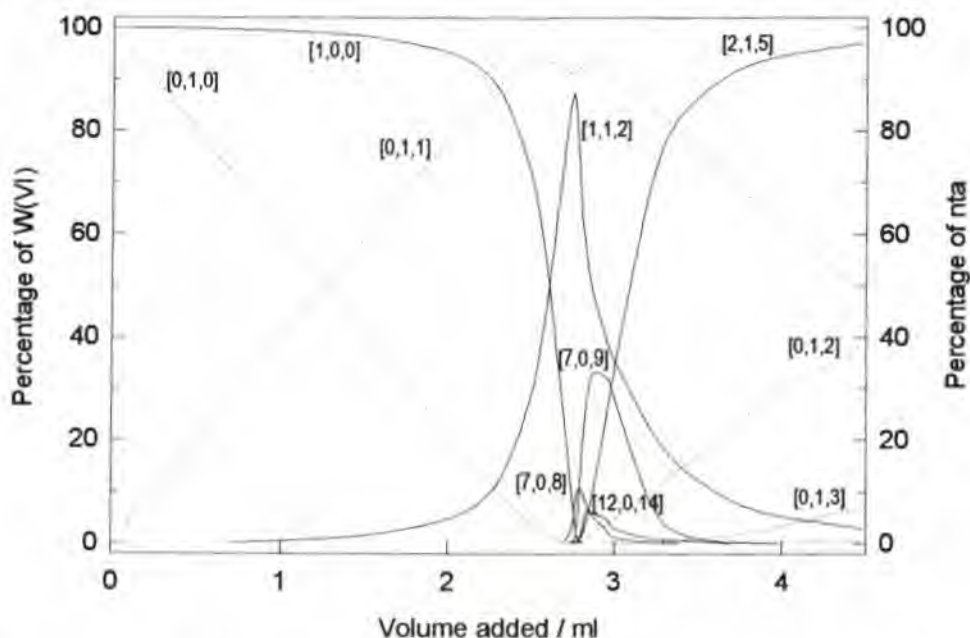


Fig. 3.8.11 Concentration of tungstate(VI)-nta complexes *before equilibrium*, expressed as a percentage of the total tungsten(VI) concentration, as a function of titrant (1 M HCl) volume added to a 25 ml solution, with the total concentrations of tungstate(VI) and nta 0.01 M and 0.1 M, respectively.

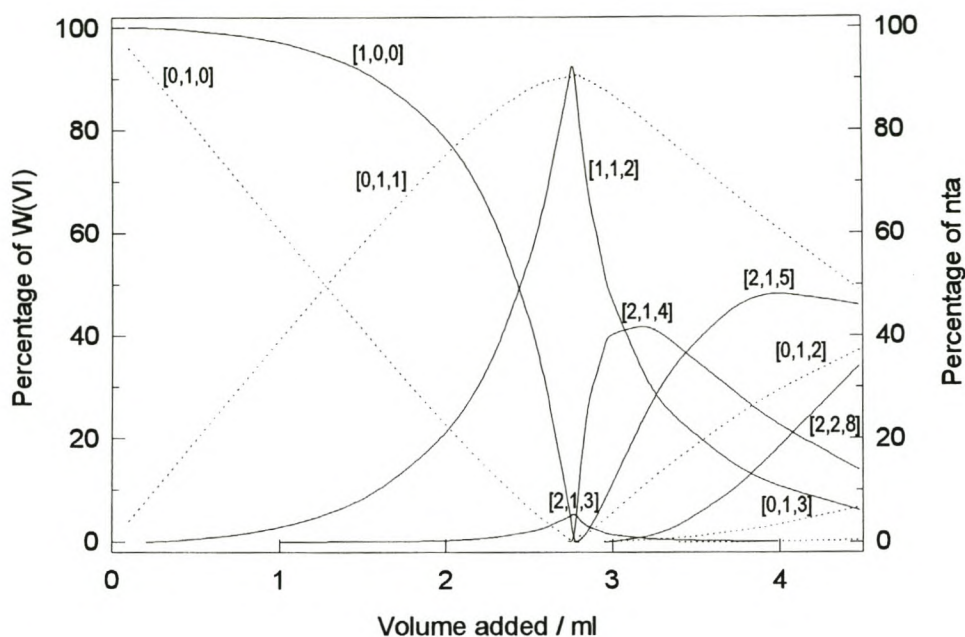


Fig. 3.8.12 Concentration of tungstate(VI)-nta complexes *at equilibrium*, expressed as a percentage of the total tungsten(VI) concentration, as a function of titrant (1 M HCl) volume added to a 25 ml solution, with the total concentrations of tungstate(VI) and nta 0.01 M and 0.1 M, respectively.

3.8.2.2 Enthalpimetric data and analysis

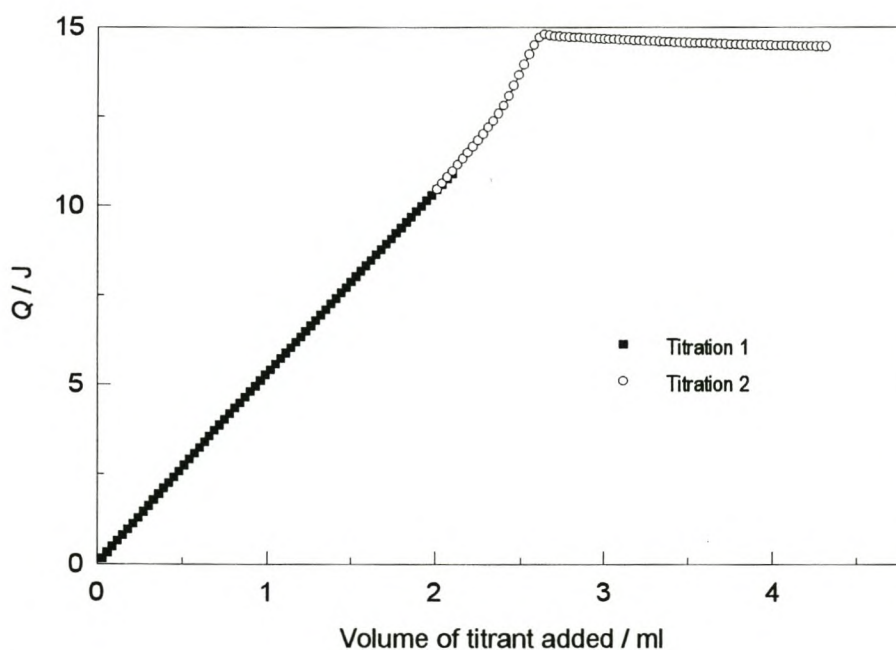


Fig. 3.8.13 Measured heat, Q , as a function of the volume of titrant added to 25 ml of a solution of 0.01 M tungstate(VI) and 0.1 M nta.

Due to the slow reactions that occur as soon as complexation starts upon acidification of the tungstate-nta solution, enthalpimetric data from a continuous (relatively fast) titration is expected to be an inaccurate account of the heat developed due to the formation of the species present *at equilibrium*. Calorimetric titrations were, nevertheless, undertaken in the hope that some of the data would be useful, at least in a *qualitative way* (Appendix 1). The two titrations were planned so, that the data from the one could be added to the other to be used together, as one titration. The experimental power curve shows a region of a "non-steady state" at the stage of the titration where 2.55 to 2.9 ml of titrant is added, which is where slow reactions are known to occur. The heat from this concatenated titration is plotted against volume of titrant added (Fig. 3.8.13).

The following discussion on the shape of the Q curves is based on the two distribution curves, Fig. 3.8.11 and 3.8.12, which were calculated for conditions similar to the calorimetric titration using the equilibrium and non-equilibrium model.

The almost straight line of the Q curve (Fig. 3.8.13) up to the addition of ~ 1 ml titrant is consistent with the sharp decrease in the concentration of [0,1,0] and the concomitant increase in its protonated species, [0,1,1] predicted by both models. (The concentrations of the other species present are practically constant.)

Both models predict a further sharp decrease in the concentration of [0,1,0] and increase of [0,1,1] for the addition of a further 1 ml of titrant. However the two different distribution curves show a significant difference in the decrease of [1,0,0] and increase of the first nta complex, [1,1,2]. The equilibrium model predicts the formation of 21% of [1,1,2] after addition of 2 ml, opposed to only 5% predicted by the non-equilibrium-model. The continued (almost) straight line of the Q curve up to the addition of 2 ml can best be explained by the absence of significant amounts of [1,1,2], in other words, better by the non-equilibrium-model, which also predicts a very sharp increase in the formation of [1,1,2] at added volume = 2.3 , and explains the inflexion in the Q curve at that point.

The inflexion at 2.6 ml cannot be ascribed to a particular feature of either distribution curves as it is not at the expected 2.7 ml where [1,1,2] reaches a maximum. At about 2.6 ml, the non-equilibrium-model predicts the formation and increase of polymeric tungstates, whereas the equilibrium-model predicts the formation and increase of other complexes, like [2,1,3], [2,1,4] and [2,1,5]. It is impossible to choose between these models for an explanation for the inflexions, especially if it is considered that the non-equilibrium-model would in any case be inaccurate.

It is believed that the "late" first inflexion in the Q curve (at ~2.3 ml and not at ~ 1.5 ml) is sufficient confirmation, that the formation of the [1,1,2] complex is a slow process.

Semi-quantitative analysis

Despite the inaccuracy of the enthalpimetric data, a few calculations of enthalpies were attempted. It was hoped that the values obtained would at least give an indication of the order of magnitude of the enthalpies.

Having established, in a qualitative way, that the *non-equilibrium-model* was the best model for formation of species during the enthalpimetric titration, it was decided to use this model for the initial calculations of enthalpies.

For the first calculations only the first 43 data points (volume 0 to 2.55) were used. Calculations based on the non-equilibrium-model (Fig. 3.8.11) show that only two reactions take place in this region: the protonation of nta, [0,1,0], to form [0,1,1] and the formation of the [1,1,2] complex (~30%). A reasonable fit was obtained (considering the rather inaccurate data) when the enthalpies of [0,1,1] and [1,1,2] were calculated simultaneously. The obtained values are: $\Delta H_{011}^{\circ} = 22.2 \text{ kJ mol}^{-1}$ and $\Delta H_{112}^{\circ} = 55.4 \text{ kJ mol}^{-1}$ (Table 3.8.4).

For the second calculation the data pertaining to the addition of 2.9 - 4.0 ml of titrant were added to the previous data. The model shows that, by the omission of the non-steady state data, the inclusion of the tungsten polyanions in the model was not necessary. The two reactions represented by the additional data are: the further protonation of nta to form [0,1,2] and the complex formation of [2,1,5]. The following enthalpies were obtained: $\Delta H_{011}^{\circ} = 22.2 \text{ kJ mol}^{-1}$, $\Delta H_{012}^{\circ} = 57.2 \text{ kJ mol}^{-1}$, and $\Delta H_{215}^{\circ} = 91.3 \text{ kJ mol}^{-1}$. For this calculation, the following known values (Table 3.8.2) pertaining to the protonation of nta were used: $\Delta H_{012}^{\circ} = 24.4 \text{ kJ mol}^{-1}$, $\Delta H_{013}^{\circ} = 26.6 \text{ kJ mol}^{-1}$ (Table 3.8.4).

All the data were used in the third and final calculation. As in the second calculation, known ΔH_{012}° and ΔH_{013}° values were used, as well as previously determined values for the enthalpy for the formation of the polytungstates (Table 2.7). Once again, considering the inaccuracies, a fair fit was obtained with the enthalpy values, $\Delta H_{011}^{\circ} = 22.2 \text{ kJ mol}^{-1}$, $\Delta H_{112}^{\circ} = 60.8 \text{ kJ mol}^{-1}$ and $\Delta H_{215}^{\circ} = 86.9 \text{ kJ mol}^{-1}$ (Table 3.8.4).

Table 3.8.4 Different calculations of ΔH° and $T\Delta S^{\circ}$ values for the formation of some W(VI)-nta complexes using the non-equilibrium model. (1 M (Na)Cl at 298.15 K)

calculation:	1	2	3
COMPLEX	ΔH° (kJ mol ⁻¹)	ΔH° (kJ mol ⁻¹)	ΔH° (kJ mol ⁻¹)
[0,1,1]	22.2	22.2	22.2
[0,1,2]	-	24.4 #	24.4 #
[0,1,3]	-	26.6 #	26.6 #
[1,1,2]	55.4	57.2	60.8
[2,1,5]		91.3	86.9

fixed values

(It was also attempted to use the equilibrium model for the calculation of the enthalpy changes for the formation of its complexes. It is interesting that enthalpy values for the formation of [1,1,2] were about the same as when the non-equilibrium-model was used, but that of [2,1,3], [2,1,4], [2,1,5] and [2,2,8] were most unlikely and the fit, expectedly, was poorer.)

It is to be emphasized that the attempt to quantify the enthalpy for the formation of [1,1,2] and [2,1,5] was rather more playful than scientific in nature, and the results prone to be flawed. The enthalpy values which were obtained (calculation 3, Table 3.8.4), however, don't seem to be totally unrealistic. At this point a

choice has to be made to (1) disregard these values completely or to (2) accept them as rough estimates. If, however, they are accepted as rough estimates, they might as well be used to calculate rough estimates for the change in entropy for the formation of the complexes.

Table 3.8.5 Calculated ΔH° and $T\Delta S^\circ$ values for the formation of some W(VI)-nta complexes. (Approximate values based on non-equilibrium model.) (1 M (Na)Cl at 298.15 K)

COMPLEX	$\log\beta_{pqr} \pm 3\sigma$	ΔG° (kJ mol ⁻¹)	ΔH° (kJ mol ⁻¹)	$T\Delta S^\circ$ (kJ mol ⁻¹)
W-nta (based on non-equilibrium-model)				
[1,1,2]	16.9	-96	-60.8	35
[2,1,5]	33.2	-189	-86.9	103

These thermodynamic values pertain to a non-equilibrium condition, since the model used in calculation of the change in enthalpy was a non-equilibrium model. The value calculated for the entropy term for the formation of [1,1,2], $T\Delta S^\circ = 35$ kJ mol⁻¹, is surprisingly close to the value $T\Delta S^\circ = 32$ kJ mol⁻¹ pertaining to the [1,1,2] molybdate-nta complex (given the uncertainties in the W-nta system). Seeing that it is common for the entropy terms of a specific predominant Mo-complex to be almost the same as for its analogue W-complex, it might be argued that the similarity of the values is not a coincidence. If it is no coincidence, it might be argued further, that a good approximation of the entropy term at *equilibrium* conditions is the same, namely 35 kJ mol⁻¹. If this is the value for the entropy term, the enthalpy for equilibrium condition must be calculated using the ΔG° for equilibrium conditions, which can be calculated from the formation constant at equilibrium conditions, namely $\log\beta_{pqr} = 17.66$. The thermodynamic values pertaining to equilibrium conditions, based on the above arguments, are shown in Table 3.8.6.

No ΔH° and $T\Delta S^\circ$ values could be obtained for the formation of the [2,1,5] complex. If the same arguments are used as in the case of the [1,1,2] complex - if it is assumed that the $T\Delta S^\circ = 103$ kJ mol⁻¹ pertaining to non-equilibrium condition is also valid for equilibrium condition, the ΔH° for the formation of [2,1,5] can also be calculated in the same way as for the [1,1,2] complex. These thermodynamic values are also shown in Table 3.8.6.

Table 3.8.6 Proposed ΔH° and $T\Delta S^\circ$ values for the formation of some W(VI)-nta complexes at equilibrium. (1 M (Na)Cl at 298.15 K)

COMPLEX	$\log\beta_{pqr} \pm 3\sigma$	ΔG° (kJ mol ⁻¹)	ΔH° (kJ mol ⁻¹)	$T\Delta S^\circ$ (kJ mol ⁻¹)
W-nta (based on equilibrium-model)				
[1,1,2]	17.66 ± 0.05	-100.8	-66 #	35 (assumed)
[2,1,5]	33.85 ± 0.10	-193.2	-90 #	103 (assumed)

Calculated value, based on assumed entropy term, which was borrowed from non-equilibrium values.

Although these values were obtained in a tentative manner, they are not more unrealistic than those in Table 3.8.5. They may, therefore, be proposed as the best estimates for the thermodynamic values at equilibrium conditions.

Chapter 4

Discussion

4.1 COMPARISON OF Mo(VI) AND W(VI) COMPLEXATION

All the different species identified in the systems investigated are summarized in Table 4.1. They are arranged by ligands (different columns) and by the charge of the species (different rows, indicated in the last column). The complexes which were identified in both the tungstate-ligand and molybdate-ligand systems are written in bold. Molybdate-ligand complexes which have no tungstate analogues are written in plain font, and the few tungstate-ligand complexes which have no molybdate analogues are written in italics. In this format, the similarities between the molybdate and tungstate-ligand models are emphasized.

More molybdate complexes of a particular ligand were identified than tungstate complexes. Almost all tungstate complexes have molybdate analogues and most of the *major* molybdate complexes have tungstate analogues. Those molybdate complexes which have no tungstate analogues are usually complexes of which the ratio, molybdate : ligand, is greater than 1 or having a relatively high degree of condensation. The identification of these molybdate complexes was possible because data could be collected at conditions which favoured their formation, *i.e.* relatively high concentrations of molybdate and an excess of molybdate. Due to slow reactions in solutions with an excess or a high concentration of tungstate, equilibrium data could not be obtained for such conditions. Had this been possible, it is probable that the tungstate models would have comprised more species, and could have been even more similar to the molybdate model. The very few complexes that occur *only* in the tungstate-ligand system are protonated or deprotonated species of a major complex that exists in both the molybdate- and tungstate-ligand systems.

The similarity between the molybdate and tungstate complexes of a particular ligand, particularly regarding the major species, is striking and was achieved despite attempts to prove the models incorrect by testing a wide variety of additional species and using various combinations of data sets. It is believed that this degree of similarity was not, and could not have been, achieved by following a subjective course of analysis, *i.e.*, steering the model-search in a direction in order to produce similar models. For this reason it is believed that even the minor complexes identified by the use of speciation programs are most probably not fictitious. The similarity between models of complexation of molybdate or tungstate with closely related ligands is also striking, for example, the models for complexation with lactate and mandelate, and for complexation with malate and citrate, and malate and aspartate (Table 4.1). The mutual agreement between the models gives more credence to the individual models.

Table 4.1 clearly shows that complexes $[1,1,r]$, $[1,2,r]$, $[2,2,r]$, $[2,1,r]$ as well as $[4,2,r]$ and $[4,4,r]$ occur regularly as major species. They can now be proposed to be *typical* species for these and related systems. The presence of $[1,2,r]$ complexes, particularly under conditions of excess ligand, is the most noticeable feature of the complexation of molybdate and tungstate with α -hydroxycarboxylates, particularly if the

hydroxy and carboxy groups are the only potential donor-groups present. The additional β -carboxylates of malate, citrate (and aspartate) allow a greater variety of complex types to form due to the extra donor oxygens. Tartrate can be regarded as a special α -hydroxycarboxylate ligand due to the presence of two chemically equivalent, vicinal α -hydroxycarboxylate groups, which can be involved equally in complexation. This unique feature gives rise to a host of minor complex species which have only been identified in the tartrate-systems, but which are, although unusual, quite plausible (Fig. 4.13).

When comparing the distribution curves in Chapter 3, it is obvious that the monomeric complexes [1,1,*r*] and [1,2,*r*] are usually the first complexes to form upon acidification, whereas the major dimeric and tetrameric [2,1,*r*] and [4,2,*r*] complexes are usually only formed at lower pH. This is not unexpected since the (uncomplexed) dimeric molybdate species are only important at lower pH.

The relationship between the molybdate and tungstate systems is further emphasized in **Figures 4.1.1-5** where the ΔG° values (per metal) associated with the formation of the different types of molybdate and tungstate complexes are compared. These figures clearly show that the tungstate complexes are generally significantly more stable than the molybdate complexes, the ΔG° values being about 7-11 kJ mol⁻¹ greater for the tungstate complexes. The stabilities of the Mo-complexes, [1,1ox,*r*], [2,2ox,*r*], [1,1nta,*r*], [2,2nta,*r*] and [2,1tart,2] are more comparable to those of their tungstate analogues. Comparing only molybdate complexes it is seen that the stabilities of the [1,2lac,1], [1,2man,1] and [1,2asp,*r*] complexes are much lower than that of the other [1,2,*r*] complexes and the stabilities of the [1,1man,1], [1,1mal,1], [1,1cit,1] and [1,1asp,*r*] complexes are much lower than that of the other [1,1,*r*] complexes.

The values for the change in free energy and enthalpy (per metal) associated with the formation of the different types of molybdate complexes are compared in the **Figures 4.2.1-5**. The contribution of the enthalpy to the free energy is clearly illustrated, and the contribution of the entropy term ($T\Delta S^\circ$) is implied by the difference between ΔG° and ΔH° . For most of the molybdate-complexes (for which the enthalpy could be calculated) ΔH° contributes more to the overall stability than $T\Delta S^\circ$. Generally the ΔG° for the formation of successively protonated complexes increases significantly (e.g. [1,2cit,4], [1,2cit,5], [1,2cit,6] or [1,1nta,2], [1,1nta,3], [1,1nta,4]), whereas the ΔH° often changes very little, which implies that the entropy term is usually the important driving force for the protonation of these complexes (as illustrated in Fig. 4.4.2). This favourable entropy term is mainly the result of the removal of a proton (with a very high charge density and concomitant ability to create localized solvent order) from the system. The ΔH° for the [1Mo,2,*r*] complexes are generally very similar (~ -80 kJ mol⁻¹), the aspartate complexes being exceptions (Fig. 4.2.1). Except for the [1Mo,1asp,*r*] complexes (with a particularly small ΔH°) the enthalpy change for the [1Mo,1,*r*] complexes is either about -50 or -70 kJ mol⁻¹ (Fig. 4.2.2). For the [2Mo,2,*r*] complexes a $\Delta H^\circ/\text{Mo}$ of about -60 to -70 kJ mol⁻¹ is typical (Fig. 4.2.3) whereas for the [2Mo,1,*r*] complexes the typical $\Delta H^\circ/\text{Mo}$ value is lower, between about -40 to -60 kJ mol⁻¹ (Fig. 4.2.4). The $\Delta H^\circ/\text{Mo}$ for the trimeric and tetrameric tartrate complexes are very similar to the [1,2,*r*] complexes (about -80 kJ mol⁻¹). The $\Delta H^\circ/\text{Mo}$ value for the other tetrameric complexes ([4,4,*r*] and [4,2,*r*]) is about -60 kJ mol⁻¹, with the exception of the [4,4asp,*r*] for which $\Delta H^\circ/\text{Mo}$ is particularly small, about 30 kJ mol⁻¹ (Fig. 4.2.5).

The differences in the values for the change in free energy, enthalpy and entropy (per metal) associated with the formation of related molybdate and tungstate complexes are shown in the **Figure 4.3**. A positive difference indicates that the particular quantity (ΔG° , ΔH° , $T\Delta S^\circ$) is more favourable for the tungstate complex.

The differences between the overall stability of the [1,2,*r*] molybdate and tungstate complexes of the α -hydroxycarboxylate ligands are particularly similar (Fig. 4.3), the difference in energy being 9.3 kJ mol^{-1} , on average. Both the enthalpy and entropy changes are more favourable for the tungstate complexes. For the [1,2tart,*r*] complexes the enthalpy and entropy contribute almost equally to the greater stability of the tungstate complexes, whereas the enthalpy is the main contributor for the other complexes of α -hydroxycarboxylate ligands.

The differences in the free energy of the [1W,1,*r*] and [1Mo,1,*r*] complexes of the α -hydroxycarboxylate ligands are in the range $7\text{-}11 \text{ kJ mol}^{-1}$ (Fig. 4.3). For some complexes, such as the [1,1mal,*r*] and the [1,1cit,1], the sole reason for the greater stability of the tungstate complexes is the more favourable enthalpy, since the difference in entropy is slightly in favour of the molybdate complexes. It is interesting to compare the ΔG° , ΔH° and $T\Delta S^\circ$ values in favour of the [1W,1cit,*r*] complexes. The enthalpy factor in favour of the stability of the [1W,1cit,*r*] complexes thus decreases almost linearly upon protonation whereas the entropy factor increases almost linearly, while the difference in free energy change is very similar for all the [1,1cit,*r*] complexes.

The differences in both enthalpy and entropy for the molybdate and tungstate complexes [2,2cit,5], [2,1tart,2], [2,1tart,3] and [4,4mal,11] are particularly large, but the enthalpy favours the tungstate whereas the entropy favours the molybdate complexes, resulting in the tungstate complexes being only slightly more stable than the molybdate complexes (Fig. 4.3).

The calculated ΔG° , ΔH° and $T\Delta S^\circ$ for the protonation of the ligand species are shown in **Fig 4.4.1**. All the protonations which take place at carboxylate groups in the ligand are mainly entropy driven, the enthalpy contribution being very small but favourable (except for the protonation of oxalate, for which the enthalpy change is slightly unfavourable). The change in free energy associated with the protonation of a ligand species decreases for each successive protonation mainly because of the decrease in the entropy factor which most likely is a result of the charge density of the ligand species becoming progressively smaller upon protonation. This also explains the greatest change in entropy for the protonation of the highly charged [0,1cit,0] species, compared to all other ligand protonations, except for [0,1nta,0].

The thermodynamic values for the protonation of [0,1nta,0] are clearly different from the rest, indicating the protonation of the amino group, which is almost equally entropy and enthalpy driven. The ΔH° and $T\Delta S^\circ$ values for the protonation of [0,1nta,3] was not calculated, but the trend set by the other values suggest a probable value of ~ 1 and $\sim 4 \text{ kJ mol}^{-1}$ for ΔH° and $T\Delta S^\circ$, respectively (Appendix 4).

The ΔG° values for the protonation of 73 molybdate and tungstate complexes were calculated from ΔG° values for the formation of a complex $[p,q,r]$ and its protonated form $[p,q,r+1]$. The ΔH° and $T\Delta S^\circ$ could be calculated for 53 of these complexes and are shown in Fig. 4.4.1-2. Due to the predominance of the [1,2,2] lactate and mandelate complexes in their respective systems, the ΔH° and $T\Delta S^\circ$ for the formation of other lactate and mandelate complexes could not be calculated from experimental data. For this reason, only the ΔG° values for the protonation of the lactate and mandelate complexes could be calculated. Nevertheless, the similarity of the ΔG° values for the protonation of related lactate and mandelate complexes is striking.

The ΔG° , ΔH° and $T\Delta S^\circ$ values for the protonation of the molybdate and related tungstate complexes are often very similar, for instance, for the protonation of the molybdate and tungstate complexes, [1,1ox,2], [1,2mal,2], [1,2mal,3], [1,1mal,1], [1,1mal,2], [1,1cit,1], [1,1cit,2], [1,1cit,3], [1,2tart,2], and [1,2tart,3]. However, the thermodynamic values for the protonation of some other molybdate complexes are significantly different from those for the related tungstate complex. The ΔG° values for the protonation of [2Mo,2cit,4] and [2W,2cit,4] complexes, for instance, do not differ very much, but the protonation of the molybdate complex is entirely entropy driven, whereas the protonation of the tungstate complex is mainly enthalpy driven. Similarly, the ΔG° values for the protonation of [2Mo,1tart,3] and [2W,1tart,3] complexes are not very different, but in this case the protonation of the molybdate complex is entirely enthalpy driven, whereas the protonation of the tungstate complex is entirely entropy driven.

In some systems complexes $[p,q,r]$ and $[2p,2q,2r]$ were identified. This enabled the calculation of the thermodynamic values for the dimerization of these $[p,q,r]$ complexes, which are shown in Fig. 4.5 (positive values of the quantities (ΔG° , ΔH° and $T\Delta S^\circ$) are in favour of dimerization). The dimerization of [1Mo,1ox,3], [1W,1ox,3] and [2Mo,1mal,4] is favoured by both enthalpy and entropy, but is mostly entropy driven. The dimerization of other complexes is either solely enthalpy driven, like the dimerization of [1Mo,1mal,2], [1W,1mal,2], [1Mo,1cit,2] and [1W,1cit,2], or solely entropy driven, like the dimerization of [1W,1ox,2], [1W,1mal,1], [1Mo,1cit,3], [1Mo,1nta,4] and [2Mo,1cit,5].

The different comparisons of thermodynamic values (the trends and obvious exceptions) which are presented in figures 4.1 - 4.5 were *all* taken into account when attempting to propose structures for the complexes. The proposed structures are presented in section 4.2 without much explanation. The consistency of the proposed structures and the thermodynamic evidence, or the reasons for proposing specific structures are illustrated and discussed in section 4.3.

Table 4.1 Summary of all the complexes identified in all the complex systems investigated $[p,q,r]$: Mo(VI) and W(VI) complexes $[p,q,r]$: Mo(VI)-complexes only $[p,q,r]$: W(VI)-complexes only

M-ox	M-lac	M-man	M-mal	M-cit	M-tart	M-asp	M-nta	n-
				$[1,1,1]^4$				
			$[1,1,1]^3$	$[1,1,2]^3$			$[1,1,2]^3$	3-
$[1,1,2]^2$		$[1,1,1]^2$	$[1,1,2]^2$	$[1,1,3]^2$		$[1,1,1]^2$	$[1,1,3]^2$	2-
$[1,1,3]$	$[1,1,2]$	$[1,1,2]$	$[1,1,3]$	$[1,1,4]$		$[1,1,2]$	$[1,1,4]$	1-
	$[1,1,3]$	$[1,1,3]$						0
			$[1,2,2]^4$	$[1,2,4]^4$	$[1,2,2]^4$			4-
	$[1,2,1]^3$	$[1,2,1]^3$	$[1,2,3]^3$	$[1,2,5]^3$	$[1,2,3]^3$	$[1,2,1]^3$		3-
$[1,2,4]^2$	$[1,2,2]^2$	$[1,2,2]^2$	$[1,2,4]^2$	$[1,2,6]^2$	$[1,2,4]^2$	$[1,2,2]^2$		2-
	$[1,2,3]$	$[1,2,3]$						1-
			$[2,2,2]^6$	$[2,2,4]^6$				6-
			$[2,2,3]^5$	$[2,2,5]^5$				5-
$[2,2,4]^4$	$[2,2,2]^4$		$[2,2,4]^4$	$[2,2,6]^4$				4-
$[2,2,5]^3$	$[2,2,3]^3$		$[2,2,5]^3$		$[2,2,5]^3$		$[2,2,7]^3$	3-
$[2,2,6]^2$	$[2,2,4]^2$	$[2,2,4]^2$					$[2,2,8]^2$	2-
		$[2,2,5]$						1-
				$[2,1,3]^4$	$[2,1,2]^4$		$[2,1,3]^4$	4-
			$[2,1,3]^3$	$[2,1,4]^3$	$[2,1,3]^3$		$[2,1,4]^3$	3-
	$[2,1,3]^2$	$[2,1,3]^2$	$[2,1,4]^2$	$[2,1,5]^2$	$[2,1,4]^2$		$[2,1,5]^2$	2-
$[2,1,5]$	$[2,1,4]$	$[2,1,4]$			$[2,1,5]$	$[2,1,4]$	$[2,1,6]$	1-
	$[2,1,5]$	$[2,1,5]$				$[2,1,5]$		0
				$[4,2,9]^5$				5-
$[4,2,8]^4$			$[4,2,8]^4$	$[4,2,10]^4$				4-
			$[4,2,9]^3$					3-
			$[4,2,10]^2$					2-
				$[4,4,11]^9$				9-
					$[4,4,8]^8$			8-
$[4,4,9]^7$					$[4,4,9]^7$			7-
$[4,4,10]^6$								6-
			$[4,4,11]^5$					5-
						$[4,4,9]^3$		3-
						$[4,4,10]^2$		2-
						$[2,4,8]$		0
					$[3,4,6]^8$			8-
					$[3,4,8]^6$			6-
					$[4,3,8]^6$			6-
					$[4,5,8]^{10}$			10-
					$[4,5,9]^9$			9-

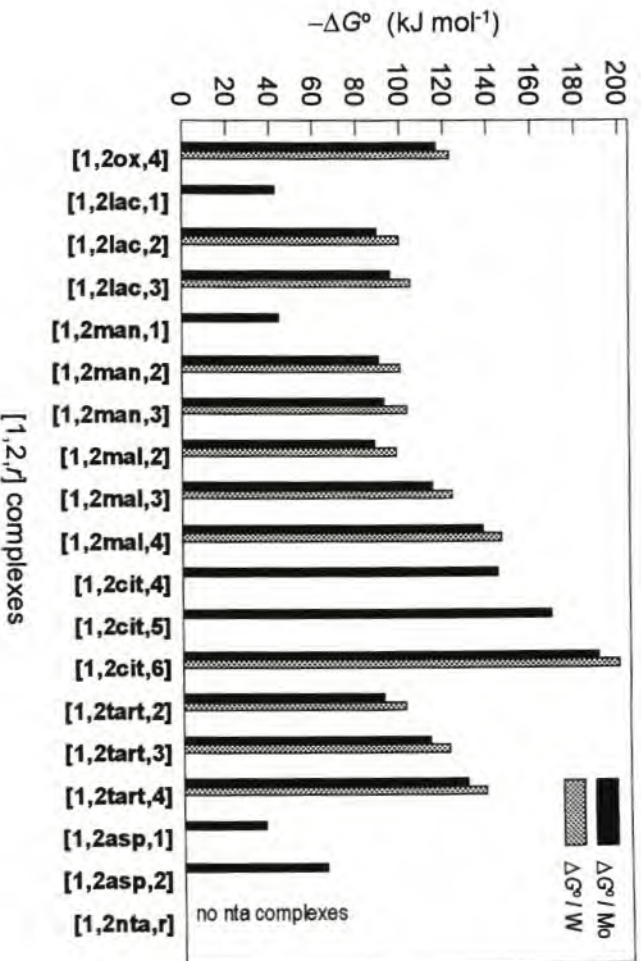


Fig. 4.1.1 The ΔG° (per metal) for the formation of molybdate(VI) and tungstate(VI) [1,2,r] complexes.

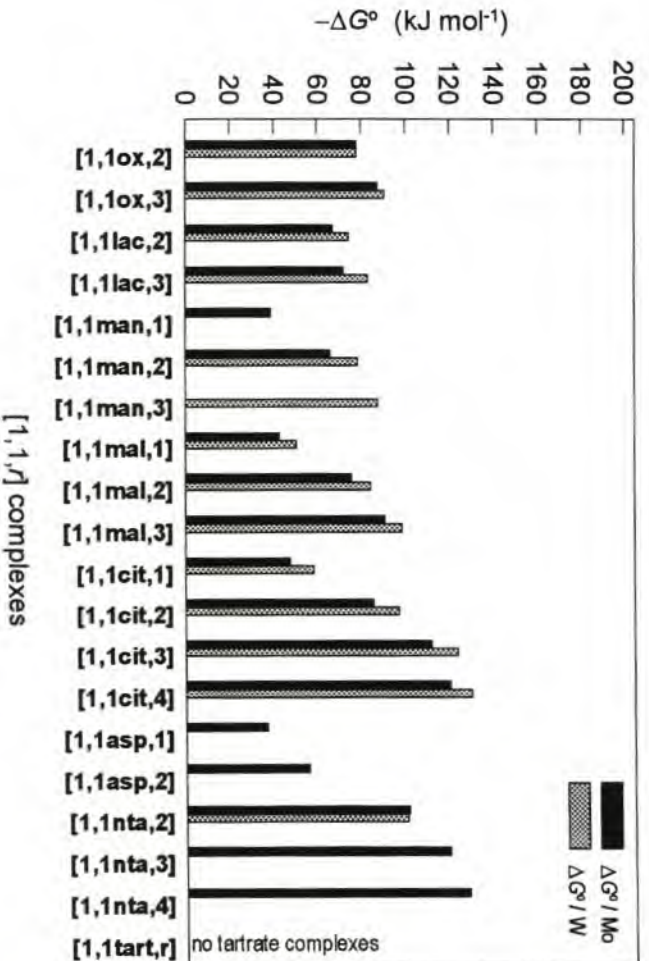


Fig. 4.1.2 The ΔG° (per metal) for the formation of molybdate(VI) and tungstate(VI) [1,1,r] complexes.

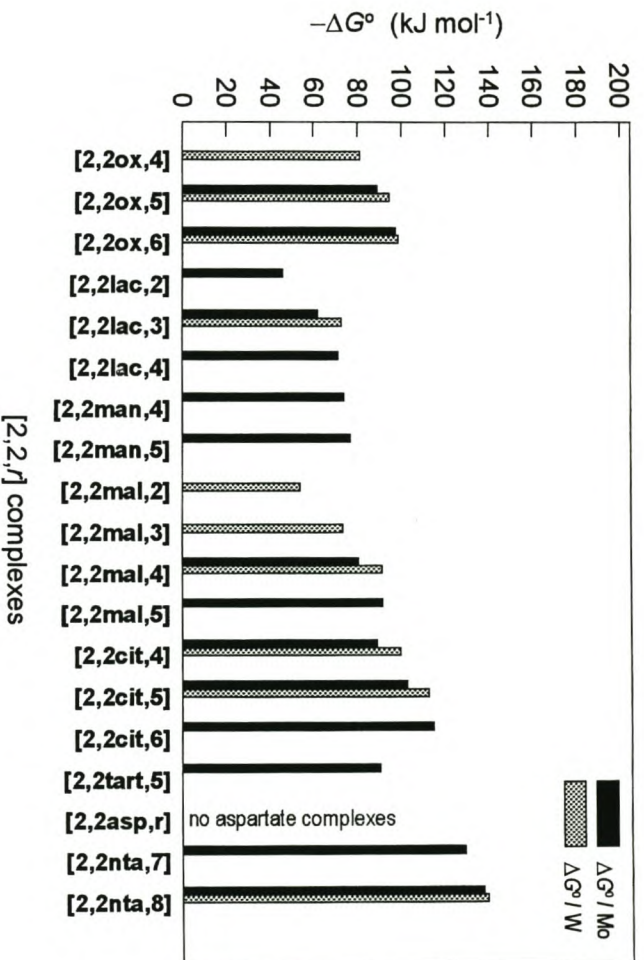


Fig. 4.1.3 The ΔG° (per metal) for the formation of molybdate(VI) and tungstate(VI) [2,2,r] complexes.

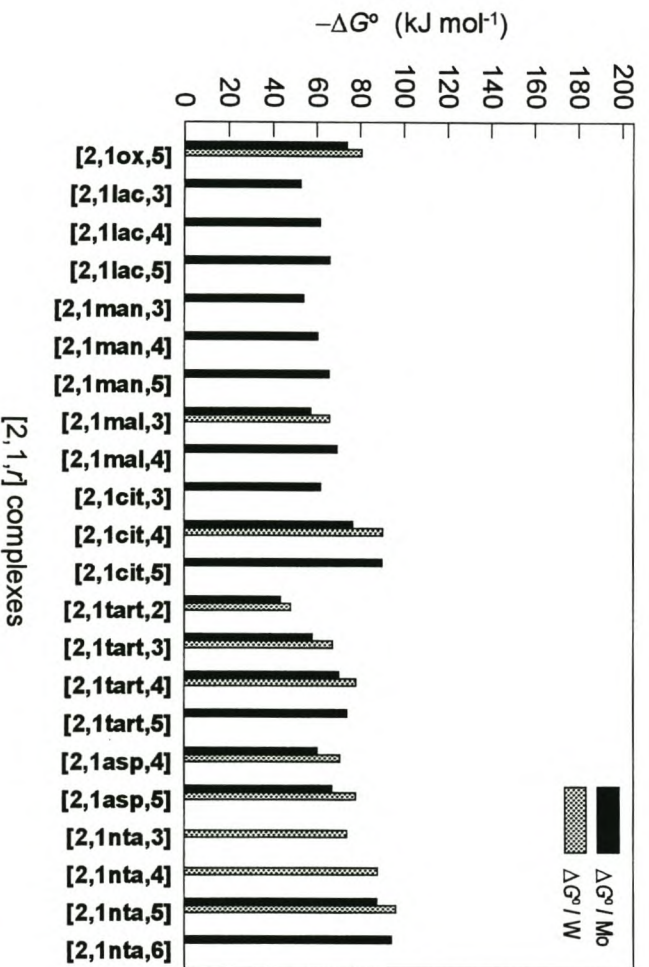


Fig. 4.1.4 The ΔG° (per metal) for the formation of molybdate(VI) and tungstate(VI) [2,1,r] complexes.

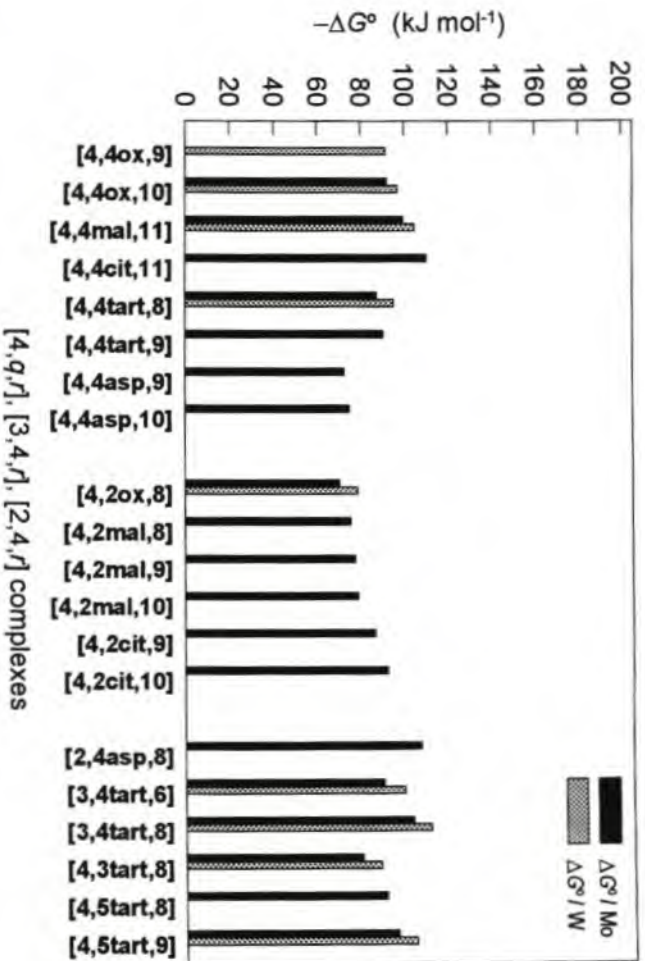


Fig. 4.1.5 The ΔG° (per metal) for the formation of molybdate(VI) and tungstate(VI) [4,4,r], [3,4,r], [2,4,r] complexes.

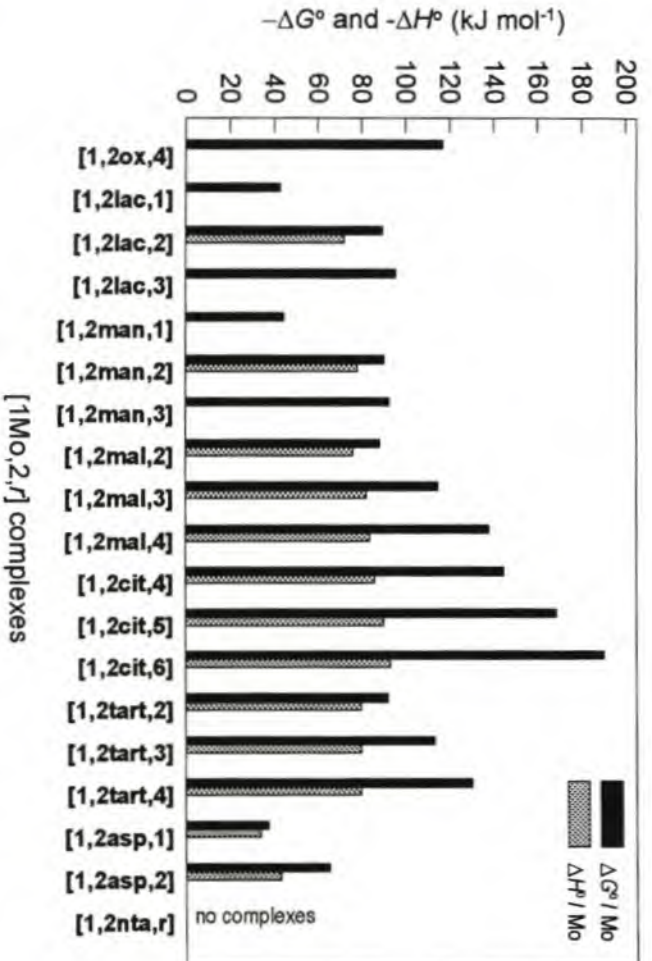


Fig. 4.2.1 Comparison of ΔG° /Mo and ΔH° /Mo for the [1,2,r] molybdate(VI) complexes.

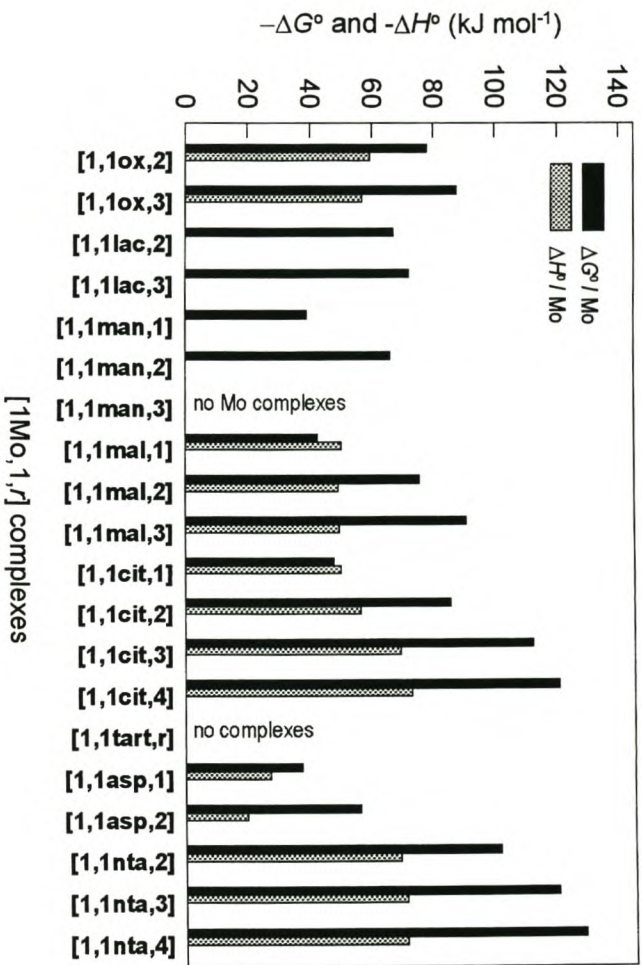


Fig. 4.2.2 Comparison of $\Delta G^\circ / \text{Mo}$ and $\Delta H^\circ / \text{Mo}$ for the [1, 1,r] molybdate(VI) complexes.

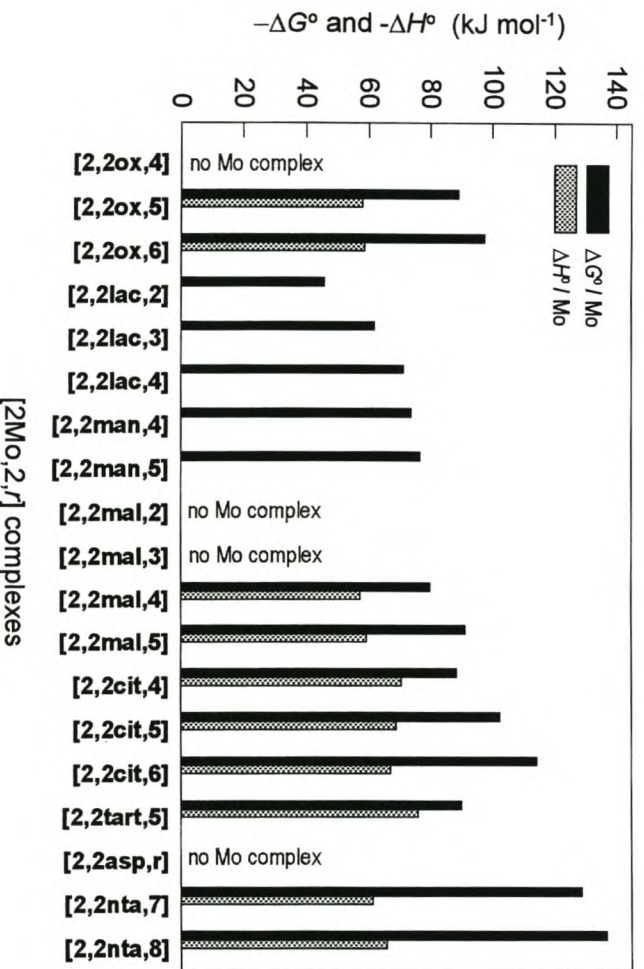
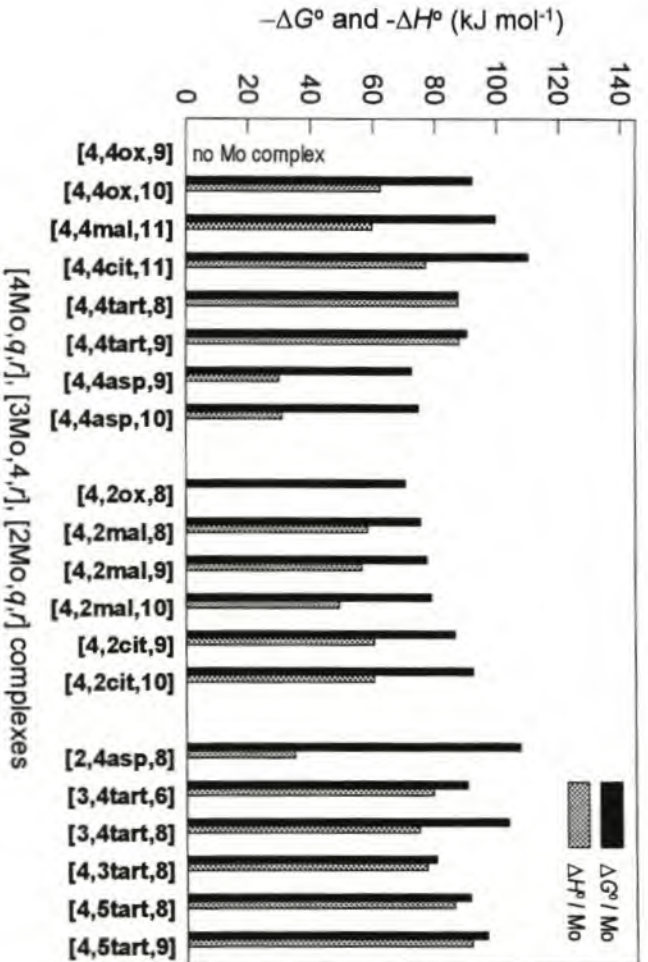
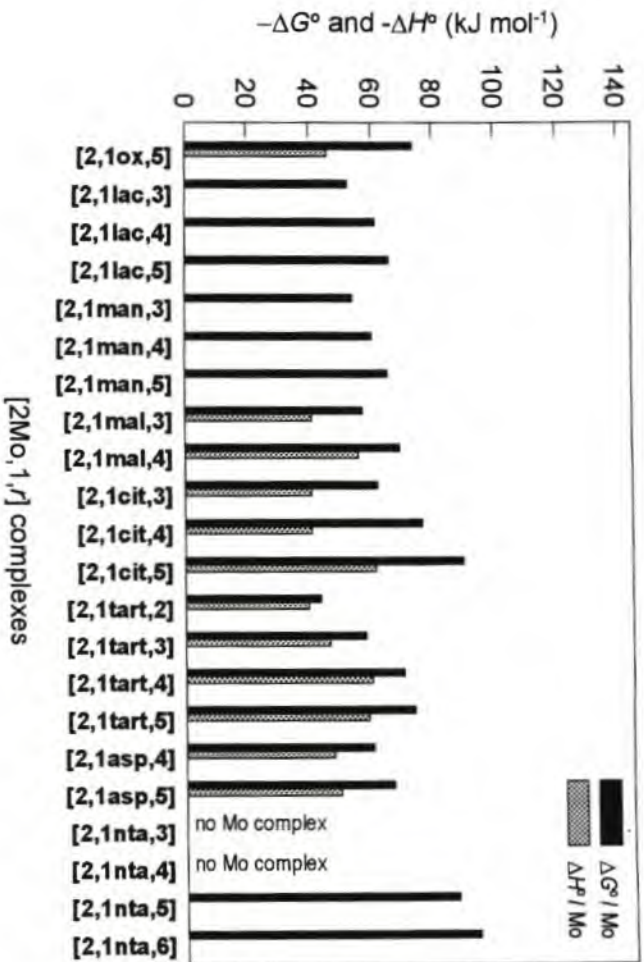


Fig. 4.2.3 Comparison of $\Delta G^\circ / \text{Mo}$ and $\Delta H^\circ / \text{Mo}$ for the [2,2,r] molybdate(VI) complexes.



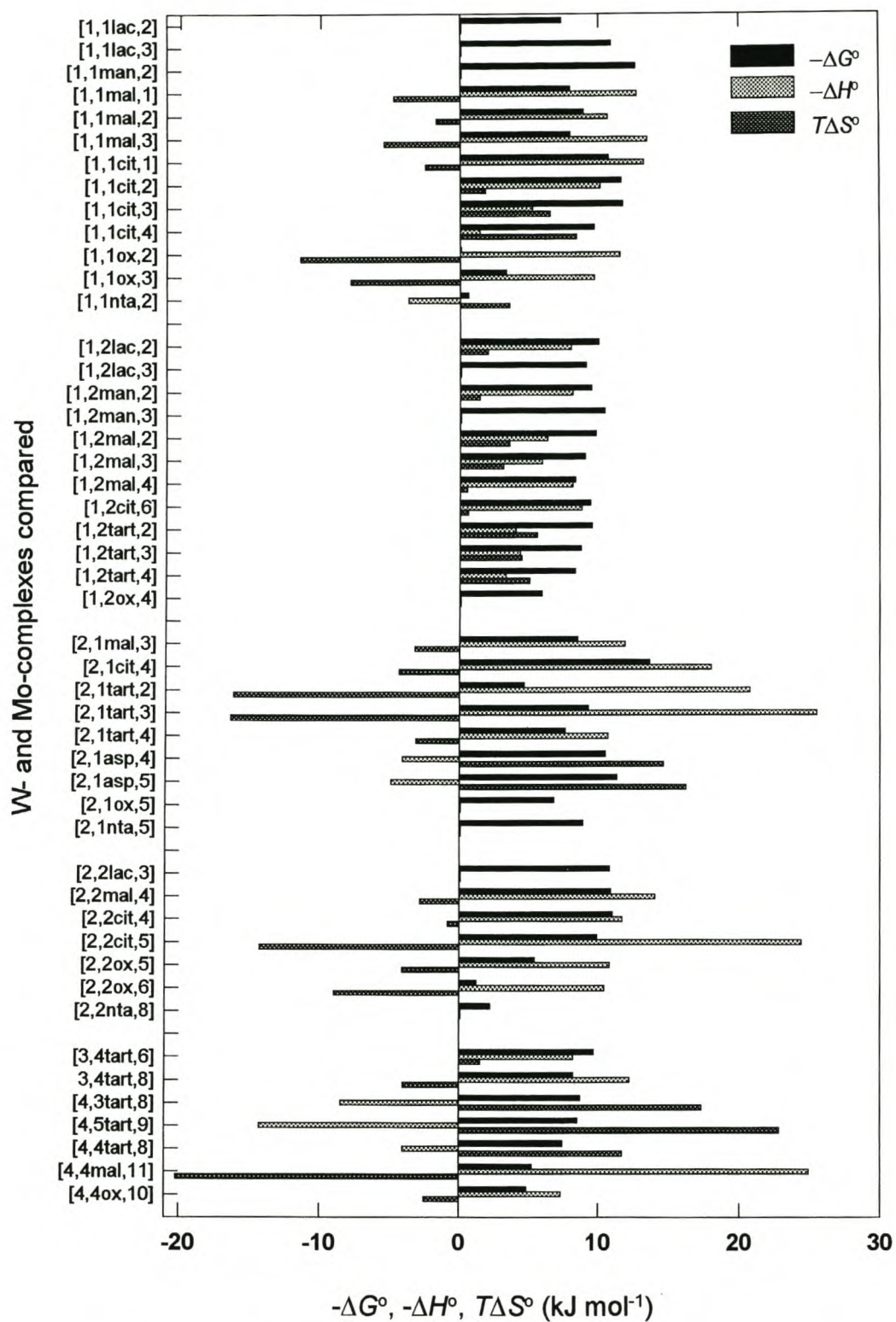


Fig. 4.3 The difference in the values of ΔG° , ΔH° and $T\Delta S^\circ$ (per metal) for the formation of tungstate(VI) and molybdate(VI) complexes of the same stoichiometry $[p,q,r]$. (A positive difference indicates that the particular quantity is more favourable for the tungstate(VI) complex than for the molybdate(VI) complex.)

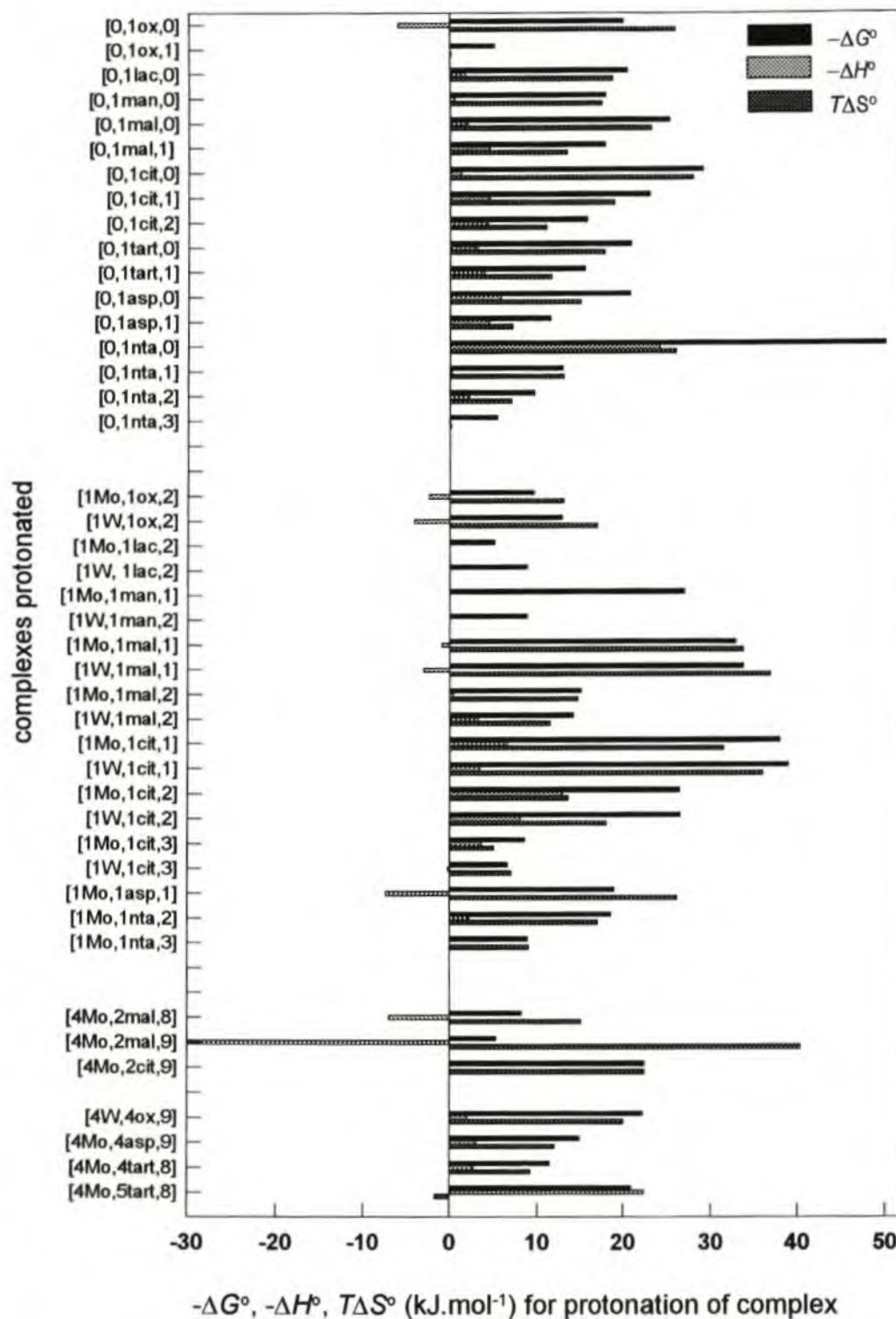


Fig. 4.4.1 The ΔG° , ΔH° and $T\Delta S^\circ$ values for the protonation of the ligands and the [1,1,*r*] and [4,*q*,*r*] complexes. (Positive values of the particular quantities are in favour of protonation.)

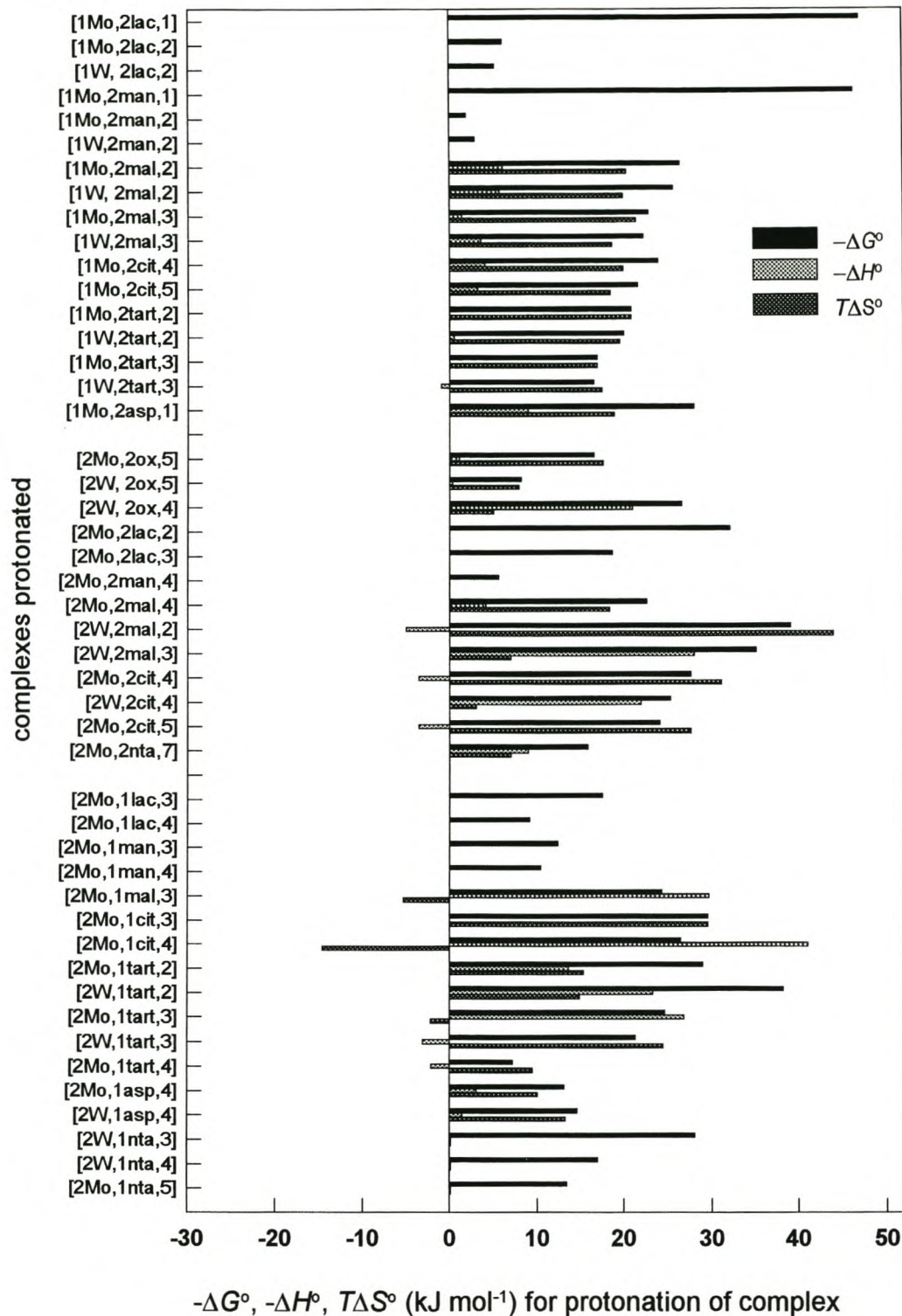


Fig. 4.4.2 The ΔG° , ΔH° and $T\Delta S^\circ$ values for the protonation of the [1,2,*r*], [2,2,*r*] and [2,1,*r*] complexes. (Positive values of the particular quantities are in favour of protonation.)

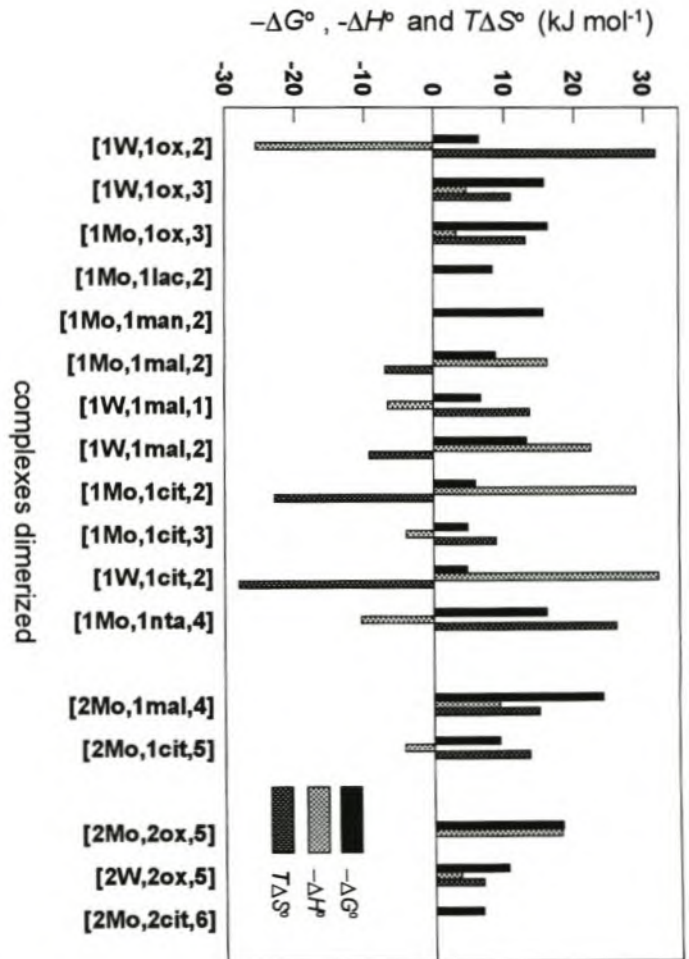


Fig. 4.5 The ΔG° , ΔH° and $T\Delta S^\circ$ for the dimerization of some complexes.

4.2 PROPOSED STRUCTURES FOR THE COMPLEXES

The existence of a specific complex species in a solid does not necessarily imply that the same complex exists in solution. However, some previous studies have led to the conclusion that the structure of a complex in solution often resembles the structure of the complex as a solid. Typically, if a complex in a crystal has a MO_2 or MO_3 core ($M = Mo$ or W), this configuration is retained in the solution, or if a ligand binds didentate or tridentate, the mode of chelation is also retained. The known structures of some molybdate and tungstate complexes in solids were therefore used as the basis for proposing structures for other related complexes as far as possible.

Only a few Mo and W- complexes of the ligands investigated have previously been isolated as solids. The structures of some have been proposed based on chemical or spectroscopic analyses, but relatively few structures (particularly of W-complexes) were determined by X-ray crystallographic analysis. Furthermore, in the light of these few X-ray structures and other evidence, some of the previously proposed structures of related complexes must be questioned. The complex anions which have been identified by X-ray analysis of their salts, as well as other plausible proposed structures are tabulated and shown in the Appendix 3.

By inspection of these complexes (Appendix 3) the following typical features for complexes of Mo and W with the ligands in question are identified ($M = Mo$ or W) :

- general: octahedral conformation of the ligands around the metal,
- [1,1,*r*] an MO_2 or MO_3 core with didentate chelation and further OH or H_2O ligands,
or an MO_3 core with tridentate chelation,
- [1,2,*r*] an MO_2 core with didentate chelation of two ligands,
- [2,2,*r*] an M_2O_5 core with didentate chelation on each M and a further OH or H_2O ligand on each M,
an M_2O_5 core with tridentate chelation on each M,
- [4,2,*r*] two doubly bridged M_2O_6 cores connected *via* one mutual O (to form a M_4O_{11} core) with two ligands, each bound tridentate to one M_2O_6 core and monodentately to the other core.

Some of these features have been combined previously [95,94] to propose structures for complexes such as the $[2Mo,1cit,4]^{2-}$ and $[2Mo,2cit,4]^{6-}$ (Appendix 3).

Complexes with the same stoichiometry as the complexes determined by X-ray crystallography (Appendix 3, Fig. A3), have now been identified by potentiometric analysis as major species in the model describing a particular system. This is not necessarily proof of the existence of all the calculated species in solution, but a strong indication that the calculated species are not fictitious. Of all the solid complexes for which

structures have been proposed previously (Appendix 3, Fig. A3, A4), only the $[1\text{Mo}, 2\text{ox}, 2]$ complex was not identified in solution. The structures of these complexes in solution are proposed to be the same as in the solid, especially since the thermodynamic values strongly support the different structures (*cf.* 4.3).

Structures were also proposed for the rest of the complexes identified in solution. The common structural features (above) have been incorporated as far as possible, and modified as little as possible when needed. Where different structures with the correct charge could be pictured, the known thermodynamic values were used to choose the more probable structure. Of particular importance, in this regard, were the values for the change of enthalpy and entropy for the formation of these complexes, the thermodynamic values for the protonation of the ligand itself, the protonation and dimerization of the complexes and the difference between the values pertaining to the molybdate and tungstate complexes. (These different thermodynamic relationships have been presented graphically in Figures 4.1.1 - 4.5). The following structures are proposed and consistent with the different thermodynamic quantities.

The structure formulas are summarized in tables to facilitate comparison. (Where the same structures are proposed for a particular pair of molybdate and tungstate complexes, the formula is printed in bold (M=Mo,W). Where the structures differ, the metal is specified.) An index number is assigned to each complex and shown in the tables which are used in the accompanying figures and the ensuing discussion.

4.2.1 $[1,2,r]$ complexes

Table 4.2.1 Proposed structures of the $[1,2,r]$ complexes. (Compare Fig. 4.6)

index	$[1,2,r]^{n-}$	Formula(structure)	X-ray structure	comment
A1	$[1,2\text{ox}, 4]^{2-}$	$[\text{MO}_2(\text{ox})_2]$		
A2	$[1,2\text{lac}, 1]^{3-}$	$[\text{MoO}_3(\text{lac})_2]$		one di-, one monodentate
A3	$[1,2\text{lac}, 2]^{2-}$	$[\text{MO}_2(\text{lac})_2]$		
A4	$[1,2\text{lac}, 3]^{-}$	$[\text{MO}_2(\text{lac})_2(\text{H}_2\text{O})]$		one di-, one monodentate
A5	$[1,2\text{man}, 1]^{3-}$	$[\text{MoO}_3(\text{man})_2]$		one di-, one monodentate
A6	$[1,2\text{man}, 2]^{2-}$	$[\text{MO}_2(\text{man})_2]$		
A7	$[1,2\text{man}, 3]^{-}$	$[\text{MO}_2(\text{man})_2(\text{H}_2\text{O})]$		one di-, one monodentate
A8	$[1,2\text{mal}, 2]^{4-}$	$[\text{MO}_2(\text{mal})_2]$		
A9	$[1,2\text{mal}, 3]^{3-}$	$[\text{MO}_2(\text{Hmal})(\text{mal})]$		
A10	$[1,2\text{mal}, 4]^{2-}$	$[\text{MO}_2(\text{Hmal})_2]$	known	
A11	$[1,2\text{cit}, 4]^{4-}$	$[\text{MoO}_2(\text{Hcit})_2]$		
A12	$[1,2\text{cit}, 5]^{3-}$	$[\text{MoO}_2(\text{H}_2\text{cit})(\text{Hcit})]$		
A13	$[1,2\text{cit}, 6]^{2-}$	$[\text{MO}_2(\text{H}_2\text{cit})_2]$		
A14	$[1,2\text{tart}, 2]^{4-}$	$[\text{MO}_2(\text{tar})_2]$		
A15	$[1,2\text{tart}, 3]^{3-}$	$[\text{MO}_2(\text{Htar})(\text{tar})]$		
A16	$[1,2\text{tart}, 4]^{2-}$	$[\text{MO}_2(\text{Htar})_2]$	known	
A17	$[1,2\text{asp}, 1]^{3-}$	$[\text{MoO}_3(\text{asp})_2]$		one di-, one monodentate
A18	$[1,2\text{asp}, 2]^{2-}$	$[\text{MoO}_2(\text{asp})_2]$		

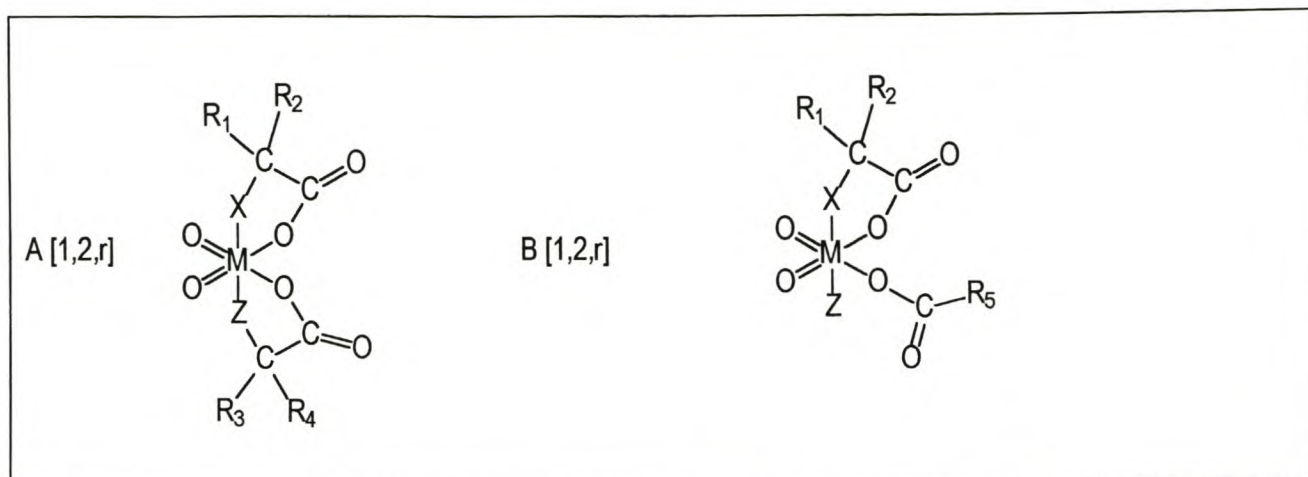


Fig. 4.6 Proposed structures for the $[1,2,r]$ complexes. (See tables below for assignment of groups.)

Structures A $[1,2,r]$

index	$[1,2,r]$	X	Z	R1	R2	R3	R4
A1	$[1,2ox,4]^{2-}$	O	O	O	-	O	-
A3	$[1,2lac,2]^{2-}$	O	O	CH ₃	H	CH ₃	H
A6	$[1,2man,2]^{2-}$	O	O	Ph	H	Ph	H
A8	$[1,2mal,2]^{4-}$	O	O	CH ₂ COO ⁻	H	CH ₂ COO ⁻	H
A9	$[1,2mal,3]^{3-}$	O	O	CH ₂ COO ⁻	H	CH ₂ COOH	H
A10	$[1,2mal,4]^{2-}$	O	O	CH ₂ COOH	H	CH ₂ COOH	H
A11	$[1,2cit,4]^{4-}$	O	O	CH ₂ COO ⁻	CH ₂ COOH	CH ₂ COO ⁻	CH ₂ COOH
A12	$[1,2cit,5]^{3-}$	O	O	CH ₂ COO ⁻	CH ₂ COOH	CH ₂ COOH	CH ₂ COOH
A13	$[1,2cit,6]^{2-}$	O	O	CH ₂ COOH	CH ₂ COOH	CH ₂ COOH	CH ₂ COOH
A14	$[1,2tart,2]^{4-}$	O	O	CH(OH)COO ⁻	H	CH(OH)COO ⁻	H
A15	$[1,2tart,3]^{3-}$	O	O	CH(OH)COO ⁻	H	CH(OH)COOH	H
A16	$[1,2tart,4]^{2-}$	O	O	CH(OH)COOH	H	CH(OH)COOH	H
A18	$[1,2asp,2]^{2-}$	NH ₂	NH ₂	CH ₂ COO ⁻	H	CH ₂ COO ⁻	H

Structures B $[1,2,r]$

index	$[1,2,r]$	X	Z	R1	R2	R5
A2	$[1,2lac,1]^{3-}$	O	O	CH ₃	H	CH(OH)-CH ₃
A4	$[1,2lac,3]^{-}$	O	H ₂ O	CH ₃	H	CH(OH)-CH ₃
A5	$[1,2man,1]^{3-}$	O	O	Ph	H	CH(OH)-Ph
A7	$[1,2man,3]^{-}$	O	H ₂ O	Ph	H	CH(OH)-Ph
A17	$[1,2asp,1]^{3-}$	NH ₂	O	CH ₂ COO ⁻	H	"CH(NH ₂)COOH"

4.2.2 [1,1,*r*] complexesTable 4.2.2 Proposed structures of the [1,1,*r*] complexes. (Compare Fig. 4.7)

index	[1,1, <i>r</i>] ⁿ⁻	Formula(structure)	X-ray structure	comment
B1	[1,1ox,2] ²⁻	[MO ₃ (ox)(H ₂ O)]	known	didentate
B2	[1,1ox,3] ⁻	[MO ₂ (ox)(H ₂ O)(OH)]		didentate
B3	[1,1lac,2] ⁻	[MO ₂ (lac)(H ₂ O)(OH)]		didentate
B4	[1,1lac,3]	[MO ₂ (lac)(H ₂ O) ₂]		didentate
B5	[1,1man,1] ²⁻	[MoO ₃ (man)(OH)(H ₂ O)]		monodentate
B6	[1,1man,2] ⁻	[MO ₂ (man)(H ₂ O)(OH)]		didentate
B7	[1,1man,3]	[WO ₂ (man)(H ₂ O) ₂]		didentate
B8	[1,1mal,1] ³⁻	[MO ₃ (mal)(H ₂ O)]		didentate
B9	[1,1mal,2] ²⁻	[MO ₃ (Hmal)(H ₂ O)]		didentate
B10	[1,1mal,3] ⁻	[MO ₂ (Hmal)(H ₂ O)(OH)]		didentate
B11	[1,1cit,1] ⁴⁻	[MO ₃ (cit)(H ₂ O)]		didentate
B12	[1,1cit,2] ³⁻	[MO ₃ (Hcit)(H ₂ O)]		didentate
B13	[1,1cit,3] ²⁻	[MoO ₂ (OH)(Hcit)]		tri-dentate
B13b	[1,1cit,3] ²⁻	[WO ₃ (H ₂ cit)(H ₂ O)]		didentate
B14	[1,1cit,4] ⁻	[MoO ₂ (Hcit)(H ₂ O)]		tri-dentate
B14b	[1,1cit,4] ⁻	[WO ₂ (OH)(H ₂ cit)(H ₂ O)]		didentate
B15	[1,1asp,1] ²⁻	[MoO ₃ (asp)]	known	tri-dentate
B16	[1,1asp,2] ⁻	[MoO ₃ (asp)(H ₂ O)]		didentate
B17	[1,1nta,2] ³⁻	[MO ₃ (nta)]	known	tri-dentate
B18	[1,1nta,3] ²⁻	[MoO ₃ (Hnta)]		tri-dentate
B19	[1,1nta,4] ¹⁻	[MoO ₂ (Hnta)(OH)]		tri-dentate

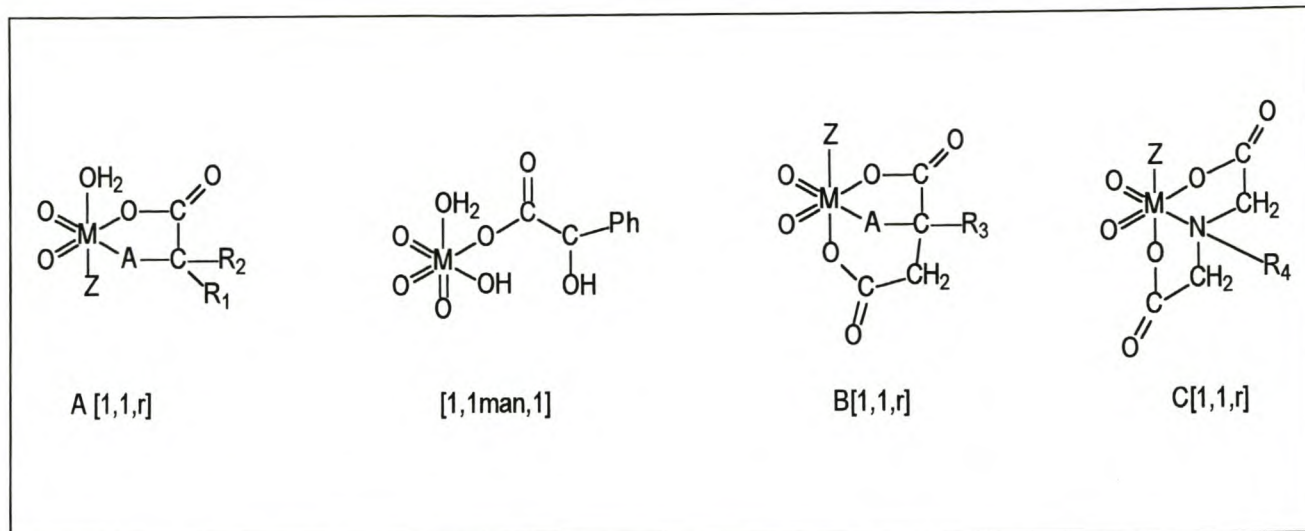


Fig. 4.7 Proposed structures for the [1,1,r] complexes. (See tables below for assignment of groups.)

Structures A [1,1,r]

index	[1Mo,1,r]	[1W,1,r]	A	Z	R1	R2
B1	[1,1ox,2] ²⁻	[1,1ox,2] ²⁻	O	O	-	-
B2	[1,1ox,3] ⁻	[1,1ox,3] ⁻	O	OH	-	-
B3	[1,1lac,2] ⁻	[1,1lac,2] ⁻	O	OH	-	H
B4	[1,1lac,3]	[1,1lac,3]	O	H ₂ O	-	H
B5	[1,1man,1] ²⁻	monodentate				
B6	[1,1man,2] ⁻	[1,1man,2] ⁻	O	OH	-	H
B7	-	[1,1man,3]	O	H ₂ O	-	H
B8	[1,1mal,1] ³⁻	[1,1mal,1] ³⁻	O	O	CH ₂ COO ⁻	H
B9	[1,1mal,2] ²⁻	[1,1mal,2] ²⁻	O	O	CH ₂ COOH	H
B10	[1,1mal,3] ⁻	[1,1mal,3] ⁻	O	OH	CH ₂ COOH	H
B11	[1,1cit,1] ⁴⁻	[1,1cit,1] ⁴⁻	O	O	CH ₂ COO ⁻	CH ₂ COO ⁻
B12	[1,1cit,2] ³⁻	[1,1cit,2] ³⁻	O	O	CH ₂ COO ⁻	CH ₂ COOH
B13	structure B	[1,1cit,3] ²⁻	O	O	CH ₂ COOH	CH ₂ COOH
B14	structure B	[1,1cit,4] ⁻	O	OH	CH ₂ COOH	CH ₂ COOH
B16	[1,1asp,2] ⁻	-	NH ₂	O	CH ₂ COOH	H

Structures B [1,1,r]

index	[1Mo,1,r]	[1W,1,r]	A	Z	R3	
B13b	[1,1cit,3] ²⁻	structure A	O	OH	CH ₂ COOH	
B14b	[1,1cit,4] ⁻	structure A	O	H ₂ O	CH ₂ COOH	
B15	[1,1asp,1] ²⁻	-	NH ₂	O	H	

Structures C [1,1,r]

index	[1Mo,1,r]	[1W,1,r]	-	Z	R4	-
B17	[1,1nta,2] ³⁻	[1,1nta,2] ³⁻	-	O	CH ₂ COO ⁻	-
B18	[1,1nta,3] ²⁻		-	O	CH ₂ COOH	-
B19	[1,1nta,4] ¹⁻		-	OH	CH ₂ COOH	-

4.2.3 [2,2,*r*] complexesTable 4.2.3 Proposed structures of the [2,2,*r*] complexes. (Compare Fig. 4.8.1 , 2)

index	[2,2, <i>r</i>] ⁿ⁻	Formula (structure)	X-ray structure	comment
C1	[2,2ox,4] ⁴⁻	[W ₂ O ₅ (ox) ₂ (OH) ₂]		oxalate bridge
C2	[2,2ox,5] ³⁻	[M ₂ O ₅ (ox) ₂ (H ₂ O)(OH)]		one oxalate / M-centre
C3	[2,2ox,6] ²⁻	[M ₂ O ₅ (ox) ₂ (H ₂ O) ₂]	known	one oxalate / M-centre
C4	[2,2lac,2] ⁴⁻	[Mo ₂ O ₅ (lac) ₂ (OH) ₂]		lactate bridge
C5	[2,2lac,3] ³⁻	[Mo ₂ O ₅ (lac) ₂ (H ₂ O)(OH)]		one lactate / Mo-centre
C5b	[2,2lac,3] ³⁻	[W ₂ O ₅ (lac) ₂ (H ₂ O)(OH)]		lactate bridge
C6	[2,2lac,4] ²⁻	[Mo ₂ O ₅ (lac) ₂ (H ₂ O) ₂]		one lactate / Mo-centre
C7	[2,2man,4] ²⁻	[Mo ₂ O ₅ (man) ₂ (H ₂ O) ₂]		one mandelate / M-centre
C8	[2,2man,5] ⁻	[Mo ₂ O ₅ (man) ₂ (H)(H ₂ O) ₂]		protonation position unknown
C9	[2,2mal,2] ⁶⁻	[W ₂ O ₅ (mal) ₂ (OH) ₂]		malate bridge
C10	[2,2mal,3] ⁵⁻	[W ₂ O ₅ (mal)(Hmal)(OH) ₂]		malate bridge
C11	[2,2mal,4] ⁴⁻	[M ₂ O ₅ (Hmal) ₂ (OH) ₂]		one malate / M-centre
C12	[2,2mal,5] ³⁻	[Mo ₂ O ₅ (Hmal) ₂ (OH)(H ₂ O)]		one malate / M-centre
C13	[2,2cit,4] ⁶⁻	[M ₂ O ₅ (cit) ₂]	known	one citrate / M-centre
C14	[2,2cit,5] ⁵⁻	[Mo ₂ O ₅ (Hcit)(cit)]		one citrate / M-centre
C15	[2,2cit,6] ⁴⁻	[Mo ₂ O ₅ (Hcit) ₂]		one citrate / M-centre
C14b	[2,2cit,5] ⁵⁻	[W ₂ O ₅ (Hcit)(cit)]		citrate bridge between W's
C16	[2,2nta,7] ³⁻	[Mo ₂ O ₅ (Hnta)(nta)]		one nta / M-centre
C17	[2,2nta,8] ²⁻	[Mo ₂ O ₅ (Hnta) ₂]	known	one nta / M-centre
C18	[2,2tart,5] ³⁻	[Mo ₂ O ₂ (tart) ₂ Mo ₂ O ₂]		two tartrate bridges

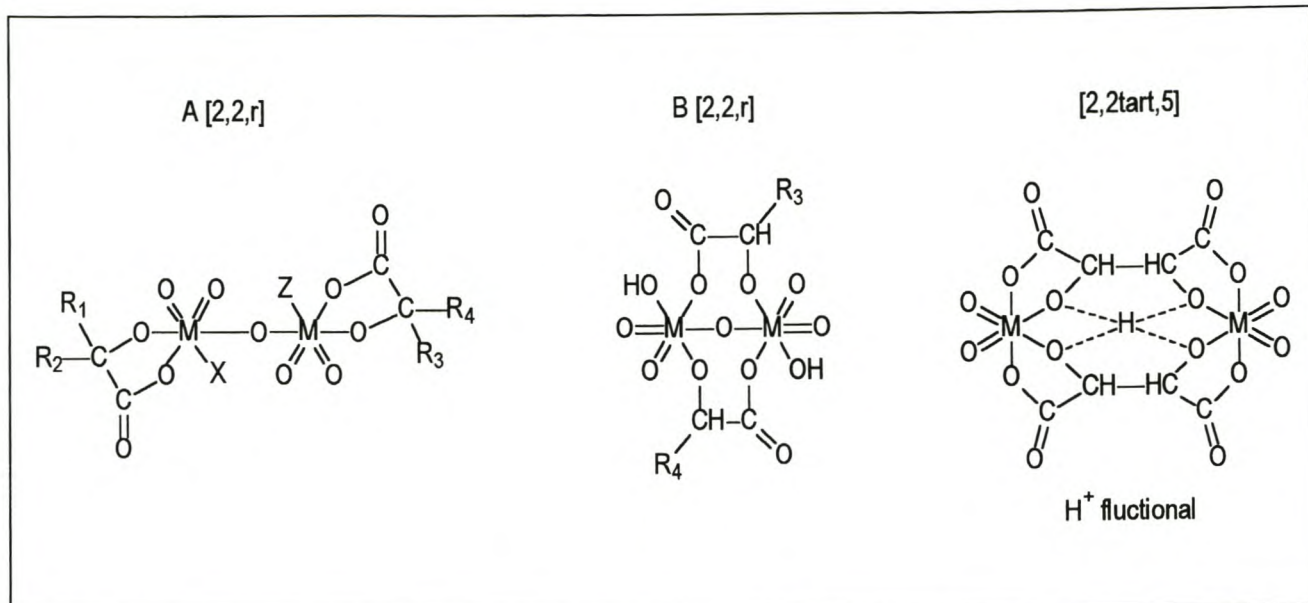


Fig. 4.8.1 Proposed structures for the [2,2,r] complexes. (See tables below for assignment of groups.)

Structures A [2,2,r]

index	[2,2,r]	X	Z	R1	R2	R3	R4
C2	[2,2ox,5] ³⁻	H ₂ O	OH	O	-	O	-
C3	[2,2ox,6] ²⁻	H ₂ O	H ₂ O	O	-	O	-
C5	[2,2lac,3] ³⁻	H ₂ O	OH	CH ₃	H	CH ₃	H
C6	[2,2lac,4] ²⁻	H ₂ O	H ₂ O	CH ₃	H	CH ₃	H
C7	[2,2man,4] ²⁻	H ₂ O	H ₂ O	Ph	H	Ph	H
C8	[2,2man,5] ⁻	H ₂ O	H ₂ O	Ph(H)	H	Ph	H
C11	[2,2mal,4] ⁴⁻	OH	OH	CH ₂ COOH	H	CH ₂ COOH	H
C12	[2,2mal,5] ³⁻	H ₂ O	OH	CH ₂ COOH	H	CH ₂ COOH	H

Structures B [2,2,r]

index	[2,2,r]	X	Z	R3		R4	
C1	[2,2ox,4] ⁴⁻	OH	OH	O		O	
C9	[2,2mal,2] ⁶⁻	OH	OH	CH ₂ COO ⁻		CH ₂ COO ⁻	
C10	[2,2mal,3] ⁵⁻	OH	OH	CH ₂ COOH		CH ₂ COO ⁻	
C4	[2,2lac,2] ⁴⁻	OH	OH	CH ₃		CH ₃	
C5b	[2,2lac,3] ³⁻	H ₂ O	OH	CH ₃		CH ₃	

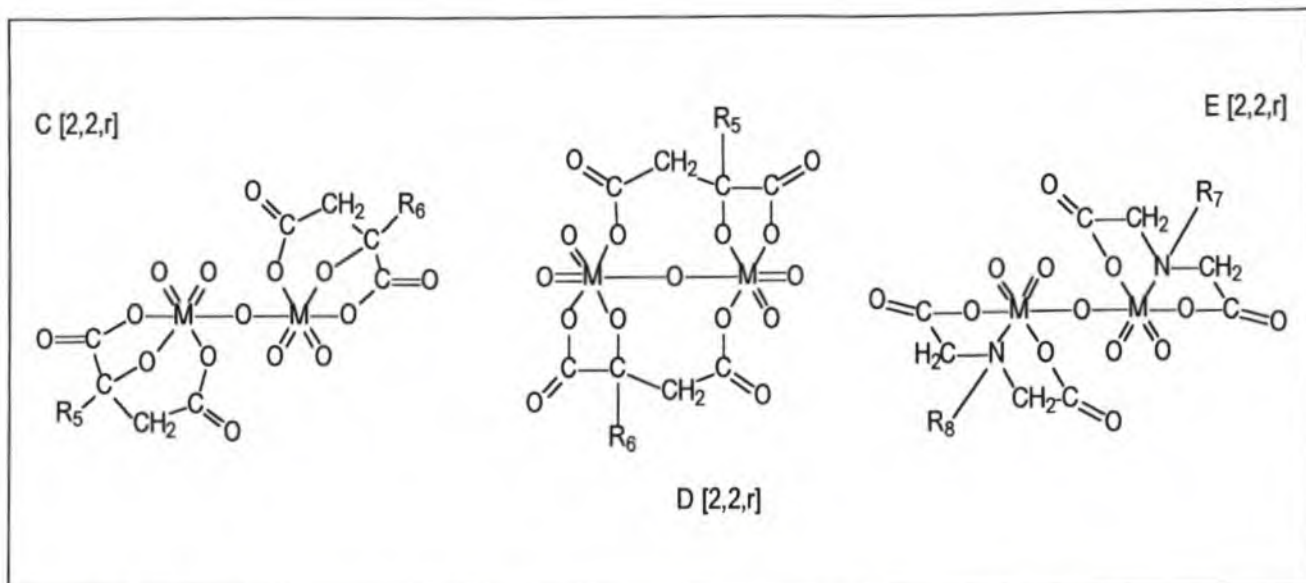


Fig. 4.8.2 Proposed structures for the [2,2,*r*] complexes. (See tables below for assignment of groups.)

Structures C [2,2,*r*] and E[2,2,*r*]

index	[2Mo,2, <i>r</i>]	[2W,2, <i>r</i>]	R5	R7	R6	R8
C13	[2,2cit,4] ⁶⁻	[2,2,4] ⁶⁻	CH ₂ COO ⁻	-	CH ₂ COO ⁻	-
C14	[2,2cit,5] ⁵⁻	structure D	CH ₂ COO ⁻	-	CH ₂ COOH	-
C15	[2,2cit,6] ⁴⁻	-	CH ₂ COOH	-	CH ₂ COOH	-
C16	[2,2nta,7] ³⁻	-	-	CH ₂ COO ⁻	-	CH ₂ COOH
C17	[2,2nta,8] ²⁻	[2W,2,8]	-	CH ₂ COOH	-	CH ₂ COOH

Structures D [2,2,*r*]

index	[2Mo,2q, <i>r</i>]	[2W,2q, <i>r</i>]	R5	R6
C14b	structure B	[2,2cit,5] ⁵⁻	CH ₂ COO ⁻	CH ₂ COOH

4.2.4 [2,1,*r*] complexes

Table 4.2.4 Proposed structures of the [2,1,*r*] complexes. (Compare Fig. 4.9.1 , 2 , 3)

index	[2,1, <i>r</i>] ⁿ⁻	Formula(structure)	NMR structure	comment
D1	[2,1ox,5] ⁻	[M₂O₅(OH) (ox) (H₂O)₂]		M-O-M, M-OH-M + ox bridge
D2	[2,1lac,3] ²⁻	[Mo ₂ O ₆ (lac)(H ₂ O) ₂]		two M-O-M + lac bridge
D3	[2,1lac,4] ⁻	[Mo ₂ O ₅ (OH) (lac)(H ₂ O) ₂]		M-O-M, M-OH-M+ lac bridge
D4	[2,1lac,5]	[Mo ₂ O ₄ (OH) ₂ (lac)(H ₂ O) ₂]		two M-OH-M + lac bridge
D5	[2,1man,3] ²⁻	[Mo ₂ O ₆ (man)(H ₂ O) ₂]		two M-O-M + man bridge
D6	[2,1man,4] ⁻	[Mo ₂ O ₅ (OH) (man)(H ₂ O) ₂]		M-O-M, M-OH-M+man brdg
D7	[2,1man,5]	[Mo ₂ O ₄ (OH) ₂ (man)(H ₂ O) ₂]		two M-OH-M + lac bridge
D8	[2,1mal,3] ³⁻	[M₂O₆ (mal) (H₂O)₂]		two M-O-M + cit bridge
D9	[2,1mal,4] ²⁻	[Mo ₂ O ₅ (OH) (mal)(H ₂ O)]		tri-dentate
D10	[2,1cit,3] ⁴⁻	[Mo ₂ O ₆ (cit) (H ₂ O) ₂]		two M-O-M + cit bridge
D11	[2,1cit,4] ³⁻	[M₂O₆ (Hcit) (H₂O)₂]		two M-O-M + cit bridge
D12	[2,1cit,5] ²⁻	[Mo ₂ O ₅ (OH)(Hcit)(H ₂ O)]	known	tri-dentate
D13	[2,1tart,2] ⁴⁻	[MoO ₂ (OH) ₂ (tart) MO ₂ (OH) ₂]		tart bridge only
D13b	[2,1tart,2] ⁴⁻	[W ₂ O ₅ (tart) (OH) ₂]		W-O-W bridge + tart bridge
D14	[2,1tart,3] ³⁻	[Mo ₂ O ₅ (tart)(OH)(H ₂ O)]		Mo-O-Mo bridge + tart bridge
D14b	[2,1tart,3] ³⁻	[W ₂ O ₆ (tart)(H ₂ O)]		W-O ₂ -W + tart bridge
D15	[2,1tart,4] ²⁻	[M ₂ O ₅ (tart)(OH)(H ₂ O)]		M-O ₂ -M + tart bridge
D16	[2,1tart,5] ⁻	[Mo ₂ O ₄ (tart)(OH) ₂ (H ₂ O)]		Mo-O ₂ -Mo + tart bridge
D17	[2,1asp,4] ⁻	[M₂O₅ (asp)(OH) (H₂O)]		Mo-O ₂ -Mo + asp bridge
D18	[2,1asp,5]	[M₂O₄ (asp)(OH)₂ (H₂O)]		Mo-O ₂ -Mo + asp bridge
D19	[2,1nta,3] ³⁻	[W ₂ O ₆ (nta) (OH) (H ₂ O)]		W-O ₂ -W + nta bi. bridge
D20	[2,1nta,4] ³⁻	[W ₂ O ₆ (nta) (H ₂ O)]		W-O ₂ -W + nta tri. bridge
D21	[2,1nta,5] ²⁻	[M ₂ O ₆ (Hnta) (H ₂ O)]		M-O ₂ -M + nta tri. bridge
D22	[2,1nta,6] ⁻	[Mo ₂ O ₅ (Hnta) (OH) (H ₂ O)]		M-O ₂ -M + nta tri. bridge

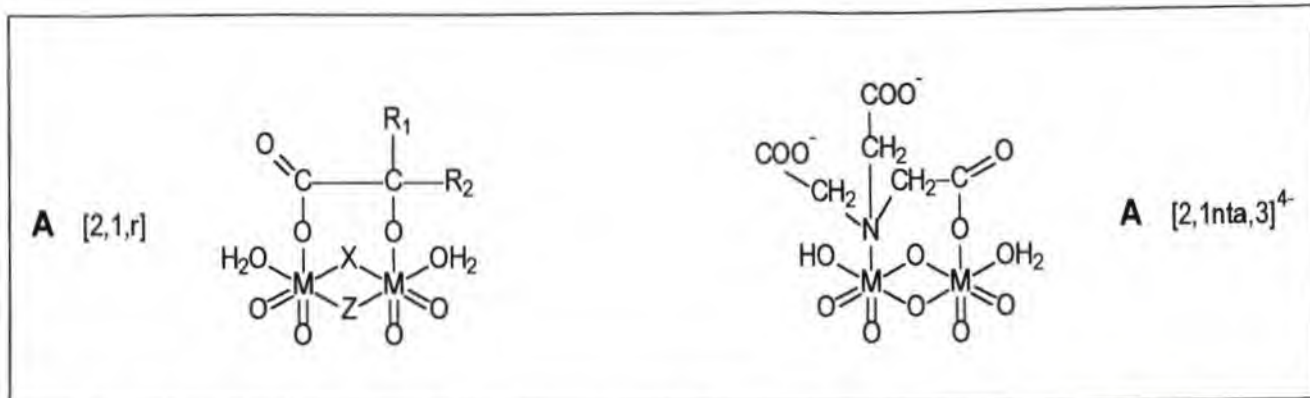


Fig. 4.9.1.1 Proposed structures for [2,1,*r*] complexes. (See table below for assignment of groups.)

Structures A [2,1,*r*]

index	[1,2, <i>r</i>]	X	Z	R1	R2
D1	[2,1ox,5] ⁻	O	OH	O	H
D2	[2,1lac,3] ²⁻	O	O	CH ₃	H
D3	[2,1lac,4] ⁻	O	OH	CH ₃	H
D4	[2,1lac,5]	OH	OH	CH ₃	H
D5	[2,1man,3] ²⁻	O	O	Ph	H
D6	[2,1man,4] ⁻	O	OH	Ph	H
D7	[2,1man,5]	OH	OH	Ph	H
D9	[2,1mal,3] ³⁻	O	O	CH ₂ COO ⁻	H
D10	[2,1cit,3] ⁴⁻	O	O	CH ₂ COO ⁻	CH ₂ COO ⁻
D11	[2,1cit,4] ³⁻	O	O	CH ₂ COOH	CH ₂ COO ⁻
D19	[2,1nta,3] ³⁻	-	-	-	-

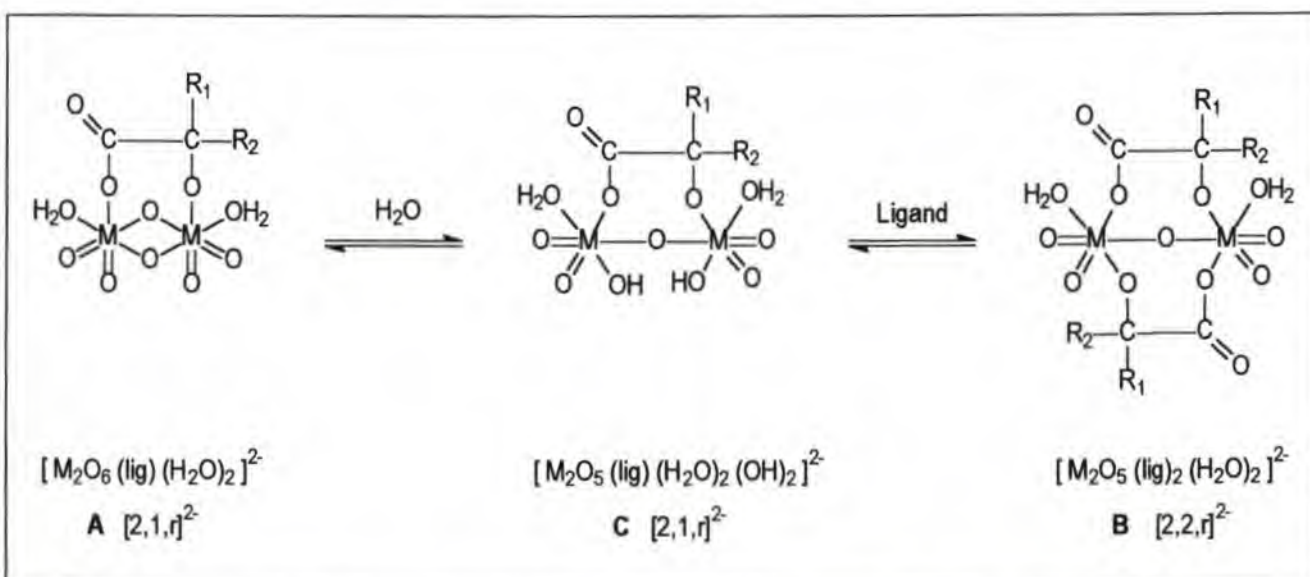


Fig. 4.9.1.2 Relationship between proposed structures for [2,1,*r*] complexes of type A (Fig. 4.9.1.1) and the proposed structures for [2,2,*r*] complexes of type B (Fig. 4.8.1).

The type C [2,1,*r*]-complexes are possible alternatives to the type A [2,1,*r*]-complexes.

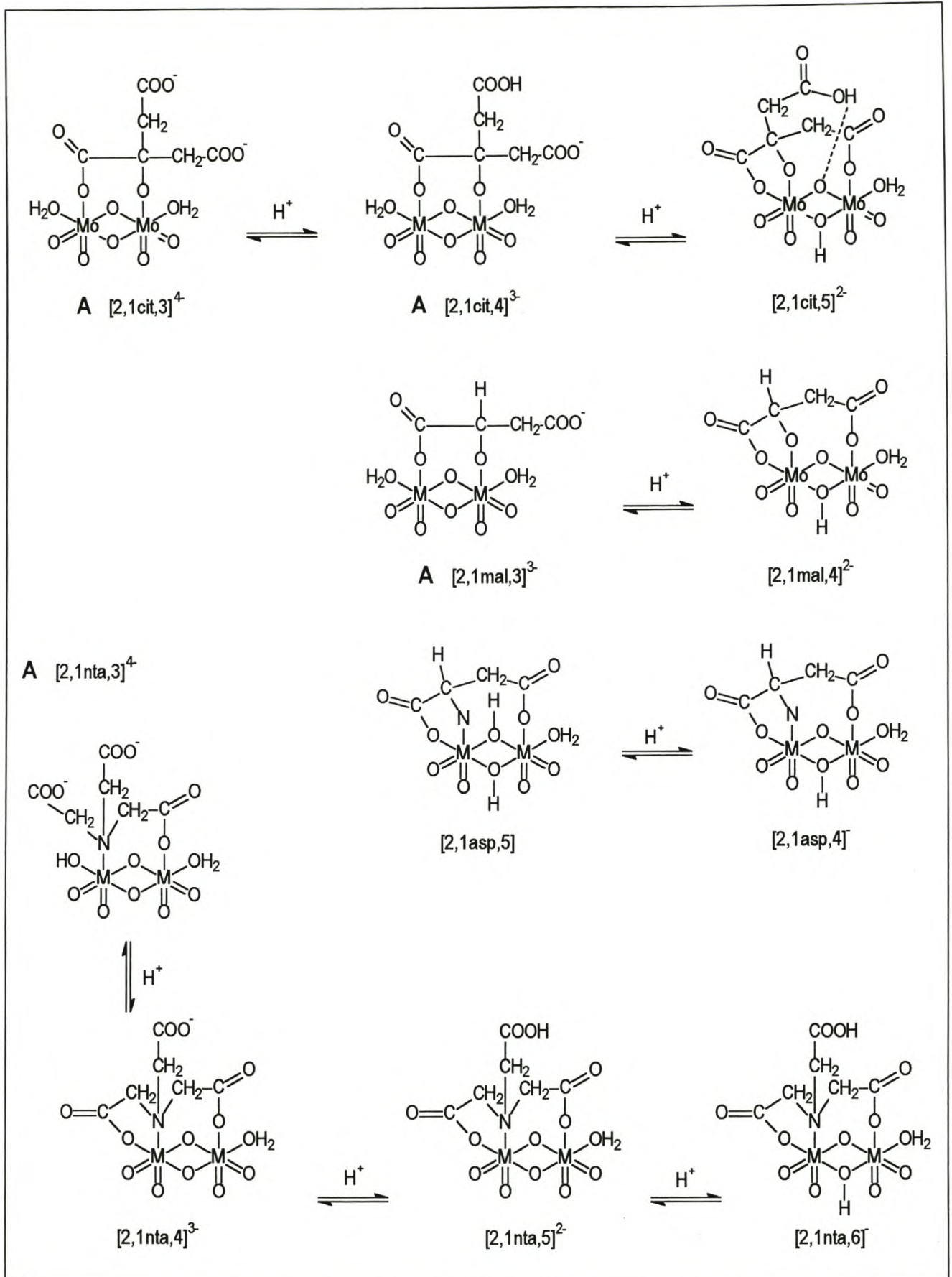


Fig. 4.9.2 Proposed structures for [2,1,*r*] complexes of malate, citrate, aspartate and nta.

(Type A structures are also presented in Fig. 4.9.1)

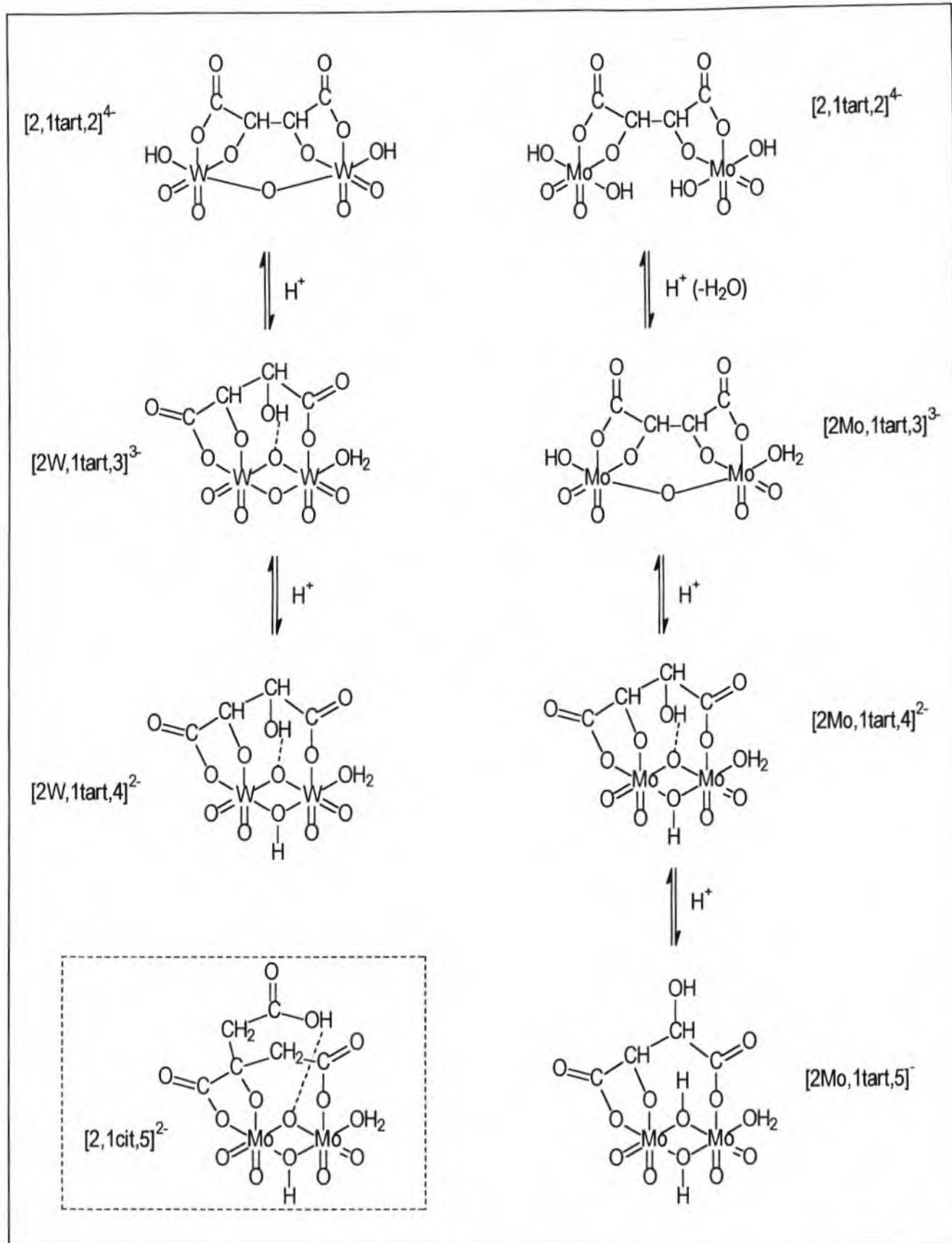


Fig. 4.9.3 Proposed structures for $[2,1,r]$ complexes of tartrate.

4.2.5 [4,2,*r*] complexes

Table 4.2.5 Proposed structures of the [4,2,*r*] complexes. (Compare Fig. 4.10)

index	[4,2, <i>r</i>] ⁿ⁻	Formula (structure)	X-ray structure	comment
E1	[4,2mal,8] ⁴⁺	[Mo ₄ O ₁₁ (mal) ₂]	known	
E2	[4,2mal,9] ³⁻	[Mo ₄ O ₁₁ (mal)(Hmal)(H ₂ O)]		
E3	[4,2mal,10] ²⁻	[Mo ₄ O ₁₁ (Hmal) ₂ (H ₂ O) ₂]		
E4	[4,2cit,10] ⁴⁺	[Mo ₄ O ₁₁ (Hcit) ₂]	known	
E5	[4,2cit,9] ⁵⁻	[Mo ₄ O ₁₁ (Hcit)(cit)]		
E6	[4,2cit,8] ⁶⁻	[Mo ₄ O ₁₁ (cit) ₂]		identified only at 2°C
E7	[4,2ox,8] ⁴⁺	[M ₄ O ₁₂ (ox) ₂ (H ₂ O) ₄]		

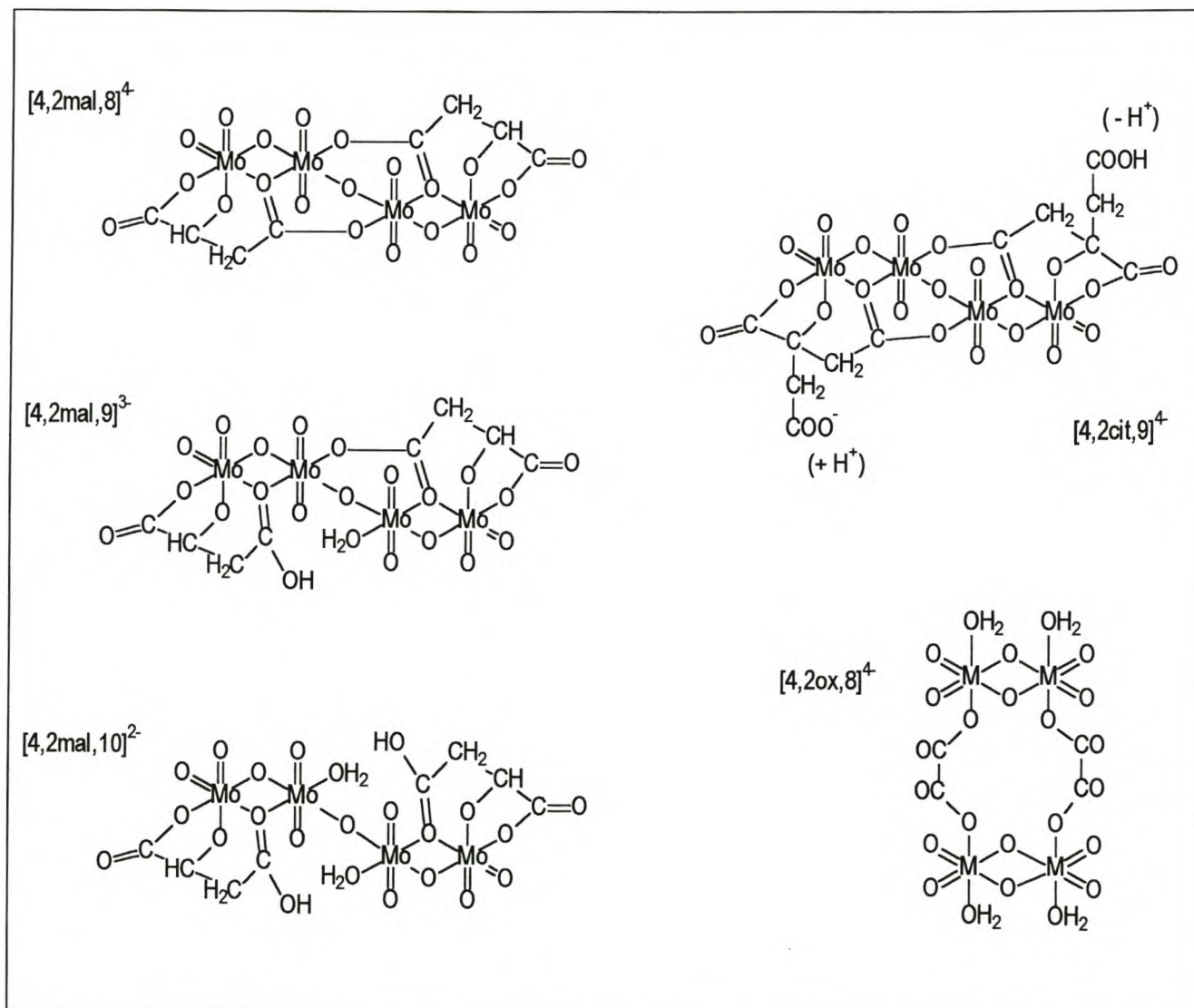


Fig. 4.10 Proposed structures for the [4,2,*r*] complexes. (Probable sites for the protonation and deprotonation of [4,2cit,9] are shown.)

4.2.6 [4,4,*r*] complexesTable 4.2.6 Proposed structures of the [4,4,*r*] complexes. (Compare Fig. 4.11.1-2)

index	[4,4, <i>r</i>] ⁿ⁻	Formula(structure)	comment
F1	[4,4tart,8] ⁸⁻	[(MO ₂ (tart)) ₄]	ring
F2	[4,4tart,9] ⁷⁻	[(MO ₂ (tart)) ₄ (H)]	ring , H ⁺ suspended in ring
F3	[4,4ox,10] ⁶⁻	[M ₄ O ₁₀ (OH) ₂ (ox) ₄]	ring
F4	[4,4ox,9] ⁷⁻	[W ₄ O ₁₁ (OH) ₁ (ox) ₄]	ring
F5a	[4,4mal,11] ⁵⁻	[M ₄ O ₈ (mal) ₄ (H ₂ O) ₃ (OH)]	ring
F5b	[4,4mal,11] ⁵⁻	[M ₄ O ₉ (mal) ₃ (Hmal)(H ₂ O)]	chain
F5c	[4,4mal,11] ⁵⁻	[M ₄ O ₈ (mal) ₄ (OH)(H ₂ O)]	chain
F5d	[4,4mal,11] ⁵⁻	[M ₄ O ₈ (mal) ₃ (Hmal)(OH) ₂]	chain
F6a	[4,4cit,11] ⁹⁻	[Mo ₄ O ₈ (cit) ₄ (H ₂ O) ₃ (OH)]	ring
F6b or	[4,4cit,11] ⁹⁻	[Mo ₄ O ₉ (cit) ₃ (Hcit)(H ₂ O)]	chain
F6c or	[4,4cit,11] ⁹⁻	[Mo ₄ O ₈ (cit) ₄ (OH)(H ₂ O)]	chain
F6d or	[4,4cit,11] ⁹⁻	[Mo ₄ O ₈ (cit) ₃ (Hcit)(OH) ₂]	chain
F7a	[4,4asp,11] ¹⁻	[Mo ₄ O ₈ (asp) ₄ (H ₂ O) ₃ (OH)]	ring imaginary complex
F7b	[4,4asp,11] ²⁻	[Mo ₄ O ₉ (asp) ₃ (Hasp)(H ₂ O) ₄]	chain imaginary complex
F8a	[4,4asp,10] ²⁻	[Mo ₄ O ₈ (asp) ₄ (H ₂ O) ₂ (OH) ₂]	ring deprotonation of H ₂ O of 7a
F8b	[4,4asp,10] ²⁻	[Mo ₄ O ₉ (asp) ₃ (Hasp) (H ₂ O) ₃ (OH)]	chain deprotonation of H ₂ O of 7b
F8c	[4,4asp,10] ²⁻	[Mo ₄ O ₉ (asp) ₄ (H ₂ O) ₄]	chain deprotonation of Hasp of 7b
F9a	[4,4asp,9] ³⁻	[Mo ₄ O ₈ (asp) ₄ (H ₂ O) ₁ (OH) ₃]	ring deprotonation of H ₂ O of 8a
F9b	[4,4asp,9] ³⁻	[Mo ₄ O ₉ (asp) ₃ (Hasp) (H ₂ O) ₂ (OH) ₂]	chain deprotonation of H ₂ O of 8b
F9c	[4,4asp,9] ³⁻	[Mo ₄ O ₉ (asp) ₄ (H ₂ O) ₃ (OH)]	chain deprotonation of Hasp of 8b
F9d	[4,4asp,9] ³⁻	[Mo ₄ O ₉ (asp) ₄ (H ₂ O) ₃ (OH)]	chain deprotonation of H ₂ O of 8c

F7a,b are possible ring or chain structures for an imaginary [4,4asp,11] , related to [4,4mal,11] and [4,4cit,11].

Structures F8a,b,c and F9a,b,c,d are seen as deprotonated forms of F7a and F7b

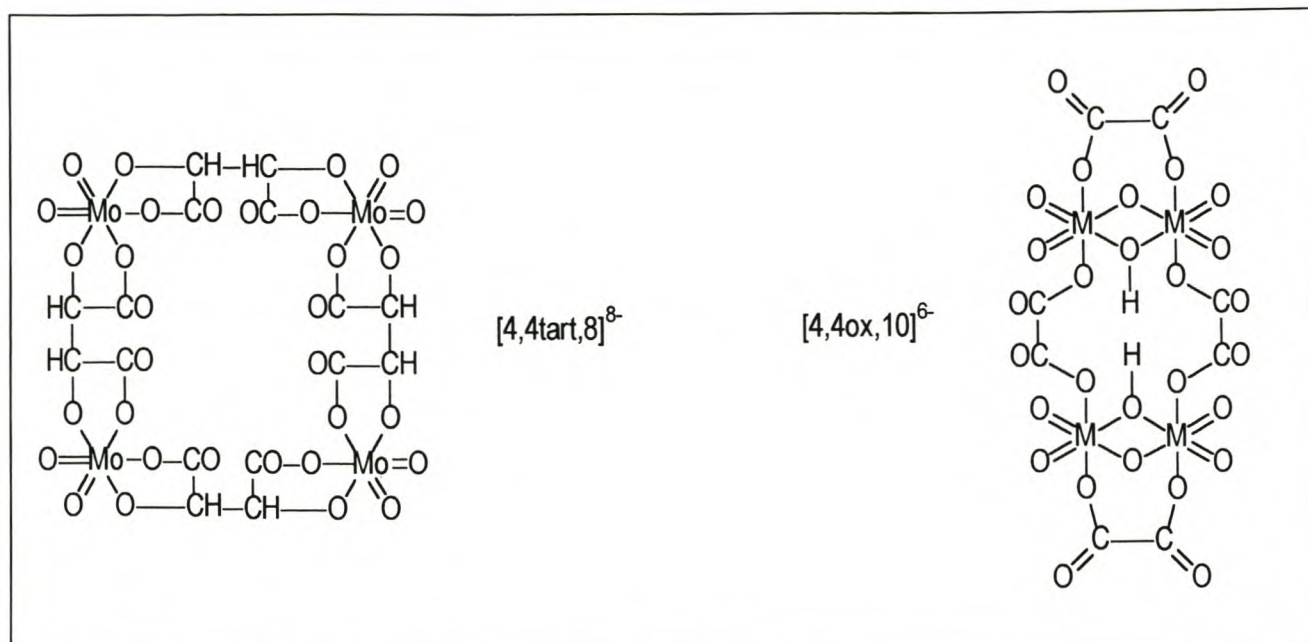


Fig. 4.11.1 Proposed structures for the [4,4,*r*] tartrate and oxalate complexes.

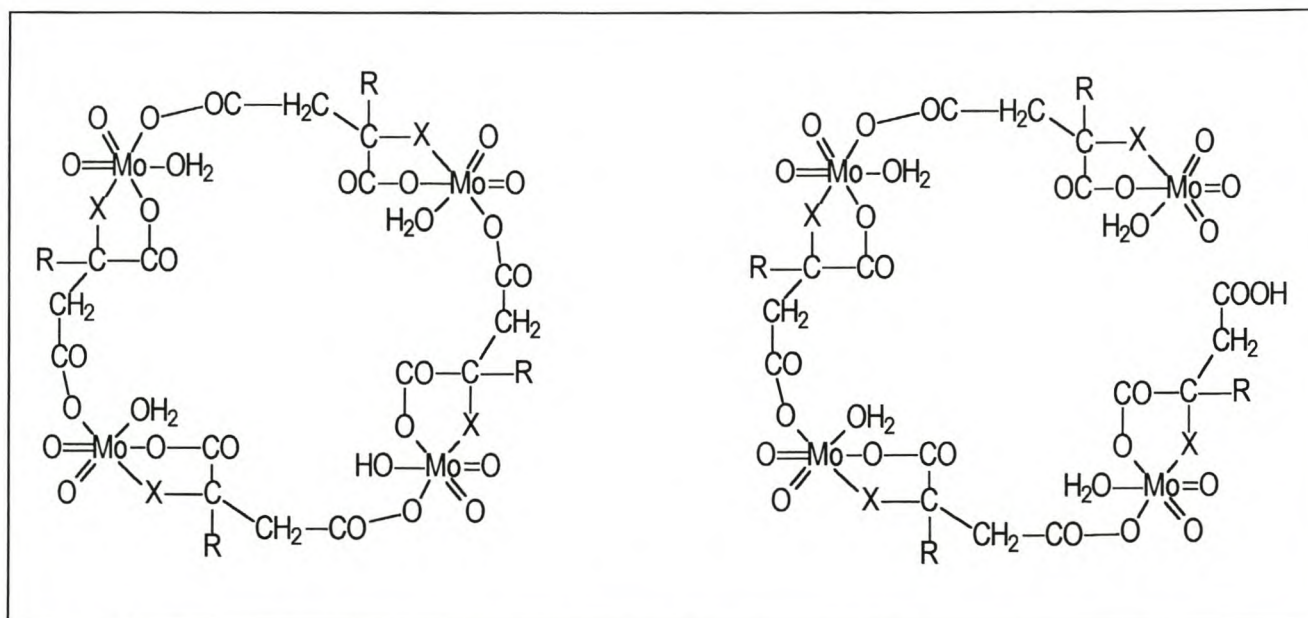
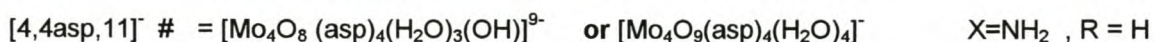
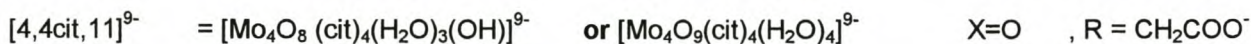


Fig. 4.11.2 Proposed ring or chain structures for the [4,4,*r*] citrate, malate and aspartate complexes.

RING - structure

CHAIN - structure



[4,4asp,11][#] was not identified, but its two deprotonated forms, [4,4,10]²⁻ and [4,4,9]³⁻, were identified with possible structures, F8a,b,c and F9a,b,c,d (Table 4.2.6).

4.2.7 [2,4asp,r] , [3,4tart,r] , [4,3tart,r] and [4,5tart,r] complexes

Table 4.2.7 Proposed structures of the [2,4,r], [3,4,r], [4,3,r] and [4,5,r] complexes (cf. Fig.4.12-13).

index	[4,4,r] ⁿ⁻	Formula(structure)		comment
G1	[2,4asp,8] ⁰⁻	[Mo ₂ O ₅ (Hasp) ₂ (H ₂ asp) ₂]		
G2	[3,4tart,6] ⁶⁻	[Mo ₃ O ₆ (tart) ₄]		tart-(Mo-tart) ₃
G3	[3,4tart,8] ⁶⁻	[Mo ₃ O ₆ (tart) ₂ (Htart) ₂]		Htart-(Mo-tart) ₂ -Mo-Htart
G4	[4,5tart,8] ¹⁰⁻	[Mo ₄ O ₈ (tart) ₅]		tart-(Mo-tart) ₄
G5	[4,5tart,9] ⁹⁻	[Mo ₄ O ₈ (Htart)(tart) ₄]		Htart-(Mo-tart) ₄
G6	[4,3tart,8] ⁶⁻	[Mo ₄ O ₈ (tart) ₃ (H ₂ O) ₂ (OH) ₂]		(Mo-tart) ₃ -Mo

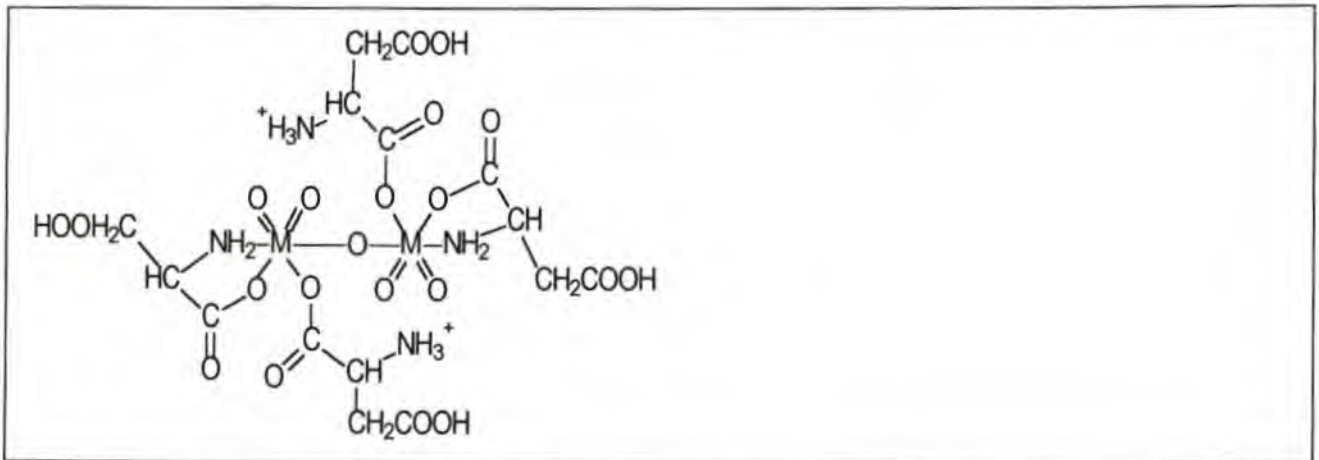


Fig. 4.12 Proposed structure for the [2,4,r] aspartate complex.

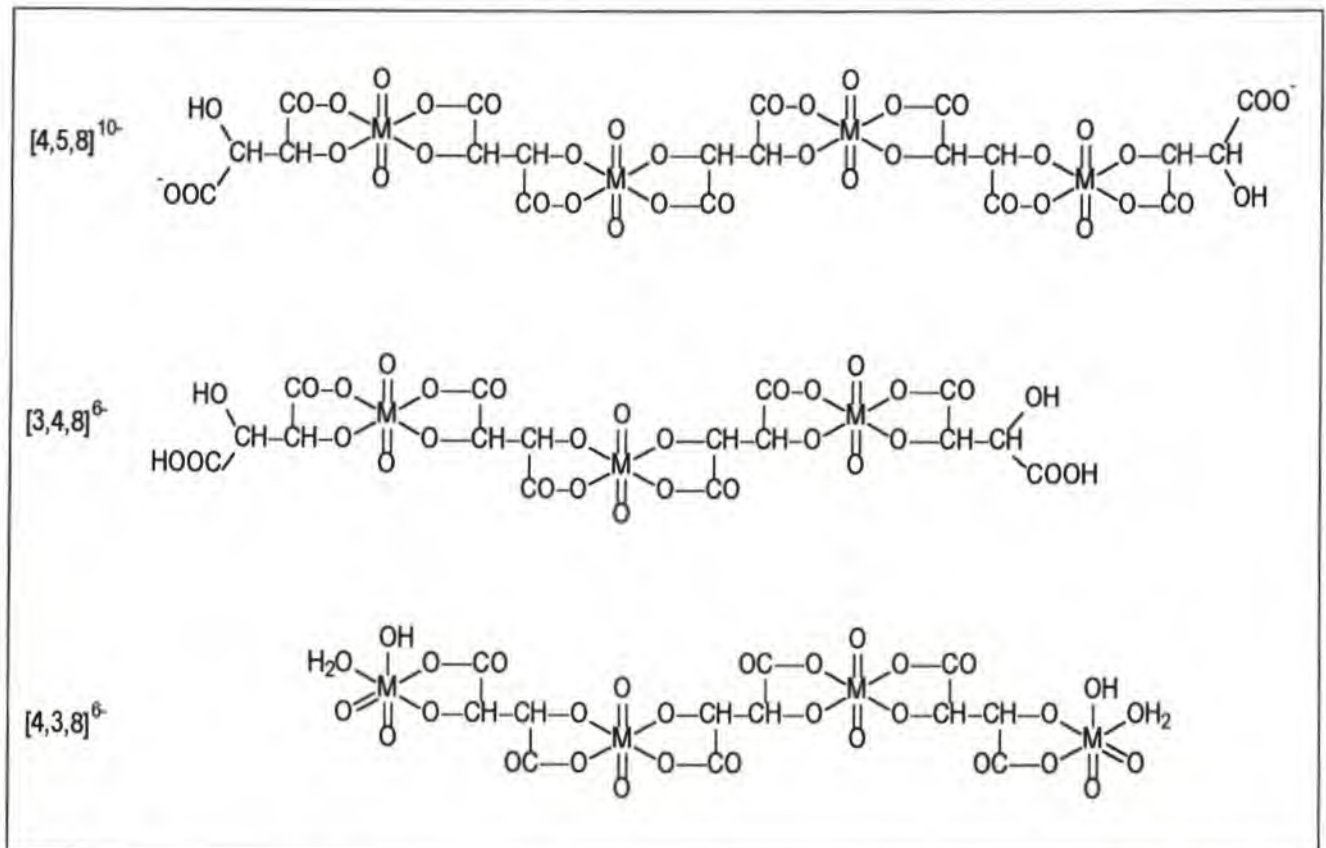


Fig. 4.13 Proposed structures for some polymeric [3,4,r], [4,3,r] and [4,5,r] tartrate complexes.

4.3 STRUCTURE AND THERMODYNAMIC VALUES

Quite a number of structural types have been proposed (Section 4.2) with due consideration to the thermodynamic evidence (Section 4.1). Some complexes have expected structures (*cf.* 4.1) while others, often minor complexes, have structures with features which have not been proposed before. In the following section it is shown that the usual and unusual structures proposed and the thermodynamic values pertaining to their formation, protonation and dimerization are consistent. Arguments based on thermodynamic quantities are used in proposing some complexes, and sometimes the structures are used to "rationalize" the thermodynamic values. Based on the trends observed and the proposed structures, some thermodynamic values, which could not be calculated, are also proposed. These values are included in the list of thermodynamic values shown in Appendix 4.

4.3.1 [1,2,*r*] complexes

Most of the [1Mo,2,*r*] complexes have the same basic structure (Fig. 4.6) in which two ligands are didentately bound to a MO₂-core and which explains the very similar values for ΔH° of about -80 kJ mol⁻¹ (Fig. 4.2.1). The ΔG° value for the formation of [1,2ox,4] is much greater than those of the [1,2,*r*] complexes of the unprotonated α -hydroxycarboxylates, [1,2lac,2], [1,2man,2], [1,2mal,2] and [1,2tart,2]. Although the basic structure of the [1,2ox,4] complex is the same, the mechanism for its formation must be different to the mechanism for the formation of the [1,2,*r*] α -hydroxycarboxylate complexes: The hydroxy proton of the α -hydroxycarboxylate ligands must be removed at some stage, at a high energy cost (pK~11.5), whereas the two bonding oxygens of oxalate are already deprotonated. (Two water molecules are formed during the formation of the α -hydroxycarboxylate complexes as well as the oxalate complex). The ΔH° for the [1Mo,2ox,4], which could not be determined from the experimental data, is therefore proposed to be more favourable for the formation of the oxalate complex than for the other [1,2,*r*]. It is proposed that the ΔH° values for the formation of [1Mo,2ox,4] is ~ 20 % greater than for [1Mo,2lac,2], (the structure of which is the closest to [1Mo,2ox,4]), based on the 20% difference in the ΔH° values for the formation of the respective [1Mo,1ox,2] and [1Mo,1mal,2] complexes (4.3.2.1) which are also formed *via* different mechanisms (Appendix 4). Similarly it is proposed that the ΔH° values for the formation of [1W,2ox,4] is probably ~ 18 % greater than for the [1W,2lac,2], based on the 18% difference in the ΔH° values for the formation of the respective [1W,1ox,2] and [1W,1mal,2] complexes. A very tentative experimental value could be obtained for [1W,2ox,4] (-88 kJ mol⁻¹), which indicates that the value derived by comparing other values is of the right order of magnitude (-94 kJ mol⁻¹). It is believed that the value derived for [1Mo,2ox,4] is also fairly accurate (-86 kJ mol⁻¹).

No [1,2nta,*r*] complexes were identified. The fact that some [1,2asp,*r*] were identified (even if their stability is particularly low due to the weaker nitrogen donor) shows that the absence of [1,2nta,*r*] is not due to the presence of a nitrogen donor instead of an oxygen donor of the hydroxy acids or oxalate, but simply due to steric hindrances caused by two large nta-ligands which have to bind didentate to one MO₂-core. A nta-

ligand was proposed to bind didentate to the larger dimeric core of the [2,1nta,3] complex, but in this case the size of the nta causes no hindrance (Fig. 4.9.2).

The structures of the [1,2mal,*r*] and [1,2tart,*r*] are very similar (the only difference being an OH group on the tartrate instead of an H-group on the malate). This is consistent with their very similar thermodynamic values (Fig. 4.2.1).

The difference in the ΔG° values for the formation of the [1,2cit,*r*] and the [1,2mal,*r*] complexes of the same charge is about 54 kJ mol^{-1} (Fig. 4.2.1). The main reason for the greater stability of these citrate complexes is the more favourable entropy factor ($\sim 45 \text{ kJ mol}^{-1}$). The change in enthalpy for the three citrate complexes is, however, also generally slightly greater than for the three malate complexes (by $\sim 9 \text{ kJ mol}^{-1}$). This consistency in the values gives more credence to the "approximate" (guessed) values for the change in enthalpy for the formation of [1Mo,2cit,5] and [1Mo,2cit,4] which were used in the calculations (*cf.* 3.5.1.4).

The protonation of [1,2mal,2] and of [1,2mal,3] are both, almost equally, entropy driven (Fig. 4.4.2). This is also the case for the protonation of [1,2cit,4] and [1,2cit,5] and of [1,2tart,2] and [1,2tart,3]. It clearly shows that the successive protonations of the complexes are simply due to the protonation of unbound acetate groups of each of the two ligands bound to the metal centre (Fig. 4.6).

The ΔG° values for the formation of [1Mo,2man,2] and [1Mo,2lac,2] are very similar, but the ΔH° value is slightly greater (and the $T\Delta S^\circ$ value slightly smaller) for the mandelate complex than for the lactate complex. This suggests that the phenyl group of the mandelate (as opposed to the methyl group of the lactate) might contribute to the bonding to the metal in a small way (Fig. 4.2.1).

The structures [1,2lac,2], [1,2man,2] and [1,2asp,2] have no obvious place for *deprotonation*. Structures have, therefore, been proposed for their deprotonated counterparts, [1,2lac,1], [1,2man,1] and [1,2asp,1], in which one ligand binds didentate and the other binds monodentate to a MO_3 -core (Fig. 4.6). Due to one fewer five-membered ring, it can be expected that the ΔH° values for such structures would be much smaller than for the other [1,2,2] complexes and it would explain the particularly small ΔG° values for [1,2lac,1], [1,2man,1] and [1,2asp,1] (Fig. 4.2.1). (ΔH° values for these complexes are proposed in Section 4.3.6.)

Similarly the structures [1,2lac,2] and [1,2man,2] have no obvious place for *protonation* unlike, for instance, [1,2mal,3], [1,2cit,4] and [1,2tart,2] which have free carboxylates. Whereas the ΔG° values for the latter complexes increase significantly upon protonation (Fig. 4.2.1), the ΔG° values for [1,2lac,3] and [1,2man,3] are very similar to the values for [1,2lac,2] and [1,2man,2]. Structures have, therefore, been proposed for the complexes [1,2lac,3] and [1,2man,3] in which one ligand binds didentate and the other binds monodentate to a $\text{MO}_2(\text{OH}_2)$ -core (Fig. 4.6). The ΔH° values for these structures are probably small and similar to the values of the [1,2lac,1] and [1,2man,1] species. (ΔH° values for these complexes are proposed in Section 4.3.6.)

The malate and aspartate ligands differ only in the one nitrogen donor of the aspartate instead of an oxygen donor in the malate. The ΔH° values for the $[1,2\text{mal},r]$ complexes is almost double the value of the $[1,2\text{asp},r]$. This shows that the amino bond to the metal is very weak compared to the oxygen-metal bond.

The differences in the ΔG° values of the $[1\text{Mo},2,r]$ and $[1\text{W},2,r]$ complexes of the hydroxycarboxylates are very similar, the average difference being 9 kJ mol^{-1} (Fig. 4.3). This is consistent with the similar structures proposed for tungstate- and molybdate complexes of the same stoichiometry. For the lactate, mandelate, malate and citrate complexes the main reason for the greater stability of the tungstate complexes is the more favourable change in enthalpy, but for the tartrate complexes, the enthalpy and entropy terms are almost equally in favour of the tungstate complex.

4.3.2 $[1,1,r]$ and $[2,2,r]$ complexes

4.3.2.1 Didentate chelation to one metal alone.

In a number of $[1,1,r]$ and $[2,2,r]$ complexes the ligands are proposed to bind didentate to one metal alone, forming a stable five-membered chelate ring per metal (*cf.* oxalate and α -hydroxy-carboxylate complexes of structure type A in Fig. 4.7 and Fig. 4.8.1). The ΔH° values (which could be calculated) of these molybdate complexes fall in a relatively narrow range, between $50\text{-}60 \text{ kJ mol}^{-1}$ per metal (Fig. 4.2.2 and 3).

The ΔH° values for the $[1\text{Mo},1\text{mal},r]$ and $[1\text{Mo},1\text{cit},1]$ complexes are particularly close ($\sim 50 \text{ kJ mol}^{-1}$). It is, therefore, proposed that the ΔH° values for the structurally related $[1\text{Mo},1\text{lac},2]$, $[1\text{Mo},1\text{lac},3]$ and $[1\text{Mo},1\text{man},2]$, which could not be determined experimentally, are also -50 kJ mol^{-1} (Appendix 4), and the $T\Delta S^\circ$ values are 17, 22, -11 and 16 kJ mol^{-1} , respectively. It can be seen from Fig. 4.3 that the greater stability of the related $[1,1,r]$ tungstate complexes is mainly due to a greater ΔH° value (by $\sim 12 \text{ kJ mol}^{-1}$). It is, therefore, proposed that the ΔH° values for the $[1\text{W},1\text{lac},2]$, $[1\text{W},1\text{lac},3]$, $[1\text{W},1\text{man},2]$ and $[1\text{W},1\text{man},3]$ are -62 kJ mol^{-1} ($-50\text{-}12$), and the $T\Delta S^\circ$ values are -11, 16, 17 and 26 kJ mol^{-1} , respectively (Appendix 4).

Although it can be pictured that the $[1\text{Mo},1\text{man},2]$ can be deprotonated at the OH, to form $\text{MoO}_3(\text{man})\text{H}_2\text{O}$, the relatively great ΔG° value associated with the protonation of $[1,1\text{man},1]$ (-27 kJ mol^{-1}) suggests that a structural change takes place upon protonation of $[1,1\text{man},1]$. It is, therefore, proposed that the mandelate is only monodentately bound to the Mo-centre. (Possibly the Ph-group also contributes slightly to the coordination of mandelate.) Such a $[1,1\text{man},1]$ complex is inevitably much less stable than the didentately bound $[1,1\text{man},2]$ complex, which explains the extremely low percentage concentration of $[1,1\text{man},1]$ (Fig. 3.3.2) and the absence of the related $[1,1\text{lac},1]$ complex. It can also be seen as an intermediate for the formation of the $[1,1\text{man},2]$ complex as well as the $[1,2\text{man},1]$, which appears at the same pH and in which one of the mandelates also only binds monodentately (Fig. 4.14). The $[1,2\text{man},1]$ can, in turn, be seen as an intermediate for the formation of the major complex $[1,2\text{man},2]$.

The ΔH° values for the [2Mo,2mal,r] and [2Mo,2ox,r] complexes are also particularly close, about -117 kJ mol^{-1} (Fig. 4.2.3). It is, therefore, proposed that the ΔH° values for the structurally related [2Mo,2lac,3], [2Mo,2lac,4], [2Mo,2man,4] and [2Mo,2man,5] are also -115 kJ mol^{-1} , and the $T\Delta S^\circ$ values are 9, 28, 33 and 38 kJ mol^{-1} , respectively (Appendix 4). It can be seen from Fig. 4.3 that the greater stability of the [2W,2ox,r], compared to the [2Mo,2ox,r], is mainly due to the greater ΔH° value (by -10 kJ mol^{-1} per metal). Similarly, the greater stability of the [2W,2mal,4], compared to the [2Mo,2mal,4], is mainly due to a greater ΔH° value (by -14 kJ mol^{-1} per metal) for the tungstate complex. These differences are of the same order as the typical difference between the [1,1,r] molybdate and tungstate complexes mentioned above (12 kJ mol^{-1}).

Despite the fact that the ΔH° values for the [1W,1ox,r] and [2W,2ox,r] are greater than those of the corresponding [1Mo,1ox,r] and [2Mo,2ox,r] complexes, the overall stability of these tungstate and molybdate complexes are very similar (Fig. 4.3). This is due to the fact that these molybdate complexes are favoured significantly by entropy compared to their tungstate analogues. (In the case of the α -hydroxycarboxylate complexes, the tungstate complexes are usually also favoured by entropy or the entropy factor is insignificant).

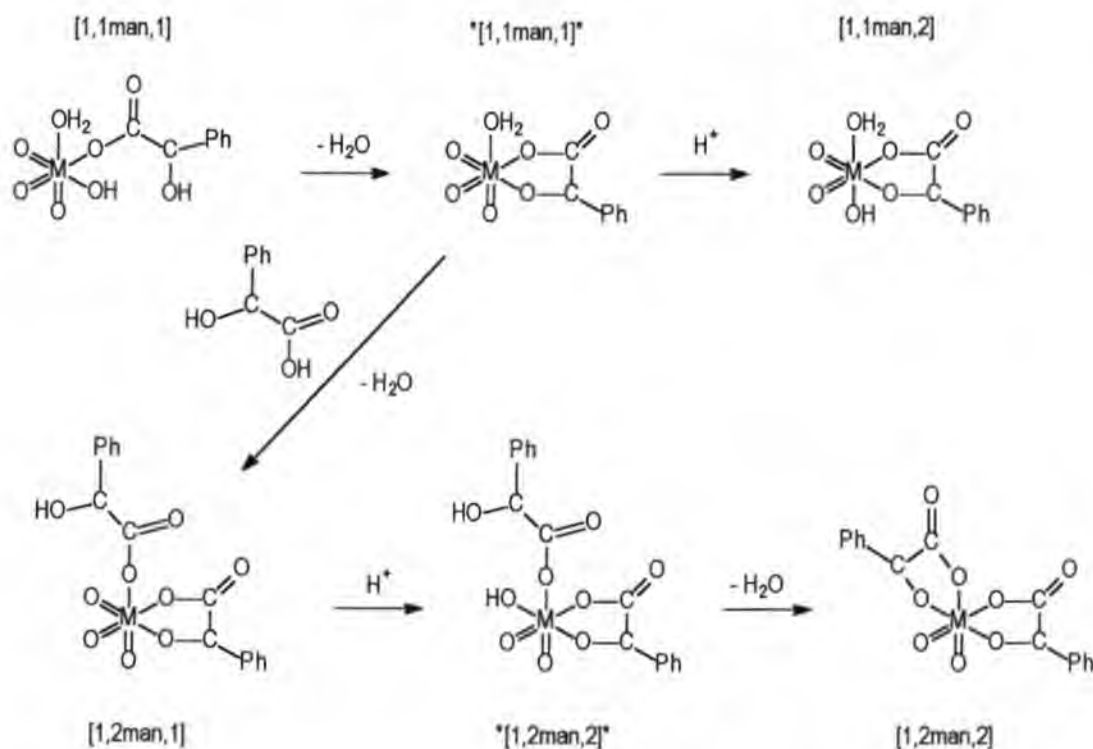


Fig. 4.14 Possible relationship between [1,1man,1], [1,1man,2], [1,2man,1] and [1,2man,2].

The overall stability and structures of the [1Mo,1ox,2] and [1Mo,1mal,2] complexes are very similar. The mechanisms for their formation must, however, be different since the oxalate (with two nucleophilic oxygens available) can be seen as simply entering the coordination sphere of molybdenum, whereas the hydroxy-oxygen of malate must be deprotonated at some stage in order to act as a donor. This difference in

mechanism is reflected in the significant difference in the change in enthalpy and entropy for their formation. The ΔH° value for the formation of the malate complex is less favourable (by 10 kJ mol^{-1}), due to the high cost of deprotonating the hydroxy-oxygen ($\text{pK} \sim 11.5$) (which is only partly recovered by the formation and bonding of a water molecule). The value for the entropy change, however, is more favourable than for the oxalate complex (by 7 kJ mol^{-1}), because of the structure being less restricted due to the non-coordinating substituents of malate. Similarly, the ΔH° value for the formation of the [1W,1mal,2] is also 10 kJ mol^{-1} less favourable than for the [1W,1ox,2].

The ΔH° and $T\Delta S^\circ$ values for the dimerization of both [1W,1mal,2] and [1Mo,1mal,2] could be calculated. As can be seen from Fig. 4.5, the change in enthalpy is 6 kJ mol^{-1} more favourable for the dimerization of the [1W,1mal,2] than of [1Mo,1mal,2] and the change in the entropy term is 2 kJ mol^{-1} less favourable. Since both dimerizations are simply due to elimination of a water molecule, this difference can be ascribed mainly to the difference in the W-OH and Mo-OH bonds of the monomers and the newly established W-O-W or Mo-O-Mo bonds of the respective dimers. It could indicate that the W-OH bond is weaker than the Mo-OH bond, or that the W-O-W is stronger than the Mo-O-Mo bond, or both.

It can be assumed that the simple dimerization of [1Mo,1lac,2] and [1Mo,1man,2] by the elimination of water would also be solely enthalpy driven like the dimerization of [1Mo,1mal,2] (dimerization of [1Mo,1mal,2] : $\Delta H^\circ = -16 \text{ kJ mol}^{-1}$ and $T\Delta S^\circ = -7 \text{ kJ mol}^{-1}$). It is interesting that the proposed values (Appendix 4) for the formation of the monomers, [1Mo,1lac,2], [1Mo,1man,2], and the dimers, [2Mo,2lac,4] and [2Mo,2man,4], indeed produce very similar values for the dimerization of the monomers. The proposed ΔH° and $T\Delta S^\circ$ values for the dimerization of [1Mo,1lac,2] are: $\Delta H^\circ = -16 \text{ kJ mol}^{-1}$ and $T\Delta S^\circ = -6 \text{ kJ mol}^{-1}$ and for [1Mo,1man,2] : $\Delta H^\circ = -15 \text{ kJ mol}^{-1}$ and $T\Delta S^\circ = 1 \text{ kJ mol}^{-1}$.

The monomers, [1Mo,1ox,3] and [1Mo,1lac,2], are proposed to have the same structure, and their dimerized forms, [2Mo,2ox,6] and [2Mo,2lac,4], too (Fig. 4.7 and 4.8.1). The dimerization of [1Mo,1ox,3], however, is mainly entropy driven, although it is also favoured slightly by enthalpy. The Mo-OH bond in the oxalate monomer is probably stronger than in the lactate monomer because of the difference between the ligands, and is therefore broken at higher energy cost.

The thermodynamic values for the dimerization of [1Mo,1ox,3] and [1W,1ox,3] are very similar (Fig. 4.5). This is consistent with the similar structures proposed for both the monomers and the dimers.

The [1Mo,1cit,3] and [1Mo,1cit,4] complexes are believed to be tridentately bound since the ΔH° values for their formation are much more favourable (by $\sim 18 \text{ kJ mol}^{-1}$) than for the [1Mo,1cit,1] and [1Mo,1cit,2] which are believed to be didentately bound. The [1W,1cit,3] and [1W,1cit,4] complexes, however, are proposed to be didentately bound since the ΔH° values for the formation of the [1W,1cit,3] and [1W,1cit,4] complexes are *only* $\sim 9 \text{ kJ mol}^{-1}$ more favourable than for [1W,1cit,1] and [1W,1cit,2]. (It is possible that the non-chelating carboxylic acid groups are involved in hydrogen bonding within the monomer, so that the distinction between di- and tri-dentate chelation becomes difficult.) The ΔG° values for formation of [1W,1cit,3] and [1W,1cit,4] are, nevertheless, greater than for the molybdate analogues by a similar amount

than of the other [1,1,*r*] complexes mentioned above (Fig. 4.3). The main reason for the greater stability is the more favourable entropy term for the formation of the tungstate complex, the enthalpy factor being favourable but relatively small. This can be regarded as an illustration of the drive to minimize the *free energy* of a molecule, not necessarily to minimize the enthalpy or to optimize the entropy. It is, for example, conceivable that under slightly different conditions (medium, temperature) it would be possible that the energy distribution of the [1W,1cit,3] complex would be in favour of tridentate bonding as in the case of the [1Mo,1cit,3] complex. In such a case the values for ΔH° and $T\Delta S^\circ$ might possibly be -81 (69+12) and 43 kJ mol⁻¹, respectively. The only reason for the greater stability of the [1W,1cit,3] complex, compared to the [1Mo,1cit,3] complex, would then be the greater change in enthalpy, as in the case of the other pairs of complexes of the same structure (Fig. 4.3).

4.3.2.2 Tridentate chelation to one metal alone.

Previous structure determinations showed that the ligands are tridentately bound in the complexes [2,2cit,4], [1Mo,1nta,3] and [2,2nta,8] in crystals [84-85, 88-90]. The distinctly greater values for the ΔH° for the [1Mo,1cit,3], [1Mo,1cit,4], [1Mo,1nta,*r*], [2Mo,2cit,*r*] and [2Mo,2nta,*r*] than for the rest of the [1,1,*r*] and [2,2,*r*] indicate that these complexes in solution are also tridentately bound (Fig.4.2.2 and 3). It is interesting that the ΔH° values for the formation of these nta complexes are rather similar to the citrate complexes, since the citrate uses three oxygen donors whereas nta uses two oxygen donors and one weaker nitrogen donor. This can be ascribed to the greater stabilizing effect of the two five-membered rings of the nta-complex, compared to one five- and one six-membered ring stabilizing the citrate complexes. The greater overall stability of the [2,2nta,*r*] complexes, compared to the [2,2cit,*r*] complexes, is mainly due to a greater $T\Delta S^\circ$ for their formation (clearly indicated in Fig. 4.2.3).

The greater stability of the [2W,2cit,4] complex, compared to [2Mo,2cit,4], is due to a more favourable enthalpy change (by 12 kJ mol⁻¹ per metal) for the formation of the tungstate complex, which has already been shown to be typical for similar structures (Fig. 4.3). The difference in the overall stability of the [2W,2cit,5] and [2Mo,2cit,5] complexes is almost the same as between [2W,2cit,4] and [2Mo,2cit,4], but the ΔH° of the tungstate complex exceeds that of the molybdate complex by 24 kJ mol⁻¹ per metal, whereas the $T\Delta S^\circ$ is distinctly in favour of the molybdate complex. The [2W,2cit,5] clearly has more bonds. A structure was proposed (Fig. 4.8.2) in which each citrate binds through three oxygens (as in [2Mo,2cit,5]), but in a way that two additional bridges are formed across the existing M-O-M bridge.

The difference in overall stability of [1W,1nta,2] and [2W,2nta,8] and their respective molybdate analogues is minimal (~2 kJ mol⁻¹ per metal) compared to the typical difference between similar molybdate- and tungstate complexes of hydroxycarboxylates (Fig. 4.3). The difference in the ΔH° values of the [1,1nta,2] complexes of molybdate and tungstate is slightly in favour (by 3.7 kJ mol⁻¹) of the molybdate complex. The only reason for the greater stability of the tungstate complex is the slightly more favourable entropy change (by 4.3 kJ mol⁻¹). The difference in ΔH° values could not be calculated for the [2,2nta,8] complexes of molybdate and tungstate. Since the [2,2nta,8] almost certainly is a simple dimer of [1,1,2] (Fig. 4.7 + 4.8.2), it is proposed that the difference in ΔH° and $T\Delta S^\circ$ for the formation of the [2W,2nta,8] and [2Mo,2nta,8] is

also 3.7 and 4.3 kJ mol⁻¹ per metal in favour of the molybdate and tungstate complexes, respectively. The ΔH° and $T\Delta S^\circ$ values for the formation of the [2W,2nta,8] are, therefore, proposed to be -126 and 149 kJ mol⁻¹, respectively (Appendix 4).

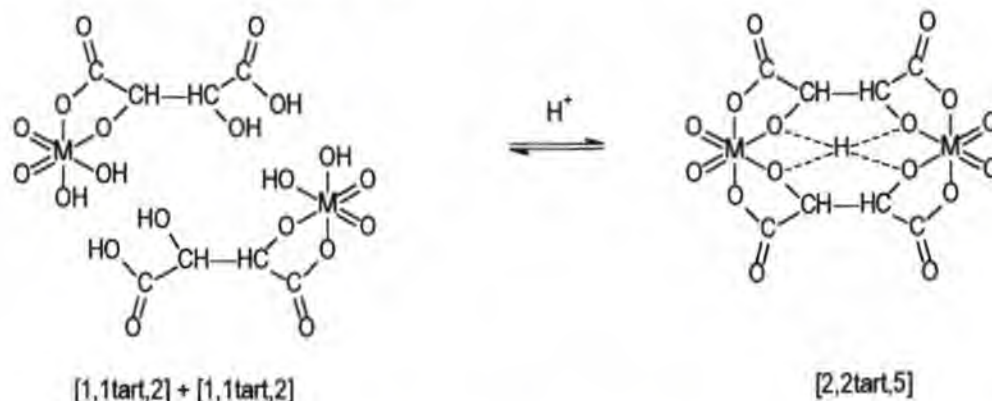
The overall stability of the [1,1asp,1] complex is extremely low (Fig. 4.2.2), because of a particularly small value for the ΔH° (-27 kJ mol⁻¹) despite the tridentate bonding of the aspartate *via* two oxygen and one nitrogen donors (Fig. 4.7). The enthalpy for the formation of the tridentate [1,1nta,*r*] complexes is more than double the value for the [1,1asp,1]. The main difference between the chelation of nta and aspartate must be the presence of two stable five-membered rings in the nta complex, compared to the one five- and one less stable, six-membered ring in the aspartate complex, although the extra carboxylate group of the nta could also affect the donor capabilities of the nitrogen.

Although the ΔG° for the formation of [1,1asp,2] is significantly greater than for the [1,1asp,1] complex, the ΔH° is even smaller than for the formation of [1,1asp,1] (Fig. 4.2.2). The entropy change for the protonation of [1,1asp,1] is unusually great (Fig. 4.4.1). It is therefore proposed that the protonation does not take place at the oxo ligand of [1,1asp,1], but that protonation takes place at the chelated β -carboxylate oxygen, whereupon the β -carboxylate leaves the coordination sphere in favour of a water molecule. The aspartate is thus proposed to bind only didentate (as mentioned in section 4.3.1), which explains the extremely small enthalpy, as well as the much smaller percentage concentration compared to the [1,1asp,1] complex (Fig. 3.7.2).

It is noteworthy that the tridentate [1Mo,1asp,1]²⁻ complex is even weaker than the very weak [1,1,2]²⁻ molybdate-succinic acid complex ($\log \beta \sim 11.5$) previously determined [139]. In the latter complex it is assumed that the two carboxylic oxygens (which are separated by -CH₂-CH₂-) bind didentate forming a seven-membered chelate ring only. The change in entropy for the formation of the [1Mo,1suc,2] complex might be greater than for the [1Mo,1asp,2], but this comparison still shows that the extra bonding *via* the nitrogen does not stabilize the complex very much. In the light of the already low stability of [1,1asp,1] it is not surprising that no [2,2asp,*r*] complexes were identified.

Although ΔG° for the [2Mo,2tart,5] complex is not particularly great, the value for ΔH° per metal is slightly greater than for the tridentate [2,2,*r*] complexes and is similar to the values typical for the [1,2,*r*] complexes (Fig. 4.2.3). Although the possibility of tridentate chelation is not excluded, a structure was proposed which is related to [1,2,*r*] complexes (Fig. 4.8.1) in the sense that each Mo-centre is chelated by two ligands *via* two stable five-membered rings. Unlike the [1,2,*r*] complexes, the two ligands form a bridge between two, otherwise, separate Mo-centres. The [1,1,*r*] complexes have been identified in all the systems studied, except in the tartrate systems. The absence of [1,1tart,*r*] complexes can, however, be rationalized in terms of the presence and structures of [1,2tart,*r*] and [2,2tart,5]. Firstly, the presence of [1,2tart,*r*] complexes shows that there is a great tendency for two tartrates to bind to one Mo-centre. Secondly, should a [1,1tart,*r*] complex be formed by didentate chelation of one Mo-centre, there is no reason for the remaining uncomplexed, chemically equivalent α -hydroxycarboxylate group not to bind didentate to another Mo-

centre. These two factors considered, it seems obvious that any [1,1tart,r] complex formed would immediately be dimerized to a [2,2tart,5] complex.



The [1Mo,1cit,3] and [1Mo,1nta,4] complexes are both tridentately bonded by the ligands. Simple dimerization by elimination of water leads to the proposed [2Mo,2cit,6] and [2Mo,2nta,8] complexes. Both these dimerizations are solely entropy driven (Fig. 4.5) unlike the enthalpy driven dimerization of the didentate monomer [1,1mal,2] (Section 4.3.2.1). It seems therefore, that the bond energy has been minimized to such an extent (through one five and one six-membered ring) in the tridentate monomers [1Mo,1cit,3] and [1Mo,1nta,4] that the M-O-M bond formed through dimerization does not lower the bond energy further. In contrast, the bond energy of the [1,1mal,2] (which is stabilized by only one five-membered ring) can be lowered significantly by the formation of an M-O-M bond. (The additional six-membered ring on the tridentate monomers stabilizes the structure more than the additional M=O on the didentate monomer.)

(Further discussion on the dimerization of [1,1mal,2] and [1,1cit,3] in section 4.3.2.4)

4.3.2.3 Monodentate chelation to two different metal centres.

The values for ΔG° for the formation of the complexes [2W,2lac,3] and [2W,2mal,3] are almost identical and relatively small compared to the other [2W,2,r] complexes (Fig. 4.1.3). The ΔG° value for the formation of [2W,2mal,2] is even smaller, but its ΔH° value (-119 kJ mol^{-1}) is similar to that of its protonated form [2W,2mal,3] (-114 kJ mol^{-1}). The lower stability (mainly as a result of a lower enthalpy) seems only plausible if the structures of these complexes are different to the other [2,2,r] complexes in which the ligands bind didentate or tridentate, but forming at least one stable five-membered ring. For this reason a different structure was proposed (structure B, Fig. 4.8.1) in which the two ligands bind monodentate to each metal centre of a dimeric M_2O_5 core. Although these structures are not stabilized by five-membered rings, the ligands stabilize the structure somewhat by forming two additional bridges across the dimeric core. The ΔG° values for the protonation of [2W,2mal,2] and [2W,2mal,3] are similar and particularly great (Fig. 4.4.2). The first protonation is entirely entropy driven, whereas the second protonation is mostly enthalpy driven. This is consistent with the different structures proposed for [2W,2mal,3] and [2W,2mal,4] (structure B and A structures, respectively, Fig. 4.8.1). The protonation of the [2W,2mal,2] is due to the protonation of the free β -carboxylate, which is typically entropy driven, resulting in a complex [2W,2mal,3] with basically the same structure as [2W,2mal,2]. The protonation of [2W,2mal,3], however, results in an enthalpy driven rearrangement of groups, resulting in a structure with two stable five-membered rings (B \rightarrow A, Fig.4.8.1).

The stability of the [2Mo,2lac,2] complex is also particularly low compared to the other [2Mo,2,r] complexes (Fig. 4.1.3). For this reason it is proposed that the structure of this molybdate complex is similar to the structure of [2W,2mal,2] (Fig. 4.8.1, B). Since the ΔG° for the protonation of [2Mo,2lac,3] is much smaller than for the protonation of [2W,2mal,3] (Fig. 4.4.2), it is proposed that the protonation of [2Mo,2lac,3] does not result in a major rearrangement of groups (as the protonation of [2W,2mal,3]). It is proposed that the structure of [2Mo,2lac,3] is similar to the [2Mo,2lac,4]. The rearrangement of groups thus takes place, already at the protonation of [2Mo,2lac,2] and is the reason for the particularly great ΔG° value for the protonation of [2Mo,2lac,2]. This rearrangement is probably enthalpy driven as is the rearrangement due to the protonation of [2W,2mal,3]. It is interesting that the *proposed* thermodynamic values for the formation of [2Mo,2lac,2] and [2Mo,2lac,3], indeed, result in enthalpy and entropy values for protonation of [2Mo,2lac,2] (-25 and +7 kJ mol⁻¹, respectively) very similar to the experimentally determined values for the protonation of [2W,2mal,3] (-28 and 7 kJ mol⁻¹, respectively).

A structure of [2W,2ox,4] could be pictured as being a result of the simple deprotonation of the water ligand on the [2W,2ox,5] complex (Fig. 4.8.1) to form a hydroxy ligand, similar to the proposed deprotonation of [2Mo,2mal,5] to form [2Mo,2mal,4] (Fig. 4.8.1). This would, however, not explain why the protonation of such a [2W,2ox,4] complex is mostly enthalpy driven, whereas the protonation of [2Mo,2mal,4] is mainly entropy driven (Fig. 4.4.2). The ΔG° and ΔH° values for the protonation of [2W,2ox,4] are almost as great as for the protonation of [2W,2mal,3], which has been proposed to cause a change in structure (previous paragraph). For this reason it is proposed that the structure of [2W,2ox,4] is similar to that of [2W,2mal,3] and that protonation of [2W,2ox,4] also leads to an enthalpy driven structural rearrangement similar to the protonation of [2W,2mal,3] (B \rightarrow A fig.4.8.1). The proposed ΔH° value for the formation of [2W,2ox,4] is thus -114 kJ mol⁻¹, the same as the value for the formation of [2W,2mal,3] (Appendix 4). This value compares relatively favourably with the two tentatively calculated values which were calculated based on two different models A and B (Table 3.1.4).

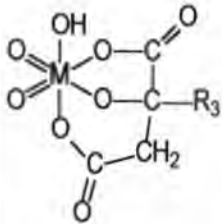
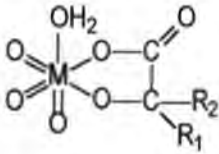
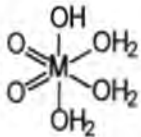
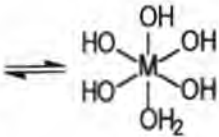
It can be assumed that the ΔH° value for the formation of [2W,2lac,3] is also -114 kJ mol⁻¹ and that the value for $T\Delta S^\circ$ therefore is 38 kJ mol⁻¹ (Appendix 4). Based on the typical difference of ~12 kJ mol⁻¹ per metal between the ΔH° values of tungstate and molybdate complexes of the same structure, the ΔH° value for the formation of [2Mo,2lac,2] is proposed to be -90 kJ mol⁻¹ and the $T\Delta S^\circ$ value, therefore, 2 kJ mol⁻¹ (Appendix 4).

The structures of [1W,1ox,2] and [1W,1ox,3] have been proposed to be very similar (Fig. 4.7., A). The dimerization of [1W,1ox,2] is, however, solely entropy driven, the enthalpy change being very unfavourable, whereas the dimerization of [1W,1ox,3] is mostly entropy driven, the enthalpy change being slightly favourable too. (Fig. 4.5). This is consistent with the proposed structure of [2W,2ox,6] which is stabilized by two five-membered rings, and the proposed structure of [2W,2ox,4] which contains no stable five-membered rings (Fig. 4.8.1, A, B). The loss of bonds and the gain in freedom upon dimerization of [1W,1ox,2] is reflected in the very favourable entropy change and unfavourable enthalpy change.

4.3.2.4 Dimerization of monomeric octahedral Mo

It has been mentioned (*cf.* 4.3.2.1 and 2) that the simple dimerization of the complex [1Mo,1mal,2] is solely enthalpy driven, the ΔH° and $T\Delta S^\circ$ values being -16 and -7 kJ mol^{-1} , respectively, but that the simple dimerization of the complex [1Mo,1cit,3] is solely entropy driven, the ΔH° and $T\Delta S^\circ$ values being $+4$ and $+9$ kJ mol^{-1} , respectively (as illustrated below). Both dimerizations are the result of the elimination of a water molecule and result in the formation of an Mo-O-Mo bond. The respective modes of chelation (didentate or tridentate) are believed to be retained in the products of dimerization, namely [2Mo,2mal,4] and [2Mo,2cit,6].

It has been mentioned (*cf.* 4.3.2.2) that the bond energy seemingly has been minimized to such an extent in the tridentate monomer [1Mo,1cit,3] (through one five and one six-membered ring) that the M-O-M bond formed through dimerization does not lower the bond energy further, but that, in contrast, the bond energy of the [1,1mal,2] (which is stabilized by only one five-membered ring) can be lowered significantly by the formation of an M-O-M bond. The dimerization of an octahedral molybdate species, such as the [1,0,3]⁺ species (with no stable five-membered ring) should therefore be favoured by enthalpy to an even greater extent than for the dimerization of the didentate [1,1mal,2]. If the enthalpy change for such a dimerization is proposed to be more favourable by the same amount as the difference between the values pertaining to the dimerization of [1Mo,1mal,2] and [1Mo,1cit,3], and if the entropy change is less favourable by the same amount as the difference between the values for the dimerization of [1Mo,1mal,2] and [1Mo,1cit,3], the following values are obtained: $\Delta H^\circ = -36$ kJ mol^{-1} and $T\Delta S^\circ = -23$ kJ mol^{-1} . It is interesting that these values are relatively close to the values determined by Cruywagen [140] for the dimerization of the [1,0,3]⁺ molybdate species in 3 M Na(H)ClO₄ medium: $\Delta H^\circ = -32$ and $T\Delta S^\circ = -19$ kJ mol^{-1} .

				
Monomer:	[1,1cit,3] ²⁻	[1,1mal,2] ²⁻	[1,0,3] ⁺	
$\Delta H^\circ_{\text{dimerization}}$	+4 kJ mol^{-1}	-16 kJ mol^{-1}	-36 kJ mol^{-1} (proposed value)	
$T\Delta S^\circ_{\text{dimerization}}$	+9 kJ mol^{-1}	-7 kJ mol^{-1}	-23 kJ mol^{-1} (proposed value)	

4.3.3 [2,1,r] complexes

When the Figures 4.1.1-5 are compared it is obvious that the ΔG° values per metal for the [2,1,r] complexes are generally smaller than for the other type of complexes. This is mainly due to the small ratio of ligand to metal in these complexes.

The complexes [2Mo,1mal,3], [2Mo,1cit,3] and [2Mo,1cit,4] have very similar ΔH° values (-82 kJ mol^{-1}) (Fig.4.2.4). The same structures are proposed for these complexes, as well as for the [2Mo,1lac,*r*] and [2Mo,1man,*r*] complexes (Type A complexes, Fig. 4.9.1.1). The ligand binds monodentate to each of the metal centres of a M_2O_6 core. The octahedral conformation is achieved by an additional water ligand on each of the metal centres. Although no stable five-membered ring is formed, the ligand stabilizes the dimeric metal core by forming a further bridge across the dimer. Since the difference in the ΔH° values of [2Mo,1mal,3] and [2W,1mal,3] as well as between [2Mo,1cit,4] and [2W,1cit,4] is the main reason for the greater stability of the respective tungstate complexes (Fig. 4.3) it was proposed that the tungstate complexes have similar structures.

It is proposed that the ΔH° values for the formation of the [2Mo,1lac,*r*] and [2Mo,1man,*r*] complexes (which could not be calculated experimentally) are also -82 kJ mol^{-1} (Appendix 4). The $T\Delta S^\circ$ values, calculated from these proposed ΔH° values, for the [2Mo,1lac,3], [2Mo,1lac,4] and [2Mo,1lac,5] complexes are very similar to the $T\Delta S^\circ$ values calculated for their mandelate analogues. This agreement indicates that the structures and the thermodynamic values are consistent.

The [2,1ox,5] complexes are proposed to have the same structure as the [2,1mal,3] complexes (Fig. 4.9.1.1, structure A). (The difference in the ΔG° values of [2W,1ox,5] and [2W,1mal,3] is almost the same as between [2Mo,1ox,5] and [2Mo,1mal,3], namely $\sim 31 \text{ kJ mol}^{-1}$.) The ΔG° values of the [2,1ox,5] complexes are much greater than those of similar complexes of α -hydroxycarboxylates, but it has been shown that the ΔG° values for oxalate complexes of [1,1,*r*], [1,2,*r*] and [2,2,*r*] are also greater than for similar complexes of α -hydroxycarboxylates. This is explained by the high energy cost of removing the proton from the hydroxy group of the α -hydroxycarboxylates in order to enable complexation *via* the oxygen (compared to the oxygen of oxalate which is readily available for complexation). In the case of the [2,1,*r*] complexes, this is reflected by the 10 kJ mol^{-1} difference between the ΔH° value for the formation of [2Mo,1mal,3] and the very tentative value for the formation of [2Mo,1ox,5], in favour of the latter.

Alternative structures (C, Fig. 4.9.1.2) have been shown for the structures which are mentioned above (A). Structures (A) are, however, preferred to structures (C), since a di- μ -oxo bridge probably stabilizes a structure (A) more than the M-O-M bridge of a structure (C). The structures (C) and (A) are very closely related, the former being the result of hydrolysis of structures (A). As is indicated in Fig. 4.9.1.2 the structures (C) are also closely related to [2,2,*r*] complexes with structure B of Fig. 4.8.1. These relationships between the structures (C) and (B) and therefore between structures (A) and (B), give more credence to all these proposed structures (A,B,C), which have not been proposed before.

The ΔH° values for the formation of [2Mo,1cit,5], [2Mo,1tart,4] and [2Mo,1tart,5] are similar and relatively large (Fig. 4.2.4). The ΔH° values (per metal) for the formation of the [2,1asp,*r*] complexes are also regarded as relatively large (compared to [1,1,*r*] and [1,2,*r*] aspartate complexes). The ligands are believed to be bonded *via* three donors in these complexes. The α -hydroxy-carboxylate or α -amino-carboxylate

groups bind didentate to one metal of the dimeric core and the β -carboxylate group binds monodentate to the other metal of the dimeric core (Fig. 4.9.2). Thus the ligand forms an additional bridge across the dimeric core but also introduces a stable five-membered ring into the structure. In the case of [2Mo,1cit,5] and [2Mo,1tart,4], it is likely that the free OH of tartrate and citrate stabilizes the structure further by hydrogen bonding with the M-O-M oxygen. The M-O-M bond is believed to be protonated in the [2Mo,1tart,5], so that this stabilization by hydrogen bonding is absent in [2Mo,1tart,5]. This could explain why the ΔH° values for the formation of [2Mo,1tart,5] is 4 kJ mol^{-1} less favourable than for the formation of [2Mo,1tart,4] (Fig. 4.9.3).

The ΔG° and ΔH° values for the formation of the [2W,1tart,4] complex, are both about 10 kJ mol^{-1} per metal greater than for the formation of its molybdate counterpart, [2Mo,1tart,4]. This has been proposed to be typical of similar molybdate and tungstate structures before. It is logical and consistent, therefore, to propose the same structure for [2Mo,1tart,4] and [2W,1tart,4]. Because the ΔH° value for the formation of the [2W,1tart,3] is very similar to [2W,1tart,4], the structures are also proposed to be similar. This is consistent with the entropy driven protonation of [2W,1tart,3] (Fig. 4.4.2), which is typical of simple protonations (without major structural changes).

The above-mentioned structures, [2,1mal,4] and [2,1cit,5], having more bonds than [2,1mal,3] and [2,1cit,4], are consistent with the enthalpy driven protonation of [2,1mal,3] and [2,1cit,4] (Fig. 4.4.2). The similar structures of [2,1cit,3] and [2,1cit,4] are consistent with the entropy driven protonation of the uncomplexed carboxylate of the former complex (Fig. 4.4.2).

The overall stability of the [2,1nta,4] and [2,1nta,5] complexes is so high, that it seems reasonable that the nta also binds in a similar fashion (Fig. 4.9.2). The ΔG° value for the [2W,1nta,3] complex, however, is 28 kJ mol^{-1} smaller than for the [2,1nta,4] complex. Such a difference has been shown to indicate different structures. For this reason it is proposed that the nta binds only didentate in the [2W,1nta,3] complex. This is the only nta complex in which nta is believed to bind didentate. This structure, and the lower stability of [2W,1nta,3] "explains" the absence of the related [2Mo,1nta,3] complex.

The structures for [2W,1tart,3], [2M,1tart,4] and [2Mo,1tart,5] have been discussed above. The following thermodynamic evidence suggests that the structures for [2Mo,1tart,3], [2W,1tart,2] and [2Mo,1tart,2] are neither like their protonated forms, nor like the proposed structures for [2Mo,1mal,3], [2Mo,1cit,3] and [2Mo,1cit,4] and, furthermore, that the structures of [2W,1tart,2] and [2W,1tart,3] differ from their respective molybdate analogues:

The ΔH° value for the formation of [2W,1tart,2] is about 20 kJ mol^{-1} per metal more favourable, and the $T\Delta S^\circ$ about 16 kJ mol^{-1} per metal less favourable than for [2Mo,1tart,2], which strongly suggests different structures for [2W,1tart,2] and [2Mo,1tart,2], with the tungstate complex having more bonds. For exactly the same reasons, the [2W,1tart,3] complex is also assumed to have more bonds than its molybdate counterpart, [2Mo,1tart,3]. Different structures for [2W,1tart,3] and [2Mo,1tart,3] are also consistent with the entropy driven protonation of the former and the enthalpy driven protonation of the

latter. Similarly, different structures for [2W,1tart,2] and [2Mo,1tart,2] are also consistent with the much greater enthalpy change associated with the protonation of the [2W,1tart,2] compared to the protonation of [2Mo,1tart,2], the change in entropy being almost the same. The ΔH° values for the formation of [2Mo,1tart,3] and [2W,1tart,2] are too great to indicate the same structures as for the type-A structures ([2Mo,1mal,3], [2Mo,1cit,3] and [2Mo,1cit,4]), but too small to indicate the same structures as for the [2,1tart,4] complexes.

This slightly unusual thermodynamic evidence has led to the suggestion of different structures than discussed before (Fig. 4.9.3): The two vicinal α -hydroxy carboxylate groups of tartrate are bonded in the same way, through didentate chelation, to different metal centres in the proposed structures for [2Mo,1tart,2], [2Mo,1tart,3] and [2W,1tart,3]. The structure for [2Mo,1tart,2] closely resembles the proposed structure for the [2Mo,2tart,5] complex as well as the polymeric [3,4tart,r], [4,3tart,r], [4,4tart,4] and [4,5tart,r] complexes. The [2W,1tart,2] has an extra W-O-W bond, which is the result of water elimination of a structure similar to [2Mo,1tart,2]. This is consistent with the greater number of bonds of the [2W,1tart,2] compared to [2Mo,1tart,2]. The protonation of [2Mo,1tart,2] is proposed to lead to the formation of an additional Mo-O-Mo bond by elimination of water, resulting in a structure which is similar to the proposed structure of [2W,1tart,2]. (This is consistent with the 14 kJ mol⁻¹ per metal more favourable ΔH° value for the formation of [2W,1tart,2] compared to [2Mo,1tart,3]. The much more favourable $T\Delta S^\circ$ value for the latter complex is due to the higher degree of protonation.)

4.3.4 [4,2,r] complexes

The same structures are proposed for the [4,2mal,8] and [4,2cit,10] complexes in solution as have been determined in solids [78-80, 82-83]. The only difference between the two structures is an additional uncoordinated β -carboxylic acid group of each citrate (Fig. A3, Appendix 3). The obvious site for deprotonation of [4,2cit,10] is this uncoordinated β -carboxylic acid group. This is consistent with the entropy driven (Fig. 4.4.1) protonation of [4,2cit,9], which is very typical for a simple protonation of an uncoordinated carboxylate group. Unlike the [4,2cit,10] complex, the [4,2mal,8] complex does not have uncoordinated β -carboxylic acid groups which can be deprotonated. It is thus understandable that no [4,2mal,7] complex was identified. The complexes [4,2mal,9] and [4,2mal,10] were, however, identified. The ΔG° value for the first protonation of [4,2mal,8] is relatively small (Fig. 4.4.2). The unfavourable enthalpy change and favourable, but relatively small, entropy change (compared to protonation of carboxylates) indicates that the protonation of [4,2mal,8] is accompanied by a loss of a Mo-malate bond which decreases the rigidity of the structure slightly. It is proposed that the β -carboxylate which binds *via* both carboxylate oxygens in the [4,2mal,8] complex, when protonated, binds only *via* one oxygen, and that a water ligand enters the coordination sphere to maintain octahedral conformation. The one ligand bridge across the Mo-O-Mo bond is thus broken upon protonation (Fig. 4.10). The remaining ligand bridge still ensures some rigidity about the Mo-O-Mo bond. A similar break of the remaining ligand bridge across the Mo-O-Mo bond is proposed to take place upon further protonation of [4,2mal,9]. This leaves the Mo-O-Mo bond, which connects two sizeable dimers, much more free to rotate and bend. This is consistent with the exceptionally favourable

change in entropy and unfavourable change in enthalpy for the protonation of [4,2mal,9] compared to the protonation of [4,2mal,8] (Fig. 4.4.1).

The [4,2mal,8] complex predominates at pH~3 and the protonated species [4,2mal,9] and [4,2mal,10] are important species at pH 2-1. It can be assumed that upon further acidification the remaining Mo-O-Mo bond would be vulnerable to protonation which would probably lead to the formation two dimeric complexes. The complex [2,1mal,4] was also identified as a minor complex at pH~3. The dimerization of [2,1mal,4] to form the [4,2mal,8] is favoured both by enthalpy and entropy (Fig. 4.5), which explains the large dimerization constant and the predominance of [4,2mal,8] above the [2,1mal,4] complex at pH~3.

The [4,2cit,10] complex is important only at pH~1 where the [2,1cit,5] complex dominates. The dimerization constant for [2,1cit,5] is much smaller than for the [2,1mal,4], mainly because the enthalpy change is unfavourable (the entropy change is very similar). The favourable ΔH° for the dimerization of [2,1mal,4] and the unfavourable ΔH° for the dimerization of [2,1cit,5] is consistent with the proposed hydrogen bonding which stabilizes the [2,1cit,5], and not the [2,1mal,4]. (Apart from this difference, the structures of [2,1mal,4] and [2,1cit,4] and of their dimerization products, [4,2mal,8] and [4,2cit,10], are very similar). The small dimerization constant explains the dominance of the [2,1cit,5] complex over the [4,2cit,10] complex. The very similar structures of [4,2cit,10] and [4,2mal,8] suggest that the citrate complex can probably also be protonated to [4,2cit,11] and [4,2cit,12] at pH < 1 (beyond the experimental range of this investigation).

The complexes [4W,2ox,8] and [4Mo,2ox,8] have been identified as possible minor species. The enthalpy and entropy factors could not be determined, but the ΔG° values are comparable to the other [4,2,r] complexes (Fig. 4.1.5). The difference in the ΔG° values of the tungstate and molybdate complex, 9 kJ mol⁻¹ per metal, compares well with the typical difference between similar complexes. Since each oxalate has only two donor oxygens, it is obvious that the structure of [4,2ox,8] cannot be the same as the related malate and citrate complexes. The oxalate binds monodentate to a metal centre of two separate dimeric molybdate cores (Mo₂O₈(H₂O)₂) in the proposed structure (Fig. 4.10). The two oxalates thus form two bridges between dimeric molybdenum resulting in a very symmetric structure. Since no stable five-membered rings are formed it is understandable that the stability of such an oxalate complex is smaller than that of the malate and citrate complexes. On the one hand it is expected that, because of the absence of stable five-membered rings, the ΔH° (and ΔG°) values for [4,2ox,8] would be smaller than for the [4,2mal,8], but on the other hand there is no need to deprotonate a hydroxy group at high energy cost as during the formation of the malate complex. It is proposed that the ΔH° value for the [4Mo,2ox,8] is at least -200 kJ mol⁻¹ and that the value for the [4W,2ox,8] could be about -30 kJ mol⁻¹ more favourable (Appendix 4).

4.3.5 [3,4,r], [4,3,r], [4,4,r], [4,5,r] and [2,4,8] complexes

The ΔG° values per metal for the [3,4,r], [4,3,r], [4,4,r], and [4,5,r] complexes are all relatively great compared to the values in general (Fig. 4.1.5). Even the values pertaining to the [4,4asp,r] complexes are large compared to most other amino complexes. The formation of the tartrate complexes, [3,4tart,r],

[4,3tart,r], [4,4tart,r] and [4,5tart,r], is solely or mainly enthalpy driven (Fig. 4.2.5), the ΔH° values averaging about -85 kJ mol^{-1} per molybdenum. The structures are all essentially polymeric chains of MO_2 -tartrate units (Fig. 4.11.1 and 4.13). This is a consequence of the unique nature of tartrate, which consists of two vicinal α -hydroxycarboxylate groups that tend to bind didentate to two separate metal-centres. The structures [1,2tart,2], [2,1tart,2] and [2,2tart,5] can also be regarded as related structures (Fig. 4.6, 4.8.1 and 4.9.3). The ring structures of [4,4tart,8] and [2,2tart,5] complexes are merely special polymeric chains, with no end and no beginning. In these structures each MO_2 -metal centre is bound by the maximum number of five-membered rings possible (two) and all the possible oxygen donors of each tartrate are used in bonding. It is thus not surprising that the formation of the highly ordered ring structure of [4,4tart,8] is almost solely enthalpy driven ($\Delta G^\circ \approx \Delta H^\circ$).

The [4,4tart,8] complex is protonated to form [4,4tart,9]. The ΔG° for this reaction, which is mainly entropy driven, is relatively small (Fig. 4.4.4). This result concurs with the absence of free β -carboxylates which would have been easily protonated. The [4,4tart,8] is very symmetrical with no single obvious site for protonation. It is believed, however, that a proton can be accepted by the molecule due to the presence of eight C=O groups in relatively close proximity. The proposed structure of [4,5tart,8], however, has two free β -carboxylates (Fig. 4.13). The ΔG° for the protonation of [4,5tart,8] is typical of protonation of two free β -carboxylates, although the calculated ΔH° value is unusually large (Fig. 4.4.4). It is possibly an indication that, if one end of the chain is neutralized by protonation, the chain is able to curl up due to hydrogen bonding. The unusually large ΔH° value might, however, simply be due to the enthalpy calculation based on an oversimplified model (*cf.* 3.5.1).

The ΔG° values for the tungstate complexes [3,4,r], [4,3,r], [4,4,r], and [4,5,r], are $\sim 8 \text{ kJ mol}^{-1}$ per metal greater than for their molybdate analogues (Fig. 4.3), which has been shown to be quite typical for complexation of molybdate and tungstate with α -hydroxycarboxylates.

Although citrate potentially has four oxygen donors, it typically binds *via* three donors only, probably simply due to steric hindrances. The malate and aspartate ligands bind tridentate at the most. The [4,4cit,r], [4,4mal,r] and [4,4asp,r] complexes, therefore, cannot have the same structure as [4,4tart,8]. The structures proposed are, however, also polymeric chains or rings (Fig. 4.11.2). The ligands typically bind didentate (*via* the α -hydroxycarboxylate or the α -amino-carboxylate) to one metal centre and monodentately (*via* the β -carboxylate) to another metal centre ([2,1,r] and [2,2,r] complexes). It has been shown that different chain or ring structures can be pictured which are consistent with the charge of the complex (Table 4.2.6, Fig. 4.11.2). Unfortunately too little thermodynamic evidence could be gathered that might have helped to discriminate between them. The protonation of the [4,4asp,9] complex is solely entropy driven ($T\Delta S^\circ = 12 \text{ kJ mol}^{-1}$), but this could indicate protonation of either an uncomplexed carboxylate or a hydroxy ligand. Fewer five-membered rings are formed than in the [4,4tart,8] which explains the significantly smaller ΔH° values (Fig. 4.2.5). Despite the smaller enthalpy values, the overall stability of the citrate and malate

complexes is greater than that of the tartrate complex, due solely to a substantially more favourable entropy change.

The oxalate ligand, with only two available oxygen donors, clearly precludes similar structures for the tentatively identified [4Mo,4ox,10] and [4W,4ox,10] complexes. A structure is therefore proposed which resembles the proposed structures for [4,2ox,8] and [2,1ox,5] (Fig. 4.10 and Fig. 4.9.1). It is of some consolation that these three types of complexes, in which the ligands always only bind monodentately to separate metal cores, are structurally related: This relationship lends more credence to the individual proposals, which, on their own, might seem far-fetched.

The very unusual [2Mo,4asp,8] complex was identified as a possible minor complex. The ΔH° value calculated is particularly small (Fig. 4.2.5), and the formation reaction is thus mainly entropy driven. The only structure which could be pictured (with the correct charge) is shown in Fig. 4.12. It is a dimeric form of the proposed [1,2asp,1] structure (Fig. 4.6). The two monodentately bonded aspartate ligands and the single Mo-O-Mo bridge connecting two large substructures are consistent with the great entropy and small enthalpy contribution to the overall stability. Once again the structural relationship between two unusual structures ([1,2asp,1] and [2,4asp,8]) gives more credence to the individual structures.

4.3.6 Protonations

The ΔG° for the protonation of complexes at an unbound β -carboxylate group typically varies between -16 and -40 kJ mol⁻¹. (Examples are: protonation of [1,2mal,2], [1,2mal,3], [1,2cit,4], [1,2cit,5], [1,2tart,2], [1,2tart,3], [1,1mal,1], [1,1cit,1], [1W,1cit,2], [1,1nta,2], [2,2mal,2], [2Mo,2cit,4], [2Mo,2cit,5] and [2,1cit,3]). The ΔG° values may be very similar or may be greater than the ΔG° values for the protonation of the ligand alone. The ΔH° values for these protonations are usually very small (< -5 kJ mol⁻¹), the main driving force being the change in entropy.

The ΔG° values for the protonation of complexes at a M=O, M-OH and M-O-M oxygens typically vary between -6 and -18 kJ mol⁻¹. The entropy factor is also the main driving force for this protonation. (Examples are: [1,1ox,2], [1,1lac,2], [1,1man,2], [1,1mal,2], [1,1cit,3], [1,1nta,3], [2,2ox,5], [2,2lac,3], [2,2mal,4], [2,2lac,2], [2,1lac,3], [2,1man,3], [2,1ox,5], [2,1lac,4], [2,1man,4], [2,1asp,4], [2,1nta,5], [2W,1tart,3], [2Mo,1tart,4]).

A few protonations are proposed to result in complexes with fewer bonds between the metal and the ligand investigated, for instance the protonation of [1,2man,2], [1,2lac,2], [1,1asp,1], [4,2mal,8] and [4,2mal,9]. The ΔG° values for the protonation of these complexes are usually small (about -5 kJ mol⁻¹), except for the protonation of [1,1asp,1] for which the value is -28 kJ mol⁻¹. The ΔH° and $T\Delta S^\circ$ values could only be calculated for the protonation of the latter three complexes. In each case the enthalpy is significantly unfavourable and the reaction solely entropy driven (Fig. 4.4.1-2). It is proposed that the ΔH° values for the formation of [1Mo,2lac,3] and [1Mo,2man,3] are about -60 kJ mol⁻¹ (distinctly smaller than for the

didentately bound [1Mo,2lac,2] and [1Mo,2man,2], respectively) and the ΔH° values for the formation of [1W,2lac,3] and [1W,2man,3], about -70 kJ mol^{-1} ($\sim 10 \text{ kJ mol}^{-1}$ more favourable than the respective molybdate complexes). The protonation of [1Mo,2lac,2] and [1Mo,2man,2] would then be entropy driven, with the respective $T\Delta S^\circ$ values, $+18 \text{ kJ mol}^{-1}$ and 20 kJ mol^{-1} . Similarly the protonation of [1W,2lac,2] and [1W,2man,2] would then be entropy driven, with $T\Delta S^\circ$ values, $+15 \text{ kJ mol}^{-1}$ and 19 kJ mol^{-1} , respectively (Appendix 4).

A few protonations are proposed to result in complexes with more bonds between the metal and the ligand investigated, for instance the protonation of [1Mo,2man,1], [1Mo,2lac,1], [1Mo,1man,1], [2Mo,2lac,2], [2W,1nta,3], [2W,2ox,4], [1Mo,2asp,1], [2Mo,1mal,3], [2W,2mal,3], [1Mo,1cit,2], [2W,2cit,4], [2Mo,1cit,4], [2Mo,1tart,2], [2W,1tart,2], [2Mo,1tart,3] and [4Mo,5tart,8]. The ΔG° values for the protonation of these complexes are usually relatively great, between -28 and -48 kJ mol^{-1} (Fig. 4.4.1-2). The ΔH° and $T\Delta S^\circ$ values could be calculated for the protonation of the latter nine complexes. The enthalpy is distinctly favourable for these protonations (ΔH° between -13 and -40 kJ mol^{-1}); some protonations are even solely enthalpy driven. In the previous paragraph ΔH° values have been proposed for the complexes [1Mo,2lac,3] and [1Mo,2man,3] (-60 kJ mol^{-1}). The complexes [1Mo,2lac,1] and [1Mo,2man,1] are proposed to have the same basic structures as [1Mo,2lac,3] and [1Mo,2man,3] (Fig. 4.6). For this reason it is proposed that the ΔH° values for the formation of [1Mo,2lac,1] and [1Mo,2man,1] are also about -60 kJ mol^{-1} (Appendix 4). The protonation of [1Mo,2lac,1] and [1Mo,2man,1] would then be favoured by enthalpy and entropy, with ΔH° values, -12 kJ mol^{-1} and -18 kJ mol^{-1} , respectively and $T\Delta S^\circ$ values, $+35 \text{ kJ mol}^{-1}$ and $+29 \text{ kJ mol}^{-1}$, respectively.

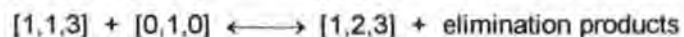
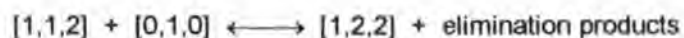
Mandelate is proposed to bind monodentate in the complex [1Mo,1man,1] (Fig. 4.7). A ΔH° value of -35 kJ mol^{-1} is proposed for the formation of [1Mo,1man,1] (Appendix 4). This value is significantly smaller than the proposed value for the [1Mo,1man,2] in which the mandelate is didentately bound (-50 kJ mol^{-1}). The protonation of [1Mo,1man,1] is thus proposed to be favoured by enthalpy and entropy, with ΔH° and $T\Delta S^\circ$ values, -15 kJ mol^{-1} and 12 kJ mol^{-1} , respectively.

4.3.7 Comparison of [1,2,2] and [1,1,2] complexes

Comparison of the distribution of [1,1,2] and [1,2,2] in the Mo-oxalate, Mo-lactate, Mo-mandelate, Mo-malate, Mo-citrate and Mo-aspartate systems, particularly at high pH where molybdate is first complexed upon acidification, reveals that

- the [1,1,2] predominates in the absence of [1,2,2] in the oxalate systems,
- that [1,2,2] predominates in the lactate and mandelate systems where the [1,1,2] is a minor species,
- that both [1,1,2] and [1,2,2] are important in the malate systems, and
- that only [1,1,2] exists in the citrate systems and not the [1,2,2] complex.

In order to establish a possible reason for the different ratios of $[1,1,r]$ to $[1,2,r]$ complexes in the different systems the relative stabilities of some $[1,2,r]$ and $[1,1,r]$ have been studied. The difference in thermodynamic values for the formation of some $[1,1,r]$ and $[1,2,r]$ complexes of the same ligand and with the same number of protons (r) are shown in Fig. 4.15 below. These differences amount to the thermodynamic values for the addition of a further ligand to a $[1,1,r]$ complex, for example:



Unfortunately changes of enthalpy and entropy for the formation of these complexes could not all be determined experimentally or to the same degree of certainty; it is only in the malate and aspartate system (where both species are important enough) where these values were determined for both the $[1,1,2]$ and $[1,2,2]$ complexes. In the lactate and mandelate system the $[1,2,2]$ complexes predominate to such an extent, that the enthalpy and entropy for the formation of the minor species $[1,1,r]$ could not be determined from experimental data. Values for the formation of $[1,1\text{lac},2]$ and $[1,1\text{man},2]$ have, however, been proposed (*cf.* 4.3.1 and Appendix 4). Based on these proposed values, the comparison could also be made for these systems. The ΔH° value for the formation of $[1,2\text{cit},4]$ was fixed at an approximate value during the calculation of the ΔH° values for the other citrate complexes, so that the comparison is less significant as that for the malate system.

The thermodynamic values (ΔG° , ΔH° , $T\Delta S^\circ$) for the addition of the ligands show three distinct types:

- A** The values for the addition of a ligand to $[1\text{Mo},1\text{mal},2]$, $[1\text{W},1\text{mal},2]$ and $[1\text{Mo},1\text{asp},2]$ are very similar. The ΔG° values are relatively small (about -10 kJ mol^{-1}), the ΔH° value for the addition is favourable (about -24 kJ mol^{-1}), and the $T\Delta S^\circ$ terms are distinctly unfavourable for the addition (about -10 kJ mol^{-1}).
- B** The values for the addition of a ligand to $[1\text{Mo},1\text{mal},3]$, $[1\text{W},1\text{mal},3]$, $[1\text{Mo},1\text{lac},2]$ and $[1\text{Mo},1\text{man},2]$ are very similar. The ΔG° values are greater (about -23 kJ mol^{-1}), the ΔH° values are favourable (about -24 kJ mol^{-1}), and the $T\Delta S^\circ$ terms are generally insignificant for the addition.
- C** The values for the addition of citrate to $[1\text{Mo},1\text{cit},4]$ is unusual (compared to the other available values). The ΔG° value is also relatively large (about -23 kJ mol^{-1}), but the ΔH° value and the $T\Delta S^\circ$ term are almost equally favourable for the addition.

In the following paragraphs it will be shown that these groupings are not incidental, since they correspond with the different structures of the different $[1,1,r]$ complexes (Fig. 4.7) and the respective products of addition, $[1,2,r]$ (Fig. 4.6).

The enthalpies for the additions can be rationalized as follows: The type A $[1,1,2]$ complexes have the general structure $\text{MO}_3(\text{OH}_2)\text{ligand}$ (didentate chelation *via* five-membered ring), the type B, $\text{MO}_2(\text{OH}_2)(\text{OH})\text{ligand}$ (didentate chelation *via* five-membered ring), and the type C, $\text{MO}_2(\text{OH}_2)\text{ligand}$ (tridentate chelation *via* five- and six-membered rings). The similar and relatively great ΔH° values for the

addition of ligand to the [1,1,2] complexes of type A and B are the result of the formation of an additional stable five-membered ring. Although an additional five-membered ring is also formed at the addition of a ligand to [1Mo,1cit,4], the concomitant loss of a six-membered ring results in a relatively small ΔH° value for the addition of ligand.

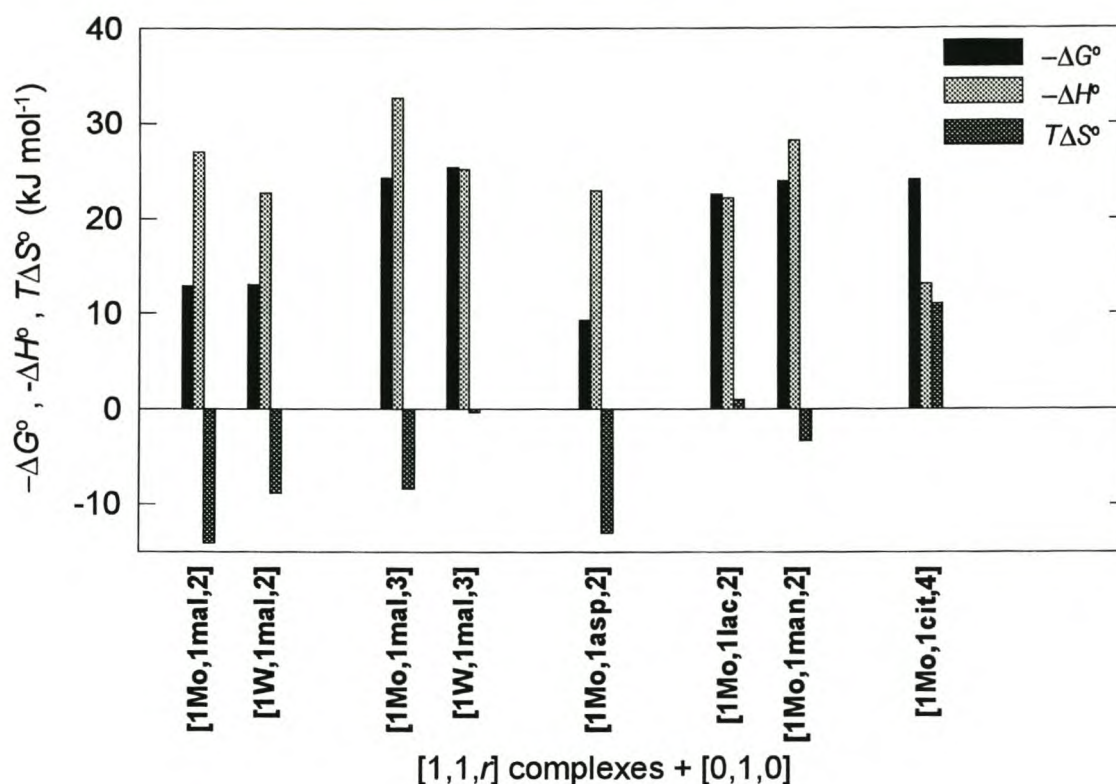


Fig. 4.15 Thermodynamic values for the addition of a ligand to some [1,1,*r*] complexes.

The gain in entropy due to the formation of two water molecules is less than the loss of entropy due to the combination of the charged ligand and the charged [1,1,*r*] complex of type A and B to form one charged molecule, since the net change in entropy is unfavourable for the addition. (The change in entropy for the simple dimerization of *e.g.* [1,1mal,2] is also unfavourable despite the formation of a water molecule). The addition of citrate to [1,1cit,4] (type C) results in the formation of only one water molecule, but, while citrate binds tridentate to the molybdate centre of [1,1cit,4], it only binds didentate to the molybdate centre of [1,2cit,4]. The distinctly favourable entropy change for the addition of citrate to [1,1cit,4] indicates that this loss of rigidity/order due to the detachment of the β -carboxylates (from tridentate to didentate) is the dominant entropy factor. Thus, the significantly favourable entropy change for the addition of a citrate to [1,1cit,4] opposed to the unfavourable entropy change for the addition of ligand to type A and B complexes seems reasonable.

The more unfavourable entropy change for the addition of type A complexes, compared to the type B complexes can also be rationalized: The addition products of the ligand and type A [1,1,*r*] complexes, [1,2mal,2] and [1,2asp,2], both have two uncoordinated β -carboxylates. On the other hand, the addition products of ligand and type B [1,1,*r*] complexes, [1,2mal,3], [1,2lac,2] and [1,2man,2], only have one uncoordinated β -carboxylate (mal), or none at all (lac, man). It is conceivable that the two uncoordinated β -carboxylates, which carry a fairly localized negative charge, establish localized solvent order, resulting in a more unfavourable entropy change than for ligand additions to type B complexes.

The predominant [1,1ox,2] complex, $\text{MO}_3(\text{OH}_2)\text{ligand}$ (didentate chelation *via* five-membered ring), has a type A structure. The addition of oxalate ([0,1ox,0]), which has no hydroxy groups, by elimination of two waters (as in the case of the addition of a ligand to the other type A [1,1,*r*] complexes) is not possible because there are not enough hydrogens available. (This is in agreement with the proposed model, which contains no [1,2,2] complex.) The addition of oxalic acid, however, which has two hydroxy groups, is possible through the elimination of water molecules, resulting in the complex [1,2ox,4]. Due to the formation of an additional five-membered ring, the change in enthalpy is expected to be favourable, and the driving force of the reaction (as for the addition of ligands to type A and B [1,1,*r*] complexes). The reaction product, [1,2ox,4] is similar to the reaction products, [1,2lac,2] and [1,2man,2], in the sense that it contains no uncomplexed β -carboxylates which could establish localized solvent order. The change in entropy is therefore expected to be similar to that of the addition of the ligand to [1,2lac,2] and [1,2man,2]. The thermodynamic values for the addition of oxalic acid ([0,1ox,2]), calculated from the *experimental* values for the formation of [1,1ox,2] and the *proposed* values for the formation of [1,2ox,4] (Appendix 4), indeed show that the enthalpy is the driving force and that the entropy change is very similar to the values for the addition of ligand to [1,2lac,2] and [1,2man,2].

The addition of citrate to [1,1cit,1] by elimination of water is not possible because there are not enough protons in the reactants (as with the addition of oxalate to [1,1ox,2]), or viewed differently, the reaction would be possible through the elimination of two hydroxy-anions. The charge of the products would however result in greater solvent order. The unfavourable entropy change would prohibit the reaction.

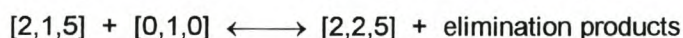
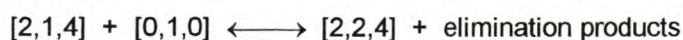
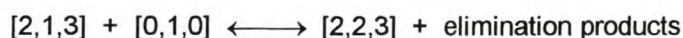
The [1,1cit,2] complex is similar to the type A [1,1,*r*] complexes. The change in enthalpy for the addition of citrate to [1,1cit,2] would probably be as favourable ($\Delta H^\circ \sim -24 \text{ kJ mol}^{-1}$) as for similar additions to type A [1,1,*r*] complexes, due to the formation of an additional five-membered ring. The resulting [1,2cit,2] complexes, would have four negatively charged uncomplexed β -carboxylate groups, which would result in even greater order of the solvent than the [1,2mal,2] and [1,2asp,2] (type B products). The change in entropy is expected to be very unfavourable for the addition of citrate to [1,1cit,2] ($T\Delta S^\circ \sim -24 \text{ kJ mol}^{-1}$). The reaction will thus not take place as the favourable enthalpy change for the formation of the [1,2cit,2] is balanced by the favourable entropy change for the formation of [1,1cit,2].

The [1,1cit,3] complex is similar to the type C complex [1,2cit,4]. The ΔH° for the addition of citrate to [1,1cit,3] is expected to be only as favourable as for the addition of citrate to [1,1cit,4]. The three negatively charged uncomplexed β -carboxylate groups of the [1,2cit,3] would result in a much greater solvent order

than the two of [1,2cit,4]. It is conceivable that the relatively small enthalpy change is as favourable as the entropy change is unfavourable, resulting in an unfavourable change in free energy. This is consistent with the absence of the [1,2cit,3] in the model.

4.3.8 Comparison of [2,1,*r*] and [2,2,*r*] complexes

The relative stabilities of some [2,2,*r*] and [2,1,*r*] can be considered. The difference in thermodynamic values for the formation of some [2,2,*r*] and [2,1,*r*] complexes of the same ligand and number of protons (*r*) are shown in Fig. 4.16 (values are in favour of [2,2,*r*]). These differences amount to the thermodynamic values for the addition of a further ligand to a [2,1,*r*] complex, for example:



Unfortunately changes of enthalpy and entropy for the formation of these complexes could not all be determined experimentally. The enthalpy and entropy values pertaining to the lactate and mandelate complexes are based on proposed values (Appendix 4).

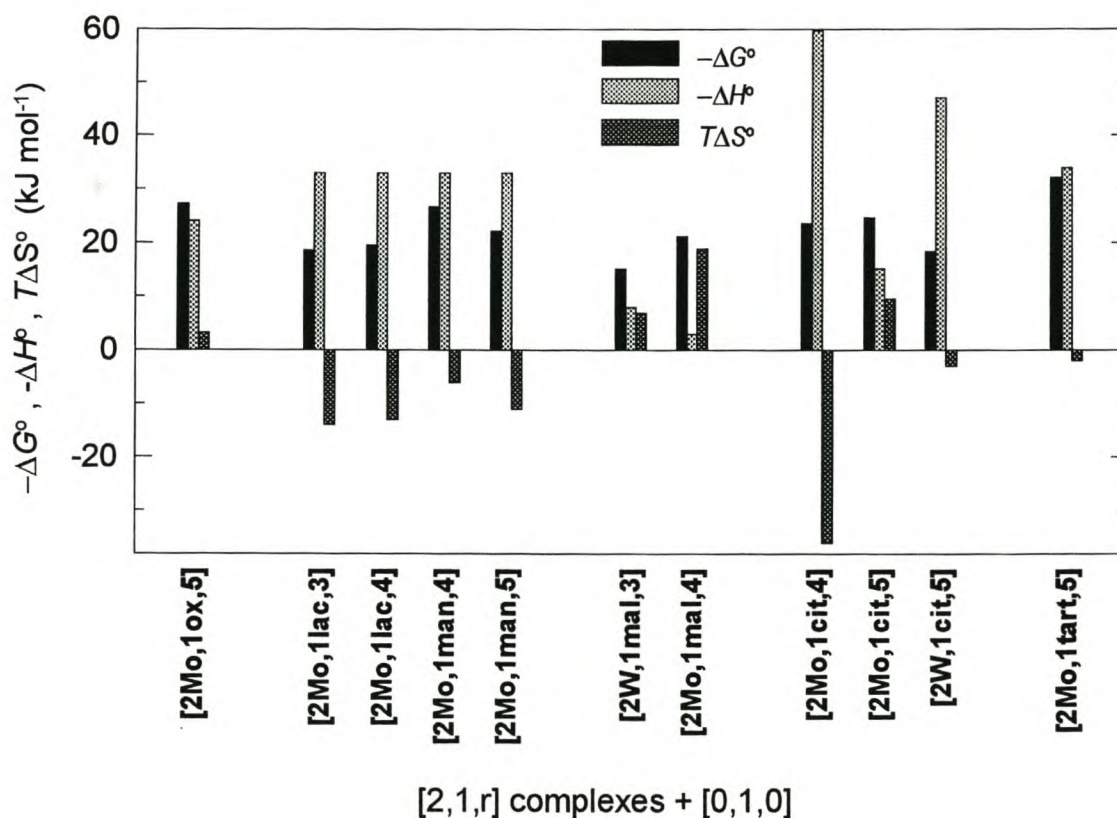


Fig. 4.16 Thermodynamic values for the addition of a ligand to [2,1,*r*] complexes.

The [2,1ox,5], [2,1lac,3], [2,1lac,4], [2,1man,4], [2,1man,5], [2W,1mal,3] are proposed to have similar structures, where the ligand binds monodentate to different metal centres of a dimer (Fig. 4.9.1.1). The products of the addition of a ligand and elimination of water of the first 5 complexes (molybdate complexes) are also similar (Fig. 4.8.1): Each ligand binds didentate *via* a five-membered ring to one metal centre of the dimer. According to the proposed or tentatively calculated thermodynamic values for the formation of these complexes, the change in enthalpy is the sole (or main) driving force for the addition and condensation (Fig. 4.16). This is similar to the addition of ligands to most [1,1,*r*] complexes (4.3.7). The entropy gain upon elimination of water obviously is not as great as the entropy loss due to chelation of a further ligand. The addition of a ligand and the elimination of water of the [2W,1mal,3], however, is assumed to result in a different type of structure (Fig. 4.8.1). The second ligand merely leads to a second ligand bridge, and no five-membered rings are formed as for the former additions. The change in enthalpy is, understandably, also less favourable.

The product of the addition of malate to [2,1mal,4], namely [2,2mal,4], is proposed also to have two stable five-membered rings, but the malate is already bonded *via* a five-membered ring to one metal centre in the [2,1mal,4] with the β -carboxylate also forming a bridge across the dimer. The net gain in enthalpy is, therefore, minimal, compared to the addition of ligand to the above mentioned [2,1,*r*] complexes which are not stabilized by a five-membered ring. According to the proposed structures, the additional ligand bridge across the metal dimer as well as one of the M-O-M bridges are broken, resulting in a product, [2,2mal,4] which is more free to rotate and bend than the reactant [2,1mal,4]. This explains the favourable entropy change for the addition of malate to [2,1mal,4].

The [2,1cit,4] is assumed to have the same structure as the [2,1mal,3], but the enthalpy change for the addition of citrate to [2,1cit,4] is very large (much greater than for addition to [2,1mal,3]). This is due to tridentate chelation of each citrate to the [2,2cit,4] dimer (Fig. 4.8.2). Despite the elimination of three water molecules, the entropy change is unfavourable due to the much higher degree of bonding established. Although the citrates are also tridentately bonded in the [2,2cit,5] as in the [2,2cit,4] complex, the change of enthalpy is not particularly large since the [2,1cit,5] complex is already stabilized *via* a five-membered ring as well as a ligand bridge across the dimer, unlike the [2,1cit,4]. The flexibility gained across the M-O-M bond as well as the two water molecules eliminated result in a favourable entropy change for the addition of citrate to [2,1cit,5].

The [2W,1cit,5] is proposed to be similar to [2Mo,1cit,5] (Fig. 4.9.2). Although the citrate binds to the metal *via* three oxygens in both the [2W,2cit,5] and [2Mo,2cit,5], each citrate forms a bridge across the M-O-M bond in the [2W,2cit,5] (unlike the [2Mo,2cit,5]), resulting in a much more rigid tungstate structure compared to the molybdate structure (Fig. 4.8.2). The change in enthalpy is thus much greater than for the addition of citrate to [2Mo,1cit,5]. Concomitantly the entropy change for the formation of this rigid structure is very unfavourable, despite the elimination of two water molecules.

The extraordinary great change in free energy, solely due to a very great change in enthalpy for the addition of tartrate to the proposed [2,1tart,5] complex can also be rationalized by the very rigid proposed structure for [2,2tart,5] in which each Mo-centre is chelated *via* two five-membered rings, and in which all four possible oxygen donors of tartrate have been used in complex formation (4.8.1).

4.4 COMPARISON WITH LITERATURE

The values for the protonation constants of the ligands agree very well with the available literature values for similar media and temperature. (These values are presented in the relevant tables in Chapter 3).

4.4.1 Oxalate complexes

The [2Mo,2ox,6] and [1Mo,1ox,2] complexes, of which structures have been determined before, have been found to exist in solution too [75-77]. Beltrán [91] proposed the [1Mo,2ox,2], [2Mo,2ox,4] and [2Mo,2ox,5] complexes in solids, but only the latter was now identified in solution. The tungstate complex, [2W,2ox,4] was, however, identified as well as the protonated form of [1Mo,2ox,2], namely the [1Mo,2ox,4] complex. The [1Mo,2ox,2] is proposed to be highly unlikely (*cf.* 4.3.7). The evidence of Beltrán concerning the [2Mo,2ox,4] is not necessarily contradictory to the results of the present investigation as it is possible that under slightly different conditions the [2Mo,2ox,4] could exist (like its tungstate counterpart). The complexes identified by potentiometry and spectrophotometry previously [2], [1Mo,1ox,2], [2Mo,2ox,5], [2Mo,2ox,6], have been confirmed, but complexes [1Mo,1ox,3], [2Mo,1ox,5] and [1Mo,2ox,4] have now been identified as additional minor species in this investigation. The existence of a complex $[\text{WO}_3(\text{ox})]^{2-}$, suggested previously [103], was confirmed in this investigation, but as one species of a W-oxalate model which is very similar to the Mo-oxalate model.

4.4.2 Lactate and mandelate complexes

The calculated formation constant of the $[\text{1Mo,2lac,2}]^{2-}$ complex, $\log\beta_{122} = 15.71$, can be compared with the approximate value of 14.7 calculated from NMR measurements by Gil and co-workers [93,104]. Beltrán-Porter *et al.* [92] proposed the [2Mo,2lac,4] complex at pH~2, as well as its protonated form [2Mo,2lac,5] in 0.5 M NaClO₄ medium. The [2Mo,2lac,4] complex was identified in this investigation but not the [2Mo,2lac,5]. (The related [2Mo,2man,5] complex was however identified.) The different models don't necessarily contradict, as the medium of investigation was different, but it is possible that the now identified/proposed [1,1,2], [1,1,3], [1,2,3], [2,1,4], [2,1,5] complexes, which all occur at very low pH, were previously collectively ascribed to the complex [2Mo,2lac,5] (*cf.* Fig. 3.2.2).

The existence of a dilactate complex $[\text{WO}_2(\text{lac})_2]^{2-}$ at pH~5 has previously been deduced from proton and ¹³C NMR measurements [93] but the stoichiometry of a much weaker complex at the same pH could not be established. Our investigation has confirmed the existence of the [1W,2lac,2] complex and has shown that at pH~5 two additional, very minor species, namely [2W,2lac,3] and [1W,1lac,2] exist. After the results of our investigation were published, Hlaibi *et al.* reported a $\log\beta_{122} = 18.15$ for the [1W,2lac,2] complex and, once again, speculated on a possible existence of a [2W,2lac,*r*] complex [97]. (This value was larger than our value, because the authors did not take into account the presence of a small amount of minor complexes when calculating the value.)

The [1Mo,2man,2] and [1W,2man,2] were identified previously and approximate values for their formation constants, $\log\beta_{122} = 14.8$ (Mo) and $\log\beta_{122} = 15.8$ (W), were obtained from NMR data [93]. These values are both 1 to 2 log units smaller than our values (Table 3.3.1 and 3.3.3). The new models also include minor species, [1Mo,1,r], [2Mo,2,r], [2Mo,1,5] and [1W,1,r], [2W,2,r].

Benzilate is very similar to mandelate, the former having an additional phenyl group instead of a proton on the α -carbon. A potentiometric investigation of the molybdate-benzilate system in the pH range 2-7 led to the identification of the [1,2,2] and [2,2,4] complexes and the calculation of their formation constants ($\log\beta_{122} = 17.35$ and $\log\beta_{224} = 29.07$ in 0,1 M NaNO₃) [141]. As expected, this system is very similar to the Mo-mandelate system over the same pH range (Fig. 3.3.2). Based on this similarity it is proposed that a [2,2,5] benzilate complex probably exists at pH < 2 (like the [2,2man,5] in the mandelate system.) An ammonium salt of the [1,2,2] benzilate complex was prepared and characterized by X-ray crystallography. This structure is the same as the structures proposed for the [1,2,2] complexes (Fig. 4.6).

4.4.3 Malate complexes

Many species, with varying molybdate:malate ratios (1:1, 2:2, 4:4, 1:2, 2:1, 4:2) have been proposed in different previous studies [25-33], but the combination of complexes proposed are often contradictory [28,30,31]. The different reports can be rationalized by our Mo-malate model which consists of 14 complexes of 6 different molybdate:malate ratios: Because of the overlap of equilibria it is very difficult to accurately identify species under isolated conditions; it is almost impossible to avoid the presence of at least a few minor species, which, if not taken account of, will lead to misinterpretations of data. One exception would be conditions of substantial excess of malate, but that would only lead to the identification of the [1,2,r] complexes.

The results of two of the previous investigations of the Mo-malate system are of particular interest, and discussed in the following sections.

4.4.3.1 Previous NMR investigation (Mo-malate) [30]

Since the thorough investigation by Caldeira *et al.* [30] resulted in the proposal of several species under different conditions, it is of particular interest to see whether their results are consistent with the results of our investigation.

The interpretation of the Job curves constructed from NMR data by Caldeira *et al.* could not conclusively identify the complexes. The authors proposed the existence of one complex with 2:1 (possibly a [4,2,r] complex), one complex of 1:1, and two complexes with 1:2 stoichiometry. The reaction model now proposed (Table 3.4.1) was employed to calculate the distribution of species pertaining to conditions of the two NMR investigations by Caldeira. The one experiment was conducted at a constant pH=5, and the other at pH=5.5. In both experiments the concentration of the molybdate and malate were varied, but with the constraint of [Mo]+[malate]=1 M. The calculated distribution curves are shown in Fig. 4.17.1 and Fig. 4.17.2. The main complex species predicted by the model correlates extremely well with the maxima of the Job curves identified by the authors as complex a, b, c and d. This model thus confirms that complex-c is the [4,2,8] complex and that complex-d has a 1:1 stoichiometry, now proposed to be the [2,2,4]

complex. The complex-b and complex-a are clearly the [1,2,2] and [1,2,3] complex. The distinct NMR spectra observed for these two complexes showed that they cannot just differ in the degree of protonation and geometrical isomers were suggested [30].

4.4.3.2 Previous polarimetric study (Mo-malate) [31].

The results of the present investigation also concur with the conclusions of a polarimetric study regarding the stoichiometry and approximate stability regions of the six complexes [1,1,1], [1,1,2], [1,2,2], [2,2,4], [2,2,5] and [4,2,8]. In particular, there is a close correlation between the change in rotatory power and the distribution curves of the [4,2,8] complex with the change in malic acid/molybdate ratio at constant pH values of 3 and 4 (Fig. 4.18.1 and Fig.4.18.2). The values obtained by graphical extrapolation for the formation constants of three complexes namely, $\log\beta_{111} = 8.2$ (7.47), $\log\beta_{122} = 13.9$ (15.48) and $\log\beta_{224} = 22.6$ (28.06) differ appreciably from those now determined (shown in brackets). However, considering the complexity of the system, the extrapolated values should be regarded as reasonable approximations.

Complexes with varying tungstate:malate ratios (1:1, 2:2, 2:1, 1:2) have been proposed in the previous investigations of the tungstate-malate system by Gil and Cervilla [34-36]. These results are discussed in the light of our model which consists of 11 complexes of 5 different tungstate:malate ratios.

4.4.3.3 Previous NMR investigation (W-malate) [34].

The Job curves constructed by Gil *et al.* [34] from NMR data at pH 3.0, 4.3 and 5.5 show one 1:1, one 2:1 and two 1:2 complexes. Using our tungstate-malate model, distribution curves were calculated for the same conditions of their experiments which are shown in Fig. 4.19. Calculations show that the proposed 1:2 complexes are the [1,2,2], [1,2,3] and [1,2,4] now identified; the peaks of the Job curves coincide in each case with the maximum percentage concentration of the particular complex. The 1:1 complex shown by the authors to be concentration dependent and for which a 2:2 stoichiometry was suggested corresponds with the [2,2,4]. They also found indications of a 2:1 species which can be associated with the [2,1,3] complex, but in view of the high concentrations used (and excess of tungstate) it could just as well be a [4,2,8] complex analogous to the molybdenum complex isolated in the solid state [78-80].

4.4.3.4 Previous polarimetric study (W-malate) [36].

The polarimetric measurements clearly showed the difference in optical activity of solutions when either molybdate or tungstate is in excess (actually twenty-five-fold). With malate in excess the change in optical activity with pH as reported by these authors correlates well with the distribution of the [1,1,1], [1,2,2] and [1,2,4] complexes (Fig. 4.20); due to considerable overlap of stability regions of the complexes it is not surprising that their *D* vs pH curve does not show an inflexion at the pH where the [1,2,3] occurs in maximum percentage concentration. The interpretation of this curve by these authors in terms of the formation of only one 1:2 complex, but two 2:2 complexes can not therefore be accepted which also implies that the interpretations of Gil *et al.* regarding the existence of 1:2 complexes were correct. However, it is now clear that the 1:1 complex of Cervilla *et al.*, which occurs at high pH, is indeed a [1,1,1] complex and therefore different from the 1:1 complexes of Gil *et al.* which are in fact dimers. The existence of dimeric complexes in solutions with an excess of tungstate has also been postulated by Cervilla *et al.*

The present reaction model clearly accommodates quite well the experimental data of these two research groups and successfully resolves the conflicting interpretations.

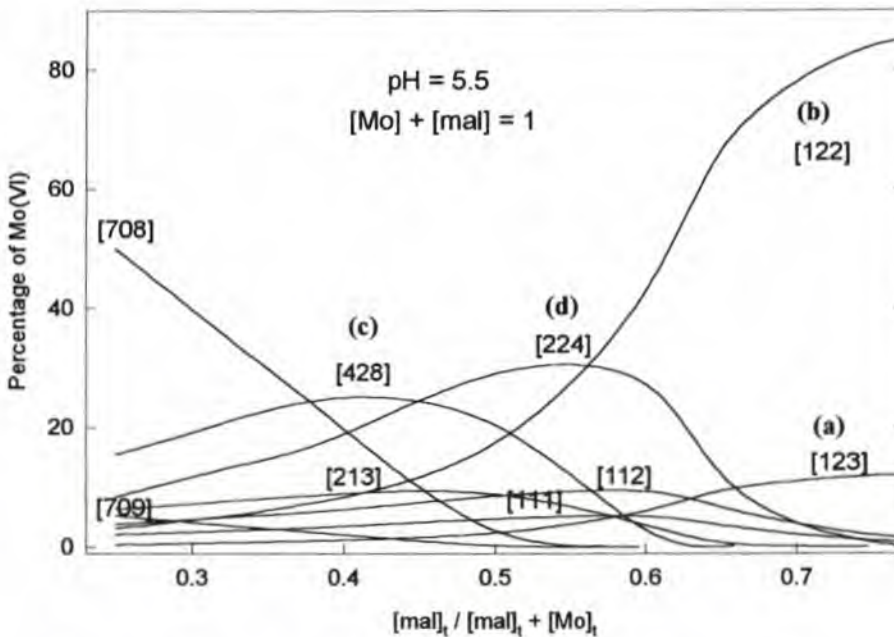
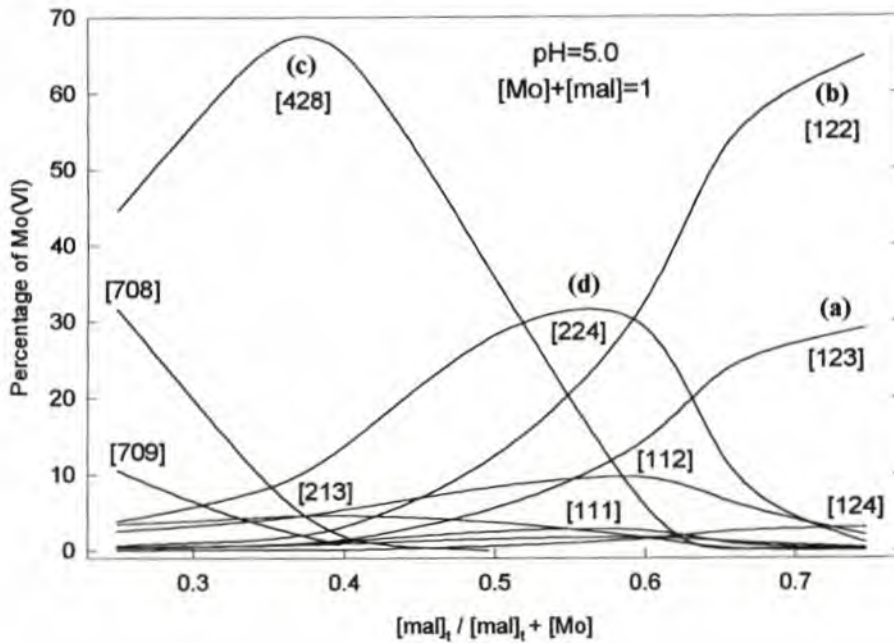


Fig. 4.17.1 (Top) Distribution of Mo(VI)-malate complexes at pH=5 as a function of the fraction of total malate concentration to the total concentration of complexing species (Mo+mal), which equals 1 M.

Fig. 4.17.2 (Bottom) Distribution of Mo(VI)-malate complexes at pH=5.5 as a function of the fraction of total malate concentration to the total concentration of complexing species (Mo+mal), which equals 1 M.

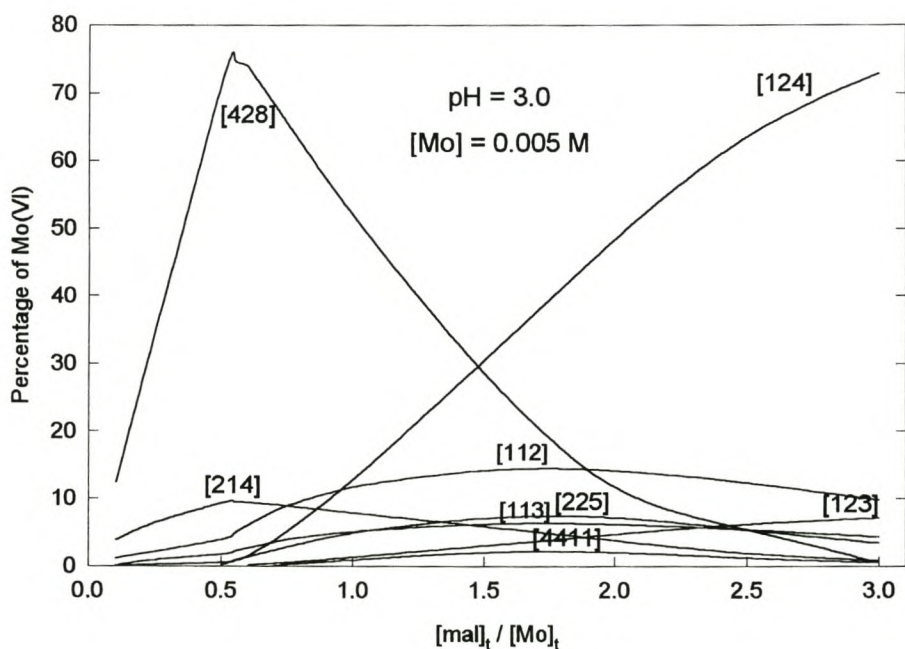
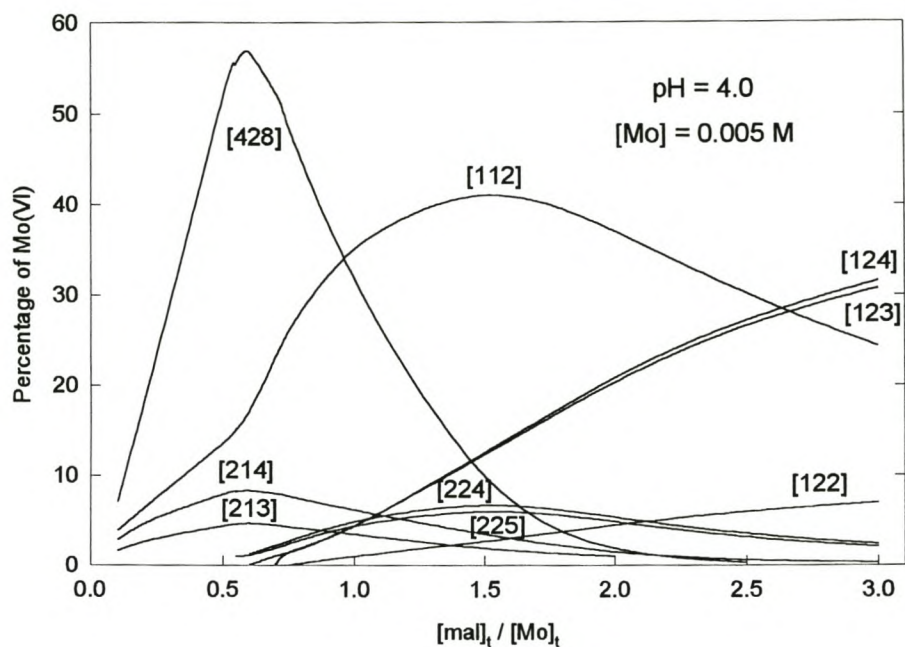


Fig. 4.18.1 (Top) Distribution of Mo(VI)-malate complexes at pH=4 and for [Mo(VI)]=0.005 M, expressed as a percentage of the total molybdenum(VI) concentration as a function of [mal]/[molybdate].

Fig. 4.18.2 (Bottom) Distribution of Mo(VI)-malate complexes at pH=3 and for [Mo(VI)]=0.005 M, expressed as a percentage of the total molybdenum(VI) concentration as a function of [mal]/[molybdate].

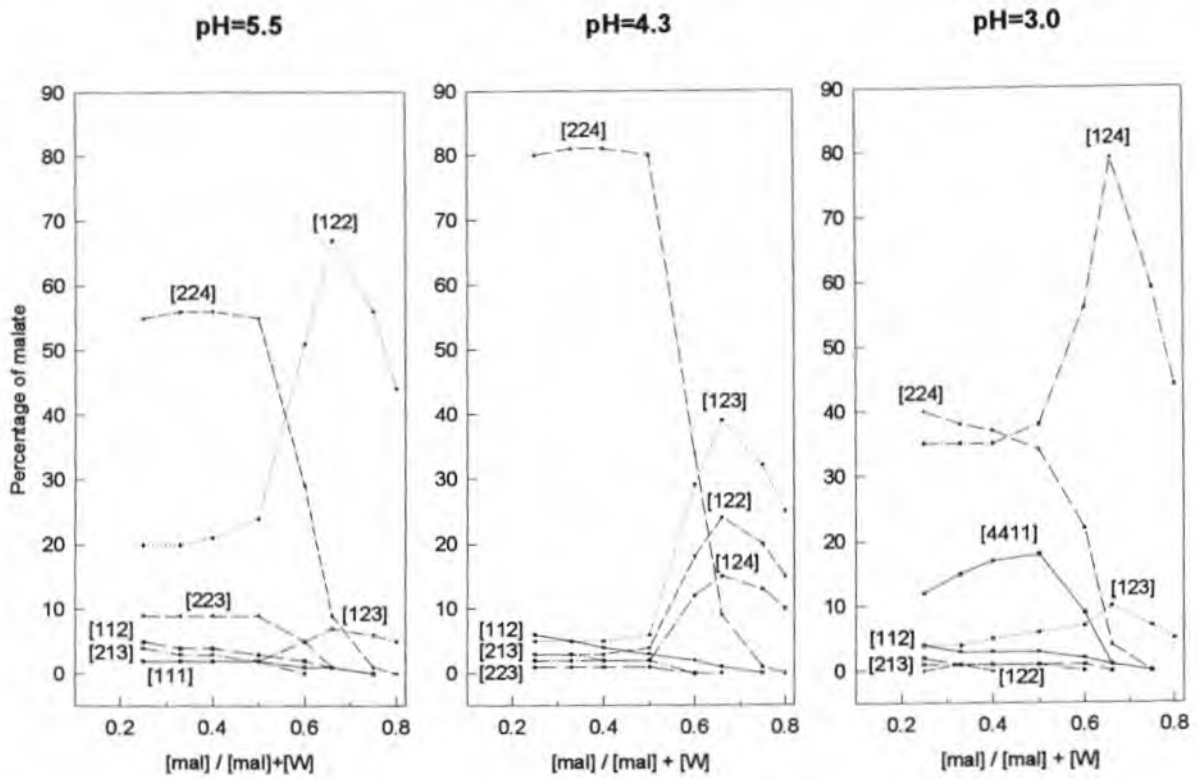


Fig. 4.19 Concentration of tungstate(VI)-malate complexes at pH 5.5, 4.3, 3.0, expressed as a percentage of the total malate concentration, as a function of the fraction of total malate concentration to the total concentration of complexing species ($W+mal$), which equals 1 M.

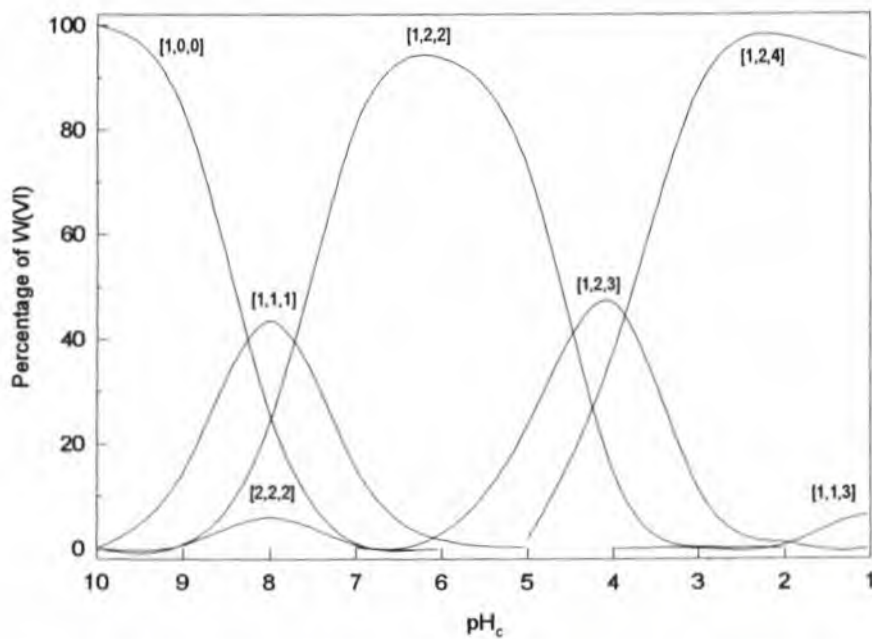


Fig. 4.20 Concentration of tungstate(VI)-malate complexes, expressed as a percentage of the total molybdenum(VI) concentration, as a function of pH_c . The total concentrations of tungstate(VI) and malate are 0.01 M and 0.25 M, respectively.

4.4.4 Citrate complexes

Of the previous investigations the investigation by Cruywagen [37] has contributed most in understanding the equilibria in the Mo-citrate system as it established equilibrium constants and other thermodynamic parameters for the formation of some major complexes, namely the mononuclear [1,1,1], [1,1,2] and [1,1,3] complexes as well as two dinuclear complexes, namely, [2,1,4] and [2,1,5].

A mononuclear compound, $K_4[MoO_3(cit)] \cdot H_2O$ and two dinuclear compounds $K_6[Mo_2O_5(cit)_2] \cdot 7H_2O$ and $K_4[Mo_2O_5(Hcit)_2] \cdot 5H_2O$, which correspond to [1,1,1], [2,2,4] and [2,2,6], respectively, have been obtained by precipitation from aqueous solution and have been characterized by a variety of chemical methods [94]. A complex of composition $M_4[Mo_2O_5(OH)(H_2O)(Hcit)] \cdot 0.5H_2O$ where M is K^+ or NH_4^+ , and which corresponds to [2,1,5] has also been reported [95]. The isolation of molybdenum(VI) citrate complexes in crystalline form suitable for X-ray structural analysis has proved to be quite difficult, but two types of structures, tetranuclear citrate complexes, $[K_4[(MoO_2)_4O_3(cit)_2] \cdot 6H_2O$ and $[Me_3N(CH_2)_6NMe_3]_2[Mo_4O_{11}(Hcit)_2] \cdot 12H_2O$ [82,83], corresponding to [4,2,10] and a dinuclear complex, $K_2Na_4[(MoO_2)_2O(cit)_2] \cdot 5H_2O$ [86], corresponding to [2,2,4], have been determined by single-crystal X-ray analysis.

The complexes previously proposed by Cruywagen as well as complexes which have been identified in solids have now been identified as major species in our model which consists of 16 complexes of six different molybdate: citrate ratios (Table 3.5.1).

Most of the polarographic methods for the determination of molybdenum(VI) are based on the reduction of a molybdenum complex. The ligand used, usually an α -hydroxycarboxylic acid such as lactic, malic or citric acid, is typically present in large excess [38-45]. The polarographic reduction of molybdenum(VI) in the presence of citric acid has been investigated by several authors, but the interpretation of the results has been hampered by a lack of knowledge about the identity and stability regions of the electroactive complex species, as well as that of the reduced products [39-43]. The [1,1,1] complex could, however, be identified by polarographic methods at 2°C in slightly alkaline solution and an approximate constants for its formation was determined. This value ($\log \beta_{111} = 8.4$) is close to our value pertaining to 25°C, but is 0.6 log units smaller than our value pertaining to 2°C. The identification of the species is in agreement with the model in the respect that it is the only complex which is present at $pH > 8$.

The formation in solution of either one or two complexes with a tungsten(VI) to citrate ratio of 1:1 has been reported by several authors [47-53]. A complex with a 1:2 tungstate: citrate ratio has also been proposed by some of these investigators [49,51,53]. From the results of a spectrophotometric, polarimetric and NMR study Cervilla *et al.* [53] concluded that, in addition to a 1:1 and a 1:2 complex, two dimeric complexes with a tungstate: citrate ratio of 2:2 also exist in solution. Despite agreement among investigators about the tungstate: citrate ratio of some complexes, conclusions about the proton stoichiometry as well as the stability regions of most complexes were contradictory. For the 1:2 complex, for example, negative charges of

2- and 6-, respectively, [51,53] have been assigned. Recently a dinuclear tungsten(VI) citrate complex, $\text{Na}_6[\text{W}_2\text{O}_5(\text{cit})_2]\cdot 10\text{H}_2\text{O}$, has been structurally characterized by X-ray analysis [84,85].

The results of our investigation are in agreement with those of Cervilla *et al.* [53] as far as the existence of [1,1,1] and [2,2,4] complexes are concerned. However, the proton stoichiometry of the [1,2,6] and [2,2,5] complexes in our model differs from that of the other two complexes proposed by these authors, namely [1,2,3] and [2,2,7].

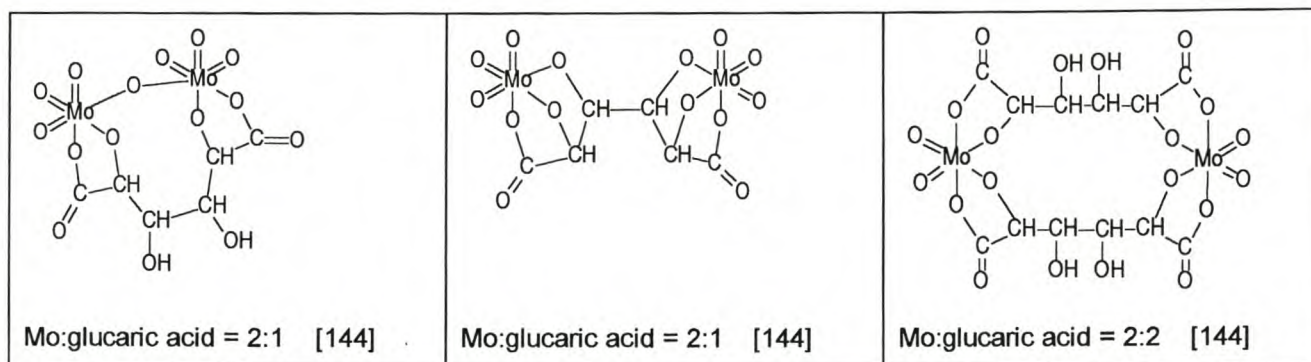
4.4.5 Tartrate complexes

The best model obtained from our previous potentiometric investigation [142] consisted of the monomeric species, [1,2,2], [1,2,3], [1,2,4], the dimeric species, [2,1,4], [2,1,5] and the tetrameric species, [4,4,7], [4,4,8], [4,4,9], [4,2,6] and [4,2,7]. Judging by their greater percentage concentration under the experimental conditions, the major complexes were the monomeric and dimeric complexes as well as the tetrameric [4,4,8] complex. (This model confirmed the existence of a [1,2,*r*] and polymeric complexes proposed before [54-62].) The model now proposed, calculated from a broader data base, consists of the same major complexes as in the old model, but several new minor complexes were identified. The complexes [4,4,7], [4,2,6] and [4,2,7] of the previous model were obviously collectively representing a number of species. The structures of these species could only be interpreted as polymeric chains (Fig. 4.13), which suggest that many more such complexes could exist with varying chain lengths and differing degree of protonation. The new model, therefore, most probably is still too simple to represent the true minor species, but it is believed to give a better idea of the type of complexes that exist than the old model. The existence of the polynuclear complexes is supported by the identification of similar minor species in the tungstate-tartrate system.

A number of previous investigations have produced evidence for polymer formation in the molybdate and tungstate tartrate systems [56-57,59-60]. No specific polymeric complexes have been proposed, except for the [2Mo,2,4] [96] and [2W,2,4] [97] complexes. Very simple ring structures for these complexes were proposed on the basis of NMR evidence. However, no [2,2,4] complexes were identified in our investigation of the molybdate or tungstate tartrate systems. The ring structure of the [2,2,4] as proposed by these authors has exactly the same features as the [4,4,8] complex now proposed (Fig. 4.11.1). It is believed that the NMR signals, which led to the proposal of the [2,2,4] structure, could just as well be interpreted in terms of the [4,4,8] complex.

Based on NMR evidence a [2Mo,1,2] complex has also been proposed before [96]. This structure, which can be regarded as a small chain and a precursor to polymerization, is identical to the structure now proposed (Fig. 4.9.3). It is noteworthy that the molybdate:tartrate ratio of the first isolated tartrato peroxo complex of molybdate, is also 2:1 [143] and that X-ray structure determination revealed that two, otherwise separate Mo-centres are bridged by the tartrate in an identical manner as in the [2Mo,2tart,4] complex (Fig. 4.9.3).

Different structures have been proposed for the [2Mo,1tart,2] and [2W,1tart,2] complexes (Fig. 4.9.3). In both structures tartrate forms a bridge between the metal centres. Whereas the W-centres are also connected via a W-O-W bond, the Mo-centres do not share an oxygen. In this regard it is interesting that two complexes in the molybdate-glucaric acid system [144], both with a metal:ligand ratio 2:1, also differ in the same respect: In both complexes the Mo-centres are bridged by the ligand (which is related to tartrate), but the Mo-centres in one complex share an oxygen, whereas the Mo-centres in the other don't. The same authors also proposed a molybdate-glucaric acid complex with a metal:ligand ratio 2:2. A simple ring structure was proposed, which is very similar to the structure now proposed for the [2Mo,2tart,5] complex (Fig. 4.8.1).



4.4.6 Aspartate complexes

The identification of the [1,1,1] complex is in agreement with the results of previous equilibrium studies [66,98-101] and with the isolation in solid state of a complex with composition $K_2[MoO_3(asp)] \cdot H_2O$ [100]. The rest of the model now proposed does, however, not agree with the recently reported model [66] consisting of [1,1,1], [2,2,4], [2,2,5] and [2,2,6] pertaining to a different ionic medium, i.e., 0.1 M $NaNO_3$. This model was based on only three potentiometric titrations with molybdate to aspartate ratios of 1:4, 1:5 and 1:10 for an initial molybdate concentration of 0.002 - 0.003 M. Our model fits our data much better ($\sigma = 1.44$) than the model mentioned above ($\sigma = 4.36$) (Table 3.7.2).

The formation constant $\log\beta_{111} = 6.54$, which converts to the value 16.12 when expressed in terms of the unprotonated aspartate, L^{2-} , as the reacting species, can be compared with the values 16.01 (0.1 M $NaNO_3$) [66], 15.74 (1 M $NaCl$, 18°C) [99], 16.79 (0.16 M KNO_3) [98] and 18.2 (0.1 M $NaClO_4$, 25°C) [67].

Rabenstein [98] investigated complexation of molybdate and tungstate with aspartate and concluded that no complexation of tungstate and aspartate occurs in the pH-range in which a 1:1 molybdate-aspartate complex predominates. This is in agreement with our model, consisting only of [2W,1asp,4] and [2W,1asp,5], which predicts that complexation only takes place at $pH < 4$.

4.4.7 Nta complexes

The structures of the [1,1,2] and the [2,2,8] complexes, which have been isolated in the solid state, have been determined previously [88-90,102]. The formation constant obtained for the [1Mo,1,2] complex, $\log\beta_{112} = 17.78$, can be compared with the values previously reported for different ionic media namely, 17.90 (0.5 M NaClO₄) [71], 18.09 (1 M NaClO₄) [102] and 18.60 (3 M NaClO₄) [72]. The [1,1,2] and the [2,2,8] complexes have now been confirmed in both the Mo-nta and W-nta systems, which are described by models consisting of nine Mo-nta complexes and six W-nta complexes, respectively.

The value for the change of enthalpy for the formation of the [1Mo,1,2] complex, $\Delta H_{112}^{\circ} = -77 \text{ kJ mol}^{-1}$, which has previously been estimated from the change in $\log\beta_{112}$ with temperature [73], shows reasonable agreement with that obtained in the present investigation (-69 kJ mol^{-1}). No other enthalpy values for complex formation of molybdate with nta have been reported.

Chapter 5

Concluding remarks

Potentiometric investigations formed the basis of the study of the complexation of molybdate(VI) and tungstate(VI) with the different ligands, namely, oxalate, lactate, mandelate, malate, citrate, tartrate, aspartate and nta. It is the best method for identifying the many overlapping equilibria in these systems and for calculating the formation constants of the resulting complexes. When the analysis of the data indicated the existence of many species, however, the results were met with some concern. On the one hand many species were expected, particularly if the ligand has more than two possible donors for chelation, but on the other hand, there was no physical evidence for the existence of, particularly, the minor species identified by the program. The best strategy was therefore to select conditions, and collect data with great care and to test a wide range of species (from plausible to unlikely test-species) against the developing models in very many different combinations. Such a thorough search for species should result in a model that best represents each system. At the end of the investigation all the tungstate(VI) and molybdate(VI) complexes identified could be summarized in Table 4.1 highlighting similarities and differences between systems, such as:

- the similarity between the complexation of molybdate(VI) and tungstate(VI) with the same ligand,
- the similarity between the complexation of lactate and mandelate, ligands which differ only in the methyl and phenyl substituents,
- the similarity between the complexation of malate and citrate, the latter ligand having one additional β -carboxylate group,
- the similarity between the complexation of malate and aspartate, the latter having an amino group in the position of a hydroxy group in the former,
- the predominance of the $[1,2,r]$ complexes of α -hydroxy carboxylate ligands if the ligand is present in excess,
- the resemblance between the oxalate and nta systems, particularly regarding the predominance of the $[1,1,r]$ and $[2,2,r]$ complexes, and the absence of major $[1,2,r]$ complexes,
- the resemblance between the aspartate and nta systems regarding $[1,1,r]$ and $[2,1,r]$ complexes,
- the absence of $[1,1,r]$ and $[2,2,r]$ complexes in the tartrate systems (except for $[2\text{Mo},2\text{tart},5]$), and
- the presence of many unusual polymeric complexes in the tartrate systems.

The reasons for these similarities and differences were sometimes obvious (and expected), but some could only be rationalized after comparing the thermodynamic values for the formation, protonation and dimerization of the different complexes. Based on the previously determined structures of some of the complexes (mainly as solids) and the calculated thermodynamic values, structures were proposed for each complex identified. (Actually the attempt to rationalize the thermodynamic values in terms of the proposed

structures, and proposal of structures based on thermodynamic evidence are rather entwined.) The thermodynamic values have been shown to consistently support the different proposed structures (*cf.* 4.3). Furthermore, most of the important complexes are proposed to have features that are typical of the few structures which have been determined by, for example, X-ray crystallographic analysis (*cf.* 4.2). The structural features of some other complexes needed to be adapted slightly in order to obtain structures with the required charge. As few as possible different types of structures were proposed. Structures for different protonated forms of a complex, for instance, were proposed to be essentially the same, except if the thermodynamic values strongly suggested otherwise. Structures of higher symmetry were preferred to structures of lower symmetry. The structures of some minor species, in particular, would clearly not be as stable as the typical (known) structures, but this is precisely the reason for them being present in low percentage concentrations only. Some of these more unstable complexes of different stoichiometry (which have not been proposed previously) have very similar features. Furthermore, they could sometimes be pictured as possible intermediate species in the formation of other, more stable complexes. Particularly in the tartrate systems, some unusual structures could be used to explain why other typical complexes were absent in this system. The structures proposed for those W-complexes which have no molybdate(VI) counterparts are usually less stable than the structures proposed for complexes which have been identified in both the W and Mo-complex systems. The absence of these few Mo-complexes are, therefore, no cause for concern.

The consistency of thermodynamic evidence and the proposed structures enabled the prediction of many of the values for the change in enthalpy and entropy which could not be calculated from the experimental data. In the Mo-lactate and Mo-mandelate systems, for instance, the enthalpy change could only be calculated for the one predominant complex, but after careful consideration of possible structures and possible relations with other systems, enthalpy (and entropy) values have been proposed for all the other minor species. This consistency was achieved even though the change in enthalpy and entropy for the formation of many complexes could not be determined, and that some approximations had to be made when the values were calculated. (This is particularly true for the investigations of complexation with tungstate(VI) where slow reactions made analysis difficult). The overall consistency contributed much to the acceptance of the individual models, perhaps even more so than the spectrophotometric analyses which were aimed at confirming a few selected major complexes, or the polarographic analysis of the complicated molybdate(VI)-citrate system.

Although potentially very useful in identifying complexes in solution and calculating their formation constants, spectrophotometric analysis proved to be much less useful than potentiometry in these investigations. No spectrophotometric investigations of the tungstate(VI) systems were possible since solutions of tungstate(VI) and the particular ligands used do not absorb in the UV-region like the solutions of molybdate(VI) and these ligands. The investigations revealed that the calculated molar absorbance spectra of complexes are often very similar, particularly complexes which differ only in the degree of protonation. For this reason it was sometimes difficult to obtain unique results using the speciation programs even though the experimental spectra were very accurate and the conditions carefully selected to represent as few species as possible.

Polarography was tried as an independent method to support the potentiometric model of the molybdate(VI)-citrate system. Complexes are, unfortunately, reduced to different species, complicating the interpretation of an already complex system. However, the analysis revealed that many different complexes indeed exist and the peaks were shown to correlate with the appearance of the complexes predicted by the model. This is strong evidence that the comprehensive model obtained from potentiometric analysis does not only "fit the data well", but that it is a true reflection of the complexity of the real system. The polarographic analysis was not extended to other systems, as it proved to be very difficult to analyse the polarograms without specialized knowledge of polarography as such. The complicated models pertaining to other systems were, however, more readily accepted due to the one-off confirmation by polarographic methods, that the real Mo-citrate system is at least as complicated as the potentiometric Mo-citrate model indicated.

Although some complexes are known to exist as solids, it does not necessarily mean that the complexes exist in solution or necessarily have the same structure. However, all except one of the complexes identified as solids have been incorporated in our models indicating that crystallized complexes are *likely* to have counterparts in solution. It seems, therefore, that further attempts at crystallizing complexes from solutions is worth its while as a possible support for the models. Thus far attempts at making crystals of complexes were generally not very successful. Our models could be useful in calculating optimum conditions for the preparation of specific complexes or predicting difficulties. The Mo-citrate model, for instance, can already be used to explain why crystals of dimeric citrate complexes have been prepared and characterized, but only one monomeric complex, [1,1cit,1] has been prepared at relatively high pH. According to the model, [1,1cit,*r*] complexes are major complexes in solution, but most occur in the same pH-region in which [2,2cit,*r*] complexes also occur, the least protonated monomeric complex, [1,1cit,1], being the exception. The model predicts that dimerization of [1,1cit,2], [1,1cit,3] and [1,1cit,4] complexes occurs upon evaporation of a molybdate(VI)-citrate solution, but that [1,1cit,1] has the chance of retaining its identity as there is no competing complex at pH = 8. Similarly the model for complexation with tartrate and the proposed structures of the species explain the particular difficulty in crystallizing tartrate complexes: The various polymeric chain complexes exhibit an inclination for polymerization which is probably the reason why most attempts lead to the formation of a "jam" instead of crystals.

Specific molybdate(VI)-proton and tungstate(VI)-proton models were used to represent possible uncomplexed molybdenum or tungsten species during calculations of complexation models. These models are regarded as "good", mainly because they predict the pH of a wide range of molybdate/HCl or tungstate/HCl solutions very accurately. Although many of the species in these models can be regarded as certain, some are still uncertain. (Since starting the investigation the existence of the polymolybdate species, [7,0,11], in particular, has been regarded as doubtful. Yet it is clear that it is an excellent "placeholder" for other species, the identity of which are also uncertain at this stage.) It was of some concern whether such a model would lead to the identification of fictitious complex species. Therefore, the usually fixed formation constants of the molybdate(VI) or tungstate(VI) species, or the experimental concentrations of the molybdate(VI) or tungstate(VI) were allowed to be refined during some of the final calculations of the complexation models. The final complexation models remained unaltered. This indicated that the

molybdate(VI) or tungstate(VI) models used were, indeed, good enough in *representing* uncomplexed molybdenum or tungsten, despite the uncertainty about the true identity of some of the species. Occasionally an alternative, equally good molybdate(VI) model was used for a few calculations. The complexation models were not affected significantly, showing that the complexation model is not particularly sensitive to the exact species in the molybdate(VI) model, as long as the molybdate(VI)-proton model has a good fit for a wide range of molybdate(VI) concentrations. Furthermore, when testing the final complexation models, the titrations were ignored in which uncomplexed molybdate(VI) species were present. The best complexation models for these reduced data sets did not contradict the models calculated from the full data sets, which showed that the complexes were independent of the particular molybdate(VI)-proton model used.

The investigation shows that the stability constants of the tungstate(VI) complexes of α -hydroxycarboxylates generally exceeds that of the related molybdate(VI) complexes by ~ 1.6 log units per metal, in other words, that the change in free energy for the formation of the tungstate(VI) complexes is ~ 9 kJ mol⁻¹ per metal more favourable than for the related molybdate(VI) complexes. In the case of molybdate(VI) and tungstate(VI) complexes which are proposed to have the same structure, the main reason for the greater overall stability is usually the more favourable change in enthalpy. This is also the case for similar uncomplexed polymeric molybdate(VI) or tungstate(VI) species: The difference in the change of enthalpy for the formation of the hepta-tungstates and hepta-molybdates, for instance, is about 11 kJ mol⁻¹ per metal more favourable for the hepta-tungstate, whereas the difference in the change in entropy is insignificant. This more favourable enthalpy change for the polymerization or chelation of tungstate(VI) (compared to molybdate(VI)) reflects a greater tendency for tungstate(VI) to expand its co-ordination number from four to six (which results in an increased bond energy). If the structure of the tungstate(VI) complex has more metal-ligand bonds or has more M-O-M bridges than the molybdate(VI) complex with the same stoichiometry (e.g. [2,2cit,5]), the change in enthalpy is typically even more in favour of the tungstate(VI) complex. When the structure of the tungstate(VI) complex has fewer metal-ligand bonds or has fewer M-O-M bridges than the molybdate(VI) complex with the same stoichiometry (e.g. [1,1cit,4]), the change in entropy is particularly favourable for the tungstate(VI) complex, whereas the change in enthalpy is more comparable to or even less favourable than for the molybdate(VI) complex. The difference in free energy for such molybdate(VI) and tungstate(VI) complexes is, however, not necessarily greater than for similar structures, as the greater enthalpy change is associated with a less favourable entropy change and vice versa; since the higher degree of bonding inevitably results in a lesser degree of freedom. This illustrates that there is a drive to minimize the total free energy and that the enthalpy is not necessarily minimized or the entropy optimized.

The difference in the stability of [1Mo,1ox,r], [2Mo,2ox,4], [1Mo,1nta,r] and [2Mo,2nta,r] complexes and their respective tungstate(VI) counterparts, however, is generally almost insignificant. It was established that the change in enthalpy for the formation of the tungstate(VI) complexes, [1W,1ox,r] and [2W,2ox,r], is about 10 kJ mol⁻¹ per metal more favourable than for the molybdate(VI) counterparts (as usual), but that the entropy factor, $T\Delta S^\circ$, is about 10 kJ mol⁻¹ per metal less favourable, the net result being the similar overall stability of the molybdate(VI) and tungstate(VI) complexes. Based on the calculated thermodynamic values the similar stability of the [1W,1nta,2] and [1Mo,1nta,2] is due to the enthalpy change being slightly more favourable for the molybdate(VI) complex and the entropy change being slightly more favourable for the

tungstate(VI) complex. It is very unusual for the enthalpy change to be less favourable for the tungstate(VI) complex. This anomaly may, however, not be taken too seriously, as it is very likely that the calculated ΔH° values pertaining to the tungstate(VI)-nta complexes are too small since approximations had to be made in their calculations (*cf.* 3.8.2.2).

The accuracy of the ΔG° values, which were calculated from the fairly accurate formation constants, is generally much greater than the accuracy of the experimentally determined ΔH° values. Because the $T\Delta S^\circ$ values were calculated from the ΔG° and ΔH° values, they are not independent values and are at least as inaccurate as the ΔH° values. However, *for the sake of the discussion* of the thermodynamic values, attempting to find patterns in the systems, and in the proposal of structures, the calculated values had to be regarded as the "true" values and the ΔH° and $T\Delta S^\circ$ had to be regarded as independent values. This is the obvious weak link in the arguments used for proposing complexes. If a calculated ΔH° value were actually 10 kJ mol^{-1} less favourable than the true value, the calculated $T\Delta S^\circ$ value would be too favourable (by the same amount). This could lead to the proposal of a different structure in some cases. It is hoped, however, that the ΔH° values, and therefore also the $T\Delta S^\circ$ values, of the more important complexes are accurate enough that such a misinterpretation of the values is unlikely, especially since much more emphasis has generally been put on trends in the thermodynamic values, rather than the absolute values.

The methods used in this investigation have their shortcomings; approximations had to be made and the models were generally not substantiated by other independent methods of analysis. However, the investigation clearly shows that many more complexes exist, in varying metal-to-ligand ratios and degree of condensation and protonation, than the very few complexes previously reported in the literature. The quantitative thermodynamic values obtained experimentally for nearly 100 complexes can certainly be used with much greater confidence than the few values determined previously, which were acquired by making great approximations in the analysis. The models, even if they are proved in future to be slightly inaccurate, too simple or containing some fictitious minor species, are believed to open up possibilities of investigating the systems by different methods as they can be used to calculate optimal conditions for experimental analysis. These models could already be used successfully to explain why some previous investigations under different conditions led to the identification of different complexes. The relatively complicated models for the molybdate(VI) and tungstate(VI)-malate system, for instance, were used very successfully in interpreting (or verifying interpretations of) previously obtained NMR and polarimetric data.

Having established typical stoichiometries of the complexes of these ligands, and having suggested how the available donor groups are possibly utilized in complexation, it is now possible to predict the type of complexes of molybdate(VI) and tungstate(VI) with other, related ligands as well as their formation constants. This could be useful in the design or search of ligands which would bind to molybdate(VI) or tungstate(VI) to form complexes with peculiar characteristics for use in biological systems, for the extraction of the metals or for analytical purposes.

Appendix 1

Summary of titrations

The following tables summarize the titration conditions of the different potentiometric, spectrophotometric and calorimetric investigations.

1.1 Potentiometric titrations

The initial concentrations of the reactants in the test solution and titrant solution, the pH-range covered by the individual titrations and the number of each type of titration used (n) in the final calculation are shown. Initial volumes for the titrations were typically 50 to 90 ml. (A negative value for the [HCl] indicates a [OH] of the same magnitude.) The last column refers to comments on the particular titration or set of titrations, mainly concerning the stability of the mV-readings, which follow the table.

test solution concentrations			titrant concentrations			pH		
[Mo]	[ox ²⁻]	[HCl]	[Mo]t	[ox ²⁻]t	[HCl]t	range	n	comment
	0.05				1.001	5.1 - 1.5	1	
	0.03				0.350	6.3 - 1.5	1	
0.01	0.03				1.001	6.9 - 1.0	1	
0.02	0.03				1.001	7.3 - 1.0	1	
0.01	0.01				1.001	7.0 - 1.0	2	
0.03	0.02				1.001	7.2 - 1.0	1	
[W]	[ox ²⁻]	[HCl]	[W]t	[ox ²⁻]t	[HCl]t	pH	n	A
0.002	0.004				0.350	6.6 - 1.1	1	
0.002	0.003				0.350	6.6 - 1.2	1	
0.002	0.002				0.350	6.5 - 1.1	1	
0.002	0.001				0.350	6.5 - 1.1	1	
0.005	0.010				0.350	7.0 - 1.2	1	
0.005	0.0075				0.350	7.0 - 1.2	1	
0.005	0.005				0.350	6.9 - 1.2	1	
0.01	0.030				1.001	6.9 - 1.1	1	
0.01	0.025				0.350	6.7 - 1.1	1	
0.01	0.015				0.350	6.8 - 1.2	1	
0.02	0.04				1.001	7.3 - 1.0	1	
0.02	0.03				1.001	7.5 - 1.0	1	
[Mo]	[lac ⁻]	[HCl]	[Mo]t	[lac ⁻]t	[HCl]t	pH	n	
	0.05				0.4987	4.8 - 1.6	2	
	0.0517	0.00157			1.002	5.1 - 1.0	2	
	0.1661	0.00473			1.002	5.1 - 1.0	3	
0.01	0.05				0.4987	7.4 - 1.9	2	
0.0098	0.052				1.002	7.1 - 1.0	2	
0.005	0.01				1.002	6.5 - 1.0	2	
0.01	0.02				1.002	6.8 - 1.0	2	
0.05	0.1				1.002	7.6 - 1.0	2	
0.005	0.005				0.1000	6.5 - 2.1	1	

0.05	0.05				0.4987	6.8 - 1.9	1	
0.05	0.01				0.4987	6.9 - 1.9	1	
[W]	[lac⁻]	[HCl]	[W]t	[lac⁻]t	[HCl]t	pH	n	B
0.01	0.1				0.6933	7.8 - 2.0	2	
0.009	0.07				0.6933	7.7 - 2.0	3	
0.001	0.003				0.2973	6.5 - 2.0	2	
0.003	0.009				0.3491	7.2 - 1.8	1	
0.005	0.01				0.3491	7.3 - 2.0	1	
0.01	0.02				0.5136	7.5 - 2.0	2	
[Mo]	[man⁻]	[HCl]	[Mo]t	[man⁻]t	[HCl]t	pH	n	
	0.01				1.007	6.5 - 1.0	2	
	0.05	0.05			- 0.6356	2.0 - 11.5	2	
0.005	0.05				0.3502	7.5 - 1.6	1	
0.01	0.05				0.3502	7.4 - 1.6	2	
0.02	0.05	0.05			0.3492	2.6 - 1.2	1	
0.01	0.01	0.01			0.3492	4.9 - 1.3	2	
0.05	0.05				1.000	7.6 - 1.1	2	
0.1	0.1	0.1			1.000	5.8 - 1.1	1	
0.01	0.005	0.005			0.3492	5.1 - 1.3	2	
[W]	[man⁻]	[HCl]	[W]t	[man⁻]t	[HCl]t	pH	n	C
0.005	0.05				0.3021	8.5 - 3.0	2	
0.001	0.005				0.3021	7.3 - 2.2	2	
0.005	0.025				0.3021	8.2 - 1.0	2	
0.01	0.05				0.3021	8.5 - 2.1	1	
0.005	0.015				0.3021	8.0 - 1.5	1	
0.005	0.015				1.000	7.7 - 1.0	1	
0.02	0.1				0.3021	9.1 - 1.6	1	
0.01	0.025				0.3021	8.3 - 2.6	1	
[Mo]	[mal²⁻]	[HCl]	[Mo]t	[mal²⁻]t	[HCl]t	pH	n	
	0.05				0.999	6.5 - 1.0	2	
0.025	0.10				0.999	8.2 - 1.1	2	
0.01	0.02				0.4405	7.2 - 1.2	1	
0.005	0.005				0.4405	6.5 - 1.1	1	
0.01	0.01				0.4405	7.0 - 1.2	2	
0.05	0.05				0.999	8.2 - 1.0	2	
0.02	0.01				0.4405	7.2 - 1.2	2	
0.01	0.005				0.4405	6.7 - 1.1	2	
[W]	[mal²⁻]	[HCl]	[W]t	[mal²⁻]t	[HCl]t	pH	n	
0.01	0.04972				0.5953	8.4 - 1.9	2	
0.01	0.03007				0.5953	8.4 - 1.9	2	
0.01	0.01984				0.5955	8.3 - 1.9	2	
0.05	0.1001				1.000	9.0 - 1.8	2	
0.01	0.00994				0.5953	7.9 - 1.9	2	D
[Mo]	[cit³⁻]	[HCl]	[Mo]t	[cit³⁻]t	[HCl]t	pH	n	
0.01	0.04	0.1506			0.2503	2.1 - 7.9	2	
0.05	0.1				0.9986	8.7 - 1.0	1	

0.01	0.01				0.350	7.6 - 1.0	2	
0.05	0.05				1.000	8.3 - 1.6	2	
0.1	0.1				0.9986	9.2 - 1.0	1	
0.02	0.01				0.350	7.9 - 1.1	2	
0.01	0.01	0.05			-0.500	2.1 - 9.0	1	
[Mo]	[cit³⁻]	[HCl]	[Mo]t	[cit³⁻]t	[HCl]t	pH	n	E
-	0.02				1.002	7.0 - 1.0	2	2 °C
0.005	0.01				1.002	8.3 - 1.0	2	2 °C
0.01	0.02				1.002	8.9 - 1.0	2	2 °C
0.05	0.1				1.002	10.0 - 1.0	2	2 °C
0.01	0.01				1.002	8.6 - 1.0	2	2 °C
0.05	0.05				1.002	9.7 - 1.0	2	2 °C
0.1	0.1				1.002	10.2 - 1.0	2	2 °C
0.01	0.005				1.002	8.2 - 1.0	2	2 °C
0.02	0.01				1.002	8.8 - 7.0	2	2 °C
[W]	[cit³⁻]	[HCl]	[W]t	[cit³⁻]t	[HCl]t	pH	n	F
0.005	0.02503				0.6940	9.3 - 2.9	1	
0.05	0.2				0.9986	9.4 - 1.2	2	
0.05	0.1				0.9984	10.5 - 1.0	2	
0.1	0.2				0.9986	9.2 - 1.0	1	
0.01	0.02				0.6940	9.6 - 2.0	1	
0.05	0.075				1.000	10.4 - 1.0	1	
0.01	0.01				0.6940	9.2 - 2.0	1	
[Mo]	[tart²⁻]	[HCl]	[Mo]t	[tart²⁻]t	[HCl]t	pH	n	
	0.05				1.000	5 - 1	2	
0.02	0.01	-0.044			0.35	6.9 - 2.0	1	
0.02	0.01	0.02			1.001	5.2 - 1.0	1	
0.02	0.01	0.1426		0.1	0.2	1.0 - 1.1	1	
0.05	0.031				1.001	7.7 - 1.0	1	
0.0455	0.035				1.001	7.9 - 1.0	1	
0.05	0.05				1.001	8.0 - 1.1	1	
0.025	0.025				1.001	7.7 - 1.0	1	
0.05	0.07				1.001	8.2 - 1.0	1	
0.025	0.04				1.001	7.8 - 1.0	1	
0.01	0.045				0.350	7.9 - 2.3	1	
[W]	[tart²⁻]	[HCl]	[W]t	[tart²⁻]t	[HCl]t	pH	n	G
	0.05				1.000	5 - 1	2	
0.02	0.05				1.001	8.5 - 1.1	1	
0.02	0.04				1.001	8.7 - 1.0	2	
0.02	0.03				1.001	8.4 - 1.0	1	
0.01	0.015				0.350	8.2 - 1.3	2	
0.005	0.0075				0.350	7.6 - 1.2	1	
0.04	0.04	0.08			1.001	4.1 - 1.1	1	
0.03	0.03	0.06			1.001	4.1 - 1.0	1	
0.01	0.01				0.350	7.8 - 1.3	1	
0.005	0.005				0.350	7.3 - 1.2	1	

0.02	0.015	0.037			1.001	3.6 - 1.0	1	
0.002	-			0.1000	0.2000	6.0 - 2.4	1	
0.005	0.0075			0.1000	0.2000	7.5 - 2.7	1	
0.03	0.03	0.06		0.1000	0.2000	4.1 - 2.1	1	
[Mo]	[Hasp⁻]	[HCl]	[Mo]t	[Hasp⁻]t	[HCl]t	pH	n	
-	0.05	-0.10			1.002	10.7 - 1.1	2	
-	0.0296				1.000	3.2 - 1.1	1	
-	0.0296				-0.6356	3.0 - 9.8	2	
0.005	0.1	-0.2			1.000	10.0 - 1.0	2	
0.005	0.05	-0.1			1.000	10.0 - 1.0	2	
0.01	0.05	-0.1			1.000	10.0 - 1.2	2	
0.02	0.10				1.002	7.0 - 1.2	2	
0.05	0.25				1.002	7.5 - 2.6	2	
-	0.08488	0.1514	0.1		-		1	H1
-	0.08772	0.1231	0.1		-		1	H2
-	0.08969	0.1930	0.1		-		1	H3
-	0.09418	0.0583	0.1		-		1	H4
0.005	0.025		0.0500	0.2500	0.0500	6.7 - 5.2	2	H5
[W]	[Hasp⁻]	[HCl]	[W]t	[Hasp⁻]t	[HCl]t	pH	n	l
0.005	0.02	-0.01632			1.001	10 - 1.0	2	
0.01	0.02	-0.01632			1.001	9.9 - 1.1	1	
0.01	0.01	-0.00816			1.001	9.7 - 1.0	1	
[Mo]	[nta³⁻]	[HCl]	[Mo]t	[nta³⁻]t	[HCl]t	pH	n	
	0.02				0.999	9.9 - 1.0	2	
	0.05				0.999	10.2 - 2.0	2	J1
0.0075	0.075				0.999	7.4 - 2.0	2	J2
0.01	0.075				0.999	7.6 - 2.0	2	J3
0.01	0.05				0.999	7.3 - 1.7	2	J4
0.01	0.01				0.999	7.6 - 1.0	2	
0.05	0.05				0.999	7.7 - 1.0	2	
0.075	0.075				0.999	7.6 - 1.0	2	
0.025	0.01				0.999	5.3 - 1.0	2	
[W]	[nta³⁻]	[HCl]	[W]t	[nta³⁻]t	[HCl]t	pH	n	K
0.005	0.1	0.04767			1.001	10.4 - 2.2	2	K1
0.0025	0.02				1.001	9.7 - 1.1	2	
0.005	0.025				1.001	10.0 - 1.1	2	
0.01	0.04				1.001	10.2 - 1.1	1	
0.005	0.01				1.001	9.8 - 1.1	2	
0.01	0.015				1.001	9.9 - 1.0	2	
0.01	0.01	0.02			1.001	5.9 - 1.1	2	
0.02	0.02	0.06			1.001	2.7 - 1.0	2	
[W]	[nta³⁻]	[HCl]	[W]t	[nta³⁻]t	[HCl]t	pH	n	L
0.005	0.025				0.3507	8.3 - 2.7	1	
0.01	0.03				0.3507	9.2 - 2.3	1	
0.005	0.01				0.3507	9.4 - 1.5	1	
0.02	0.05				0.3507	9.7 - 2.1	1	

- A** Titrant was only added after the mV-readings stabilized. Slow reactions occurred when the solutions of tungstate and oxalate were acidified to $F > 0.6$ (F = degree of protonation), suggesting that possibly the tungstate was not complexed under those conditions despite the presence of the ligand. The slow reactions were more prominent in solutions with smaller excess of oxalate and higher tungstate concentration. The only titration attempted with excess of tungstate was for the conditions, 0.002 M tungstate and 0.001 M oxalate. Despite the relatively low tungstate concentration, the reactions in the pH range 4.4 - 3.3 were so slow that no mV-readings were taken until pH was lower than 3.3.
- B** Lower concentrations of tungstate or a greater excess of lactate had to be used than in the case of molybdate to prevent the slow reactions occurring in tungstate solutions acidified to $F > 0.6$ (F = degree of protonation , Appendix 5).
- C** By manually controlling the addition of acid and monitoring the stability of pH readings the absence of slow equilibria could be verified for these titrations.
- D** At pH < 4.0 preliminary calculations indicate the presence of higher than 7% isopolytungstate ions. These data were not suitable for analysis.
- E** These molybdate-citrate titrations were carried out at temperature 2°C.
- F** When citrate was in excess, stable potentials were obtained within seconds of addition of the titrant. In the case of an equimolar solution (0.05 M) of tungstate and citrate, for example, a drift in potential with time was observed which is typical of that which occurs in tungstate solutions acidified to a degree of protonation, F , > 0.6 . The highest equimolar concentration of tungstate and citrate used in the investigation, and which gave stable potentials in less than 1 min, was 0.01 M.
- G** Most titrations had regions of slow equilibria, especially at pH>4. Where the concentration of tungstate was low and the tartrate in excess, stable potentials were obtained within reasonable time after each addition of the titrant, but titrations of solutions with higher tungstate concentration and no, or little, excess of tartrate were started at pH~4 to avoid the more pronounced slow reactions.
- H1,2,3,4** Aspartate solutions acidified to pH ~ 1.8 , 2.2 , 2.6 and 3.5 respectively , titrated with 0.1 M molybdate up to a molybdate:aspartate ratio of 1:5.

- H5** The ratio of molybdate:aspartate was kept constant but the concentration increased from 0.005:0.025 to 0.025:0.125 M while the pH varied from 6.9 to 5
- I** Titrant was added manually to ensure that equilibrium was reached after every addition before taking a mV reading. The mV readings were unstable in the pH region ~ 4.2 - 2.8 directly after addition of titrant until equilibrium was attained. Equilibrium was established within about 2 minutes in the titration of the solution with the four-fold excess of aspartate and about 6 minutes in the titration of the solution with the two-fold excess. The mV readings at pH~4.2 stabilized too slowly during the titration of the equimolar solution. It was decided to "jump" this region of instability by adding a relatively large amount of titrant. At pH~3.3 only a few minutes were needed to reach equilibrium and at pH~2.8 the titration could proceed at normal speed. (It was decided to find a preliminary model, using only these three titrations. The preliminary model showed that it would be meaningless to extend the titration conditions.
- J1,2,3,4** Titrations were stopped at pH ~2 due to precipitation.
- K** Titrant was added manually to ensure that equilibrium was reached after every addition before taking a mV reading. Where mV readings stabilised within a few minutes, measurements were taken, but in regions where equilibria were established much slower, quick additions of titrant were made (without taking mV-readings) till a pH was reached where readings stabilized relatively quickly again. Accurate readings were difficult (or impossible) for the most titrations in the pH-region 8 - 4 . Slow reactions in the pH ~ 4 could indicate slow tungstate equilibria, BUT slow reactions at pH 7 - 8 cannot be ascribed to slow tungstate equilibria, as the protonation is simply not high enough. Local initial acid could result in the formation of kinetically stable ions. Another indication that these slow reactions are due to complexation and not tungstate equilibria is, that the slow equilibria seemed to be more prominent where nta was in greater excess and complexation would be encouraged.
- K1** Titration was stopped at pH~2.2 due to precipitation.
- L** A few point titrations were done. (The initial volumes were 20 ml, instead of the usual ~80 ml.) The solutions were allowed to stand for a day before determining the pH. These pH values were compared to the readings taken two days after preparation. The measurements on the different days did not differ significantly, indicating that equilibria had been established within a day. Despite the state of equilibrium, measurements in certain pH ranges were difficult because of electrode drifts. No reason for this effect could be established as it apparently happened at will, and no way could be found to avoid it. It was decided that under these circumstances it was best to take a mV reading as quickly as possible.

1.2 Spectrophotometric titrations

The initial concentrations of the reactants in the test solution and titrant solution, the pH-range covered by the titration and the number of spectra measured during the titration are shown. (A negative value for the [HCl] indicates a [OH] of the same magnitude). The last column refers to comments on the particular titration and measurement of spectra, particularly regarding the wavelength range and increments, and the path length of the cuvette.

test solution concentrations			titrant concentrations			pH		
[Mo]	[man ⁻]	[HCl]	[Mo]t	[man ⁻]t	[HCl]t	range	<i>n</i>	comment
	0.00008	0.01		0.00008	-0.01	2.1 - 4.7	7	A1
0.0002	0.001		0.0002	0.001	0.01	6.0 - 3.4	20	A2
0.00002	0.0008		0.00002	0.0008	0.01	7.0 - 2.0	20	A3
[Mo]	[mal ²⁻]	[HCl]	[Mo]t	[mal ²⁻]t	[HCl]t	pH	<i>n</i>	
	0.0016			0.0016	0.25	5.7 - 1.3	17	B
0.0001	0.0001		0.0001	0.0001	0.1	5.6 - 1.5	21	B
[Mo]	[cit ³⁻]	[HCl]	[Mo]t	[cit ³⁻]t	[HCl]t	pH	<i>n</i>	
	0.0016			0.0016	0.25	6.0 - 1.4	19	C
0.0001	0.00012		0.0001	0.00012	0.025	5.6 - 1.0	24	C
[Mo]	[Hasp ⁻]	[HCl]	[Mo]t	[Hasp ⁻]t	[HCl]t	pH	<i>n</i>	
	0.1			0.1	0.1	7.0 - 2.3		D
0.005	0.1		0.005	0.1	0.1	7.0 - 2.3	20	D
0.01	0.1		0.01	0.1	0.1	7.0 - 2.3	20	D
[Mo]	[nta ³⁻]	[HCl]	[Mo]t	[nta ³⁻]t	[HCl]t	pH	<i>n</i>	
	0.00025			0.00025	0.01	5.1 - 1.3	13	E
0.0002	0.00025		0.0002	0.00025	0.01	5.2 - 2.7	13	E

- A1** Wavelength range 206 - 250 nm; at 2 nm intervals; Quartz cuvettes of path length 1.0 cm.
- A2** Wavelength range 219 - 250 nm; at 2 nm intervals; Quartz cuvettes of path length 0.5 cm.
- A3** Wavelength range 219 - 250 nm; at 2 nm intervals; Quartz cuvettes of path length 1.0 cm
- B** Wavelength range 206 - 320 nm; at 3 nm intervals; Quartz cuvettes of path length 1.0 cm.
- C** Wavelength range 206 - 320 nm; at 3 nm intervals; Quartz cuvettes of path length 1.0 cm.
- D** Absorbances were measured against air in the wavelength range 222 - 300 nm at 2 nm intervals using a flow through quartz cuvettes [A15]. The path length was set at 0.02482 cm (calibrated length).
- The absorbance of the aspartate species at the chosen path length was small and showed only a small dependence on pH below 230 nm. (The absorbance increased rapidly only below 220 nm.) An aspartate spectrum measured against air could, therefore, simply be subtracted from the molybdate-aspartate spectra measured against air in order to get data representing complexation.
- E** Wavelength range 212 - 300 nm; at 2 nm intervals; Quartz cuvettes of path length 1.0 cm.

1.3 Calorimetric titrations

The initial concentrations of the reactants in the test solution are shown. Initial volumes for the titrations were typically 20 or 25 ml. The titrant was a solution of 1 M HCl.

A negative value for the [HCl] indicates a [OH] of the same magnitude.

Titration from previous investigation [2]

Concentrations of reactants		
[Mo]	[ox ²⁻]	[HCl]
0.05	0.05	
[W]	[ox ²⁻]	[HCl]
	0.025	
0.01	0.025	
[Mo]	[lac ⁻]	[HCl]
	0.1	
0.01	0.05	
[W]	[lac ⁻]	[HCl]
0.01	0.0497	
[Mo]	[man ⁻]	[HCl]
	0.1	
0.02	0.10	
[W]	[man ⁻]	[HCl]
	0.1	
0.02	0.10	
[Mo]	[mal ²⁻]	[HCl]
	0.02	
0.01	0.04	
0.01	0.04	
0.05	0.20	
0.05	0.20	
0.03	0.05	
0.03	0.05	
0.03	0.03	
0.03	0.03	
[W]	[mal ²⁻]	[HCl]
0.02	0.15	
0.02	0.04	
0.1	0.1	

#

Concentrations of reactants		
[Mo]	[cit ³⁻]	[HCl]
0.01	0.01	
0.04	0.04	
0.05	0.05	
[W]	[cit ³⁻]	[HCl]
0.05	0.075	
0.025	0.03	
0.01	0.01	
[Mo]	[tart ²⁻]	[HCl]
0.05	0.05	0.008
0.025	0.05	0.008
0.025	0.1	0.008
[W]	[tart ²⁻]	[HCl]
0.02	0.03	
0.02	0.04	
0.02	0.10	
[Mo]	[Hasp ⁻]	[HCl]
	0.1	
0.01	0.1	
[W]	[Hasp ⁻]	[HCl]
0.01	0.02	-0.01629
0.01	0.02	0.00246
[Mo]	[nta ³⁻]	[HCl]
	0.01	
	0.04	0.04
0.01	0.01	
0.04	0.06	0.08
[W]	[nta ³⁻]	[HCl]
0.01	0.1	
0.01	0.1	0.08

Appendix 2

Distribution of the ligand species

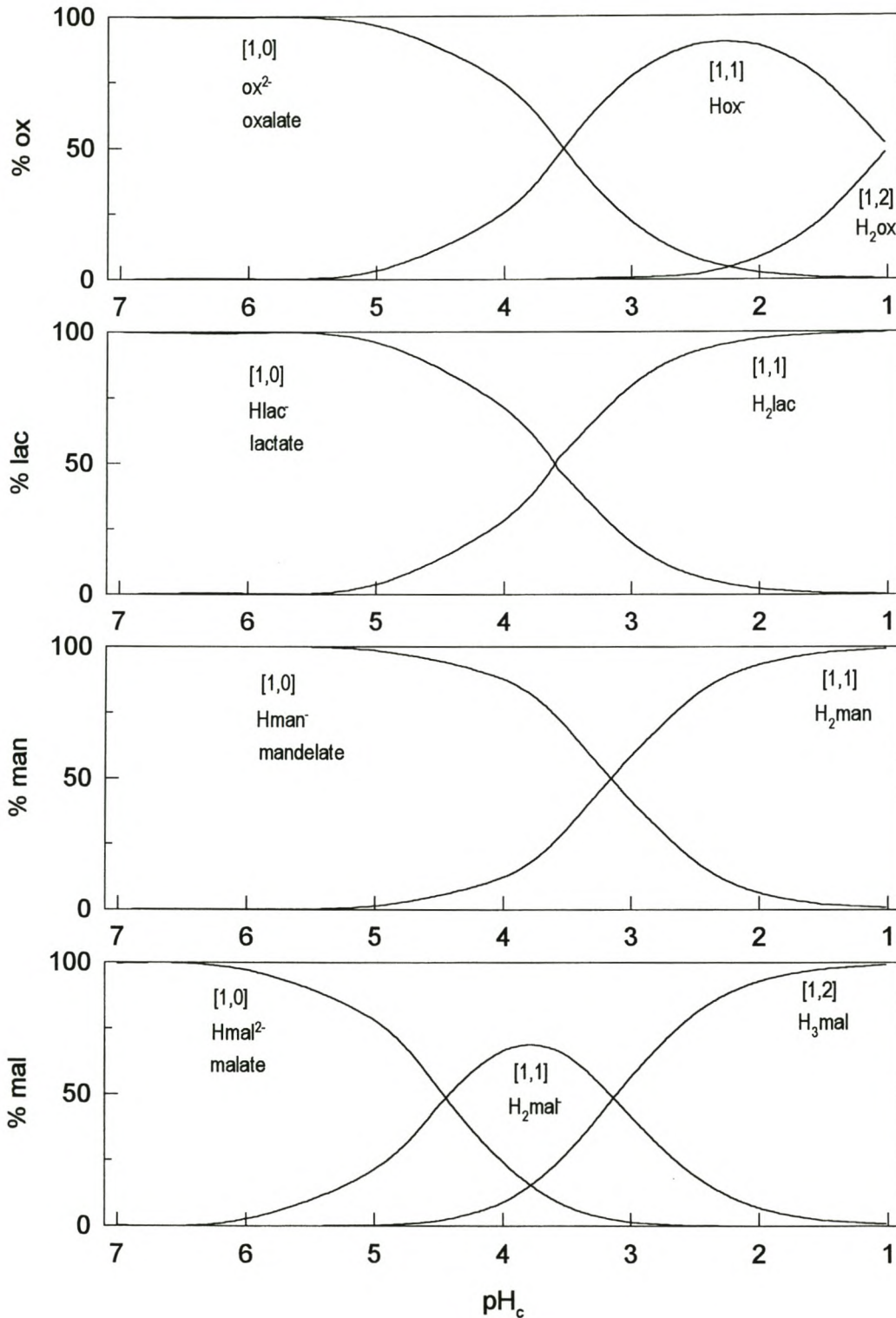


Fig. A1 Distribution of oxalate, lactate, mandelate and malate species in 1 M (Na)Cl medium at 25°C

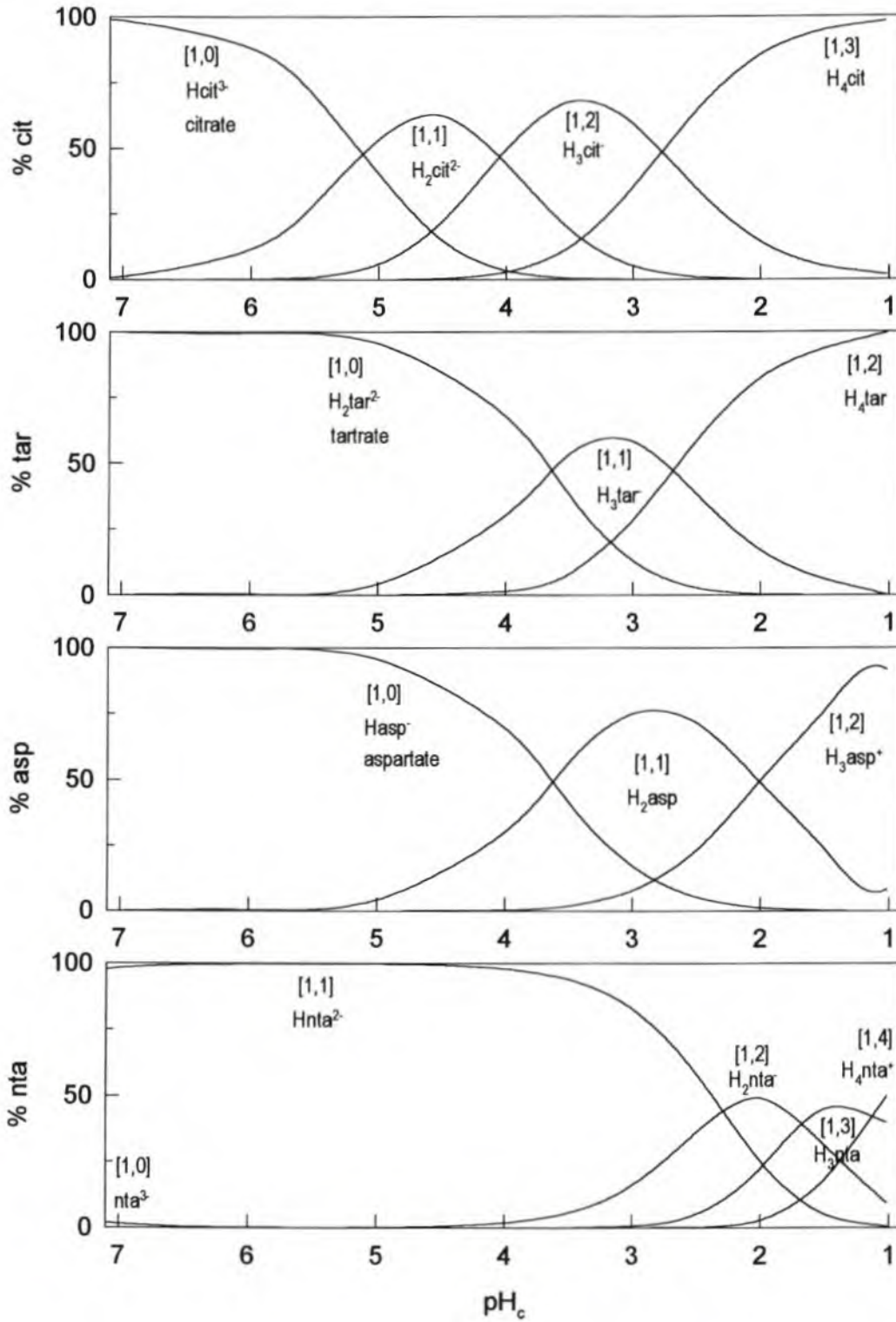


Fig. A2 Distribution of citrate, tartrate, aspartate and nta species in 1 M (Na)Cl medium at 25°C

Appendix 3

Structures previously determined

The complex anions which have been identified by X-ray analysis of their salts (and can therefore be regarded as certain), as well as other likely proposed structures are tabulated and shown in the two figures below.

Table A1. Summary of known structures of complex anions from the literature.

X-ray analysis (cf. Fig. A3)			
Complex Anions in solids	[p,q,r]	index in figure	Reference
[MoO ₃ (ox)(H ₂ O)]	[1Mo , 1ox , 2] ²⁻	A	[76,77]
[Mo ₂ O ₅ (ox) ₂ (H ₂ O) ₂]	[2Mo , 2ox , 6] ²⁻	B	[75,76]
[Mo ₄ O ₁₁ (mal) ₂]	[4Mo , 2mal, 8] ⁴⁻	C	[78-80]
[MoO ₂ (Hmal) ₂]	[1Mo , 2mal, 4] ²⁻	D	[81]
[Mo ₄ O ₁₁ (Hcit) ₂]	[4Mo , 2cit , 10] ⁴⁻	E	[82,83]
[Mo ₂ O ₅ (cit) ₂]	[2Mo , 2cit , 4] ⁶⁻	F	[86]
[V ₂ O ₅ (cit) ₂]	[2W , 2cit , 4] ⁶⁻	G	[84,85]
[MoO ₂ (Htart) ₂]	[1Mo , 2tart , 4] ²⁻	H	[87]
[MoO ₃ (nta)]	[1Mo , 1nta , 2] ³⁻	I	[88]
[Mo ₂ O ₅ (Hnta) ₂]	[2Mo , 2nta , 8] ²⁻	J	[89,90]
other analyses (cf. Fig. A4)			
Complex Anions in solids	[p,q,r]		Reference
[MoO ₂ (OH) ₂ (C ₂ O ₄) ₂] ⁴⁻	[1Mo , 2ox , 2] ⁴⁻		[91]
[Mo ₂ O ₅ (OH) ₂ (C ₂ O ₄) ₂] ⁴⁻	[2Mo , 2ox , 4] ⁴⁻		[91]
[WO ₃ (ox)] ²⁻	[1W , 1ox , 2] ²⁻		[103]
[MoO ₂ (lac) ₂] ²⁻	[1Mo , 2lac , 2] ²⁻		[93]
[Mo ₂ O ₅ (lac) ₂ (H ₂ O) ₂] ²⁻	[2Mo , 2lac , 4] ²⁻	K	[92]
[WO ₂ (lac) ₂] ²⁻	[1W , 2lac , 2] ²⁻		[93]
[MoO ₂ (man) ₂] ²⁻	[1Mo , 2man , 2] ²⁻		[93]
[WO ₂ (man) ₂] ²⁻	[1W , 2man , 2] ²⁻		[93]
[MoO ₂ (Hmal) ₂] ²⁻	[1Mo , 2mal , 4] ²⁻		[81]
[MoO ₂ (mal) ₂] ⁴⁻	[1Mo , 2mal , 2] ⁴⁻		[81]
[MoO ₂ .H(mal) ₂] ²⁻	[1Mo , 2mal , 4] ²⁻		[81]
[MoO ₃ (cit)(H ₂ O)] ⁴⁻	[1Mo , 1cit , 1] ⁴⁻	L	[94]
[Mo ₂ O ₅ (cit) ₂] ⁶⁻	[2Mo , 2cit , 4] ⁶⁻	M	[94]
[Mo ₂ O ₅ (Hcit) ₂] ⁴⁻	[2Mo , 2cit , 6] ⁴⁻		[94]
[Mo ₂ O ₅ (OH)(H ₂ O)(Hcit)] ²⁻	[2Mo , 1cit , 5] ²⁻	N	[95]
[MoO ₃ (asp)] ²⁻	[1Mo , 1asp , 1] ²⁻	O	[101]
[WO ₃ (nta)]	[1W , 1nta , 2] ³⁻		[102]

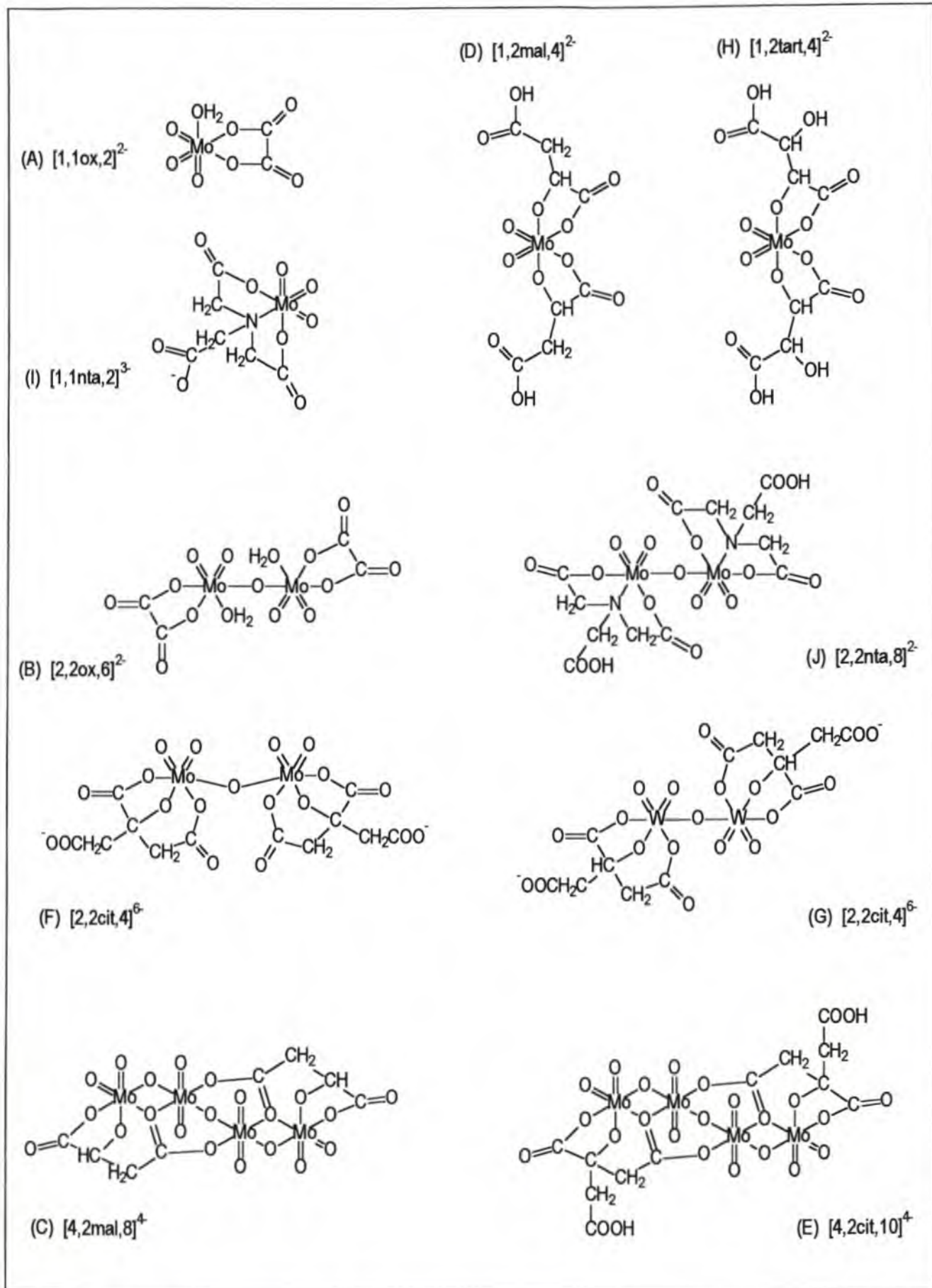


Fig. A3 Structures determined by X-ray crystallography.

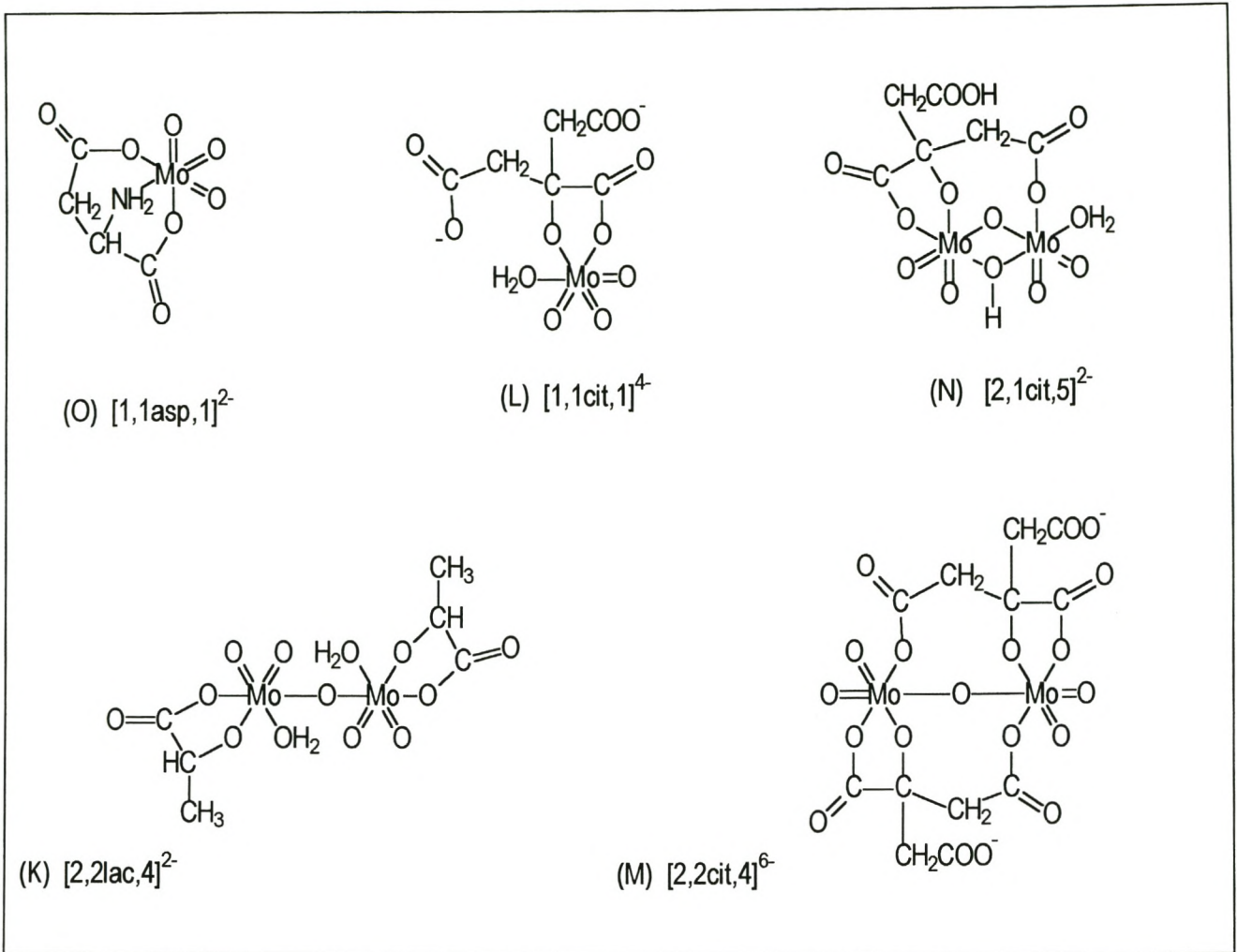


Fig. A4 Structures determined by other methods than X-ray crystallography.

Appendix 4

Summary of thermodynamic values

The following tables contain the calculated and approximate values shown in the relevant tables in Chapter 3 as well as values which were proposed in Chapter 4 which could not be calculated from the experimental data. The tables pertaining to the Mo and W-oxalate system contain values from different models (*cf.* Table 3.1.2 and 3.1.4).

proposed values in brackets (Chapter 4)

approximate values used in calculation

Mo-oxalate

COMPLEX	$\log\beta_{\text{pqr}} \pm 3 \sigma$	ΔG° (kJ mol ⁻¹)	ΔH° (kJ mol ⁻¹)	$T\Delta S^\circ$ (kJ mol ⁻¹)
[0, 1ox, 1] ⁻	3.52 ± 0.02	-20.1		
[0, 1ox, 2]	4.41 ± 0.02	-25.2		
[1Mo, 1ox, 2] ²⁻	13.65 ± 0.01	-77.9	-59.4 ± 1.0	19
[1Mo, 1ox, 3] ⁻	15.32 ± 0.19	-87.46	-57.9 ± 2.0	30
[2Mo, 2ox, 5] ³⁻	31.19 ± 0.08	-178.1	-118.1 ± 4.0	60
[2Mo, 2ox, 6] ²⁻	34.10 ± 0.05	-194.7	-118.9 ± 2.0	76
[2Mo, 1ox, 5] ⁻	25.88 ± 0.05	-147.7	-92 ± 15 [-106]	56 [42]
[1Mo, 2ox, 4] ²⁻	20.50 ± 0.19	-117.0	[-86]	[31]
[4Mo, 2ox, 8] ⁴⁻	49.50 ± 0.22	-282.4	[-200]	[82]
[4Mo, 4ox, 10] ⁶⁻	64.63 ± 0.25		-250 ± 10	119

W-oxalate

COMPLEX	$\log\beta_{\text{pqr}} \pm 3 \sigma$	ΔG° (kJ mol ⁻¹)	ΔH° (kJ mol ⁻¹)	$T\Delta S^\circ$ (kJ mol ⁻¹)
[0, 1ox, 1] ⁻	3.52 ± 0.02	-20.1	+3.17 ± 0.5	23.3
[0, 1ox, 2]	4.41 ± 0.02	-25.2	+5.18 ± 0.5	30.4-
[1W, 1ox, 2] ²⁻	13.65 ± 0.02	-78	-70.8 ± 0.5	7.1
[1W, 1ox, 3] ⁻	15.89 ± 0.32	-91	-66.7 ± 1.0	24.0
[2W, 2ox, 4] ⁴⁻	28.43 ± 0.18	-161	-116 ± 5	46
[2W, 2ox, 5] ³⁻	33.09 ± 0.04	-188	-137.7 ± 2.0	51.1
[2W, 2ox, 6] ²⁻	34.52 ± 0.31	-197	-138 ± 4	59
[2W, 1ox, 5] ⁻	28.24 ± 0.24	-161	[-128]	[33]
[1W, 2ox, 4] ²⁻	21.53 ± 0.35	-123	-87 ± 5 [96]	36 [27]
[4W, 2ox, 8] ⁴⁻	55.24 ± 0.25	-315	[-233]	[82]
[4W, 4ox, 9] ⁴⁻	64.10 ± 0.25	-366	-277 ± 5	89
[4W, 4ox, 10] ⁶⁻	67.99 ± 0.25	-388	-279 ± 5	109

Mo-lactate

COMPLEX	$\log \beta_{pqr} \pm 3 \sigma$	ΔG° (kJ mol ⁻¹)	ΔH° (kJ mol ⁻¹)	$T\Delta S^\circ$ (kJ mol ⁻¹)
[0,1lac,1] ⁻	3.60 ± 0.01	-20.53	-1.7 ± 2	18.8
[1Mo,2lac,1] ³⁻	7.46 ± 0.46	-42.67	[-60]	[-17]
[1Mo,2lac,2] ²⁻	15.71 ± 0.01	-89.67	-72 ± 2	18
[1Mo,2lac,3] ⁻	16.78 ± 0.09	-95.75	[-60]	[36]
[1Mo,1lac,2] ⁻	11.76 ± 0.03	-67.10	[-50]	[17]
[1Mo,1lac,3] ⁻	12.66 ± 0.32	-72.24	[-50]	[22]
[2Mo,2lac,2] ⁴⁻	16.07 ± 0.14	-91.70	[-90]	[2]
[2Mo,2lac,3] ³⁻	21.70 ± 0.14	-123.8	[-115]	[9]
[2Mo,2lac,4] ²⁻	24.97 ± 0.30	-142.5	[-115]	[28]
[2Mo,1lac,3] ²⁻	18.44 ± 0.38	-105.2	[-82]	[23]
[2Mo,1lac,4] ⁻	21.53 ± 0.12	-122.9	[-82]	[41]
[2Mo,1lac,5]	23.12 ± 0.14	-132.0	[-82]	[50]

W-lactate

COMPLEX	$\log \beta_{pqr} \pm 3 \sigma$	ΔG° (kJ mol ⁻¹)	ΔH° (kJ mol ⁻¹)	$T\Delta S^\circ$ (kJ mol ⁻¹)
[0,1lac,1] ⁻	3.60 ± 0.01	-20.53	-1.7 ± 2	18.8
[1W,2lac,2] ²⁻	17.47 ± 0.01	-99.72	-80 ± 2	20
[1W,2lac,3] ⁻	18.38 ± 0.11	-104.9	[-70]	[35]
[1W,1lac,2] ⁻	13.03 ± 0.07	-74.35	[-62]	[12]
[1W,1lac,3] ⁻	14.56 ± 0.13	-83.1	[-62]	[21]
[2W,2lac,3] ³⁻	25.47 ± 0.11	-145.3	[-114]	[31]

Mo-mandelate

COMPLEX	$\log \beta_{pqr} \pm 3 \sigma$	ΔG° (kJ mol ⁻¹)	ΔH° (kJ mol ⁻¹)	$T\Delta S^\circ$ (kJ mol ⁻¹)
[0,1,1] ⁻	3.15 ± 0.01	-17.98	-0.5 ± 0.5	17.5
[1Mo,2man,1] ³⁻	7.80 ± 0.30	-44.5	[-60]	[-16]
[1Mo,2man,2] ²⁻	15.93 ± 0.01	-90.03	-78.2 ± 0.5	12.7
[1Mo,2man,3] ⁻	16.27 ± 0.29	-92.8	[-60]	[33]
[1Mo,1man,1] ²⁻	6.83 ± 0.12	-39.0	[-35]	[4]
[1Mo,1man,2] ⁻	11.57 ± 0.06	-66.0	[-50]	[16]
[2Mo,2man,4] ²⁻	25.87 ± 0.03	-147.6	[-115]	[33]
[2Mo,2man,5] ⁻	26.86 ± 0.12	-153.3	[-115]	[38]
[2Mo,1man,3] ²⁻	19.00 ± 0.15	-108.4	[-82]	[26]
[2Mo,1man,4] ⁻	21.18 ± 0.24	-120.9	[-82]	[39]
[2Mo,1man,5]	23.00 ± 0.06	-131.2	[-82]	[49]

W-mandelate

COMPLEX	$\log \beta_{pqr} \pm 3 \sigma$	ΔG° (kJ mol ⁻¹)	ΔH° (kJ mol ⁻¹)	$T\Delta S^\circ$ (kJ mol ⁻¹)
[0,1man,1] ⁻	3.15 ± 0.01	-17.98	-0.5 ± 0.5	17.5
[1W,2man,2] ²⁻	17.59 ± 0.01	-100.4	-86.3 ± 0.5	14.1
[1W,2man,3] ⁻	18.09 ± 0.30	-103.2	[-70]	[33]
[1W,1man,2] ⁻	13.78 ± 0.07	-78.6	[-62]	[17]
[1W,1man,3]	15.33 ± 0.07	-87.5	[-62]	[26]

Mo-malate

COMPLEX	$\log\beta_{\text{pqr}} \pm 3 \sigma$	ΔG° (kJ mol ⁻¹)	ΔH° (kJ mol ⁻¹)	$T\Delta S^\circ$ (kJ mol ⁻¹)
[0,1mal,1] ⁻	4.44 ± 0.01	-25.3	-2.0 ± 0.1	23.3
[0,1mal,2]	7.57 ± 0.01	-43.2	-6.5 ± 0.1	36.7
[1Mo,2mal,2] ⁴⁻	15.48 ± 0.01	-88.36	-76.2 ± 0.5	12
[1Mo,2mal,3] ³⁻	20.13 ± 0.01	-114.9	-82.3 ± 0.5	33
[1Mo,2mal,4] ²⁻	24.14 ± 0.01	-137.8	-83.7 ± 0.5	54
[1Mo,1mal,1] ³⁻	7.47 ± 0.01	-42.64	-50.1 ± 1	-8
[1Mo,1mal,2] ²⁻	13.23 ± 0.01	-75.52	-49.2 ± 0.5	26
[1Mo,1mal,3] ⁻	15.87 ± 0.08	-90.59	-49.6 ± 0.5	41
[2Mo,2mal,4] ⁴⁻	28.06 ± 0.03	-160.2	-115 ± 5	46
[2Mo,2mal,5] ³⁻	32.01 ± 0.07	-182.7	-119 ± 5	64
[2Mo,1mal,3] ³⁻	20.10 ± 0.04	-114.7	-82 ± 5	32
[2Mo,1mal,4] ²⁻	24.35 ± 0.24	-139.0	-112 ± 5	27
[4Mo,2mal,8] ⁴⁻	52.92 ± 0.03	-302.1	-233 ± 5	69
[4Mo,2mal,9] ³⁻	54.35 ± 0.05	-310.2	-226 ± 5	84
[4Mo,2mal,10] ²⁻	55.27 ± 0.09	-315.5	-191 ± 10	125
[4Mo,4mal,11] ⁵⁻	69.92 ± 0.09	-399.1	-239 ± 15	160

W-malate

COMPLEX	$\log\beta_{\text{pqr}} \pm 3 \sigma$	ΔG° (kJ mol ⁻¹)	ΔH° (kJ mol ⁻¹)	$T\Delta S^\circ$ (kJ mol ⁻¹)
[0,1mal,1] ⁻	4.44 ± 0.01	-25.3	-2.0 ± 0.1	23.3
[0,1mal,2]	7.57 ± 0.01	-43.2	-6.5 ± 0.1	36.7
[1W,2mal,2] ⁴⁻	17.20 ± 0.01	-98.2	-82.5 ± 0.5	15.7
[1W,2mal,3] ³⁻	21.70 ± 0.02	-123.9	-88.2 ± 0.5	35.7
[1W,2mal,4] ²⁻	25.60 ± 0.01	-146.2	-91.8 ± 0.6	54.4
[1W,1mal,1] ³⁻	8.85 ± 0.01	-50.5	-62.8 ± 0.5	-12.3
[1W,1mal,2] ²⁻	14.78 ± 0.06	-84.4	-59.8 ± 0.5	24.6
[1W,1mal,3] ⁻	17.26 ± 0.03	-98.5	-63.0 ± 2	36
[2W,2mal,2] ⁶⁻	18.87 ± 0.06	-107.7	-119 ± 3	-11
[2W,2mal,3] ⁵⁻	25.72 ± 0.10	-146.8	-114 ± 5	33
[2W,2mal,4] ⁴⁻	31.88 ± 0.07	-182.0	-142 ± 3	40
[2W,1mal,3] ³⁻	23.07 ± 0.33	-131.7	-106 ± 20	26
[4W,4mal,11] ⁵⁻	73.60 ± 0.15	-420.1	-341 ± 30	79

Mo-citrate

COMPLEX	$\log\beta_{\text{pqr}} \pm 3 \sigma$	ΔG° (kJ mol ⁻¹)	ΔH° (kJ mol ⁻¹)	$T\Delta S^\circ$ (kJ mol ⁻¹)
[0,1cit,1]	5.12 ± 0.01	-29.2	-1.3 ± 0.1	28
[0,1cit,2]	9.17 ± 0.01	-52.4	-5.8 ± 0.1	47
[0,1cit,2]	11.94 ± 0.02	-68.2	-10.1 ± 0.1	58
[1Mo,1cit,1] ⁴⁻	8.34 ± 0.01	-47.7	-49.9 ± 0.5	-2.2
[1Mo,1cit,2] ³⁻	15.00 ± 0.01	-85.6	-56.4 ± 0.5	29.2
[1Mo,1cit,3] ²⁻	19.62 ± 0.01	-112.0	-69 ± 2	42.7
[1Mo,1cit,4] ⁻	21.12 ± 0.11	-120.5	-73 ± 2	47.6
[2Mo,2cit,4] ⁶⁻	31.02 ± 0.03	-177.1	-142 ± 2	36
[2Mo,2cit,5] ⁵⁻	35.86 ± 0.05	-204.7	-138 ± 3	67
[2Mo,2cit,6] ⁴⁻	40.08 ± 0.07	-228.8	-135 ± 4	94
[1Mo,2cit,4] ⁴⁻	25.34 ± 0.18	-144.6	-86	# 59 #
[1Mo,2cit,5] ³⁻	29.54 ± 0.11	-168.6	-90	# 79 #
[1Mo,2cit,6] ²⁻	33.34 ± 0.02	-190.3	-93 ± 5	97
[2Mo,1cit,3] ⁴⁻	21.73 ± 0.09	-124.0	-82	# 42 #
[2Mo,1cit,4] ³⁻	26.90 ± 0.06	-153.5	-82 ± 10	72
[2Mo,1cit,5] ²⁻	31.53 ± 0.03	-180.0	-123 ± 2	57
[4Mo,2cit,8] ⁶⁻	-	-		
[4Mo,2cit,9] ⁵⁻	60.76 ± 0.15	-346.8	-242	# 105 #
[4Mo,2cit,10] ⁴⁻	64.69 ± 0.11	-369.2	-242 ± 8	127
[4Mo,4cit,11] ³⁻	77.45 ± 0.24	-442.1	-308 ± 10	134
[4Mo,4cit,12] ⁵⁻	(81.33) #	(-464) #		

W-citrate

COMPLEX	$\log\beta_{\text{pqr}} \pm 3 \sigma$	ΔG° (kJ mol ⁻¹)	ΔH° (kJ mol ⁻¹)	$T\Delta S^\circ$ (kJ mol ⁻¹)
[0,1cit,1]	5.12 ± 0.01	-29.2	-1.3 ± 0.1	28
[0,1cit,2]	9.17 ± 0.01	-52.4	-5.8 ± 0.1	47
[0,1cit,2]	11.94 ± 0.02	-68.2	-10.1 ± 0.1	58
[1W,1cit,1] ⁴⁻	10.21 ± 0.01	-58.3	-63.1 ± 2.0	-5
[1W,1cit,2] ³⁻	17.03 ± 0.01	-97.2	-66.5 ± 2.0	31
[1W,1cit,3] ²⁻	21.67 ± 0.01	-123.7	-74.5 ± 2.0	49
[1W,1cit,4] ⁻	22.82 ± 0.03	-130.2	-74.3 ± 2.0	56
[2W,2cit,4] ⁶⁻	34.89 ± 0.06	-199.1	-165 ± 10	34
[2W,2cit,5] ⁵⁻	39.33 ± 0.12	-224.5	-187 ± 10	38
[1W,2cit,6] ²⁻	35.00 ± 0.03	-199.7	-102 ± 15	98
[2W,1cit,4] ³⁻	31.68 ± 0.27	-180.8	-118 ± 20	63

Mo-tartrate

COMPLEX	$\log \beta_{pqr} \pm 3 \sigma$	ΔG° (kJ mol ⁻¹)	ΔH° (kJ mol ⁻¹)	$T\Delta S^\circ$ (kJ mol ⁻¹)
[0,1tart,1] ⁻	3.660 ± 0.01	-20.9	-3.1 ± 0.1	17.8
[0,1tart,2]	6.374 ± 0.01	-36.4	-7.0 ± 0.1	29.4
[1Mo,2tart,2] ⁴⁻	16.18 ± 0.01	-92.32	-79.8 ± 1.0	12
[1Mo,2tart,3] ³⁻	19.85 ± 0.03	-113.3	-80.0 ± 1.0	33
[1Mo,2tart,4] ²⁻	22.83 ± 0.03	-130.3	-80.0 ± 1.0	50
[2Mo,1tart,2] ⁴⁻	15.33 ± 0.04	-87.47	-80 ± 5	8
[2Mo,1tart,3] ³⁻	20.39 ± 0.12	-116.3	-93 ± 12	23
[2Mo,1tart,4] ²⁻	24.70 ± 0.04	-140.9	-120 ± 4	21
[2Mo,1tart,5] ⁻	25.97 ± 0.04	-148.2	-117.9 ± 3.0	30
[2Mo,2tart,5] ³⁻	31.59 ± 0.15	-180.3	-152 ± 10	28
[3Mo,4tart,6] ⁶⁻	47.54 ± 0.39	-271.4	-239 ± 40	33
[3Mo,4tart,8] ⁶⁻	54.56 ± 0.11	-311.3	-224 ± 30	87
[4Mo,3tart,8] ⁶⁻	56.35 ± 0.09	-321.5	-310 ± 40	12
[4Mo,4tart,8] ⁸⁻	61.41 ± 0.04	-350.4	-350 ± 30	0
[4Mo,4tart,9] ⁷⁻	63.40 ± 0.33	-361.8	-353 ± 40	9
[4Mo,5tart,8] ¹⁰⁻	64.04 ± 0.12	-365.4	-345 ± 50	21
[4Mo,5tart,9] ⁹⁻	67.70 ± 0.09	-386.3	-408 ± 50	-22

W-tartrate

COMPLEX	$\log \beta_{pqr} \pm 3 \sigma$	ΔG° (kJ mol ⁻¹)	ΔH° (kJ mol ⁻¹)	$T\Delta S^\circ$ (kJ mol ⁻¹)
[0,1tart,1] ⁻	3.660 ± 0.01	-20.9	-3.1 ± 0.1	17.8
[0,1tart,2]	6.374 ± 0.01	-36.4	-7.0 ± 0.1	29.4
[1W,2tart,2] ⁴⁻	17.85 ± 0.04	-101.9	-83.8 ± 2.0	18
[1W,2tart,3] ³⁻	21.38 ± 0.05	-122.0	-84.3 ± 1.0	38
[1W,2tart,4] ²⁻	24.29 ± 0.05	-138.6	-83.30 ± 2.0	55
[2W,1tart,2] ⁴⁻	16.94 ± 0.48	-96.66	-121 ± 10	-24
[2W,1tart,3] ³⁻	23.64 ± 0.09	-134.9	-144 ± 5	-10
[2W,1tart,4] ²⁻	27.38 ± 0.09	-156.2	-141 ± 4	15
[3W,4tart,6] ⁶⁻	52.65 ± 0.11	-300.4	-263 ± 10	37
[3W,4tart,8] ⁶⁻	58.86 ± 0.26	-335.9	-261 ± 10	75
[4W,3tart,8] ⁶⁻	62.46 ± 0.12	-356.4	-275 ± 40	81
[4W,4tart,8] ⁶⁻	66.79 ± 0.09	-381.1	-334 ± 40	47
[4W,5tart,9] ⁹⁻	73.68 ± 0.13	-420.4	-351 ± 40	70

Mo-aspartate

COMPLEX	$\log\beta_{pqr} \pm 3 \sigma$	ΔG° (kJ mol ⁻¹)	ΔH° (kJ mol ⁻¹)	$T\Delta S^\circ$ (kJ mol ⁻¹)
[0,1asp,1]	3.64 ± 0.01	-20.8	-5.8 ± 0.2	15.0
[0,1asp,2] ⁺	5.65 ± 0.01	-32.3	-10.2 ± 0.6	22.1
[1Mo,1asp,1] ²⁻	6.54 ± 0.01	-37.3	-27.4 ± 0.6	10
[1Mo,1asp,2] ⁻	9.84 ± 0.12	-56.2	-20 ± 7	36
[1Mo,2asp,1] ³⁻	6.57 ± 0.10	-37.5	-34 ± 8	4
[1Mo,2asp,2] ²⁻	11.47 ± 0.04	-65.5	-43 ± 3	23
[2Mo,1asp,4] ⁻	21.20 ± 0.05	-121.0	-96 ± 2	25
[2Mo,1asp,5]	23.50 ± 0.05	-134.1	-99 ± 8	35
[4Mo,4asp,9] ³⁻	50.86 ± 0.11	-290.3	-119 ± 10	171
[4Mo,4asp,10] ²⁻	53.48 ± 0.34	-305.2	-122 ± 15	183
[2Mo,4asp,8]	37.74 ± 0.10	-215.4	-69 ± 10	146

W-aspartate

COMPLEX	$\log\beta_{pqr} \pm 3 \sigma$	ΔG° (kJ mol ⁻¹)	ΔH° (kJ mol ⁻¹)	$T\Delta S^\circ$ (kJ mol ⁻¹)
[0,1asp,-1]	-9.55 ± 0.03	+54.52	+40.3	-14.2
[0,1asp,1]	3.64 ± 0.01	-20.8	-5.8 ± 0.1	15.0
[0,1asp,2] ⁺	5.65 ± 0.01	-32.3	-10.2 ± 0.1	22.1
[2W,1asp,4] ⁻	24.88 ± 0.5	-142.0	-88 ± 10	54
[2W,1asp,5]	27.43 ± 0.5	-156.6	-89 ± 10	67

Mo-nta

COMPLEX	$\log\beta_{pqr} \pm 3 \sigma$	ΔG° (kJ mol ⁻¹)	ΔH° (kJ mol ⁻¹)	$T\Delta S^\circ$ (kJ mol ⁻¹)
[0,1nta,1] ²⁻	8.78 ± 0.01	-50.1	-24.2 ± 0.5	26
[0,1nta,2] ⁻	11.04 ± 0.01	-63.0	-24.4 ± 1.0	39
[0,1nta,3]	12.73 ± 0.01	-72.7	-26.6 ± 1.0	46
[0,1nta,4] ⁺	13.69 ± 0.05	-78.1	[-27.6]	[50]
[1Mo,1nta,2] ³⁻	17.78 ± 0.02	-101.5	-69 ± 1.0	32
[1Mo,1nta,3] ²⁻	21.02 ± 0.02	-120.0	-71.2 ± 2.0	49
[1Mo,1nta,4] ⁻	22.57 ± 0.07	-128.8	-71.2 #	58 #
[2Mo,2nta,7] ³⁻	45.16 ± 0.04	-257.8	-123 ± 4	135
[2Mo,2nta,8] ²⁻	47.95 ± 0.02	-273.7	-132 ± 2	142
[2Mo,1nta,5] ²⁻	30.74 ± 0.12	-175.5		
[2Mo,1nta,6] ⁻	33.09 ± 0.04	-188.9		

W-nta

COMPLEX	$\log\beta_{pqr} \pm 3 \sigma$	ΔG° (kJ mol ⁻¹)	ΔH° (kJ mol ⁻¹)	$T\Delta S^\circ$ (kJ mol ⁻¹)
[0,1nta,1] ²⁻	8.78 ± 0.01	-50.1	-24.2 ± 0.5	26
[0,1nta,2] ⁻	11.04 ± 0.01	-63.0	-24.4 ± 1.0	39
[0,1nta,3]	12.73 ± 0.01	-72.7	-26.6 ± 1.0	46
[0,1nta,4] ⁺	13.69 ± 0.05	-78.1	[-27.6]	[50]
[1W,1nta,2] ³⁻	17.67 ± 0.05	-100.8	-66 ± 10	35
[2W,1nta,3] ⁴⁻	25.99 ± 0.03	-148.3		
[2W,1nta,4] ³⁻	30.92 ± 0.07	-176.4		
[2W,1nta,5] ²⁻	33.84 ± 0.10	-193.1	-90 ± 10	103
[2W,2nta,8] ²⁻	48.72 ± 0.05	-278.0	[-125]	[151]

Appendix 5

Explanatory notes on F curves

The F function, stated at the beginning of Chapter 3, is defined by

$$F = (H - h + K_w / h) / (2B + nC) \quad [3.1]$$

where

H , B and C = analytical concentrations of acid, Mo(VI) or W(VI) and ligand, respectively

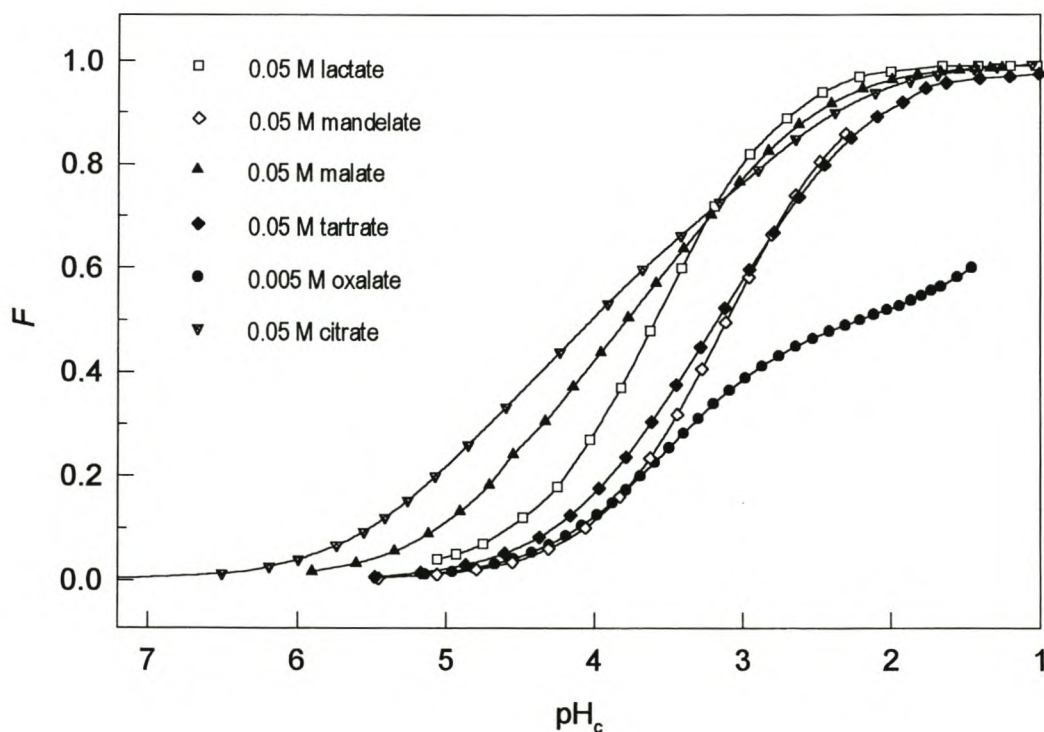
h = concentration of free H^+

n = charge on ligand

$K_w = 10^{-13.71}$ (for this medium, 1 M NaCl)

The function F thus represents the fraction of the total negative charge neutralized due to protonation. This is illustrated below by the very simple F curves which represent the titration of some of the ligands used, namely lactate, mandelate, oxalate, malate, tartrate and citrate. (These curves are also shown in the relevant figures in Chapter 3.)

(The F function differs from the well-known Z function only by a constant, resulting from the introduction of the charges (2 and n) into the function.)



The ligands lactate and mandelate have a single negative charge in their unprotonated form. Lactate is fully deprotonated at $\text{pH} > 5.5$ and fully protonated at $\text{pH} < 1$ (Appendix 2), corresponding to the degree of protonation $F = 0$ and $F = 1$, respectively. This can be seen in the curve of F vs. pH of the titration of lactate with acid. The protonation of lactate between $\text{pH} 5.5$ and 1 is indicated by the increase from 0 to 1 . The change of F is most significant (steepest slope) at $\text{pH} \sim 3.6$ where half of the lactate has been protonated, which corresponds to $F = 0.5$. The F curve representing the titration of mandelate with acid is very similar, except that protonation only starts at $\text{pH} \sim 5.2$ (Appendix 2), because of the smaller $\text{p}K$, and the curve is slightly shifted to the lower pH region.

The ligands malate and tartrate have two negative charges in their unprotonated form. Malate is fully deprotonated at $\text{pH} > 6.5$ and fully protonated at $\text{pH} < 1$ (Appendix 2). This also corresponds to the degree of protonation $F = 0$ and $F = 1$, respectively, as can be seen in the curve of F vs. pH of the titration of malate with. The double protonation of Hmal^{2-} (via H_2mal^-) takes place over a wider pH range than the single protonation of Hlac^- or Hman^- (Appendix 2), but the first and second protonation equilibria overlap to a large extent. The slope of the F curve is, therefore, generally less steep than the curve pertaining to the lactate system, and is almost constant between $\text{pH} 4.5$ and 3 . Half of the initial negative charge has been neutralized at $F = 0.5$, but in this case, the protons are distributed among both H_2mal^- and H_3mal (Appendix 2). The F curve representing the titration of tartrate with acid is very similar, except that protonation only starts at $\text{pH} \sim 5.5$ (Appendix 2), and that the features discussed above are slightly shifted to the lower pH region.

Oxalate also has two negative charges in its unprotonated form. Oxalate is fully deprotonated at $\text{pH} > 5.5$ (Appendix 2) and most of the oxalate species are singly protonated at $\text{pH} \sim 2.2$ (Hox^-). This corresponds to the degree of protonation $F = 0$ and $F = 0.5$, respectively. At $\text{pH} \sim 3.5$, equal amounts of ox^{2-} and Hox^- exist, which correspond to the value $F = 0.25$, where the slope of the F curve is the steepest. The second protonation only starts at $\text{pH} \sim 3$. An F value of 0.75 can be predicted at $\text{pH} \sim 1$ where roughly equal amounts of Hox^- and H_2ox exist. Since the two protonation equilibria overlap to a very *small* degree (unlike the case of the malate and tartrate systems), the increase in F due to the first protonation is quite distinct from the increase due to the second protonation. The resulting inflexion at $F = 0.5$ clearly indicates a major species (Hox^-) for which $r/q = 0.5$.

The citrate ligand has three negative charges in its unprotonated form. Citrate is fully deprotonated at $\text{pH} > 7$ and fully protonated at $\text{pH} < 1$ (Appendix 2). This also corresponds to the degree of protonation $F = 0$ and $F = 1$, respectively, as can be seen in the curve of F vs. pH of the titration of citrate with acid. The three protonation steps overlap significantly in the pH region 5 to 3 , hence the almost constant slope of the F curve. (The very slight inflexion at $\text{pH} \sim 3.5$ can be attributed to the presence of mostly the doubly protonated H_3cit^- .)

These examples of very simple systems show that the definition of the F function ensures that the presence of only unprotonated reactant is indicated by $F=0$ and the presence of only fully protonated species is indicated by $F=1$ (irrespective of the initial concentration and of how many protonations are involved). More importantly, inflexions have been shown to indicate the formation of a predominant species in a system.

References

1. Cotton F.A. and Wilkinson G., *Advanced Inorganic Chemistry, A comprehensive Text*, 5th edn., John Wiley & Sons, New York, p. 1371 (1988).
2. Cruywagen J.J., Heyns J.B.B. and Van de Water R.F., *J. Chem. Soc., Dalton Trans.*, 1986, 1857.
3. Spengler G. and Gansheimer J., *Angew. Chem.*, 1957, **26**, 354.
4. Mitchell P.C.H., *Chem. Soc. Rev.*, 1966, **20**, 103.
5. Atovymyan L.O. and Bokii G.B., *J. Struct. Chem.*, 1963, **4**, 524.
6. Spivack B. and Dori Z., *Coord. Chem. Rev.*, 1975, **17**, 99.
7. Gopalakrishnan J., Viswanathan B. and Srinivasan V., *J. Inorg. Nucl. Chem.*, 1970, **32**, 2565.
8. Goel S.P. and Mehrotra P.N., *Thermochim. Acta*, 1983, **68**, 137.
9. Goel S.P. and Mehrotra P.N., *Thermochim. Acta*, 1983, **70**, 201.
10. Beltrán-Porter A. and Martínez-Tamayo E., *Thermochim. Acta*, 1984, **75**, 303.
11. Tchakirian A. and Vartapetian O., *C. R. Acad. Sci. Paris*, 1952, **234**, 212.
12. Chalmers R.A. and Sinclair A.G., *J. Inorg. Nucl. Chem.*, 1967, **29**, 2065.
13. Shishkor D.A. and Velcheva B., *C. R. Acad. Bulg. Sci.*, 1964, **17**, 905.
14. Mikesova M. and Bartusek M., *Collect. Czech. Chem. Commun.*, 1978, **43**, 1867.
15. Shapiro K. Ya., Yurkevich Yu.N. and Kulukova V.V., *Chem. Abstr.*, 1968, **69**, 102644e.
16. Johansen E.S. and Jøns O., *Talanta*, 1984, **31**, 743.
17. Davies L. and Richardson R., *J. Less-Common Met.*, 1962, **4**, 104.
18. Voelter W., Bayer E., Barth G., Bunnenberg E. and Djerassi C., *Chem. Ber.*, 1969, **102**, 2003.
19. Wunsch G. and Nagen K., *Fresenius Z. Anal. Chem.*, 1979, **295**, 119.
20. Brown D.H. and Neumann D., *J. Inorg. Nucl. Chem.*, 1975, **37**, 332.
21. Shiskov D.A., *Dokl. Bolg. Akad. Nauk.*, 1971, **24**, 769.
22. Brown D.H., *J. Chem. Soc.*, 1961, 4732.
23. Banerjee S.P. and Bhattacharya A.K., *Curr. Sci.*, 1961, **30**, 380.
24. Souchay P., *Bull. Soc. Chim. Fr.*, 1989, 122.
25. Richardson E., *J. Inorg. Nucl. Chem.* 1960, **13**, 84.
26. Baillie M.J. and Brown D.H., *J. Chem. Soc.*, 1961, 3691.
27. Prasad S. and Pandey L.P., *J. Indian Chem. Soc.*, 1965, **42**, 783.
28. Cadot M. and Viossat B., *Rev. Chim. Minérale*, 1969, **6**, 727.
29. Mikanová E. and Barušek M., *Scripta. Fac. Sci. Nat. Univ. Purkynianae Brun.*, 1981, **11**, 439.
30. Caldeira M.M., Saraiva M.E.T.L. and Gil V.M.S., *Inorg. Nucl. Chem. Letters*, 1981, **17**, 295 and refs therein.
31. Beltrán A., Avalos A.C and Beltrán J., *J. Inorg. Nucl. Chem.*, 1981, **43**, 1337.
32. Mártine D.O., Feliz M.R. and Capparelli A.L., *Polyhedron*, 1988, **7**, 2708.
33. Azevedo M.D., Gomes-Costa R. and Jacobsohn K., *Enzymologia*, 1972, **43**, 105.
34. Gil V.M.S., Saraiva M.E.T.L., Caldeira M.M. and Pereira A.M.D., *J. Inorg. Nucl. Chem.*, 1980, **42**, 389 and refs therein.

35. Gil V.M.S., Saraiva M.E.T.L. and Caldeira M.M., *Inorg. Nucl. Chem. Letters*, 1981, **17**, 295.
36. Cervilla A., Ramirez J.A. and Llopis E., *Can. J. Chem.*, 1985, **63**, 1041.
37. Cruywagen J.J. and Van de Water R.F., *Polyhedron* 1986, **5**, 521 and refs therein.
38. Parker G.M., *Analytical Chemistry of Molybdenum*, Springer-Verlag, Berlin, Heidelberg (1983).
39. Meites L., *Anal. Chem.*, 1953, **25**, 1752.
40. Pecsok R.L. and Parkhurst R.M., *Anal. Chem.*, 1955, **27**, 1920.
41. Jost P., Lagrange P., Wolff M. and Schwing J.-R., *Proceedings of the Conference on the Chemistry and Uses of Molybdenum.*, University of Reading, England (1973).
42. Ogura K and Enaka Y., *Electrochim. Acta*, 1977, **22**, 833.
43. Creager S.E., Aikens D.A. and Clark H.M., *Electrochim. Acta*, 1982, **27**, 1307.
44. Day Jr R.A. and Underwood A.L., *Quantitative Analysis*, 6th edn., Prentice-Hall International, London (1991).
45. Bertotti M. and Tokoro R., *J. Electroanal. Chem.*, 1993, **360**, 39.
46. Tytko K.-H. and Trobisch U., *Gmelin Handbook of Inorganic Chemistry* (eds., Katscher H. and Schröder F.), 8th edn. Molybdenum Suppl. Vol.B 3a, Oxide Hydrates, Molybdate Ions. Springer-Verlag, Berlin (1987).
47. Rao G.S., *Proc. Nat. Acad. Sci., India, Sect. A*, 1954, **23**, 84.
48. Richardson E., *J. Inorg. Nucl. Chem.*, 1960, **13**, 84.
49. Rakhimov Kh.R. and Berdikhaliyev A., *Nauchn. Tr., Tashk. Gos. Univ.*, 1964, **264**, 142.
50. Pyatnitskii I.V. and Kravtsova L.F., *Ukr. Khim. Zh.*, 1968, **34**, 706.
51. Shiskov D.A., *Dokl. Bolg. Akad. Nauk*, 1971, **24**, 769.
52. Termendzhyan Z.Z. and Gaibakyan D.S., *Arm. Khim. Zh.*, 1971, **24**, 577.
53. Cervilla A., Ramirez J.A. and Llopis E., *Transition Met. Chem.*, 1986, **11**, 186.
54. Richardson E., *J. Inorg. Nucl. Chem.*, 1960, **13**, 84 and refs therein.
55. Clark E.R., *J. Inorg. Nucl. Chem.*, 1962, **24**, 1381.
56. Baillie M.J. and Brown D.H., *J. Chem. Soc.*, 1961, 3691.
57. Cadot M., Souchay P. and Viossat B., *Compt. Rend.*, 1966, **263**, 927.
58. Voelter W., Bayer E., Barth G, Bunnenberg E. and Djerassi C., *Chem. Ber.*, 1960, **102**, 2003.
59. Somova I.I., Tselinskii Y.K. and Mokhosev M.V., *Russ. J. Inorg. Chem.*, 1972, **17**, 79.
60. Tselinskii Y.K., Kuselmann I.I., Somova I.I. and Mokhosev M.V., *Russ. J. Inorg. Chem.*, 1973, **18**, 1725.
61. Mikanova E. and Barusek M., *Scripta Fac. Sci. Nat. Univ. Purk. Brun.*, 1981, **11**, 439.
62. Arena G., Cali R., Grasso M., Musumeci S., Sammartano S. and Rigano C., *Thermochimica Acta*, 1980, **36**, 329.
63. Castaño R., Etcebarria N. and Madariaga J.M. *J. Chem. Soc.*, 1994, 2729.
64. Brown D.H. and McPherson J., *J. Inorg. Nucl. Chem.*, 1972, **34**, 1705.
65. Singh M.K. and Srivastava M.N., *J. Inorg. Nucl. Chem.*, 1972, **34**, 2081.
66. Domènech A., Llopis E., Garcia-España E. and Cervilla A., *Transition Met. Chem.*, 1990, **15**, 525.
67. Gharib F., Zare K., Khorrami S.A. and Behju A., *J. Chem. Eng. Data*, 1995, **40**, 1214.
68. Domènech A., Llopis E., Cervilla A. and Vicente F., *Polyhedron*, 1992, **11** (12), 1517.

69. Anderegg G., *Pure Appl. Chem.*, 1982, **54**, 2693.
70. Chan S.I., Kula R.J. and Sawyer D.T., *J. Am. Chem. Soc.*, 1964, **18**, 377.
71. Collin J.-P and Lagrange P., *Bull. Soc. Chim. Fr.*, 1976, **9-10**, 1304.
72. Zare K., Lagrange P. and Lagrange J., *J. Chem. Soc., Dalton Trans.*, 1979, 1372.
73. Funahashi S., Kato Y., Nakyama M. and Tanaka M., *Inorg. Chem.*, 1981, **20**, 1752.
74. Kula R.J., *Anal. Chem.*, 1967, **10**, 1171.
75. Cotton F.A., Morehouse S.M. and Wood J.S., *Inorg. Chem.*, 1963, **3**, 1603.
76. Mentzen B.F. and Sauterau H., *J. Photochem.*, 1981, **15**, 169.
77. Nassimbeni L.R., Niven M.L., Cruywagen J.J. and Heyns J.B.B., *J. Crystallogr. Spectrosc. Res.*, 1987, **17**, 99.
78. Berg J.-E., Brandänge S., Lindblom L. and Werener P.-E., *Acta Chem. Scand.*, 1977, **A31**, 325.
79. Porai-Koshits M.A., Aslanov L.A., Ivanova G.V. and Polynova T.V., *J. Struct. Chem. (Engl. Trans.)*, 1968, **9**, 401.
80. Zhou Z-H., Yan W-B., Wan H-L. and Tsai K-R., *Chin. J. Struct. Chem.*, 1995, **14**, 255.
81. Knobler C.B., Wilson A.J., Hider R.N., Jenson I.W., Penfold B.R., Robinson W.T. and Wilkins C.J., *J. Chem Soc., Dalton Trans.*, 1983, 1299.
82. Alcock N.W., Dudek M., Grybos R., Hodorowicz E., Kanas A. and Samotus A., *J. Chem. Soc., Dalton Trans.*, 1990, 707.
83. Nassimbeni L.R., Niven M.L., Cruywagen J.J. and Heyns J.B.B., *J. Crystallogr. Spectrosc. Res.*, 1987, **17**, 373.
84. Cruywagen J.J., Saayman L.J. and Niven M.J., *J. Crystallogr. Spectrosc. Res.*, 1992, **22**, 737.
85. Llopis E., Ramirez J.A., Dominech A. and Cervilla A., *J. Chem. Soc.*, 1993, 1121.
86. Zhou Z-H., Wan H-L. and Tsai K-R., *Polyhedron* 1997, **16**, 75.
87. Robinson W.T. and Wilkins C.J., *Transition Met. Chem.*, 1986, **11**, 86.
88. Butcher R.J. and Penfold B.R., *J. Cryst. Mol. Struct.*, 1976, **6**, 13.
89. Matsumoto K., Marutani Y. and Ooi S., *Bull. Chem. Soc. Jpn.*, 1984, **57**, 2671.
90. Knobler C., Penfold B.R., Robinson, W.T., Wilkins C.J. and Yong S.H., *J. Chem. Soc. Dalton Trans.*, 1979, 248.
91. Beltrán A., Caturla F., Cervilla A. and Beltrán J., *J. Inorg. Nucl. Chem.*, 1981, **43**, 3277.
92. Beltrán-Porter A., Cervilla A., Caturla F. and Vila M.J., *Transition Met. Chem.*, 1983, **8**, 324.
93. Caldeira M.M., Ramos M.L. and Gil V.M.S., *Can. J. Chem.*, 1987, **65**, 827.
94. Samotus A., Kanas A., Dudek M., Grybos R. and Hodorowicz E., *Transition Met. Chem.*, 1991, **16**, 495.
95. Pedrosa de Jesus J.D., Farropas M. De D., O'Brien P., Gillard R.D. and Williams P.A., *Transition Met. Chem.*, 1983, **8**, 193.
96. Cavaleiro A.M.V.S.V., Gil V.M.S., Pedrosa de Jesus J.D., Gillard R.D. and Williams P.A., *Transition Met. Chem. (Weinheim, Ger.)*, 1984, **9**, 62.
97. Hlaibi M., Chapelle S., Benaïssa M. and Verchère J-F., *Inorg. Chem.*, 1995, **34**, 4434.
98. Rabestein D.L., Greenberg M.S. and Saetre R., *Inorg. Chem.*, 1977, **16**, 1241.

99. Cavaleiro A.M.V.S.V. , Gil V.M.S., Pedrosa de Jesus J.D., Gillard R.D. and Williams P.A., *Transition Met. Chem.*, 1982, **7**, 75.
100. Butcher R.J., Powell, H.K.J., Wilkens C.J. and Yong S.H., *J. Chem. Soc., Dalton Trans.*, 1976, 356.
101. Freeman M.A., Schultz F.A. and Reilley C.N., *Inorg. Chem.*, 1982, **21**, 567.
102. Miller K.F. and Wentworth R.A.D., *Inorg. Chem.*, 1978, **17**, 2769.
103. Sengupta A.K and Nath S.K., *Indian J. Chem., Sect. A*, 1981, **20**, 203.
104. Caldeira M.M. and Gil V.M.S., *Polyhedron*, 1986, **5**, 381.
105. Gil V.M.S., *Pure Appl. Chem.*, 1989, **61**, 841.
106. Chen Q. and Zubieta J., *Coord. Chem. Rev.*, 1992, **114**, 107.
107. Stiefel E., in *Comprehensive Coordination Chemistry* , ed. Wilkinson G., 1987,**3**, 1257 and 1375.
108. Gamer C.D. and Chamock J.M., in *Comprehensive Coordination Chemistry*, ed. Wilkinson G., 1987, **3**, 1329.
109. Zubieta J. and Chen Q., *Coordination Chemistry Reviews*, 1992, **114**, 107.
110. Wilkinson G., *Comprehensive Coordination Chemistry* , **87**, **2**, 461+740+961
111. Rossotti H.S., *Talanta*, 1974, **21**, 809.
112. Choat T.C., Cruywagen J.J. and Heyns J.B.B., *Anal. Chem.*, 1986, **58**, 2571.
113. Cruywagen J.J. Program written in FORTRAN for IBM compatible PC.
114. Christensen J.J., Johnston H.D. and Izatt R.M., *Rev. Sci. Instrum.*, 1968, **39**, 1356.
115. Christensen, J.J., Gardner J.W., Eatough D.J., Watts P.J. and Hart R.M., *Rev. Sci. Instrum.*, 1973, **44**, 481.
116. Cruywagen J.J. and Rohwer E.A., *unpublished work*
117. Cruywagen J.J and Van der Merwe I.F.J., *J. Chem. Soc., Dalton Trans.*, 1987, 1701.
118. Gans P., Sabatini A. and Vacca A., *J. Chem. Soc., Dalton Trans.*, 1985, 1195.
119. Vetrogen V.I., Lukyanenko N.G., Schwing-Weill M-J., Arnaud-Neu F., *Talanta*, 1994, **41**, 2105
120. Gans P., Sabatini A. and Vacca A., *Talanta*, 1996, **43**, 1739.
121. Cruywagen J.J., *Inorg. Chem.*, 1980, **19**, 552.
122. Cruywagen J.J., Heyns J.B.B. and Rohwer E.F.C.H., *J. Inorg. Nucl. Chem.*, 1978, **40**, 53.
123. Cruywagen J.J., Heyns J.B.B. and Rohwer E.F.C.H., *J. Inorg. Nucl. Chem.*, 1976, **38**, 2033.
124. Rohwer E.F.C.H. and Cruywagen J.J., *J. S. Afr. Chem. Inst.*, 1969, **22**, 198.
125. Cruywagen J.J., Heyns J.B.B., *Inorg. Chem.*, 1987, **26**, 2569.
126. Gampp H., Maeder M., Meyer C.J. and Zuberbühler A.D., *Talanta*, 1985, **32**, 95.
127. Maeder M and Zuberbuhler A.D. *Anal. Chem.*, 1990, **62**, 2220 and refs therein.
128. Leggett D.J. and McBryde W.A.E., *Anal. Chem.*, 1975, **47**, 1065.
129. Legget D.J., in *Computational Methods for the Determination of Formation Constants*, (ed. Legget D.J.) Plenum Press, New York, p.221.(1985).
130. Dixon W.J. (ed.), *BMDP Statistical Software*, University of California Press, Berkley, CA (1981).
131. Lin H-K., Gu A-X. and Chen Y-T., *Gazz. Chim. Ital.*, 1987, **117**, 23.
132. Lundqvist R., Lu J.F. and Svantesson I., *Acta Chem. Scand., Ser. A*, 1984, **38**, 3271.

133. Smith R.M. and Martell A.E., *Critical Stability Constants*, Vol. 6, Second Suppl., Plenum, New York, p. 311., (1989).
134. Powell J.E. and Neillie W.F.S., *J. Inorg. Nucl. Chem.*, 1967, **29**, 2371.
135. Cruywagen J.J. and Van de Water R.F., *Polyhedron*, 1986, **5**, 521.
136. Bottari E., Festa M.R. and Jasionowska R., *Polyhedron*, 1989, **8**, 1019.
137. Yamada S., Magase J., Fanahashi S. and Tanaka M., *J. Inorg. Nucl. Chem.*, 1976, **38**, 617.
138. Christensen, J.J., Izatt R.M. and Hansen L.D., *J. Am. Chem. Soc.*, 1967, **89**, 213.
139. Rohwer E.A., *MSc thesis*, University of Stellenbosch (1988).
140. Cruywagen J.J. and Heyns J.B.B., *paper submitted*, Dec 1999.
141. Cervilla A., Llopis E., Ribera A., Doménech A. and White A.J.P., *J. Chem. Soc. Dalton Trans.*, 1995, 3891.
142. Cruywagen J.J., Heyns J.B.B. and Rohwer E.A., *J. Chem. Soc. Dalton Trans.*, 1990, 1951.
143. Dengel A.C., Griffith W.P., Powell R.D. and Skapski A.C., *J. Am. Chem. Soc., Chem. Commun.*, 1986, 555.
144. Ramos M.L., Caldeira M.M. and Gil V.M.S. *Inorganica Chimica Acta*, 1991, **180**, 219.

Publications based on this work

- | | |
|--|---|
| Cruywagen J.J., Krüger L. and Rohwer E.A., | <i>J. Chem. Soc. Dalton Trans.</i> , 1993, 105.
(Mo/W-lac) |
| Cruywagen J.J. and Rohwer E.A., | <i>J. Chem. Soc. Dalton Trans.</i> , 1995, 3433.
(Mo/W man) |
| Cruywagen J.J., Rohwer E.A. and Van de Water R.F., | <i>Polyhedron.</i> , 1997, 16 (2), 243.
(Mo-mal) |
| Cruywagen J.J., Krüger L. and Rohwer E.A., | <i>J. Chem. Soc. Dalton Trans.</i> , 1997, 1925.
(W-mal) |
| Cruywagen J.J., Rohwer E.A. and Wessels G.F.S., | <i>Polyhedron.</i> , 1995, 14 (23-24), 3481.
(Mo-cit) |
| Cruywagen J.J., Krüger L. and Rohwer E.A., | <i>J. Chem. Soc. Dalton Trans.</i> , 1991, 1727.
(W-cit) |
| Cruywagen J.J., Heyns J.B.B. and Rohwer E.A., | <i>J. Chem. Soc. Dalton Trans.</i> , 1990, 1951.
(Mo-tart) |
| Cruywagen J.J., Heyns J.B.B. and Rohwer E.A., | <i>J. Chem. Soc. Dalton Trans.</i> , 1993, 1713.
(Mo-asp) |
| Cruywagen J.J., Heyns J.B.B. and Rohwer E.A., | <i>J. Chem. Soc. Dalton Trans.</i> , 1994, 45.
(Mo-nta) |